A Flexible and Modular Approach to [2]Ferrocenophanes with Nitrogen in Bridging Position

A Thesis Submitted to the College of

Graduate Studies and Research

in Partial Fulfilment of the Requirements

for the Degree of Doctor of Philosophy

in the Department of Chemistry

University of Saskatchewan

Saskatoon

Canada

by

Subhayan Dey

PERMISSION TO USE

In presenting this thesis in partial fulfillment of the requirements for a Postgraduate degree from the University of Saskatchewan, I agree that the Libraries of this University may make it freely available for inspection. I further agree that permission for copying of this thesis in any manner, in whole or in part, for scholarly purposes may be granted by the professor who supervised my thesis work or, in his absence, by the Head of the Department or the Dean of the College in which my thesis work was done. It is understood that any copying or publication or use of this thesis or parts thereof for financial gain shall not be allowed without my written permission. It is also understood that due recognition shall be given to me and to the University of Saskatchewan in any scholarly use which may be made of any material in my thesis.

Requests for permission to copy or to make other uses of materials in this thesis in whole or part should be addressed to:

Head of the Department

Department of Chemistry

University of Saskatchewan

Saskatoon, Saskatchewan, S7N 5C9, Canada

ABSTRACT

[*n*]Ferrocenophanes are interesting because these strained sandwich compounds can be polymerized to metallopolymers by ring-opening polymerization reactions. Although there are many strained [*n*]ferrocenophanes known, only few of them can be polymerized with controlled molecular weight and molecular weight distribution. Among them, the Me_2Si-bridged [1]ferrocenophane is the mostly explored species. To expand the possibility of accessible monomers we synthesized a new class of strained [2]ferrocenophanes. Although there are plenty of examples of symmetrically bridged [2]ferrocenophanes known, similar species with two different bridging elements are comparatively rare. In order to induce a difference in polarity over the diatomic bridge, nitrogen was introduced in the bridging position. Via a known synthetic methodology, one bromine of 1,1'-dibromoferrocene was selectively replaced by an amino group. The resulting compound was then modified into a class of easily synthesizable starting materials which were cleanly lithiated under optimized condition and in-situ reacted with different elemental dihalides to produce unsymmetrically bridged aza[2]ferrocenophanes. This is the first reported development of a modular synthetic approach towards this class of strained sandwich compounds. Aza[2]ferrocenophanes with boron, gallium, silicon, tin, and phosphorus as the second bridging element were prepared and characterized.

Among these strained compounds, only the silicon- and tin-bridged species have been investigated for ring-opening polymerizations. However, no polymeric materials were obtained from these reactions. The preparation of azaphospha[2]ferrocenophanes was surprisingly difficult and led to unexpected products like 1,1'-disubstituted ferrocenes and azacarbaphospha[3]ferrocenophane.

ACKNOWLEDGEMENTS

I am grateful to my supervisor Prof. Dr. Jens Müller for his support, guidance and encouragement during my studies as a Ph.D. student.

I would like to thank the University of Saskatchewan and Department of Chemistry for providing me with the opportunity to study here; the members of my advisory committee for their support, and the stuffs at the Saskatchewan Structural Science Centre. In particular, I am grateful to Ken Thoms for his help with mass measurements and Dr. Keith C. Brown for his help with NMR measurements.

I would like to acknowledge all present and past members of the Müller group for their help and support. In particular, I would like to acknowledge Dr. Bidraha Bagh, Hridaynath Bhattacharjee and Cao Phan Thuy My for their support and inspiration.

I am grateful to my parents Nemai Tirtha and Minu De, and wife Soumi Dutta for their love, moral support and encouragement for such a long time. I would like to convey my special thanks to Prof. Dr. Jaydip Biswas (MS, Calcutta) and Dr. Santosh M. Kumar (MS, Calcutta) for giving me a new life.

TABLE OF CONTENTS

Pages

LIST OF ABBREVIATIONS

ABBREVIATIONS

CHN……...……. elemental analysis

cod..... 1,5-cyclooctadiene

Cp..... cyclopentadiene

d……..… doublet

Fc..... $(C_5H_5)Fe(C_5H_4)$

FCP..... ferrocenophane

FDI……...…..... field desorption ionization

GPC..... gel permeation chromatography

HOMO..... highest occupied molecular orbital

HRMS……...….. high-resolution mass spectrometry

J……. coupling constant

LUMO..... lowest unoccupied molecular orbital

m……..…… multiplet

Mamx..... 2,4-di-*tert*-butyl-6-[(dimethylamino)methyl]phenyl

MCP..... metallocenophane

Mes..... 2,4,6-trimethylphenyl

MS……..…… mass spectrometry

NMR…….. nuclear magnetic resonance

OCP..... osmocenophane

PDI..... polydispersity index

pmdeta..... *N*,*N*,*N*′,*N*′′-pentamethyldiethylenetriamine

ppm..... parts per million

pst……...……. pseudo triplet

RCP..... ruthenocenophane

ROP..... ring-opening polymerization

r.t..... room temperature

s…….…….. singlet

t……..….. triplet

tmeda..... *N*,*N*,*N*′,*N*′-tetramethylethylenediamine

LIST OF FIGURES

Figures Pages

LIST OF SCHEMES

Schemes Pages

LIST OF TABLES

Tables Pages

CHAPTER 1

INTRODUCTION

Strained cyclic organic compounds have been investigated intensely over the last few decades. This is due to the fact that these compounds can produce moderate to high molecular weight organic polymers. A comprehensive review of this field is beyond the scope of the thesis and the readers are being referred to a few publications dealing with developments on strained silacycles, carbaphospha heterocycles and carbacycles.[1,2,3,4] Although aforementioned compounds have been well explored in molecular synthesis and as monomers of polymerization, their organometallic counterparts containing transition metals are comparatively less studied.

Over the last 50 years or so, a group of strained organometallic compounds, called metallocenophanes (MCPs), have been synthesized. MCPs are a class of strained cyclic organometallic species containing transition metals, which are sandwiched between two π-hydrocarbon rings. These compounds have attracted considerable attention for their ring-opening polymerizations (ROPs). This method of polymerization is important as it allows to incorporate metals in the polymer backbone. The first systematically studied example of ROP was performed by employing a Me_2Si group in the bridging position of a [1]ferrocenophane ([1]FCP, **1**, Figure 1.1).[5] Although this chemistry was reported in 1992, [*n*]MCPs were already published as early as 1957. The first metallocenophane was an unstrained [3]FCP (**2**, Figure 1.1), reported in 1957 by Rinehart Jr. *et al*.[6] A few years later, the same group reported the first [2]FCP (**3**, Figure 1.1)[7] and it was suggested that [1]FCPs will be too strained to exist.[8] However, despite of this assumption, 15 years later Osborne and co-worker successfully synthesized the first [1]FCPs which contained silicon in the bridging position.[9] Among the two strained compounds reported in this publication, one example is shown in Figure 1.1 (**4**, Figure 1.1).

To date, a large number of strained sandwich compounds with a wide variety of transition metals and bridging elements have been reported.[10] The variation of π-hydrocarbon was also achieved, such as in [*n*]MCPs of type **5** (Figure 1.1), where the sandwich moiety is composed out of two benzene rings.[10]

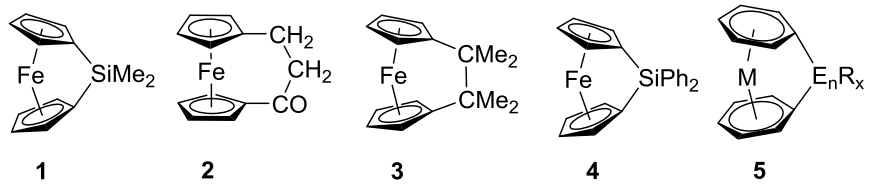

Figure 1.1. Different metallocenophanes (**1**-**4**) and a metallarenophane (**5**).

1.1. Ferrocenophanes

Ferrocene is the most common example of a metallocenes, showing two Cp rings parallel to each other. This parallel structure is due to the overlap of π orbitals of Cp ligands with s, p and d orbitals of the Fe(II) center. The short *ansa* [*n*] bridges (*n* = 1, 2, 3 etc.) compel the ferrocene moiety to change its normal geometry to a ring-tilted structure (Figure 1.2). The dihedral angle between the two Cp rings is defined as the tilt angle α, which is considered as an indication of the amount of intrinsic strain. The strain in metallocenophanes usually increases with the increase of the α angle.[10,11] In addition to the tilt angle, there are also some other geometrical features in the strained compounds: β which denotes the $Cp^{centroid}$-C^{ipso}-E angle, δ which shows the $Cp^{centroid}$-Fe-$Cp^{centroid}$ angle, and τ which defines the angle between least square plane of $Cp^{centroid}$-Fe-$Cp^{centroid}$ and E-E bridging bond vector (Figure 1.2).[10,11]

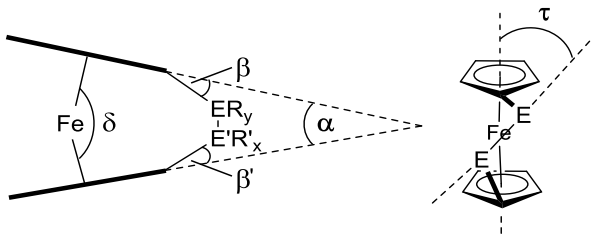

Figure 1.2. Common angles to characterize distortions in [2]FCPs.

As the number of the bridging atom increases in [*n*]FCPs, the tilt angle α decreases. For example, the tilt angle of bora[1]ferrocenophanes is around 31°,[12] whereas that of dibora[2]ferrocenophanes is around 13°.[13] The tilt angle α also increases with decreasing size of the bridging element. For example, the α angle for sila[1]ferrocenophane is 20.8(5)°,[14] whereas those for germanium- and tin-bridged [1]FCPs are 19.0(9)° and 14.1(2)°, respectively.[15,16] That means, smaller α angles are expected while moving down in a same column of the periodic table and larger α angles are expected while moving from left to right in a same row of the periodic table. For example, the α angle increases from aluminum-bridged [1]FCP [α for alumina[1]ferrocenophane is around 15°][17] to silica- [α for sila[1]ferrocenophane is around 21°][14] to phosphorus- [α for phospha[1]ferrocenophane is around 27° and borane adduct of phohpha[1]ferrocenophane is around 24.5°] bridged [1]FCP.[18,19,10] When the HOMO-LUMO gap decreases by increasing the tilt angle, a bathochromic shift of the lowest energy absorbance of the molecule is observed.[10] As a result, a gradual change in the color of [1]FCPs is observed from orange (for ferrocene) to red (for silicon- and phosphorus-bridged [1]FCPs) to purple (for boron-bridged [1]FCPs).[10]

To date, there are two well-established routes to synthesize [*n*]FCPs: the salt-metathesis and flytrap route, with the salt-metathesis reaction being the most common one.[10] This method involves the reaction of dilithio sandwich compounds of type **A** with elemental dihalides, equipped

with appropriate ligands (Scheme 1.1). One of the vital steps for the preparation of [*n*]MCPs via the salt-metathesis route is the synthesis of dilithio sandwich compounds (**A**), which is accomplished by using a lithiating reagent like butyllithium along with activators like tmeda or pmdeta (tmeda = *N*,*N*,*N*′,*N*′-tetramethylethylenediamine; pmdeta = *N*,*N*,*N*′,*N*′,*N*″-pentamethyldiethylenetetramine).[10] The less common approach for the synthesis of [*n*]MCPs is the "flytrap" method, which involves an appropriately bridged dianionic linker of type **B** and a metal dihalide (Scheme 1.1).[10] The first reported dicarbon-bridged [2]FCP **3** (Figure 1.1) was synthesized by this route, whereas the first silicon-bridged [1]FCP **4** (Figure 1.1) was prepared by the salt-metathesis reaction between dilithioferrocene·tmeda and diphenyldichlorosilane.[7,9]

Scheme 1.1. Common Synthetic Pathways to [*n*]MCPs

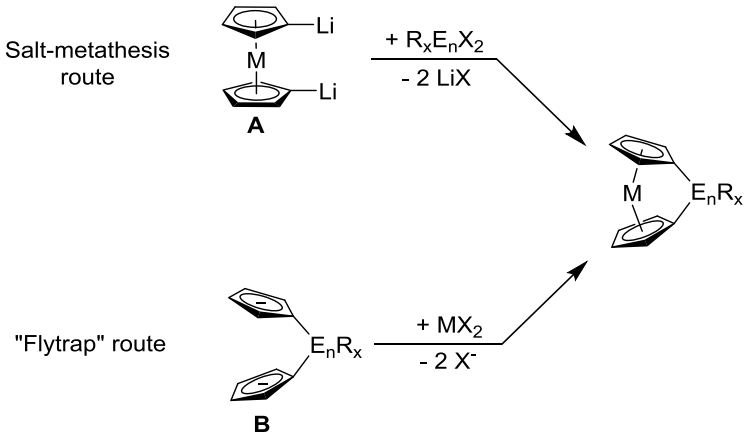

The deviation from the co-planarity to give a ring-tilted structure introduces ring-strain in [*n*]MCPs. This strain can be released by ROP, which results in polymeric materials. In practice, high-molecular-weight metallopolymers cannot be obtained by a polycondensation route (see Section 1.3). On the other hand, the chain-growth process of ROP is a very effective route to synthesize high-molecular-weight metallopolymers (see Section 1.3). Especially, [1]MCPs with large tilt angles are highly strained and are often very susceptible to release the strain by ROPs.

The ROPs of the strained MCPs has provided additional motivation to develop this exciting field.[10] As a rule of thumb, the tilt angle α plays the key role in determining the propensity toward ROP for FCPs. By calculations using density functional theory (DFT) Green showed that the energy required to tilt the Cp rings is similar to experimentally determined ΔH^{ROP} values.[20]

To date, poly(ferrocenylsilane) is the most developed subclass of metallocenophanes from ROP of strained sandwich compounds and found application in material science such as precursors to ceramics, tunable components of photonic crystal displays and redox-tunable capsules.[21,22,23] The controlled chain growth process in living ROP is another important aspect in this chemistry. In some cases, the living polymerization gives access to block co-polymers which in block sensitive solvents give nanoscopic aggregates of different morphologies such as cylinders, vesicles and spherical micelles. For an example, the block co-polymer of poly(isoprene) and poly(ferrocenylsilane) forms a core-corona type micelle structure in a mixture of xylene and decane (1 : 10), which results in a scarf-like architecture when crystallized at 70 °C.[24] These three-dimensional nanostructures show considerable potentials for applications in nanotechnology.[24,25,26]

As the field of strained ferrocenophane is being explored for last five decades, an enormous amount of material is already reported. As a result, a comprehensive overview of all published metallocenophanes is beyond the scope of this thesis. Interested readers are referred to a few recent reviews which deal with developments in this area.[10,11,20,27,28] As our main interest is about [2]FCPs, the following sections will offer an overview on the synthesis, characterization and reactivity of [2]MCPs.

1.2. [2]Metallocenophanes with Iron, Ruthenium and Osmium in the Centre

The first dicarba[2]ferrocenophane was described in 1960 (**3**, Figure 1.1), which is the first reported strained sandwich compound.[7] Since this early discovery many carbon and heteroatom-bridged [2]MCPs were synthesized.[10] Depending on the atoms present in the bridging position, this class of compounds can further be divided into symmetrically bridged [2]MCPs (**A**, Figure 1.3) and unsymmetrically bridged [2]MCPs (**B**, Figure 1.3).

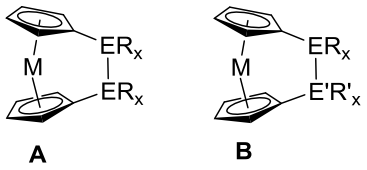

Figure 1.3. Symmetrically and unsymmetrically bridged [2]MCPs.

In the following sections, I will first give an overview of symmetrically bridged [2]FCPs, which will be followed by ruthenocene and osmocene analogs. Finally, unsymmetrically bridged [2]MCPs will be discussed.

1.2.1. Symmetrically Bridged [2]FCPs

Symmetrically bridged [2]FCPs can be divided into four subgroups: carbon-bridged [2]FCPs, boron-bridged [2]FCPs, heavier group 14-bridged [2]FCPs, and phosphorus-bridged [2]FCPs. Dicarba[2]ferrocenophanes are treated separately from the other group 14 elements as these species are more strained than their silicon, germanium, or tin counterparts and, therefore, have been more explored in terms of ROP.

1.2.1.1. Carbon-bridged [2]FCPs

The first example of a carbon-bridged [2]FCP is 1,1,2,2-tetramethyl substituted dicarbon-bridged [2]FCP (**3**), which was synthesized in a low yield by reaction of the dianionic linker **7** with $FeCl_2$ (Scheme 1.2).[7] The needed flytrap **7** was obtained by the reaction of 6,6-dimethylfulvene (**6**) and metallic sodium.[7] The yield of this reaction was improved by McGlinchey and co-workers, by using the method of direct co-condensation of 6,6-dimethylfulvene and iron vapor.[29] The X-ray crystallographic study revealed that the tilt angle of compound **3** is 23.2°, which provides evidence of intrinsic strain in the molecule.[30] Percentage yields of compound **3** were not reported in the cited publications.[7,29] The yield improvement of compound **3** from the Rinehart's synthesis to the McGlinchey's one is stated in the review article by Lee *et al*.[27]

Scheme 1.2. Synthesis of Carbon-bridged [2]FCP (3)

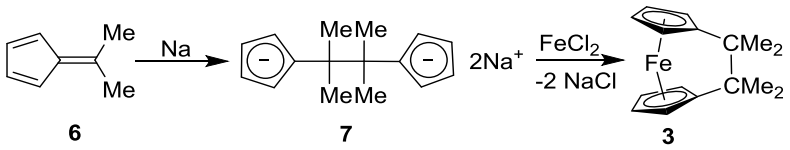

Unsaturated dicarba[2]ferrocenophanes were also synthesized and their structure and reactivity were compared with the saturated versions.[31] Tilley and co-workers synthesized the first vinyl-bridged [2]FCP (**9**) by using a McMurray coupling on 1,1'-disubstituted ferrocene derivative **8** (Scheme 1.3, yield 44%).[31] The molecular structure of compound **8**, measured by X-ray crystallography, revealed a tilt angle α of 23°, which is very similar to that of the saturated analog **3** (α = 23.2°).[30] The CH=CH-Cp angle was found as 117.8(3)° and the C=C distance as 1.315(5) Å, values that are identical with those known for alkenes.[31,27] The strained compound **9** was further used for ring-opening-metathesis polymerization, which will be discussed in Section 1.4.

Scheme 1.3. Synthesis of Vinyl-bridged [2]FCP (9)

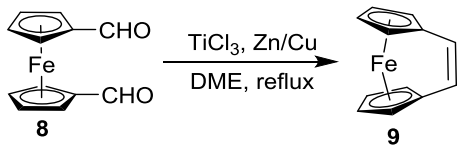

Another interesting class of unsaturated carbon-bridged [2]FCP contains phenylene moiety in the bridge and was synthesized by Yamazaki *et al.* in 1977.[32] Treatment of 1,1'-disubstituted ferrocene **10** with the acetylene-cobalt complex **11** afforded (*o*-phenylene)-bridged [2]FCP derivatives (**12**-**14**, Scheme 1.4) which showed tilt angles α in a close range of 23-24°.[32]

Scheme 1.4. Syntheses of Phenylene-bridged Carba[2]ferrocenophanes (12-14)

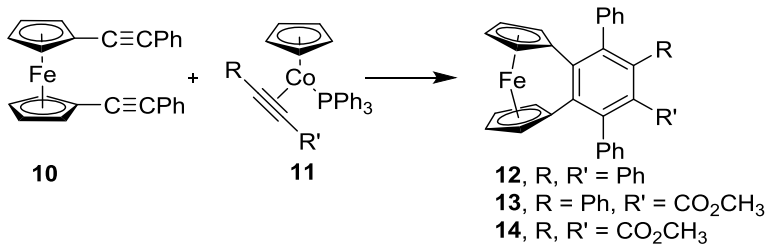

The first example of a carbon-bridged [2](1,1')[2](2,2')FCP (**17**) was synthesized via a modified flytrap route and reported in 1994 by Hafner *et al.* (Scheme 5, yield 41%).[33] By using a stoichiometric amount of *n*BuLi the tricyclic species **15** was first dilithiated and the resulting dilithio linker **16** was then reacted with $FeCl_2$. The crystallographic measurement on compound **17** revealed a tilt angle of 28.8°, which is 5.6° higher than its carbon-bridged analog **3** (Scheme 1.2).[33] Along with compound **17**, a [2](1,1')[2](2,2')zirconacenophane was also synthesized and reported by the same research group.[33]

Scheme 1.5. Synthesis of [2](1,1')[2](2,2')FCP (17)

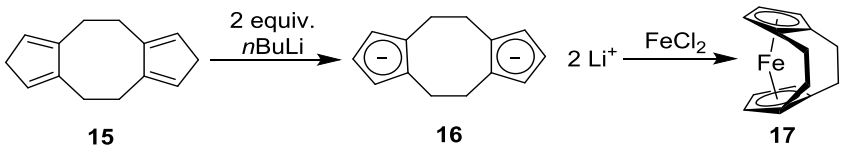

More interesting results were published when Rauchfuss and co-workers synthesized FCPs with both hydrocarbon and trisulfide bridges in the same molecule.[34] By following a general synthetic methodology, when dicarba[2]ferrocenophane **3** was lithiated and further reacted with elemental sulfur, a [2](1,1')[3](3,3')FCP **18** was obtained in a yield of 10% (Scheme 1.6).[34] By X-ray crystallographic measurement, the tilt angle of compound **15** was found as 20.21(3)°, which is ca. 3° smaller than that of the starting compound **3**.[34,30]

Scheme 1.6. Synthesis of [2](1,1')[3](3,3')FCP (18)

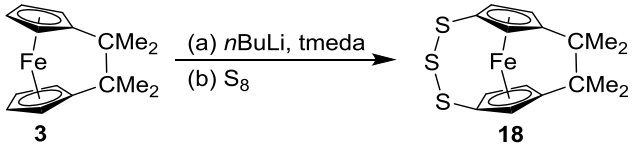

Due to their rigid conformation and substantial ring-strain, dicarba[2]ferrocenophanes show significant reactivity towards ROP.[27] The detail discussion about the ROP of these species can be found in Section 1.4.

1.2.1.2. Boron-bridged [2]FCPs

The first 1,2-dibora[2]ferrocenophane was synthesized in 1996 by Wrackmeyer and co-workers.[35] The reaction of 1,1'-dilithioferrocene (**19**) with 1,2-dichloro-1,2-bis(dimethylamino)diborane gave the dibora[2]ferrocenophane **20** in a yield of 58% (Scheme 1.7).[35]

Scheme 1.7. Synthesis of Dibora[2]ferrocenophane (20)

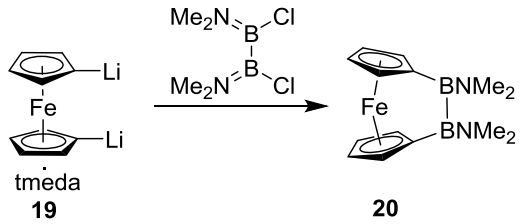

A decade later, Braunschweig and co-workers applied a flytrap approach and an alternative synthesis of compound **20** was reported.[13] In this synthesis, $FeCl_2$ was reacted with the dianionic linker **22**, which was obtained by a reaction of *n*BuLi with the bisboryl species **21** (Scheme 1.8). The dibora[2]ferrocenophane **20** was isolated in a yield of 61%, calculated from **22**.[13] The low to moderate intrinsic strain in molecule **20** is reflected by the tilt angle, which was found as 12.82(16)° from X-ray crystallography.[13] Probably due to this small tilt angle, no successful ROP has been reported on this compound. However, later, compound **20** found a way of potential application in the field of transition-metal-mediated bond activation.[36–40]

Scheme 1.8. Alternate Synthesis of Dibora[2]ferrocenophane (20)

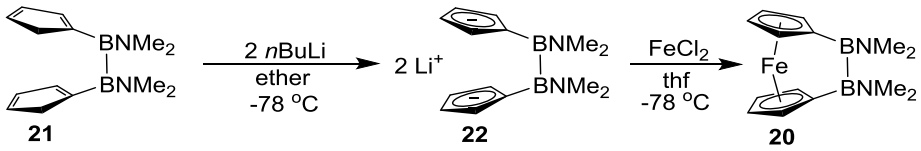

The B-B bond in compound **20** could easily be activated by certain transition metal complexes. For example, on addition of 5 mol% of $Pt(PEt_3)_3$, a $Pt(PEt_3)_2$ moiety inserted between two boron centers and the new [3]FCP **23** was formed (Scheme 1.9).[36] More interesting results were obtained when species **23** was reacted with alkynes and azobenzenes. In these two cases, diboration of the C=E (E = C, N) bonds of starting materials occurred and compounds **24** and **25**, respectively, were obtained (Scheme 1.9).[36,37] In a further reaction with isocyanides, **23** gave

[3]FCP **26** (Scheme 1.9).[38] A chromarenophane analog of compound **20** showed similar reactivity with alkynes and azobenzenes.[38] As the comprehensive review of all boron-bridged ferrocenophanes is beyond the scope of this thesis, the readers are referred to recent review articles.[39,40]

Scheme 1.9. Reactions of Dibora[2]ferrocenophane (20)

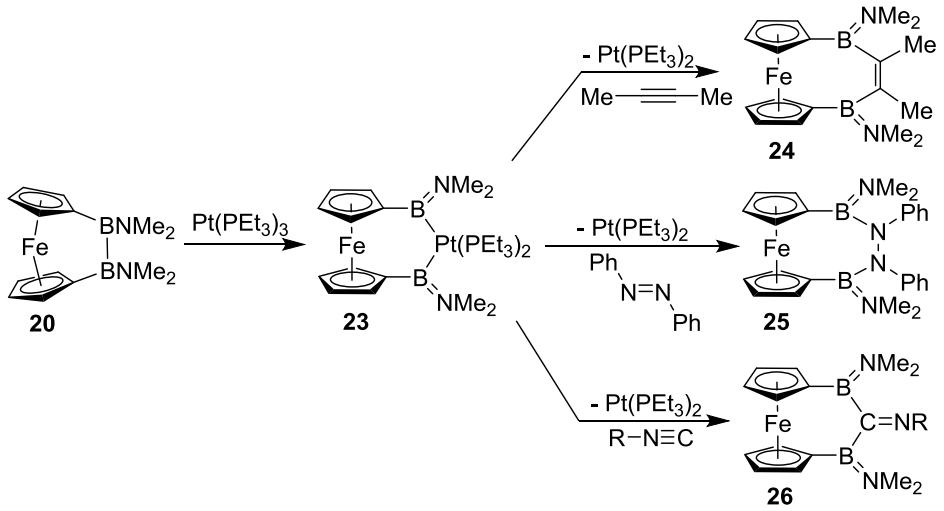

A series of new diboradicarba[4]ferrocenophanes was also synthesized via transition metal mediated diboration of selected dialkynes.[41,42] For this pathway compound **20** was first treated with catalytic amount of $Pt(PEt_3)_3$ and the resulting [3]FCP **23** was then reacted with dialkynes. Two different reaction motifs were observed in this investigation: dialkynes with no spacer unit gave diboradicarba[4]ferrocenophanes (**27**), whereas dialkynes with spacer units gave bis-diboradicarba[4]ferrocenophanes (**28**, Figure 1.4).[41,42]

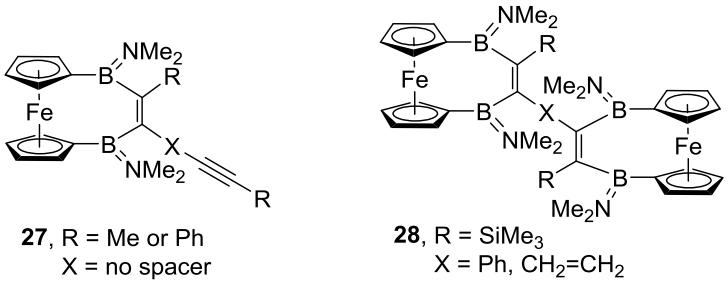

Figure 1.4. Selected examples of compounds obtained in single and double diboration of dialkynes.

1.2.1.3. Heavier Group-14-bridged [2]FCPs

The first disila- and digerma[2]ferrocenophanes were synthesized by Kumada and co-workers in 1972.[43–45] By following a flytrap route when dianionic linkers **31** and **32** were reacted with thf solutions of $FeCl_2$, compounds **33** and **34** were obtained (Scheme 1.10).[45] No percentage yield has been reported for these two compounds.[45] Species **31** and **32** were obtained from their corresponding dicyclopentadiene precursors (**29** and **30**) by reaction with *n*BuLi (Scheme 1.10a).[45] The molecular structure of compound **33**, determined by X-ray crystallography, showed a tilt angle of 4.19(2)°.[46] In 2007, Marschner and co-workers synthesized another disila[2]ferrocenophane with a $(Me_3Si)_2Si$-$Si(SiMe_3)_2$ moiety in the bridge.[47] As illustrated in Scheme 1.10b, a 1,1'-disubstituted ferrocene derivative **35** was first reacted with KO*t*Bu to afford the dianionic species **36**. When **36** was reacted with $Br(CH_2)_2Br$ the silicon-bridged [2]FCP **37** was obtained in a yield of 93%.[47] Compound **37** was further analyzed by X-ray crystallography. However, probably due to the poor quality of crystal no tilt angle for this compound was reported.[47]

Scheme 1.10. Syntheses of Disila- and Digerma[2]ferrocenophane (33, 34, and 37)

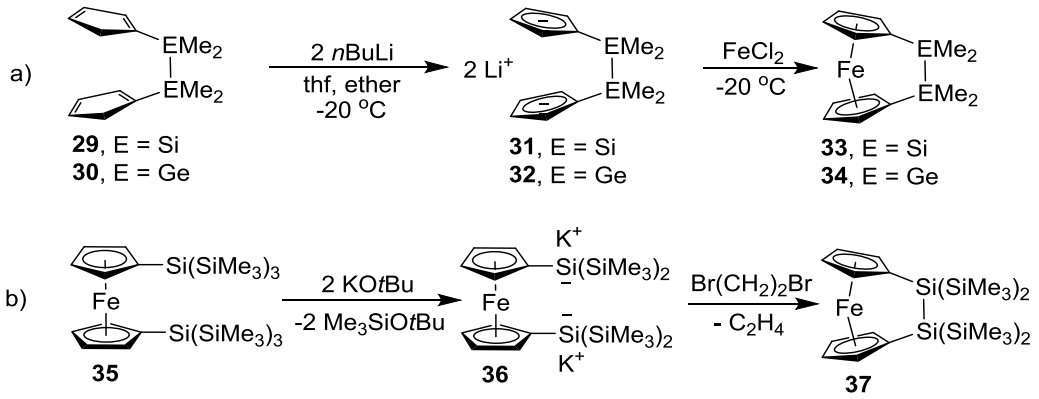

Probably due to the low intrinsic strain in the molecules, no attempt of ROP is reported on species **33** and **37**. However, further investigation revealed that the Si-Si bond in compound **33** can be activated by certain transition metal catalysts.[48] When compound **33** and certain alkynes were heated at 110 °C in the presence of catalytic amount of $Pd(PPh_3)_3$, the alkyne inserted between the two silicon centers and a class of [4]FCPs (**38** and **39**) resulted (Scheme 1.11).[48] Among the many examples reported in this publication, two selected [4]FCPs (**38** and **39**) are shown in Scheme 1.11. The X-ray crystallographic measurement on digerma[2]ferrocenophane **34** (Scheme 1.10) showed a tilt angle of 3.94°. Despite of a low intrinsic strain, this compound could be ring-open polymerized in the presence of transition metal catalysts to give metallopolymers.[49] Further detail of this reaction can be found in Section 1.4.

Scheme 1.11. Reactions of Disila[2]ferrocenophane 33

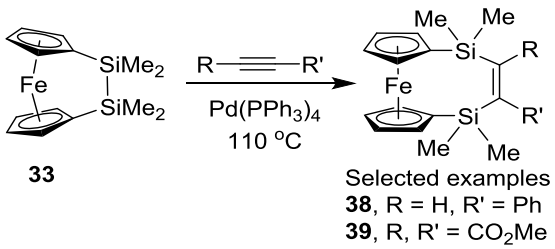

Wrackmeyer and co-workers reported the first distanna[2]ferrocenophane in 1996.[50] As illustrated in Scheme 1.12, when 1,1'-disubstituted ferrocene derivative **40** was treated with bis(trimethylsilyl)mercury, distanna[2]ferrocenophane **41** was obtained in a yield of 29%.[50] The X-ray crystallographic analysis revealed a tilt angle α of 0.7°.[50] Not surprisingly, no attempts of ROP have been reported for compound **41**. However, some reactivity of compound **41** was observed when it was reacted with the transition metal complexes. For example, upon reaction with $Pt(PPh_3)_2C_2H_4$, compound **41** gave the 1,3-distanna-2-platina[3]ferrocenophane **42**.[51] When species **42** was further reacted with alkynes, alkene moieties were introduced between two tin centers and [4]FCPs (**43** and **44**) resulted as final products.[51,52,53] Among the many examples reported in these publications, only the [4]FCPs **43** and **44** are shown in Scheme 1.12.[51,52,53]

Scheme 1.12. Synthesis and Reactions of Distanna[2]ferrocenophane (41)

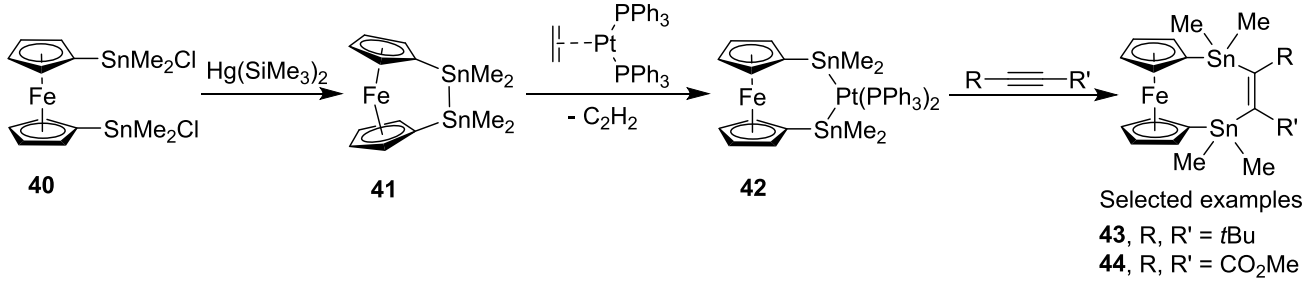

40 **41** **42**

1.2.1.4. Phosphorus-bridged [2]FCPs

The first phosphorus-bridged [2]FCP was synthesized and reported in 1984 by Allcock and co-workers.[54] As illustrated in Scheme 1.13, when 1,1'-dilithioferrocene (**19**) was reacted with 1.6 equivalents of hexachlorophosphazene, diphospha[2]ferrocenophane **45** was obtained in a yield of 1.3%.[54] The X-ray crystallographic evidence revealed that the two Cp rings in species **45** are tilted by approx 5°.[54] However, Mizuta and co-workers re-measured the published structure of compound **45** and reported the precise value of α angle as 7.7°.[55]

Scheme 1.13. Synthesis of the First Diphospha[2]ferrocenophane

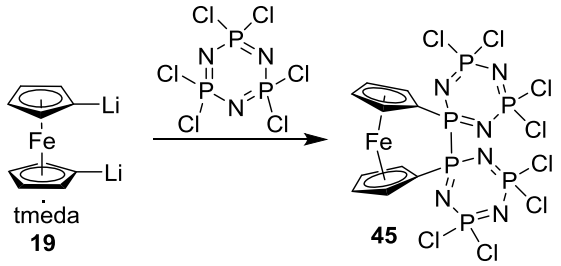

Almost 25 years after the first report, Pietschnig and co-workers synthesized the second diphospha[2]ferrocenophane using a water-induced P-P bond formation reaction.[56] As illustrated in Scheme 1.14, when bis(diphosphene) **46** was reacted with wet ether, an addition of H_2O occurred and a stable tetraphosphane oxide **47** was obtained in a yield of 95%.[56] The X-ray crystallographic measurement on compound **47** showed a tilt angle α of 11.5° which is 3.8° larger than that of the previously characterized diphospha[2]ferrocenophane **45**.[56]

Scheme 1.14. Synthesis of Diphospha[2]ferrocenophane (47) by Water-induced P-P Bond Formation

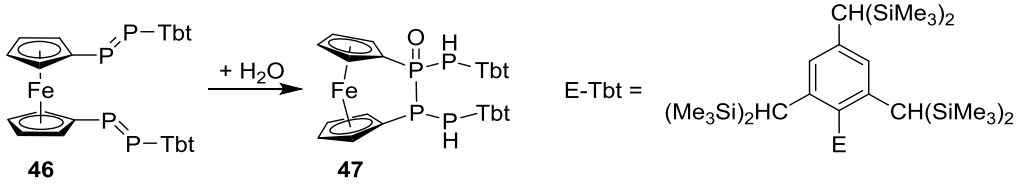

The most recent development in this field was reported in 2012 by Mizuta and co-workers.[55] As illustrated in Scheme 1.15, the aminophosphine **48** was first reacted with an ethereal solution of HCl to give the chlorophosphine **49**. Reductive coupling with magnesium afforded diphospha[2]ferrocenophane **50** in a yield of 63%.[55] Among the three [2]FCPs reported by the authors, one selected example has been depicted in Scheme 1.15.[55] The crystallographic measurement of compound **50** showed a tilt angle of 13.6°.[55]

Scheme 1.15. Synthesis of Diphospha[2]ferrocenophane (50) via Ring-closure Reaction

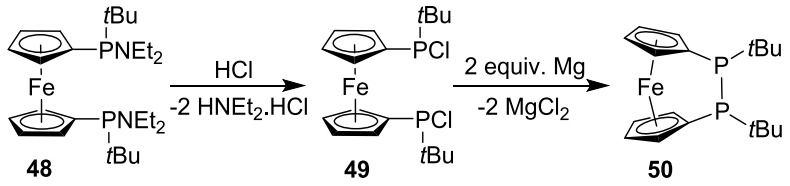

Probably due to having insufficient strain, diphospha[2]ferrocenophanes are not suitable candidates for ROPs. To the best of my knowledge, no attempt to polymerize these compounds has been reported in the literature.

1.2.2. Symmetrically Bridged [2]Ruthenocenophanes and [2]Osmocenophanes

Although plenty of examples have been reported for symmetrically bridged [2]FCPs, fewer examples are known for similar species with ruthenium and osmium. As the ruthenium and osmium have the higher covalent radii than iron, incorporation of ruthenium and osmium produces more tilted structures than their ferrocene-containing analogs [covalent radii:[57] Fe, 1.32(3) Å; Ru, 1.46(7) Å; Os, 1.44(4) Å].[10]

The first examples of carbon- and silicon-bridged [2]ruthenocenophanes ([2]RCPs) were reported by Manners and co-workers in 1994.[58,59] As illustrated in Scheme 1.16, when the dianionic linker **51** and **52** reacted with stoichiometric amounts of *cis*-$RuCl_2(DMSO)_4$, dicarba- and disila[2]ruthenocenophane (**53** and **54**) were obtained in yields of 42% and 50%, respectively.[58,59] X-ray crystallography revealed that, in comparison to dicarba- and disila[2]ferrocenophanes, the ruthenocene analogs show higher tilt angles and, therefore, higher intrinsic strain in the molecules [α angles for [2]RCPs: 29.6(5)° (**53**)[58], 7.8(5)° (**54**)[59]; α angles for [2]FCPs with the following bridging moieties in parentheses: 4.19(2)° (Si_2Me_4)[46], 21.6(5)° (C_2H_2)[10]]. As a result, the dicarba[2]ruthenocenophane **53** could be ring-open polymerized under

thermal conditions (see Section 1.4).[58] Unlike dicarba[2]ferrocenophanes, dimerization via the Ru-Ru bond formation was observed for dicarba[2]ruthenocenophane **53**, which was evidenced by X-ray crystallography.[60,61]

Scheme 1.16. Syntheses of Dicarba- and Disila[2]ruthenocenophanes (53 and 54)

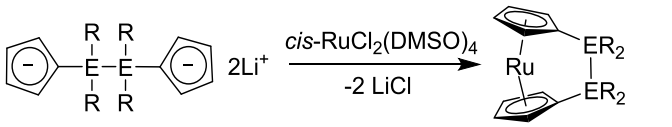

51, E = C, R = H
52, E = Si, R = Me

53, E = C, R = H
54, E = Si, R = Me

The silicon- and tin-bridged [2]osmocenophanes ([2]OCPs) were synthesized and reported by the Braunschweig's group in 2013.[62] As illustrated in Scheme 1.17, when the pmdeta-stabilized 1,1'-dilithiosmocene **55** was reacted with disilyl and distannyl chlorides, disila- and distanna[2]osmocenophanes (**56** and **57**) resulted in yields of 35% and 23%, respectively.[62] X-ray crystallography revealed that the tilt angles α of compounds **56** and **57** are significantly higher than those of ferrocenophane analogs. The α angles of silicon- and tin-bridged [2]FCPs and [2]OCPs is presented in the following: 4.3° [**33**, (Si_2Me_4)-bridged [2]FCP][46], 0.7° [**40**, (Sn_2Me_4)-bridged [2]FCP][50], 7.1° (**56**)[62], 3.58° (**57**)[62]. To the best of my knowledge, no attempts of ROP have been reported for [2]OCPs.

Scheme 1.17. Syntheses of Disila- and Distanna[2]osmocenophanes (56 and 57)

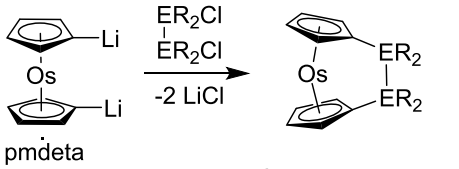

55

56, E = Si, R = Me
57, E = Sn, R = *t*Bu

1.2.3. Unsymmetrically Bridged [2]FCPs

Although, there are five major types of examples known for symmetrically bridged [2]FCPs, their unsymmetrically bridged analogs are comparatively rare. The first compound of this type, reported by Sutherland and co-workers in 1969, was equipped with nitrogen and sulfur in the bridging positions.[63] As illustrated in Scheme 1.18, when ferrocenylsulphonyl azide **58** was photolyzed at λ = 350 nm separately in cyclohexane and cyclohexene, the azathia[2]ferrocenophane **59** was produced in yields of 13% and 43%, respectively.[63] Compound **59** was further methylated using Me_2SO_4 to give a *N*-methyl derivative **60** in a yield of 73%.[63] The crystal structure of compound **59** showed a tilt angle of 23°.[64] However, no polymerization attempt on these [2]FCPs has been reported in the literature. Compounds **59** and **60** were used to report a comparison of their Mössbauer spectra with those of other known strained ferrocenophanes.[64]

Scheme 1.18. Syntheses of Azathia[2]ferrocenophanes (59 and 60)

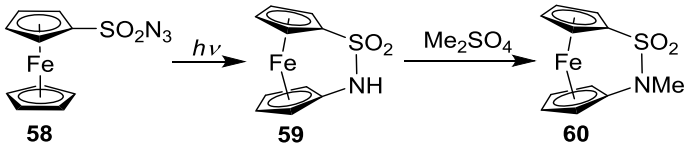

58 **59** **60**

In 1983, Wrighton and co-workers synthesized the first unsymmetrically bridged carba[2]ferrocenophane.[65] As illustrated in Scheme 1.19, a methyl substituted ferrocene derivative **61** was first dilithiated in presence of pmdeta and the dilithiated species **62** was reacted with stoichiometric amount of $SiCl_4$.[65] The resulting carbasila[2]ferrocenophane **63** was isolated in an approximate yield of 60% by vacuum sublimation of the crude reaction mixture at 125 °C.[65] When compound **63** was further reacted with excess of EtOH in hexanes, the diethoxy derivative **64** was formed, which was also purified by vacuum sublimation (Scheme 1.19).[65] Compound **63** was used as a surface derivatizing reagent (**65**, Scheme 1.19) to prepare reversible electrodes for horse heart

ferri-/ferrocytochrome *c*.[65] Neither crystal structures, nor ring-opening reactivity of compounds **63** and **64** have been reported.[65]

Scheme 1.19. Syntheses of Carbasila[2]ferrocenophane and its Reactions

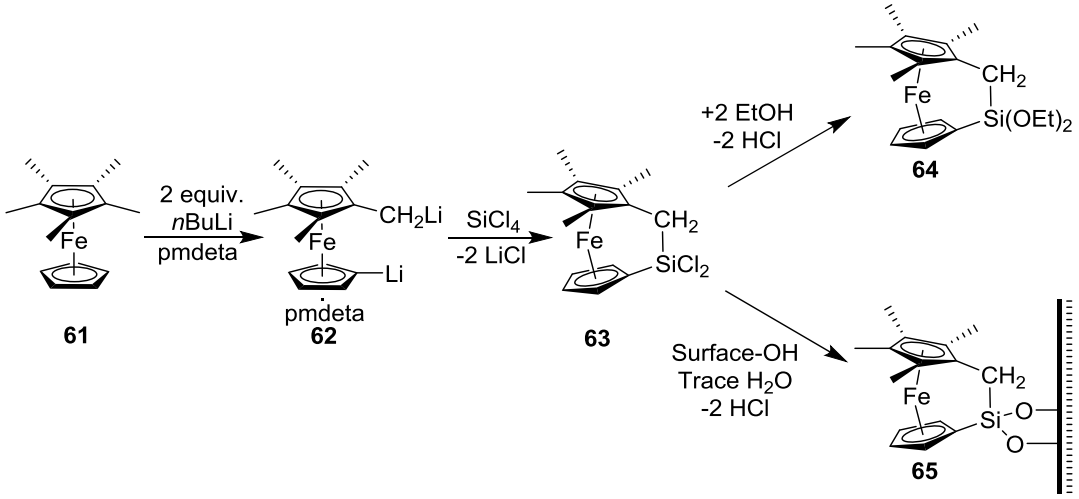

Almost two decades after this first report of unsymmetrically bridged carba[2]ferrocenophanes, Manners and co-workers reported on further examples of this kind.[66] As illustrated in Scheme 1.20, when the pmdeta-stabilized dilithio species **62** was separately reacted with the three elemental dihalides Me_2SiCl_2, $PhPCl_2$, and $MesPCl_2$, and with the sulfone derivative $S(SO_2Ph)_2$, respectively, a new family of carba[2]ferrocenophanes was formed.[66] Compounds **66-69** were isolated by recrystallization at -55 °C in yields of 26% to 56%.[66] The X-ray crystallographic evidence revealed α angles in a range of 11.8(1) to 18.51(14)°.[66] To put these values into context they can be compared to those of known [2]FCPs (bridging moieties are given in parentheses): 23.2° (C_2Me_4),[30] 21.6(5)° (C_2H_2)[10], 4.19(2)° (Si_2Me_4)[46], 3.9° (Ge_2Me_4)[49], 0.7° (Sn_2Me_4)[50], 12.82(16)° [$B_2(NMe_2)_2$],[13] 23° ($NHSO_2$)[64], 11.8(1)° (CH_2SiMe_2)[66], 15.0(4)° and 14.8(3)° (CH_2PPh)[66], 18.3(2)° (CH_2PMes)[66], 18.51(14)° (CH_2S)[66]. Due to the low intrinsic strain compound **66** did not show polymerization in any ROP conditions.[66] In contrast, carbaphospha-

and carbathia[2]ferrocenophanes **67** and **69**, respectively, ring-opened under certain conditions and afforded metallopolymers.[66] Details of ROPs of both compounds will be discussed in Section 1.4.

Scheme 1.20. Syntheses of Unsymmetrically Bridged Carba[2]ferrocenophanes (66-69)

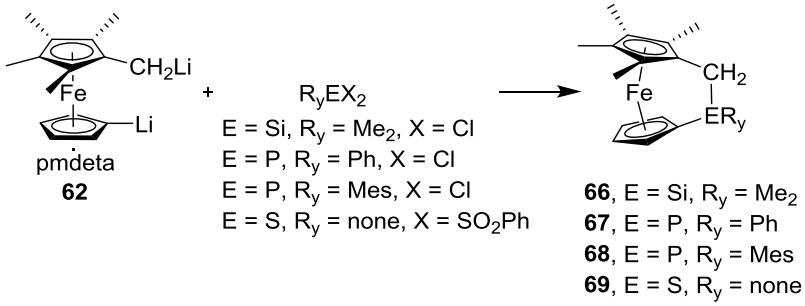

By following the similar procedure more unsymmetrically bridged carba[2]ferrocenophanes were synthesized by Manners' group.[67,68] As illustrated in Scheme 1.21, when the modified dilithoferrocene **62** was reacted with dichloro derivatives of germanium, tin, and zirconium, carbametalla[2]ferrocenophanes (**70**-**75**) were obtained in yields ranging between 19% to 49%.[67,68]

Scheme 1.21. Syntheses of Carbametalla[2]ferrocenophanes (70-75)

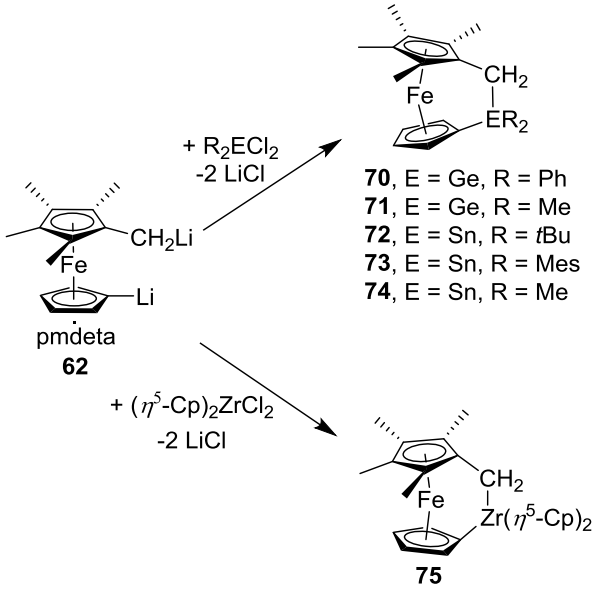

Low intrinsic strain was indicated by measured tilt angles α of germanium- and tin-bridged carba[2]ferrocenophanes [11.81(5)° (**70**), 10.99(2)° (**71**), 6.64(2)° (**72**), 7.1(1)° (**73**), and 7.5(1)° (**74**)].[67,68] As the two Cp rings were tilted in the opposite direction than usual, a negative tilt angle α = -5.5(2)° was observed for the zirconium-bridged species **75**.[68] Due to a lack of sufficient strain, none of these compounds could ring-open polymerized into metallopolymers.[67,68]

Although a few examples have been reported for unsymmetrically bridged [2]ferrocenophanes, similar species with ruthenocene and osmocene are yet to be explored.[10,11]

1.3. Polymers with Ferrocene

Natural polymers such as amber, natural rubber, and cellulose have been used by human civilization for many years. In the last century, a wide variety of synthetic organic polymers such as poly(ethylene), poly(propylene), nylon, neoprene, polyvinyl chloride, and polyvinyl butyral have been developed in chemical laboratories and manufactured on a gigantic scale by industries. Contrary to those organic polymers, metallopolymers are less developed. There two classes of metallopolymers: a polymer containing metals as the part of the backbone (main-chain metallopolymer) and a polymer containing metals in the repeating unit as pendent (side-chain metallopolymer).[69] DuPont started to explore the area of the side-chain metallopolymers by synthesizing poly(vinylferrocene) (**77**) via radical polymerization of vinyl-substituted ferrocene (**76**) in the middle of the last century (Scheme 1.22).[70] Two other ferrocene-containing side-chain metallopolymers were also synthesized by copolymerization of **76** with different monomers such as methacrylate and styrene.[70] As the side-chain metallopolymers are plenty in number and beyond the scope of this thesis, the readers are referred to recent reviews dealing with developments in this field.[69,71,72]

Scheme 1.22. Synthesis of Poly(vinylferrocene) (77)

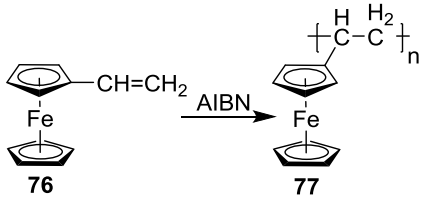

Compared to polymers containing ferrocene units as pendants which have been reported in 1955, metallopolymers with ferrocene units in the polymer backbone is a much younger class of polymers.[28] In 1982, Seyferth and Garrou *et al*. synthesized the high-molecular-weight poly(ferrocenylphosphine) **78$_n$** (M_w = 8.9-161 kDa, n = 30-550) by reacting $PhPCl_2$ with dilithioferrocene (Scheme 1.23a).[73] Rehahn and co-worker assumed that upon reaction with $PhPCl_2$, the dilithoferrocene can give phospha[1]ferrocenophane **78** which ring-open polymerized to afford **78$_n$**.[28] However, no insight about the probable *in situ* formation of species **78** was suggested by the authors in that publication.[28,73] Surprisingly, only oligomers **78$_x$** (x = 1-5) were isolated when phospha[1]ferrocenophane **78** was reacted with PhLi as an anionic initiator (Scheme 1.23b).[73]

Scheme 1.23. Synthesis of Poly(ferrocenylphenylphosphine)s 78$_n$ and 78$_x$

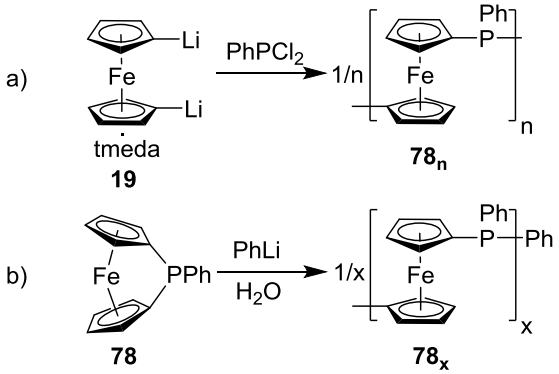

The anionic ROP of compound **78** apparently failed to give high-molecular-weight metallopolymers.[73] Probably due to this unsuccessful ROP, the investigation in this field was paused for almost a decade.[28] In 1992 Rauchfuss and Brandt *et al*. synthesized the poly(ferrocenylpersulfide) **80$_n$** (M_w = 40 kDa, n = 28-600) from trithia[3]ferrocenophane **79** by atom-abstraction ROP (Scheme 1.24).[74] A copolymer of molecular weight 25 kDa (M_w) was also synthesized by a similar ROP technique performed on a mixture of **79** and a butylated version of **79**.[74] The authors stated that the factors influencing the molecular weights of the polymers were not well understood.[74]

Scheme 1.24. Synthesis of Poly(ferrocenylpersulfide) (80$_n$)

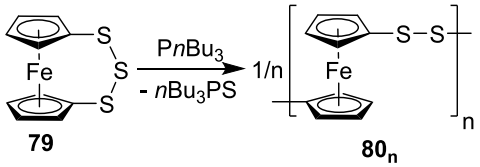

A few months later, this field got momentum when Manners and co-workers reported the first high-molecular-weight poly(ferrocenylsilane)s **1$_n$** and **81$_n$**, which were synthesized via ROP of strained [1]FCPs **1** and **81**, respectively (Scheme 1.25).[5] The molecular weight of polymer **1$_n$** was 520 kDa (M_w), however, that of **81$_n$** could not be determined due to its insolubility in organic solvents.[5] There is no doubt that this discovery started a new era of organometallic polymers.[28]

Scheme 1.25. Syntheses of Poly(ferrocenylsilane)s (1$_n$ and 81$_n$)

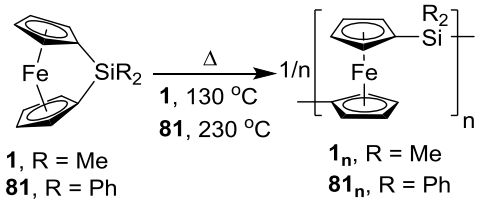

In the 1960s, mainly polycondensation routes were used to synthesize poly(metallocene)s with different bridging elements.[75,76] In 1962, poly(ferrocenylsilane) **83$_n$** was prepared by a polycondensation reaction of $FeCl_2$ and the anionic linker **82** (Scheme 1.26).[75] In 1969, compound **83$_n$** was prepared by a slightly different polycondensation method, which involved a salt-metathesis reaction between dilithioferrocene (**19**) and dimethyl silicon dichloride (Scheme 1.26).[76] However, in both the cases, only low molecular weight poly(ferrocenylsilane)s were formed.[75,76]

Scheme 1.26. Synthesis of Oligo(ferrocenylsilane) (83$_n$) via Polycondensation

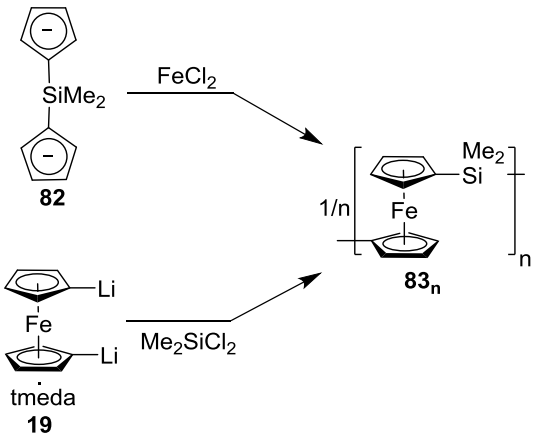

For polycondensations many species with different chain lengths are present in the reaction mixture at the same time and those species can react randomly among themselves. Therefore, a wide molecular weight distribution often results in this step-growth process. The high-molecular weight polymers can be obtained by this procedure only if two requirements are satisfied: 1) the starting materials must be highly pure; 2) the stoichiometry of the starting monomers must be precise.[28] High-molecular-weight metallopolymers were not obtained via polycondensation route, because the required high purity of starting materials are difficult to obtain and precise stoichiometry is hard to maintain. For example, dilithioferrocene·tmeda adduct always contains

tmeda varying from 2/3 to 2 per one molecule of dilithioferrocene.[77,78] Therefore, when dilithioferrocene·tmeda was used as a reagent to synthesize polymer **83$_n$** (Scheme 1.26), it is not surprising that a low-molecular-weight poly(ferrocenylsilane) was obtained.[28] In comparison to the polycondensation route, the ROP of strained [*n*]MCPs produces metallopolymers with higher molecular weight and narrower molecular-weight distribution.[28] Different methodologies, such as thermal-, anionic-, photocontrolled-, and transition-metal-catalyzed ROP have been reported in literature.[28] These methods will be discussed and each illustrated with some examples.

Thermal ROP. Manners and co-workers introduced the thermal ROP in metallocenophane chemistry for the first time in 1992, when dimethyl- and diphenylsila[1]ferrocenophanes were ring-open polymerized (Scheme 1.25).[5] The thermal ROP of strained metallocenophanes are generally performed at higher temperature in solution or in bulk. The most commonly adapted technique is heating of the strained compound in a sealed Pyrex glass tube above its melting point. As the polymers are viscous material, a change in viscosity is observed during thermal polymerization. Although this procedure affords high-molecular-weight polymers, a broad molecular weight distribution is observed for the resulting polymers. Moreover, due to the high temperature, in many cases the monomers decompose during the reaction.[28]

Very little is known about the mechanism of the thermal ROP. Even the nature of the propagating species is unknown. It is believed that the reaction mechanism involves a radical pathway.[28] To gain insight into the mechanism of thermal ROP of silicon-bridged [1]FCPs, Manners and co-workers polymerized the unsymmetrically methylated compound **84** (Scheme 1.27). The ^{1}H NMR microstructure analysis revealed that the polymerization proceeded through a non-selective cleavage of Si-Cp^H and Si-Cp^{Me} bonds.[79] More studies are needed to completely understand the mechanism of thermal ROPs.[28]

Scheme 1.27. Thermal ROP of Sila[1]ferrocenophane (84) with Unsymmetrically Substituted Cp Rings

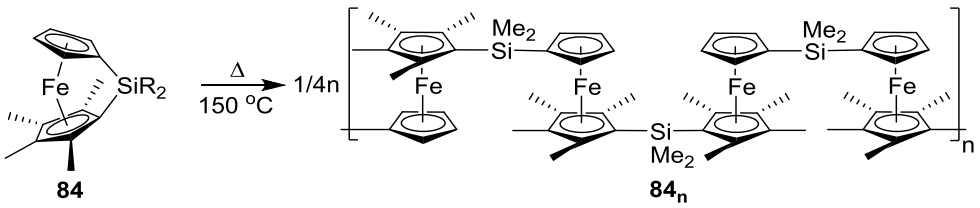

Anionic ROP. As mentioned earlier, Seyferth, Garrou, and co-workers reported the first example of an anionic ROP of the phosphorus-bridged [1]FCP, which resulted only in oligomers (Scheme 1.23b).[73] However, the first example of a successful living anionic ROP was reported by Manners *et al*. in 1994.[80] As illustrated in Scheme 1.28, when sila[1]ferrocenophane **1** was reacted with 0.1 equivalent of an anionic initiator such as ferrocenyl lithium, poly(ferrocenylsilane)s (**1$_n$**) with molecular weight of 9.5 kDa (M_w, $n \sim 29$), narrow molecular-weight distribution (PDI = 1.19), and controlled end-group structures were obtained.[80] The molecular weights of the metallopolymers were fine-tuned by varying the ratio of monomer **1** and ferrocenyl lithium.[80] Further investigation by the Manners' group revealed that the mechanism of anionic ROP involves the breakage of Cp-Si bond.[81]

Scheme 1.28. Anionic ROP of Sila[1]ferrocenophane (1)

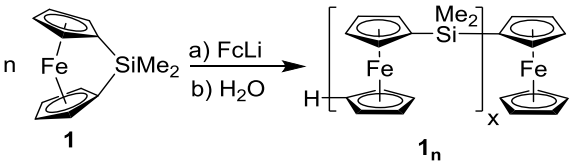

Many other anionic initiators like MeLi, *n*BuLi, *s*BuLi, and *t*BuLi have been successfully used for anionic ROPs.[81] The living anionic ROP of sila[1]ferrocenophane **1** has been used to synthesize a group of novel well-defined multiblock co-polymers constructed from poly(ferrocenylsilane), poly(styrene), and poly(dimethylsiloxane) (Scheme 1.29).[81]

Scheme 1.29. Syntheses of Block Copolymers 86_n and 87_n through the Living Polymerization

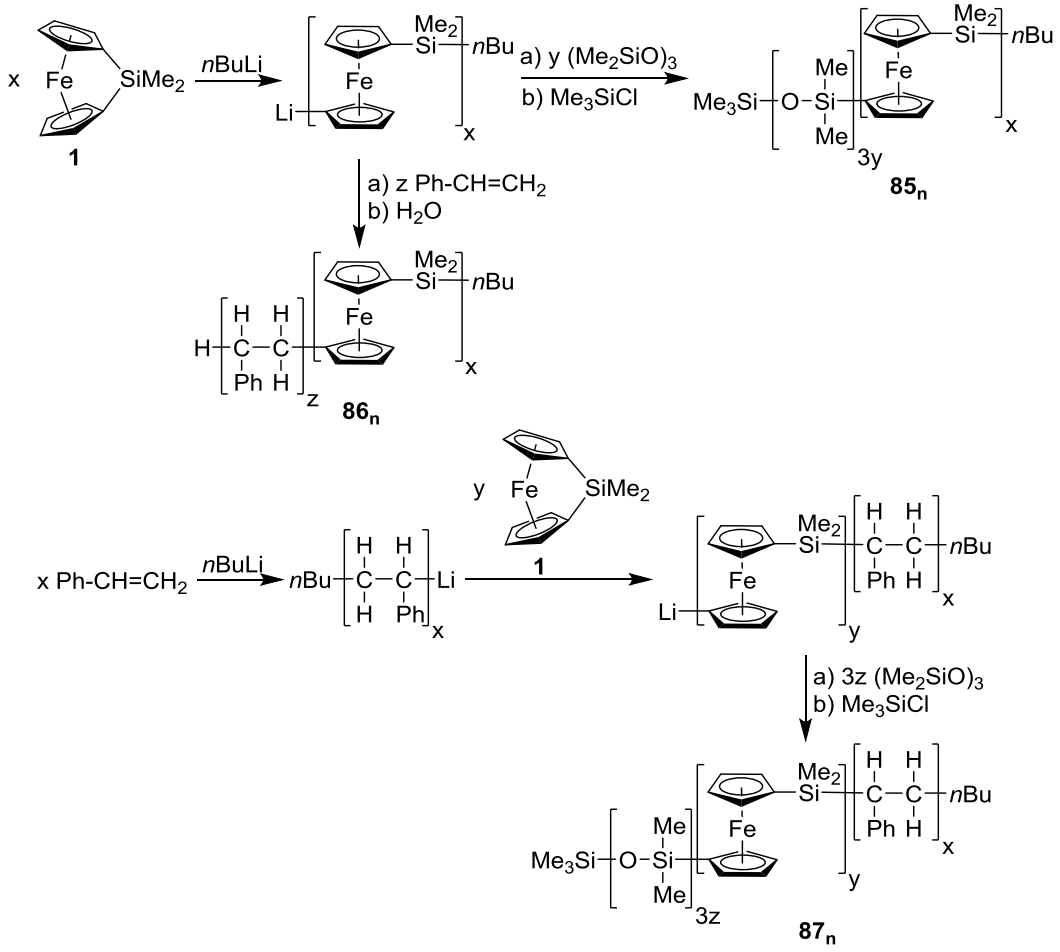

Since the thermal ROP cannot afford metallopolymers with narrow range of molecular weight distribution, anionic ROP has a high value in this field.[28] Moreover, as the anionic ROP occurs under comparatively milder condition, monomer decomposition is not an issue.[28] However, the anionic ROP is restricted to monomers having functional groups which can withstand extreme anionic condition.[28] The vital drawback of anionic ROP is that it demands a high purity level of monomers to avoid undesired chain termination.[28] Often, the latter requirement could not be achieved for many monomers.[28]

Photocontrolled ROP. In 2000, Miyoshi and co-worker described the synthesis of metallopolymers (M_w = 2.2 to 3.7 kDa, PDI = 1.71 to 1.96) of the phosphorus-bridged monomer complexes **88** via irradiation with UV light in donor solvents like thf or Me_3CN.[82] So far, these are the only examples of photocontrolled ROP of metallized phospha[1]ferrocenophanes (Scheme 1.30).[28]

Scheme 1.30. Syntheses of Metallized Poly(ferrocenylphosphine)s (88_n)

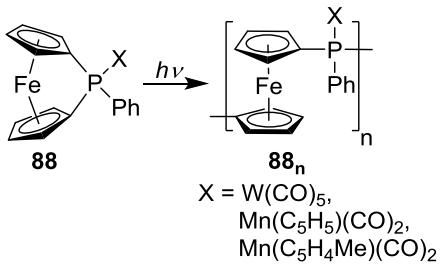

The same research group studied the mechanism of photocontrolled ROP of phosphorus-bridged [1]FCPs for the first time.[83] As illustrated in Scheme 1.31, when sulfurated phospha[1]ferrocenophane **89** was treated with an excess amount of $P(OMe)_3$ under UV-radiation, a ring slippage reaction from η^5 to η^1 occurred and intermediate **90** was formed.[83] When the similar reaction was performed with the stronger donor PMe_3, one Cp moiety completely dissociated from the iron center and species **91** was obtained (Scheme 1.31).[83] Based on this reaction, Miyoshi and co-workers proposed the mechanism of photocontrolled ROP of phospha[1]ferrocenophane, which involves the formation of active species by selective breaking of Fe-Cp bond (**91**, Scheme 1.31).[83]

Scheme 1.31. Reactivity of Sulfurated Phospha[1]ferrocenophane (89)

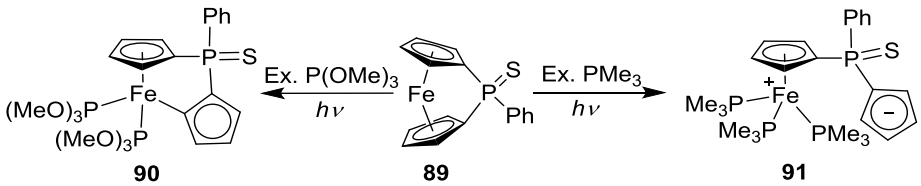

Manners *et al*. reported the first living anion-initiated photocontrolled ROP which was performed with a sila[1]ferrocenophane in 2004.[84] When compound **1** was treated with catalytic amounts of NaCp, it ring opened to form the active species **92** (Scheme 1.32).[84] In presence of UV-radiation species **92**, upon reacting with various amounts of other monomers, resulted in poly(ferrocenylsilane) $\mathbf{94_n}$, which showed molecular weight in a range of 9.7 to 78.4 kDa and a narrow molecular weight distribution (PDI = 1.04 - 1.21). [84] It was proposed that the UV-radiation weakens the Fe-Cp bond and, therefore, facilitates the attack of anionic species **92** at the iron center (Scheme 1.32).[84]

Scheme 1.32. Mechanism of Photocontrolled ROP of Sila[1]ferrocenophane

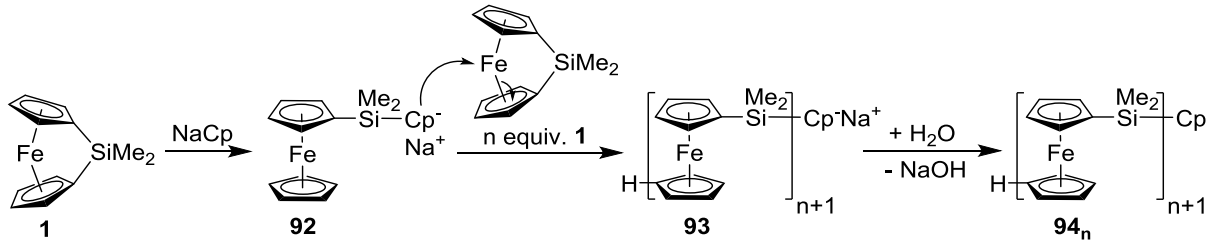

Transition-metal-catalyzed ROP. Tanaka and co-workers were the first to describe transition-metal-catalyzed ROP of [1]FCPs.[85] As described in Scheme 1.33, the treatment of sila- and germa[1]ferrocenophane, **1** and **95**, respectively, with $Pt(cod)_2$ (cod = 1,5-cyclooctadiene) resulted in high-molecular-weight metallopolymers with broad molecular weight distribution ($\mathbf{1_n}$, $M_w = 17 \times 10^2$ kDa, PDI = 2.8; $\mathbf{95_n}$, $M_w = 11 \times 10^2$ kDa, PDI = 5.2).[85] More soluble catalysts such as $Pt_2(dba)_3$ and $Pd(dba)_2$ (dba = dibenzyledeneacetone) resulted in faster polymerizations of **1**, but a lower molecular weight polymers (M_w = 300 and 150 kDa) were obtained.[85] Extremely fast polymerization (within seconds) with a bimodal molecular weight distribution (M_w = 1100 and 70 kDa) was observed when compound **1** was polymerized using $Pt(COD)_2Cl_2$ as a catalyst.[85]

Polymerization of compound **95** with $Pt_2(dba)_3$ resulted in a polymer with a molecular weight of 230 kDa (M_w) with a very broad molecular weight distribution (PDI = 9.7).[85]

Scheme 1.33. Syntheses of Poly(ferrocenylsilane) $\mathbf{1_n}$ and Poly(ferrocenylgermane) $\mathbf{95_n}$ by Transition-metal-catalyzed ROP

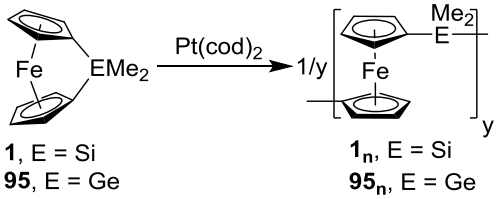

In 1995, Manners *et al*. also reported the transition-metal-catalyzed ROP of sila[1]ferrocenophane **1**, however, different metal catalysts such as $PtCl_2$, $PdCl_2$, $Pd(cod)Cl_2$ and $[Rh(cyclooctene)(\mu\text{-}Cl)]_2$ were employed.[86] Transition-metal-catalyzed ROP was initially believed to proceed through homogenous reactions.[87,28] However, subsequent studies showed that this polymerization occured heterogeneous, where colloidal metal is the main active catalyst (Scheme 1.34).[88, 28] As illustrated in Scheme 1.34, the catalyst $Pt(cod)_2$ reacts with compound **1** to give the platinasila[2]ferrocenophane **96**, which was believed to be the active catalyst until 2001. However, an intensive study suggested that the species **96** did not incorporate into the growing chain. It was proposed that the reductive elimination of the transition metal from **96**, followed by elimination of cod resulted in platinum colloids, which acted as the active species.[88] This proposal was further supported by using mercury, which acted as an inhibitor for heterogeneous reactions. [88] As no inhibitors for homogenous reactions were checked to find out if a retardation occurs, the coexistence of homogenous catalytic reaction could not be ruled out.[28]

Scheme 1.34. Proposed Mechanism of Transition-metal-catalyzed ROP

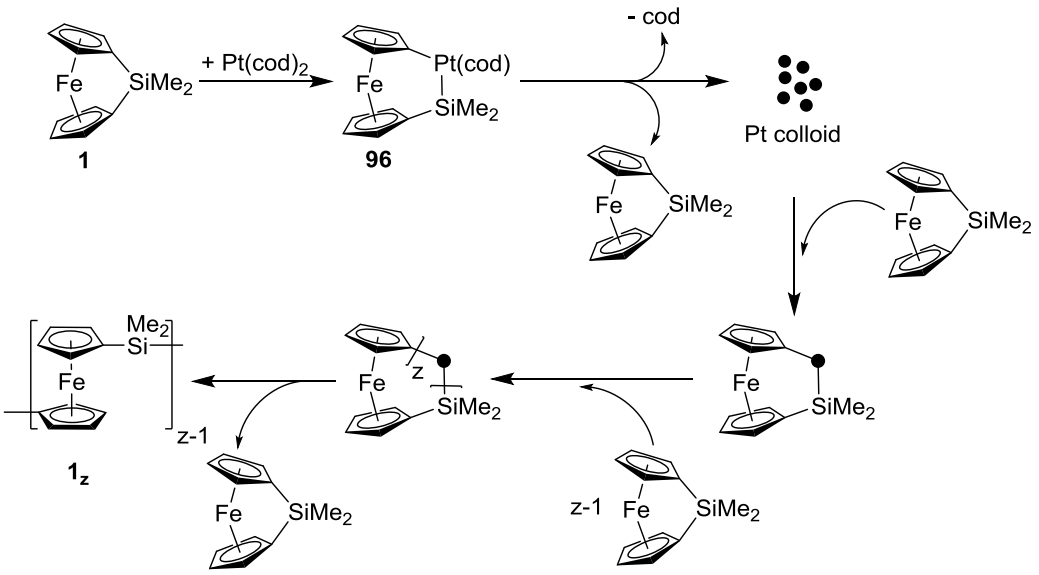

Contrary to the thermal- and anionic ROP, transition-metal-catalyzed ROP operates under milder reaction conditions and is tolerant to various functionalities of monomers.[28] Moreover, unlike anionic ROP, this method does not require high purity levels of monomers.[28]

As a large quantity of ferrocene-containing monomers and polymers could not be discussed in this thesis, an interested reader is referred to recent review articles.[10,11,20,27,28,39,40,69,71,72,89,90]

1.4. Polymers from [2]MCPs

Although there are plenty of examples known for metallopolymers derived from [1]FCPs, similar species resulting from [2]FCPs are rare. Thermal ROP of dicarba[2]ferrocenophanes were first reported by Manners and co-workers in 1993.[91] As illustrated in Scheme 1.35, when carbon-bridged [2]MCPs **53** and **97** and their di-methylated versions **98** and **99** were heated at 300 °C, metallopolymers $\mathbf{53_n}$ and $\mathbf{97_n}$-$\mathbf{99_n}$, respectively, were formed.[58,91,92] It should be noted that monomers **98** and **99** were a complex mixture of different isomers and used as such for thermal ROP.[58,91] As polymers $\mathbf{53_n}$ and $\mathbf{97_n}$ could not be dissolved in any organic solvent, they could not

be characterized by gel permeation chromatography (GPC) measurement.[58,91] While polymer **98$_n$** showed a bimodal molecular weight distribution with M_w = 81 kDa (PDI = 1.23) and 4.8 kDa (PDI = 1.37), species **99$_n$** showed a molecular weight of 12.7 kDa (M_w) with a broader polydispersity (PDI = 2.89).[58,91,92] From these results it was concluded that introducing methyl groups on Cp is necessary to produce soluble polymeric materials.[11]

Scheme 1.35. Thermal ROPs of Dicarba[2]metallocenophanes (53, 97-99)

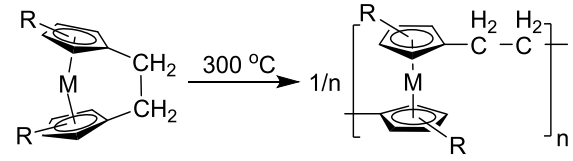

97, R = H, M = Fe
98, R = Me, M = Fe
53, R = H, M = Ru
99, R = Me, M = Ru

97$_n$, R = H, M = Fe
98$_n$, R = Me, M = Fe
53$_n$, R = H, M = Ru
99$_n$, R = Me, M = Ru

Recent studies of the thermal reactivity of dicarba[2]ferrocenophanes have been extended to species bearing non-hydrogen substituents in the bridge.[11] For example, dicarba[2]ferrocenophane **3** underwent homolytic cleavage of the C-C bridge at 240 °C, followed by a radical rearrangement to give the 1,1'-disubstituted ferrocene derivative **100** (Scheme 1.36a).[93] A different thermal behavior was observed for similar species with no or one non-hydrogen substituent in the bridge.[94] For example, upon heating of a racemic mixture of compound **101**, polymerization resulted in cyclic metallopolymers (**101$_n$**, Scheme 1.36b). Investigation into the mechanism of thermal ROP of compound **101**, involving trapping of ring-opened monomeric species, indicated that the ring-propagation proceeds via a heterolytic bond-cleavage of Fe-Cp bond.[94,11] A cartoon mechanism of thermal ROP of carbon-bridged [2]FCPs (**A**, Scheme 1.36c), postulated by Manners and co-workers,[94] is depicted in Scheme 1.36c.

Scheme 1.36. Thermal Reaction with two Different Dicarba[2]ferrocenophanes (3 and 101) and Mechanism of Thermal ROP of Dicarba[2]ferrocenophanes

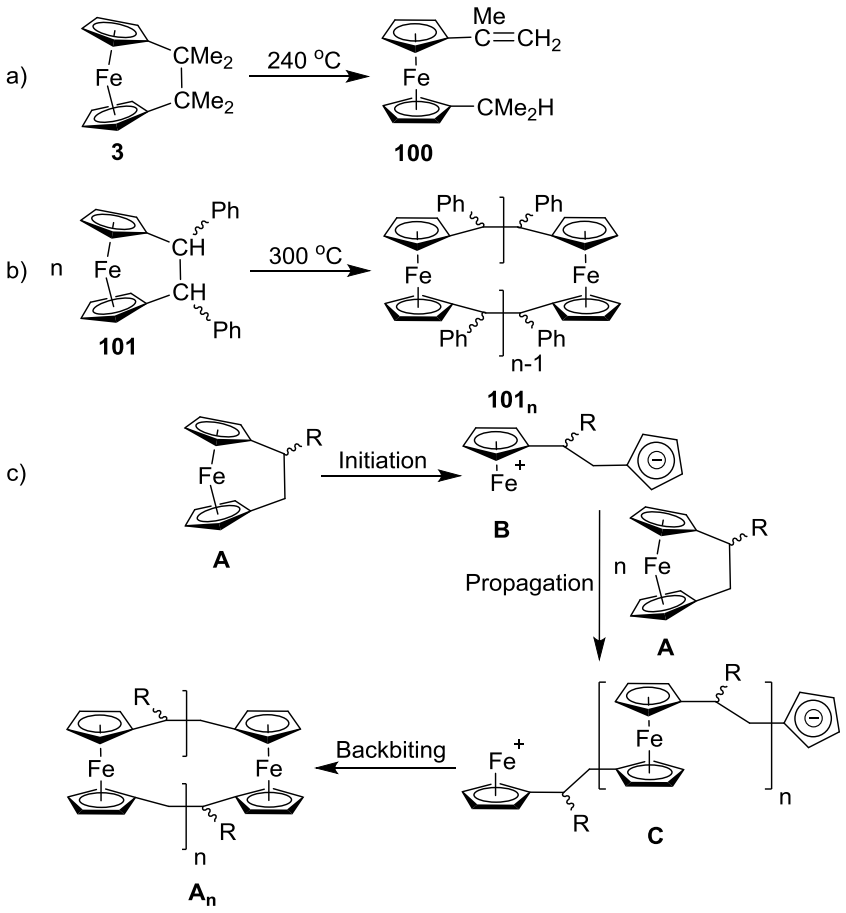

The unsaturated carbon-bridged [2]FCP **9** could be polymerized via a ring-opening-metathesis polymerization (ROMP) in presence of a molybdenum catalyst (Scheme 1.37).[31] As only insoluble materials were obtained in this reaction, characterization of polymer $\mathbf{9_n}$ could not be performed.[31] In order to synthesize a soluble polymer, compound **9** was co-polymerized with different proportions of norbornene (NBE).[31] For example, the co-polymeric material $\mathbf{102_n}$ was prepared by reacting **9** with NBE in a ratio of catalyst : **9** : NBE of 1 : 10 : 50 (Scheme 1.37).[31] Species $\mathbf{102_n}$ was partially soluble and showed a moderate molecular weight of M_w = 21 kDa and broad molecular weight distribution (PDI = 1.91).[31]

Scheme 1.37. ROMP of Dicarba[2]ferrocenophane (9) with Unsaturated Bridging Moiety

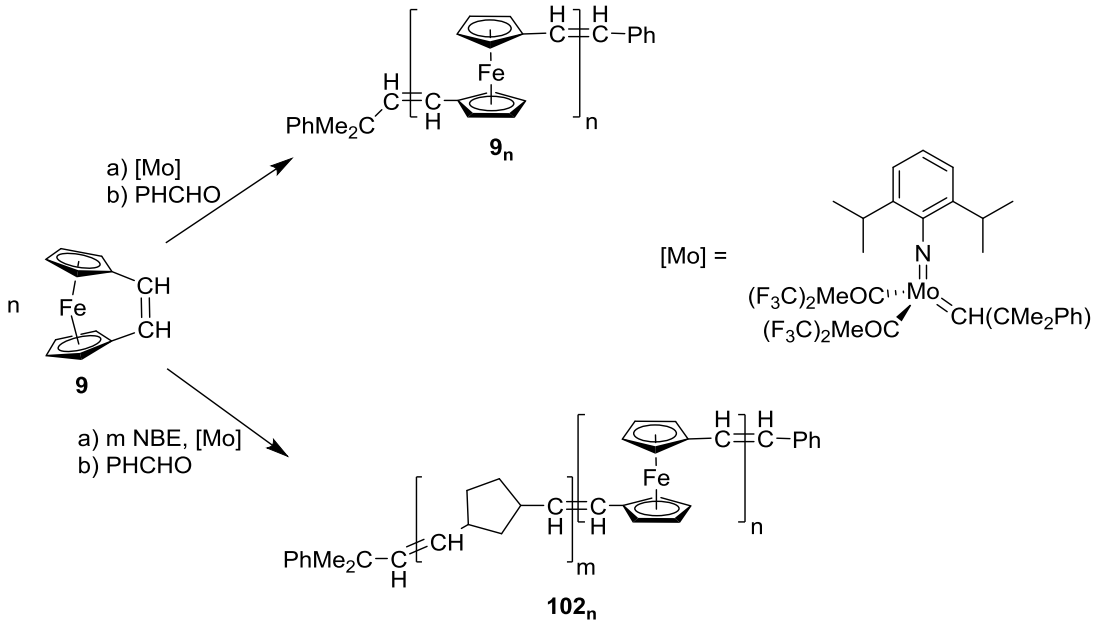

As a further development, Manners and co-workers introduced *tert*-butyl groups on Cp rings and synthesized a racemic mixture of vinyl-bridged [2]FCP (**103**, Scheme 1.38).[95] Among the racemates only one compound (**103**) has been shown in Scheme 1.38. When species **103** was polymerized in the presence of Grubbs- and Schrock-type catalysts, polymers $\mathbf{103_n}$ with a wide variety of molecular weight and polydispersity indices (M_w = 5.7 to 109 kDa, PDI = 1.30 to 2.43) were obtained (Scheme 1.38).[95] By changing the molar ratio of monomer to catalyst, the molecular weight and molecular weight distribution of polymer $\mathbf{103_n}$ could also be fine-tuned.[95]

Scheme 1.38. Syntheses of Soluble Polymers ($\mathbf{103_n}$) via ROMP

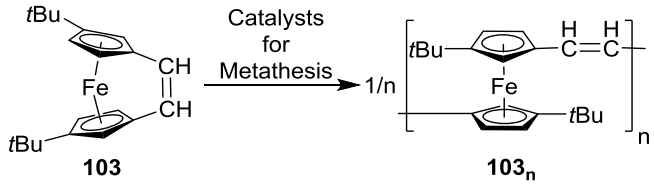

Anion-initiated photocontrolled ROP of a range of dicarba[2]ferrocenophanes has recently been reported by Manners and co-workers.[96] As shown in Scheme 1.39, compounds **104** and **105** underwent photocontrolled ROP to afford the soluble poly(ferrocenylethylene)s $\mathbf{104_n}$ and $\mathbf{105_n}$, respectively, with narrow molecular weight distribution ($\mathbf{104_n}$, PDI = 1.16 to 1.37; $\mathbf{105_n}$, PDI = 1.10 to 1.30).[96] Fine-tuning of the molecular weight of the polymers was done by varying the molar ratio of the monomer to the anionic initiator (NaCp).[96]

Scheme 1.39. Photocontrolled ROP of Dicarba[2]ferrocenophanes (104 and 105)

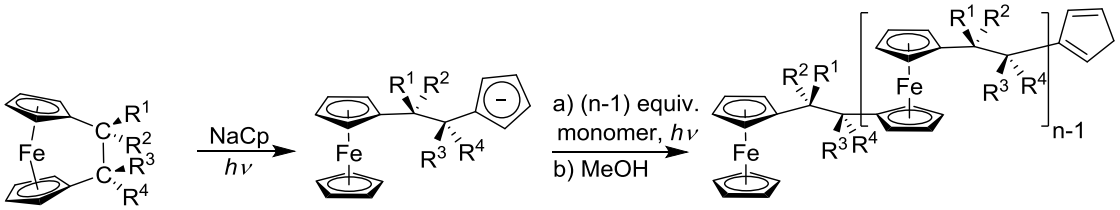

104, R^1 = Me; R^2, R^3, R^4 = H
105, R^1, R^4 = Ph; R^2, R^3 = H

106, R^1 = Me; R^2, R^3, R^4 = H
107, R^1, R^4 = Ph; R^2, R^3 = H

$\mathbf{104_n}$, R^1 = Me; R^2, R^3, R^4 = H
$\mathbf{105_n}$, R^1, R^4 = Ph; R^2, R^3 = H

Furthermore, the ability to synthesize block co-polymer $\mathbf{109_n}$ by this polymerization technique was also demonstrated through the addition of dimethylsila[1]ferrocenophane (**1**) into the "living" poly(ferrocenylethylene) macro initiator $\mathbf{108_n}$ (Scheme 1.40).[96] Two different co-polymers were synthesized by changing the ratio of **107** to **1** (**107** : **1** = 20 : 20, 7 : 7).[96] Predicted molecular weights and narrow range of molecular weight distributions were found for the block co-polymers $\mathbf{109_n}$ (M_n = 13.4 kDa, PDI = 1.18 for **107** : **1** = 20 : 20 and M_n = 7.7 kDa, PDI = 1.17 for **107** : **1** = 7 : 7).[96]

Scheme 1.40. Synthesis of Block Co-polymers (109_n) via Photocontrolled ROP of Dicarba[2]ferrocenophane (107)

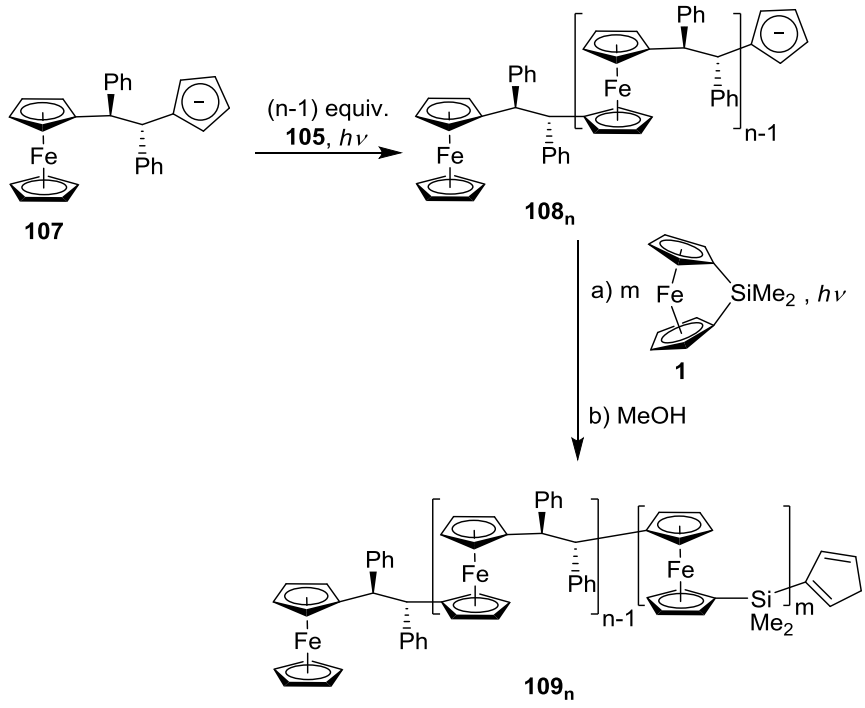

As discussed in Section 1.2.1, the heteroatom-bridged [2]FCPs have less intrinsic strain in comparison to dicarba[2]ferrocenophanes. Probably due to this reason, no successful ROP has been reported on this class of compounds, except digerma[2]ferrocenophane **34**. As illustrated in Scheme 1.41, when compound **34** was treated with catalytic amounts of transition metal catalysts [$Pd(acac)_2$, $Pd(dba)_2$, or $PtCl_2(cod)$], metallopolymers with a wide range of molecular weight and broad molecular-weight distribution were obtained [M_w = 400 kDa, PDI = 1.7 for reaction with $Pd(acac)_2$; M_w = 500 kDa, PDI 1.8 for reaction with $Pd(dba)_2$; and M_w = 20 kDa, PDI = 2.6 for reaction with $PtCl_2(cod)$].[49]

Scheme 1.41. Transition-metal-catalyzed ROP of Digerma[2]ferrocenophane (34)

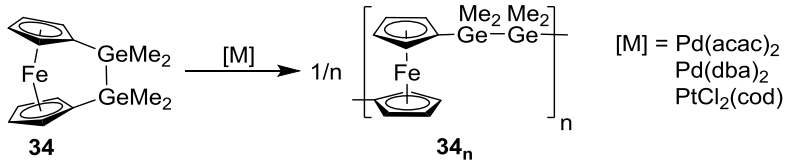

34 **34$_n$**

Although there are a handful of examples known for metallopolymers derived from symmetrically bridged [2]FCPs, related species from unsymmetrically bridged [2]FCPs are very rare. Probably due to the low intrinsic strain in [2]FCPs with CSi, CGe, CSn, and CZr atoms in bridging positions (**66**, **70**-**75**), these species could not be polymerized by any ROP method.[67,68] On the other hand, metallopolymers **67$_n$** and **69$_n$** resulted when carbaphospha- and carbathia[2]ferrocenophane **67** and **69**, respectively, were heated in evacuated Pyrex tubes (Scheme 1.42a).[66] Upon sulfurization, species **67$_n$** afforded **110$_n$** which showed a molecular weight of 120 kDa (M_w) and a broad molecular-weight distribution (PDI = 1.6; Scheme 1.42b).[66] The major part of species **69$_n$** was insoluble in common organic solvents. A small fraction of **69$_n$**, which was soluble in thf, revealed M_w of approx. 6 kDa with a PDI value of 1.1.[66]

Scheme 1.42. Thermal ROP of Carbaphospha- and Carbathia[2]ferrocenophane (67 and 69)

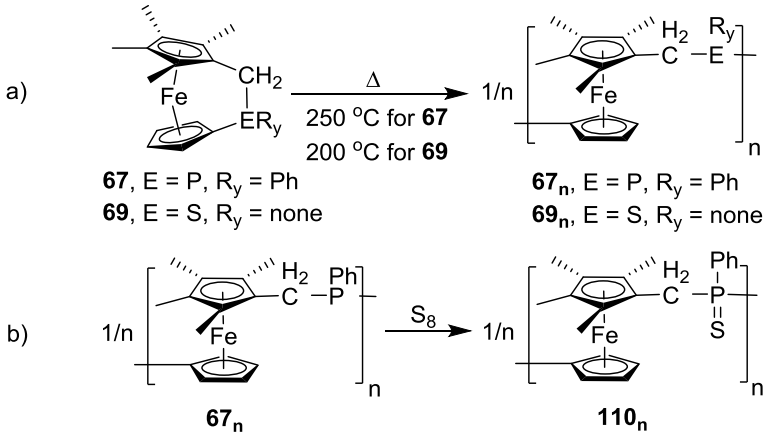

Treatment of carbathia[2]ferrocenophane **69** with cationic initiator CF_3SO_3Me and Lewis acidic initiator BF_3 (in Et_2O) resulted in an immediate color change from bright red to light orange, followed by the precipitation of polymeric materials which were mostly insoluble in common organic solvents (Scheme 1.43a).[66] The broad resonances in ^1H NMR spectrum of the soluble fraction of crude product indicated that the polymers were formed in the reaction mixture.[66] This was the first example of cationic ROP for a transition-metal-containing heterocycle.[28,66] Although no ring-opened intermediates could be detected or isolated for this reaction, a possible mechanism was proposed by Manners and co-workers (Scheme 1.43b).[66]

Scheme 1.43. Cationic ROP of Carbathia[2]ferrocenophane (69)

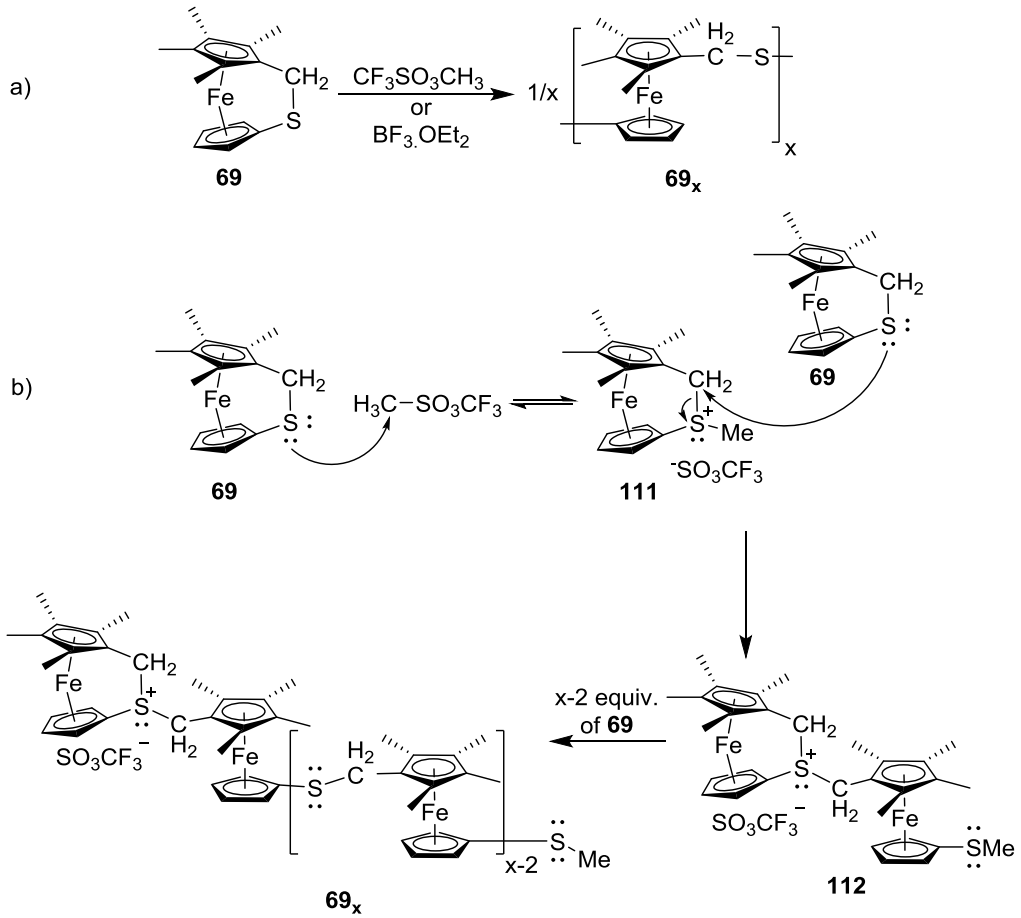

In order to generate soluble analogs for polymer $\mathbf{69_x}$, co-polymerizations with different sulfur-containing heterocycles were investigated. [66] As illustrated in Scheme 1.44, when compound **69** was heated with $(CH_2)_3S$ in a sealed Pyrex tube at 180 °C for 18 h, the random co-polymer $\mathbf{113_n}$ was formed. [66] Unlike $\mathbf{69_n}$, $\mathbf{113_n}$ was completely soluble in polar organic solvents (M_w = 300 kDa, PDI = 2.6).[66]

Scheme 1.44. Co-polymerization of Carbathia[2]ferrocenophane (69) with Trimethylene Sulfide

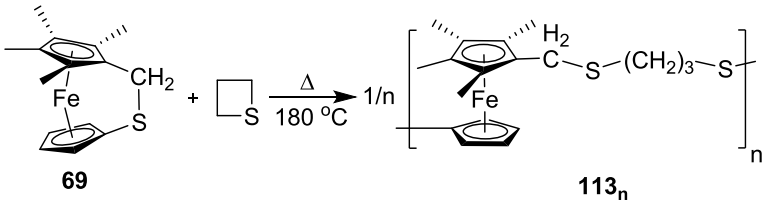

69 **113_n**

1.5. Objectives

As discussed in Section 1.2.2, the unsymmetrically bridged [2]FCPs form one of the least developed subclasses in ferrocenophane chemistry. Nearly all of the known species of this kind (**66**-**75**) have been obtained through one particular salt-metathesis reaction (Scheme 1.20 and 1.21) that results in carbon-bridged [2]FCPs.[66–68] Among these compounds, only carbaphospha[2]ferrocenophane **67** could be polymerized to give metallopolymer with a high molecular weight but broad molecular-weight distribution (Scheme 1.42).[66] When reacted in thermal and cationic conditions, carbathia[2]ferrocenophane **69** afforded insoluble polymers.

In order to expand the family of accessible monomers for ROPs, it was intended to prepare unsymmetrically bridged [2]FCPs. In order to introduce significant amounts of strain in the molecules, elements with small radii were needed in the bridge. Furthermore, we thought that a diatomic bridging moiety with a high polarity should increase the chance of ROP, initiated by polar reagents, such as *n*BuLi. Finally, due to the high abundance of natural as well as synthetic

polymers containing nitrogen in the backbone, we became interested to prepare [2]FCPs with nitrogen in bridging position (**B**, Scheme 1.45). From a retrosynthetic point of view it seems that *N*-substituted 1-amino-1'-bromoferrocenes of type **C** (Scheme 1.45) could be ideal precursors for the preparation of the targeted strained [2]FCPs of type B through the common salt-metathesis approach. The key compounds of type **C** should be accessible from 1-amino-1'-bromoferrocene (**114**, Scheme 1.45).

Scheme 1.45. Research Objective via Retro-synthesis

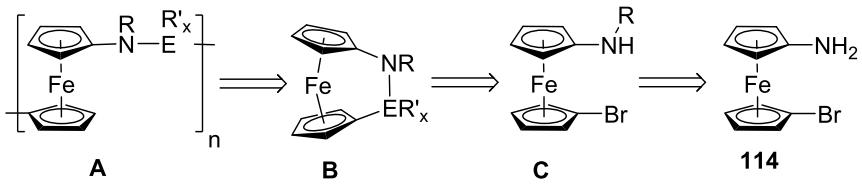

The main objective of my PhD work was to develop a family of aza[2]ferrocenophanes (**B**) with a wide variety of elements as the second different bridging atom. This approach should allow a variation of the amount of intrinsic strain in the targeted compounds. Once synthesized, the applicability of these new species as monomers for polymerizations will be explored (**B**, Scheme 1.45).

CHAPTER 2

RESULTS AND DISCUSSIONS

As outlined in Section 1.5, a salt-metathesis approach to the targeted aza[2]ferrocenophanes was proposed (Scheme 1.45). This approach required the preparation of the known compound 1-amino-1'-bromoferrocene (**114**). Consequently, explorations toward aza[2]ferrocenophanes started with the synthesis of the known species **114**.

2.1. Synthesis of 1-Amino-1'-bromoferrocene (114)

1-Amino-1'-bromoferrocene (**114**) was previously synthesized using *O*-benzylhydroxylamine as a reagent for amination.[97] In the first step of this published procedure, one bromine of 1,1'-dibromoferrocene (**115**) was replaced with lithium by using one equivalent of *n*BuLi at -78 °C.[97] The cleanliness of this selective lithium-bromine exchange reaction was tested by quenching the reaction mixture with excess amount of Me_3SiCl (Scheme 2.1). The ^1H NMR spectrum of this test reaction showed the clean formation of 1-bromo-1'-(trimethylsilyl)ferrocene (**117**).

Scheme 2.1. Monolithiation of 1,1'-Dibromoferrocene (115) Followed by Quenching

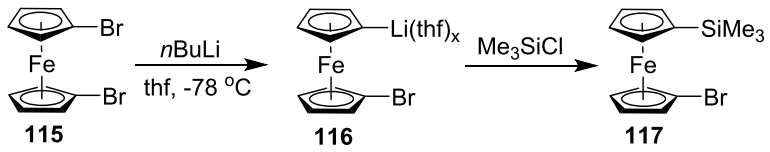

Following a known procedure, a dilute solution of *O*-benzylhydroxyl amine (2.0 mmol in 5.0 mL of thf) was dropwise added to the freshly prepared 1-bromo-1'-lithioferrocene (**116**, 2.0 mmol) at -78 °C (Scheme 2.2).[97] By an aqueous work-up, almost 1.6 mmol of bromoferrocene was obtained as a byproduct. The crude reaction mixture was further purified by column chromatography on basic alumina. The ^1H NMR spectrum of the final product showed the presence

of a small amount of the targeted species **114** along with two major impurities (**118** and **119**, Scheme 2.2). The ratio between the N*H* peaks of compounds **114** and **118** gave approximate relative amounts of those two species in isolated mixture (**114** : **118** = 1 : 3.25). The literature reports 71% and 45-55% yields of compound **114**. A yield of 71% was calculated based on the limiting reagent but the yield of 45-55% was probably based on a wrong reagent.[97] According to the reported procedure, 71% yield of compound **114** was obtained by a crystallization of crude product in hexanes at -10 °C.[97] However, repeated attempts of crystallization in different solvents and temperatures gave no crystals of compound **114** in our laboratory.

Scheme 2.2. Attempted Synthesis of 1-Amino-1'-bromoferrocene (114) Following a Previously Reported Procedure

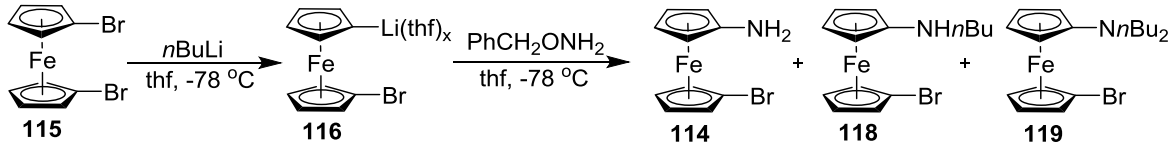

Scheme 2.3 illustrates the rational for the formation of compounds **118** and **119**. The monolithiation of 1,1'-dibromoferrocene (**115**) produced *n*BuBr as a byproduct, which was not removed from the reaction mixture. The amino group of compound **114** first reacted with *n*BuBr to produce the monosubstituted species **118**, which further reacted with a second equivalent of *n*BuBr to generate the doubly substituted species **119** (Scheme 2.3). From this mixture of products, compound **114** could not be isolated in an acceptable purity. Although, this synthesis has been described in the literature with isolated yields of 45-55% and 71% of **114**,[97] repeated attempts afforded only small amounts of the targeted compound **114** in an impure form. Therefore, an alternative pathway for **114** was needed.

Scheme 2.3. Formation of Mono- and Disubstituted 1-Amino-1'-bromoferrocene (118 and 119)

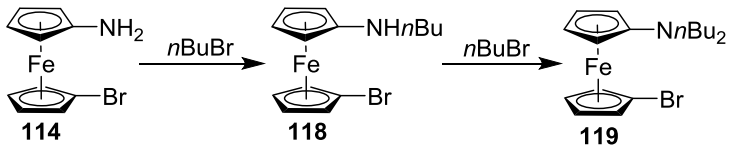

One of the best methods to prepare multi-gram quantities of aminoferrocene (**120**) is the Gabriel synthesis (Scheme 2.4).[98] In this procedure, bromoferrocene (**121**) is first reacted with phthalimide in the presence of Cu_2O (used as catalyst) to synthesize *N*-ferrocenyl phthalimide (**122**), which is then reacted with hydrazine at an elevated temperature to give aminoferrocene (**120**).[98]

Scheme 2.4. Common Synthetic Route to Aminoferrocene (120)

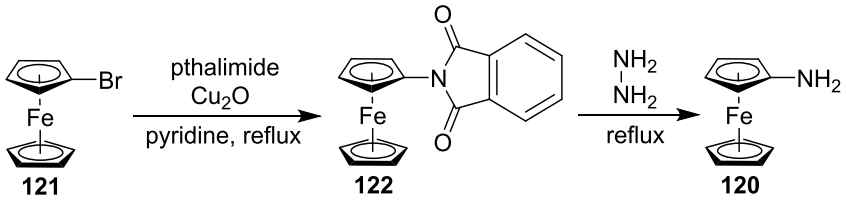

The above mentioned synthetic strategy was adapted in our chemistry. As illustrated in Scheme 2.5, 1,1'-dibromoferrocene (**115**) was first reacted with one equivalent of phthalimide in the presence of Cu_2O and, after aqueous work-up, the product was hydrazinolyzed at elevated temperature. However, this reaction resulted in **120** along with a small amount of our targeted product **114**, which could not be isolated in an acceptable purity. Therefore, another common synthetic methodology (see Scheme 2.6) was tested to add an amino group to the ferrocene moiety and, this time, 1-amino-1'-bromoferrocene (**114**) could successfully be prepared.

Scheme 2.5. Attempted Synthesis of 1-Amino-1'-bromoferrocene (114) by the Gabriel Method

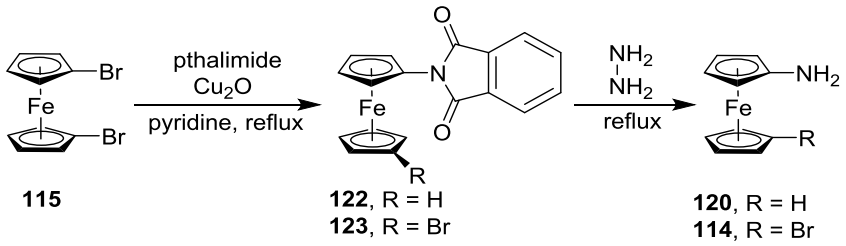

One of the oldest routes to synthesize **120** is the Curtius degradation of ferrocenyl carboxylic acid chloride (Scheme 2.6).[99] In this method, ferrocenyl carboxylic acid (**124**) is first chlorinated to the acid chloride **125**, which is then reacted with sodium azide to the corresponding azidocarbonyl ferrocene (**126**). Compound **126** is then reacted with benzyl alcohol at elevated temperature to the corresponding carbamate (**127**), which is further hydrogenolyzed in the presence of Pd/C to give aminoferrocene (**120**) as the final product (Scheme 2.6).[99]

Scheme 2.6. Synthesis of Aminoferrocene (120) by the Curtius Degradation Method

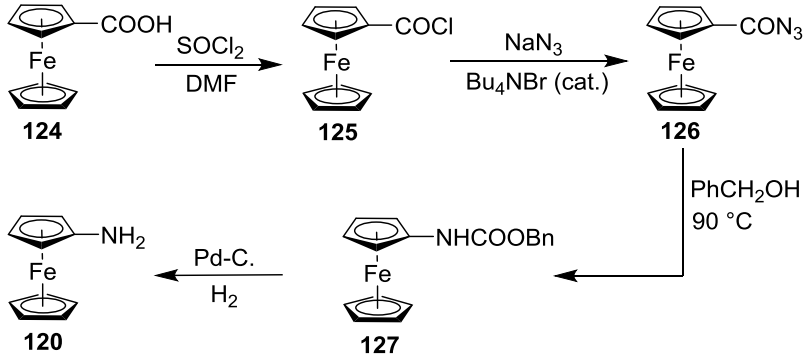

The above mentioned synthetic methodology was adapted in our chemistry (Scheme 2.7). The key compound for this pathway was 1-bromo-1'-carboxyferrocene (**128**), which was previously synthesized by the reaction of 1-bromo-1'-lithioferrocene (**116**) with dry-ice.[100] As illustrated in Scheme 2.7, the 1,1'-dibromoferrocene (**115**) was first selectively monolithiated followed by addition of an excess amount of dry-ice to the reaction mixture. Although, this

synthesis has been described in the literature with an overall isolated yield of 76%,[100] repeated attempts gave mainly bromoferrocene (**121**), carboxyferrocene (**124**) with a small amount of targeted species **128**, which could not be isolated from the reaction mixture. Therefore, we needed an alternative pathway to compound **128**. At this point, it was planned to synthesize this compound by a hydrolysis reaction from corresponding ester **129**, which was further attempted to synthesize by a known salt-metathesis reaction between species **116** and ClCOOEt (Scheme 2.8).

Scheme 2.7. Attempted Synthesis of 1-Bromo-1'-carboxyferrocene (128) Following a Previously Reported Procedure

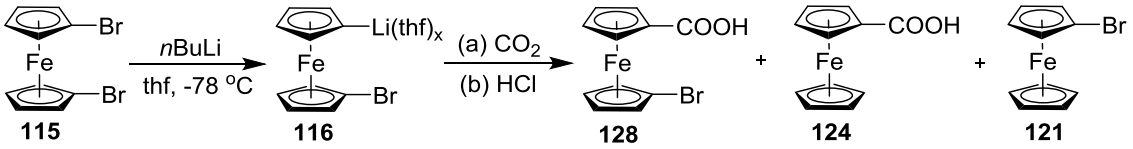

2.1.1. Synthesis of 1-Bromo-1'-(ethoxycarbonyl)ferrocene (129)

Compound **129** was previously synthesized by an *in situ* reaction of 1-bromo-1'-lithioferrocene (**116**) with ClCOOEt.[100] However, in our hands this reported synthesis resulted in a mixture of three major products: the targeted compound (**129**), a bisferrocenyl species (**130**), and (ethoxycarbonyl)ferrocene (**131**; Scheme 2.8). By column chromatography a small amount of **129**, mixed with compound **131**, could be recovered from the reaction mixture. Therefore, this synthesis needed to be improved.

Scheme 2.8. Attempted Synthesis of 1-Bromo-1'-(ethoxycarbonyl)ferrocene (129) Following a Previously Reported Procedure

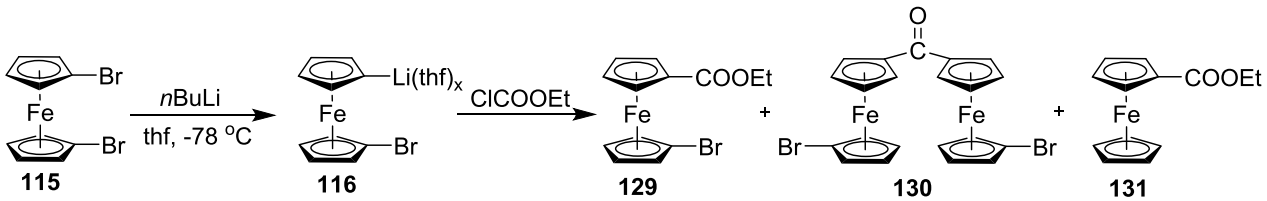

The synthesis of compound **129** is a two-step synthesis. In the second step ClCOOEt is

used, which has two leaving groups with Cl^- being a better nucleofuge than EtO^-. The first substitution on ClCOOEt by one equivalent of 1-bromo-1'-lithioferrocene (**116**) resulted in our targeted compound **129**, which then further reacted with a second equivalent of species **116** to generate the bisferrocenyl species **130**. In order to avoid this unwanted side reaction, 1-bromo-1'-lithioferrocene (**116**) was added to a large excess of ClCOOEt. After aqueous work-up and column chromatography, compound **129** was obtained in an overall yield of 72% (Scheme 2.9). In the ^1H NMR spectrum of compound **129** a triplet at δ = 1.35 and a quartet at δ = 4.29 ppm revealed the presence of COOEt group. In the Cp region, three signals at δ = 4.12, 4.41 and 4.82 ppm, in an intensity ratio of 1:2:1 were found. The intense peak at δ = 4.41 ppm is caused by the overlap of two Cp signals. This pattern indicates that **129** is a C_s symmetric molecule in solution on the NMR timescale (500 MHz).

Scheme 2.9. Synthesis of 1-Bromo-1'-(ethoxycarbonyl)ferrocene (129)

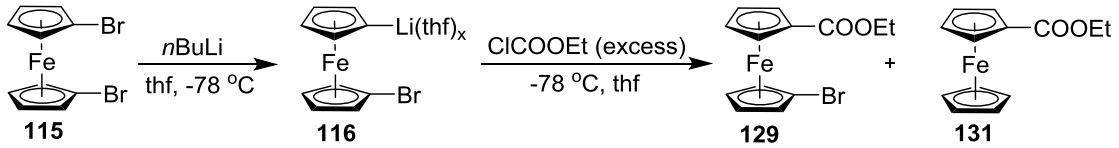

The main difficulties in synthesizing compound **129** are unwanted dilithiation of **115** and partial hydrolysis of the dilithiated product. As a result, a small amount of **131** (ca. 4%) was formed (Scheme 2.9), which could not be removed by common purification techniques (crystallization, precipitation, and chromatography). Therefore, it was decided to use species **129** contaminated with ca. 4% of (ethoxycarbonyl)ferrocene (**131**) in the next chemical transformation. As in none of the following steps the respective impurity could be removed, all of our starting materials contain 4-6% of non-brominated impurities.

2.1.2. Synthesis of 1-Bromo-1'-carboxyferrocene (128)

By following a known procedure, a solution of compound **129** (contaminated with ca. 4% of **131**) and KOH in a mixture of ethanol and water (EtOH : H_2O, 10 : 1) was refluxed for 40 h.[101] After acidic work-up, product **128** was obtained as an orange powder in a yield of 77%, containing ca. 4% of the non-brominated impurity **124** (Scheme 2.10). The ^{1}H NMR spectrum of compound **128** shows a broad signal at δ = 11.95 ppm caused by the COOH group. Four equally intense peaks in the Cp region at δ = 4.20, 4.49, 4.51, and 4.91 ppm indicate an expected C_s symmetry of the molecule.

Scheme 2.10. Synthesis of 1-Bromo-1'-carboxyferrocene (128)

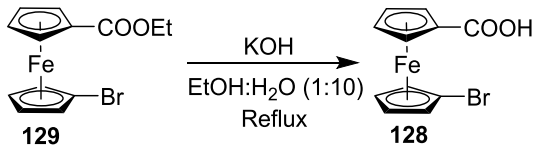

2.1.3. Synthesis of 1-Azidocarbonyl-1'-bromoferrocene (132)

As illustrated in Scheme 2.11, a solution of compound **128** (contaminated with ca. 4% of compound **124**) in CH_2Cl_2 was first treated with an excess amount of $(COCl)_2$, followed by few drops of DMF.[102] After 3 hours of stirring at room temperature, all the volatiles were removed from the reaction mixture under high vacuum. The resulting red powder, containing the acid chloride **133** (and ca. 4% of **125**), was then dissolved in CH_2Cl_2 and further reacted with an aqueous solution of NaN_3 in presence of nBu$_4$NBr as a phase transfer catalyst. After aqueous work-up, compound **132** was isolated as a brown powder (yield 93%), which contained ca. 4% of (azidocarbonyl)ferrocene (**126**) as a non-brominated impurity (Scheme 2.11). The ^{1}H NMR

spectrum of compound **132** shows four equally intense peaks in the Cp region at δ = 4.19, 4.49, 4.54, and 4.87 ppm, which indicate the presence of plane of symmetry in the molecule.

Scheme 2.11. Synthesis of 1-Azidocarbonyl-1'-bromoferrocene (132)

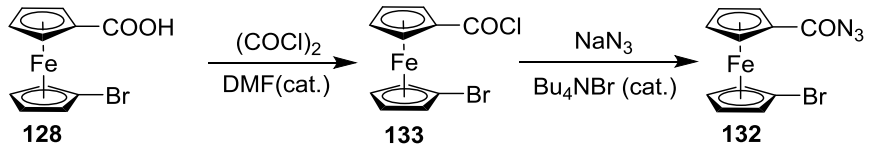

Extra care is always needed while handling organic azides. In the aforementioned reaction, as an aqueous solution of NaN_3 is used, the $(COCl)_2$ must be quantitatively removed from the reaction mixture after chlorination. Any leftover $(COCl)_2$ will form HCl upon hydrolysis, which will finally react with NaN_3 to give HN_3, a well-known highly explosive and poisonous substance. Therefore, the following simple precautionary measures were taken. First, after complete removal of all the noticeable liquids, the resulting acid chloride **133** was left for an additional 24 h under high vacuum. Second, while removing solvents with a rotary evaporator, the reaction mixture containing compound **132** was never warmed above 40 °C. Third, instead of storing compound **132** for a long time, it was consumed shortly after its preparation.

2.1.4. Synthesis of Benzyl N-(1'-bromoferrocen-1-yl)carbamate (139)

The thermal decomposition of an acyl azide (**134**) to produce an isocyanate (**135**) with a loss of N_2 gas is called Curtius rearrangement, named after Theodor Curtius, who described this reaction for the first time in 1885.[103] The resulting isocyanate **135** can then be attacked by several nucleophiles such as water, alcohols, and amines to produce primary amines (**136**), carbamates (**137**), and urea derivatives (**138**), respectively (Scheme 2.12).[103]

Scheme 2.12. Curtius Rearrangement Reactions

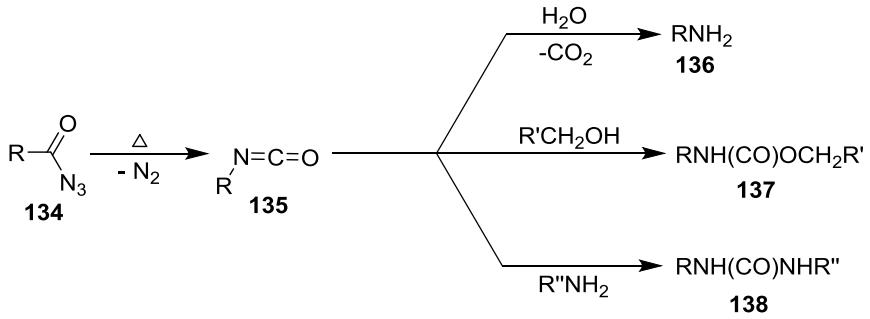

The formation of compound **138** (Scheme 2.12) has presented a common pathway to introduce a carbamate moiety on ferrocene. Ferrocenyl carbamate has been synthesized via this route, starting from corresponding acyl azide.[102] Following the similar chemical procedure, the new carbamate **139** was prepared from starting material **132** (Scheme 2.13). As illustrated in Scheme 2.13, compound **132** (contaminated with ca. 4% of compound **126**) was heated with an excess amount of benzyl alcohol resulting in a color change from burgundy-red to yellow. After removing all volatiles under high vacuum, the resulting brown solid was further purified by column chromatography. Product **139** was obtained as a golden yellow crystalline solid (yield 88%), which contained ca. 4% of benzyl N-ferrocenyl-carbamate (**127**) as the non-brominated impurity. In ^{1}H NMR spectrum the most indicative signals of compound **139** are found as a singlet at δ = 5.18 and a broad signal at δ = 6.00 ppm, which result from CH_2Ph and N*H* protons, respectively. Four equally intense peaks in the Cp region at δ = 4.04, 4.09, 4.38, and 4.52 ppm indicate that the molecule is C_s symmetric in solution on the NMR timescale (500 MHz). As compound **127** could not be removed by common purification techniques (crystallization, precipitation and chromatography), species **139** contaminated with 4% of benzyl N-ferrocenyl-carbamate (**127**) was used for the next synthetic step.

Scheme 2.13. Synthesis of Benzyl N-(1'-bromoferrocen-1-yl)carbamate (139)

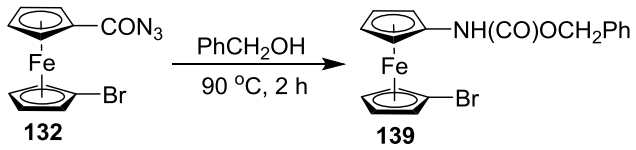

2.1.5. Synthesis of 1-Amino-1'-bromoferrocene (114)

Selective hydrogenolysis of respective carbamates in the presence of Pd-C is one of the most frequently used methods to synthesize aminoferrocenes.[99] Although it is a high-yielding procedure, the major drawback of this method is the involved hazardous chemical manipulation. Therefore, a sound technique and experienced synthetic hands are necessary to perform this reaction safely.

By following a known reaction, starting material **139** (and ca. 4% of compound **127**) was first dissolved in dry and deoxygenated *i*PrOH and, to this solution, Pd-C was slowly added by a glass funnel. The reaction flask was then purged with hydrogen by six consecutive cycles of partial evacuation and refilling. A balloon, filled with hydrogen gas, was finally placed on the reaction mixture (Scheme 2.14). After 3 hours of stirring at ambient temperature, all the insoluble materials were removed by Schlenk filtration and the resulting crude was washed with few portions of an aqueous NaOH solution.

Scheme 2.14. Synthesis of 1-Amino-1'-bromoferrocene (114)

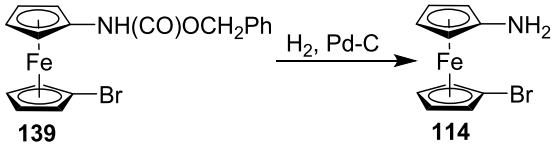

Although this reaction is well-known for its selectivity, some problems in our performed reaction surfaced. Careful evaluation of the ^{1}H NMR spectrum measured from the crude product

suggested that an additional 11% of the starting material **139** lost bromine during the reaction and resulted in aminoferrocene (**120**). However, compound **120** could partially be removed by sublimation and the targeted compound **114** was obtained in a yield of 70%. It is worth mentioning that the overall yield of compound **114**, starting from 1,1'-dibromoferrocene (**115**), was 32%. The resulting product, contaminated with ca. 6% of **120**, was used for the following. In the ^{1}H NMR spectrum the most indicative signal is found as a broad singlet at δ = 2.08 ppm which is caused by the amino group of compound **114**. Four equally intense peaks in the Cp region at δ = 3.57, 3.68, 3.71, and 4.12 ppm indicate the presence of plane of symmetry in the molecule. The ^{1}H NMR assignments of the non-brominated species **131**, **124**, **126**, **127**, and **120** can be found in the experimental section (Chapter 3).

2.2. *N*-substituted Aminobromoferrocenes

As discussed in Section 2.1, 1-amino-1'-bromoferrocene (**114**) was prepared starting from 1,1'-dibromoferrocene (**115**) in an overall yield of 32%. The final product contained ca. 6% of aminoferrocene (**120**), which could not be removed from the targeted species by common purification techniques. Therefore, **115** was used in form of a partially pure product in proceeding chemical transformations. As a result, all ferrocene derivatives were also contaminated with small amounts (2-7%) of the corresponding non-brominated impurities. The ^{1}H NMR assignments of the non-brominated species **140**, **144**, **146**, **148**, and **150** can be found in the experimental section (Chapter 3). The work, described entirely in Section 2.1, partially in Section 2.2 and mostly in Section 2.3 can be found in our recent publication.[104]

2.2.1. Lithiation of 1-Amino-1'-bromoferrocene (114)

The salt-metathesis reaction is the most suitable pathway to synthesize [*n*]FCPs. A high-yielding salt-metathesis reaction has two separate parts: a clean lithiation of the starting material and the reaction of the lithiated species with an element dihalide. As our main goal was to synthesize nitrogen-bridged [2]FCPs from compound **114**, it was important to test the efficiency of the lithiation reaction first. Therefore, by following a reported procedure,[97] a test lithiation of compound **114** was performed and an excess amount of Me_3SiCl was added in the reaction mixture, which was analyzed by ^{1}H NMR spectroscopy. However, this test reaction did not work in the anticipated way. Repeated attempts only afforded (trimethylsilylamino)ferrocene (**140**) as the major product and the trisilylated species **141** as the minor product (Scheme 2.15).

Scheme 2.15. Reported Dilithiation of Compound 114 and a Test Reaction

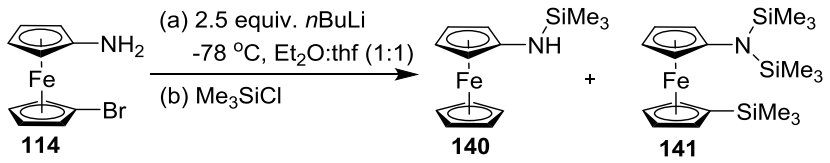

The formation of species **140** and **141** can be rationalized in the following way. Compound **114** has three possible sites for lithiation: two amino protons and one bromine atom. Upon lithiation in all three sites, compound **114** would give a trilithiated species which upon reaction with Me_3SiCl would produce compound **141**. On the other hand, an unknown intramolecular rearrangement in lithiated species resulted in compound **140** after silylation. In order to avoid such difficulties, synthesis of *N*-substituted derivatives of compound **114** were attempted.

2.2.2. Synthesis of Silyl-substituted Aminobromoferrocene (142)

By adapting a known procedure, compound **114** was silylated in the presence of Me_3SiCl.[105] The isolated product **142** was contaminated with ca. 6% of the non-brominated impurity (trimethylsilyl)aminoferrocene (**140**) (Scheme 2.16). In the ^1H NMR spectrum of compound **142**, a sharp singlet of relative intensity for nine protons at $\delta = 0.23$ and a broad singlet for one proton at $\delta = 2.42$ ppm revealed the presence of $NH(SiMe_3)$ moiety. Four equally intense signals in the Cp region at $\delta = 3.85$, 3.88, 3.99, and 4.25 ppm indicate that the molecule is C_s symmetric. Compound **142** was then dilithiated and the resulting dilithio salt was used in several salt-metathesis reactions (see Section 1.3-1.5).

Scheme 2.16. Synthesis of 1-Bromo-1'-(trimethylsilyl)aminoferrocene (142)

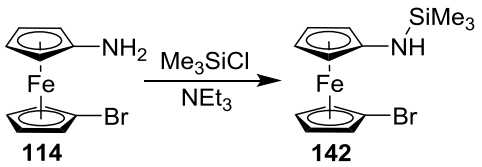

Using species **142** in salt-metathesis reactions gave FCPs that turned out to be not reactive enough to allow polymerization (see Section 1.3).[104] Therefore, other N-substituted aminobromoferrocene precursors were needed with less bulky substituents on nitrogen. The syntheses and characterization of these new species are described in the following sections.

2.2.3. Syntheses of Alkyl-substituted Aminobromoferrocenes (147 and 149)

The most common route to introduce a benzylidenimino group on a ferrocene moiety is the reaction of benzaldehyde with the corresponding aminoferrocene.[106] Although this chemical transformation produces water as a byproduct, no dehydrating agent is needed for the completion of the reaction. We adapted this well-known synthetic strategy to prepare a new ferrocenyl imine, starting from compound **114**. As illustrated in Scheme 2.17, compound **114** was first dissolved in toluene, followed by addition of benzaldehyde. The color change of the reaction mixture from yellow to burgundy red was instant. After three hours of stirring at ambient temperature, all the volatiles were removed from the reaction mixture and compound **143** was obtained as a dark red, sticky solid (yield 99%), which was contaminated with ca. 7% of (benzylidenimino)ferrocene (**144**) as the corresponding non-brominated impurity. In the ^{1}H NMR spectrum, the most indicative signals of compound **143** are found as a multiplet at δ = 7.87 and a singlet at δ = 8.48 ppm which arise from *o*-H's of phenyl and the NC*H*Ph proton, respectively. Four equally intense peaks at δ = 3.76, 4.02, 4.24 and 4.50 ppm in the Cp region indicate that the molecule is C_S symmetric in solution on the NMR timescale (500 MHz).

A similar experiment was performed, when pivalaldehyde was added to a toluene solution of compound **114**. By following a known chemical synthesis, molecular sieves were added in order to remove the water from the system.[107] Unlike the previous reaction, no significant color change was observed. After three hours the reaction mixture was filtered and all volatiles were removed from the filtrate. Compound **145** was isolated as a dark red, sticky solid (yield 96%) which was contaminated with ca. 2-3% of [(2,2-dimethylpropyliden)imino]ferrocene (**146**) as a non-brominated impurity (Scheme 2.17). In ^{1}H NMR spectrum, the most indicative signals of compound **145** are found at δ = 1.08 and 7.86 ppm which are caused by the *tert*-butyl and NC*H*t*Bu* proton, respectively. Four equally intense peaks at δ = 3.77, 3.93, 4.22, and 4.35 ppm in the Cp region indicate the presence of plane of symmetry in the molecule.

Scheme 2.17. Syntheses of Compounds 143 and 145

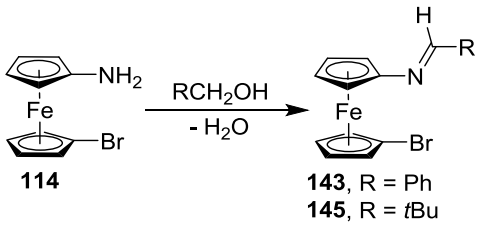

114

143, R = Ph
145, R = *t*Bu

The observed NOE correlations between NC*H*R and α-H's of Cp^{NCHR} (R = Ph, *t*Bu) revealed that the NC*H*R proton is close to the Cp^{NCHR} ring (Figure 2.1). Moreover, no NOE correlation was observed between Ph and Cp^{NCHR} for **143**, and *t*Bu and Cp^{NCHR} for **145**. Consequently, it was concluded that only the *trans*-isomers of compound **143** and **145** were formed in the above mentioned reaction sequence.

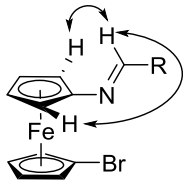

143, R = Ph
145, R = *t*Bu

Figure 2.1. Selected observed NOE correlations of compound **143** and **145** are shown by ↔. Correlations between the Cp protons have been omitted for clarity.

The transformation of imines to the corresponding amines are typically done by the reduction with ionic hydrides.[108,109] By following a known procedure, compound **143** was first dissolved in glacial acetic acid and $Na[NCBH_3]$ was added.[109] The reaction mixture instantly changed color from dark red to yellow with a simultaneous formation of hydrogen gas. After stirring overnight at ambient temperature, the reaction mixture was quenched with an aqueous NaOH solution. After aqueous work-up and column chromatography, the partially purified product was obtained as yellow solid which, upon crystallization, gave yellow crystals of the targeted compound in a yield of 46%. Like all our previous starting materials, compound **147** was contaminated with the respective non-brominated compound [ca. 2-3% of (benzylamino)ferrocene (**148**); Scheme 2.18]. In the ^{1}H NMR spectrum the most significant signals of compound **147** are found as singlets at δ = 2.42 and 3.89 ppm, resulting from the N*H* and NCH_2Ph groups, respectively. Four equally intense peaks at δ = 3.60, 3.74, 3.77, and 3.89 ppm in the Cp region indicate the presence of plane of symmetry in the molecule.

Scheme 2.18. Syntheses of Compounds 147 and 149

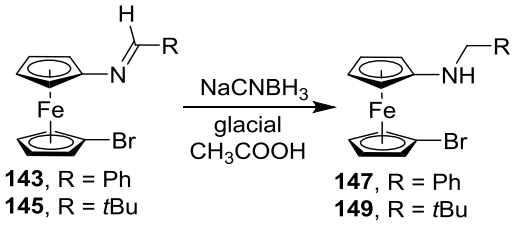

143, R = Ph
145, R = *t*Bu

147, R = Ph
149, R = *t*Bu

By following a similar procedure the neopentyl substituted 1-amino-1'-bromoferrocene (**149**) was synthesized from the corresponding imine **145** (Scheme 2.18). The reduction of compound **145** followed by aqueous work-up, column chromatography, and crystallization afforded compound **149** as a yellow waxy solid (yield 56%), which was contaminated with ca. 2-3% of (neopentylamino)ferrocene (**150**). In the ^{1}H NMR spectrum the most indicative signals of compound **149** are found as singlets at δ = 0.86 and 2.29 ppm, and a broad doublet at δ = 2.60 ppm which are resulting from *tert*-butyl, N*H*, and NC*H*$_2$*t*Bu groups, respectively. The pattern of the Cp signals (four peaks of equal intensity at δ = 3.65, 3.80, 3.82, and 4.30 ppm) indicates that the molecule is C_s symmetric on the NMR timescale (500 MHz).

2.2.4. Lithiation of 1-Bromo-1'-(trimethylsilyl)aminoferrocene (142)

Unlike ferrocene or 1,1'-dibromoferrocene (**115**), the dilithiation of compound **142** was not straightforward. Dilithiation of compound **142** at 0 °C followed by quenching with an excess amount of Me_3SiCl gave the intended product **141**, contaminated with ca. 33% of (trimethylsilyl)aminoferrocene (**140**). Although we do not have enough experimental evidence to fully understand the formation of compound **140**, proposedly this species formed as illustrated in Scheme 2.19.

Scheme 2.19. Illustration of the Side Reactions in the Dilithiation of Compound 142

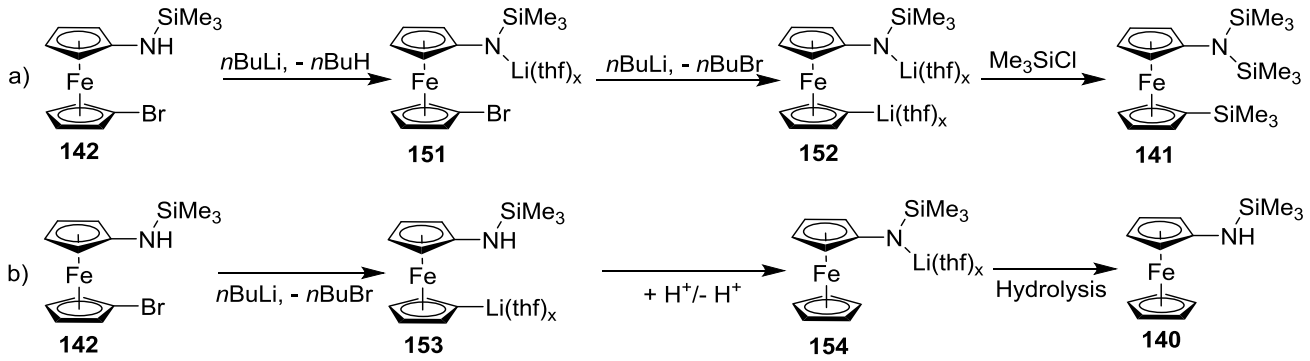

The dilithiation of compound **142** consists of the deprotonation of the amino group and a lithium-bromine exchange reaction. When the deprotonation happens on **142**, followed by lithium-bromine-exchange reaction, dilithio species **152** is formed, which upon silylation affords our intended product **141** (Scheme 2.19a). On the other hand, when compound **142** first loses bromine, monolithiated species **153** is formed. As a carbanion is more reactive than an amide, an intra- or intermolecular proton exchange reaction (from NH to Cp^-) happens and a second monolithiated species **154** is formed, which upon *in situ* hydrolysis (or protonation) gives compound **140** (Scheme 2.19b).

To test if the selective deprotonation is possible, compound **142** was reacted with a stoichiometric amount of *n*BuLi at low temperature, and the reaction mixture was quenched with excess amount of Me_3SiCl. The ^1H NMR spectrum of the reaction mixture shows that species **155** had been formed cleanly (Scheme 2.20a). In the next step, compound **142** was first lithiated at low temperature and the resulting reaction mixture was further treated with another equivalent of *n*BuLi at 0 °C. The ^1H NMR spectrum of the reaction mixture shows the clean formation of species **141** (Scheme 2.20b). Combining these two aforementioned reaction steps (Scheme 2.20b), the dilithiation of compound **142** was modified so that 2.1 equivalent of *n*BuLi was added to a -78 °C cooled solution of compound **142**. The reaction mixture was then warmed up to 0 °C and stirred

at that temperature for an additional 1 h. After quenching with an excess amount of Me_3SiCl, the ^1H NMR spectrum of the reaction mixture confirmed the formation of species **141** almost exclusively (Scheme 2.20c).

Scheme 2.20. Stepwise Dilithiation of Compound 142 Followed by Quenching

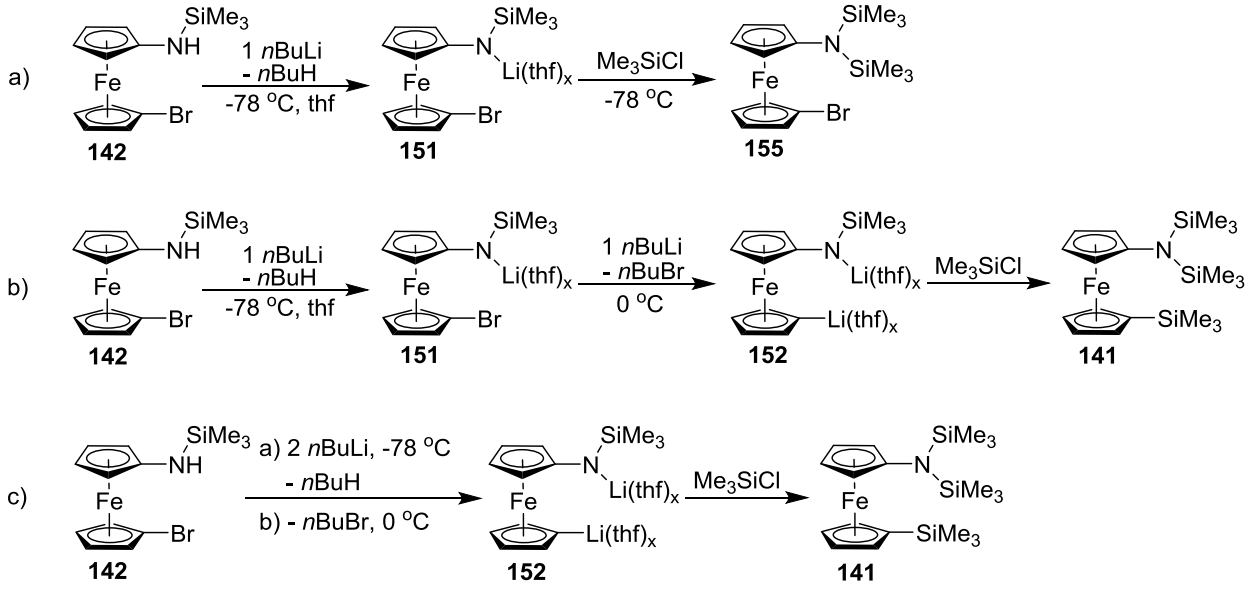

After these discoveries, in an attempt to further improve the lithiation process, the solvent of this reaction was changed from pure thf to a 9:1 mixture of hexanes and thf based on a published procedure.[110] We used this uncommon reaction mixture as it worked well for the syntheses of chiral [1]FCPs, which involved the preparation of dilithioferrocene by lithium-bromine exchange reaction.[111] Even though this mixture mainly consists of hexanes, the formed dilithio species **152** was soluble in it. From the cleanliness of the salt-metathesis reactions (discussed in Section 2.3-2.5) it was obvious that the stepwise dilithiation was working acceptably well in this solvent mixture.

2.2.5. Dilithiation of Alkyl-substituted Aminobromoferrocenes (147 and 149)

As discussed above, a stepwise reaction is needed to cleanly dilithiate starting material **142** (Scheme 2.20c). Therefore, our newly synthesized starting materials **147** and **149** were also tested by this stepwise dilithiation process, followed by quenching with an excess amount of D_2O. The ^1H NMR spectrum of the reaction mixture showed that this procedure could effectively be applied for compound **149** (Scheme 2.21). Syntheses and dilithiation of compounds **147** and **149** can be found in our recent publication.[112]

Scheme 2.21. Stepwise Lithiation of Compound 149 Followed by Quenching

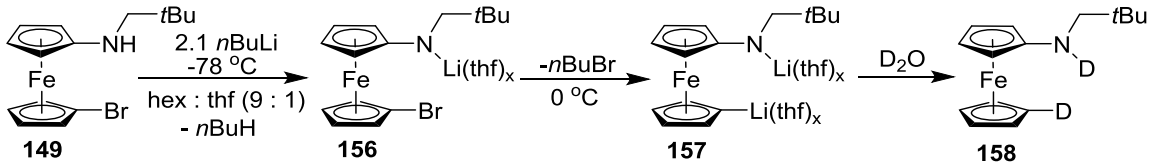

However, the stepwise dilithiation was not applicable to compound **147**. This is due to the fact that the lithiation at -78 °C led to a precipitate that did not dissolve upon increasing the temperature. Therefore, species **147** was reacted directly with 2.1 equivalents of *n*BuLi at 0 °C, which resulted in a homogenous solution. After quenching with an excess amount of D_2O, the ^1H NMR spectrum of the reaction mixture confirmed the formation of intended product **160** almost exclusively (Scheme 2.22).

Scheme 2.22. One Step Dilithiation of Compound 38 Followed by Quenching

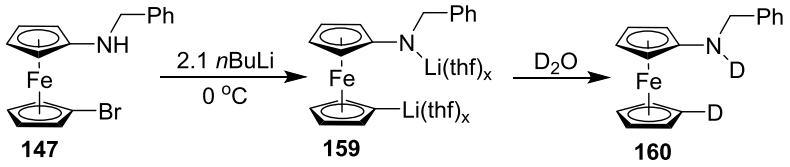

2.3. Aza[2]ferrocenophanes with Group 14 Elements in the Bridging Position

As discussed in the Section 1.2.3, the largest family of unsymmetrically bridged [2]FCPs (**A**, Figure 2.2) was developed by reacting the pmdeta-stabilized dilithio derivative of $(C_5Me_5)FeCp$ and various elemental dihalides (see Scheme 1.20 and 1.21; Section 1.2.3).[66–68] Among these strained metallocenes only carbaphospha- and carbathia[2]ferrocenophane could successfully be polymerized to afford moderate to low molecular weight metallopolymers (Section 1.4).[66]

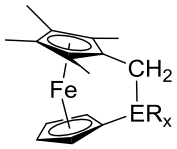

A

ER_x = S, $SiMe_2$, GeR_2, SnR_2, $PbPh_2$,PAr, $ZrCp_2$

Figure 2.2. Unsymmetrically bridged [2]FCPs synthesized by Manners and co-workers.

With limited accessibility and so far underdeveloped polymerization, we became interested in unsymmetrically bridged [2]FCPs. To develop a flexible and modular synthetic approach different starting materials (**142**, **147**, and **149**, Scheme 2.16 - 2.18) were synthesized and dilithiated. With the dilithio species in hand (**152**, **157**, and **159**, Scheme 2.20 - 2.22), salt-metathesis reactions to form [2]FCPs were explored. Scheme 2.23 illustrates a general synthetic methodology for the family of aza[2]ferrocenophanes (**A**), developed by our group.

Scheme 2.23. General Synthesis of Aza[2]ferrocenophanes (A)

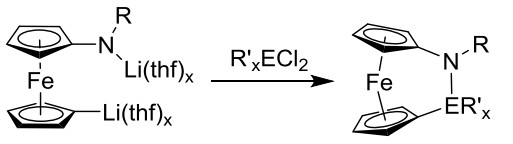

152, R = $SiMe_3$,
157, R = CH_2tBu,
159, R = CH_2Ph

A

E = Si, Sn, P, Ga, B

The previous investigation showed that Me_2Si-bridged [1]FCP (**1**) could easily be synthesized and polymerized into high molecular weight metallopolymers.[5] Therefore, our first goal was to synthesize azasila[2]ferrocenophane. Silylated 1-amino-1'-bromoferrocene (**142**), being the earliest developed starting material was chosen as the first candidate to prepare strained compounds.

2.3.1. Azasila[2]ferrocenophane (161)

Due to the fact that the silicon-bridged [1]FCPs are the most developed ferrocenophanes, in particular with respect to ROP, we chose silicon as the first candidate to prepare new aza[2]ferrocenophanes. According to the procedure published by Manners and co-workers in 1992, treatment of $(LiC_5H_4)_2Fe{\cdot}2/3$tmeda with Me_2SiCl_2 resulted in Me_2Si-bridged [1]FCP.[5] By a similar reaction between *in situ* prepared dilithio derivative **152** and Me_2SiCl_2 at -78 °C, the first azasila[2]ferrocenophane (**161**) was synthesized (Scheme 2.24). When the crude product was purified by vacuum sublimation at 45 °C, compound **161** was obtained as an analytically pure species in a yield of 53%.

Scheme 2.24. Synthesis of 2,2-Dimethyl-1-trimethylsilyl-1,2-azasila[2]ferrocenophane (161)

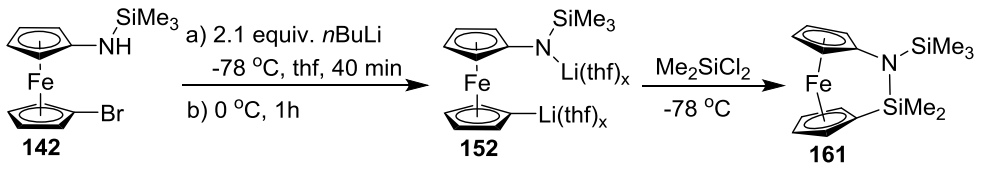

The formation of compound **161** was evident from the NMR spectroscopic data. The ^1H NMR spectrum measured from the reaction mixture after 4 hours of stirring at room temperature revealed that a clean conversion of starting materials to the intended product has happened (see Figure 2.3). The ^1H NMR spectrum of compound **161** shows four equally intense signals in the Cp

region, two for nitrogen-substituted Cp ring at δ = 3.80 and 4.23 ppm, and two for silicon-substituted Cp ring at δ = 4.27 and 4.63 ppm. This pattern of Cp signals indicates the presence of plane of symmetry in the molecule. The protons of the $NSiMe_3$ and $SiMe_2$ groups were found as two intense singlets for nine and six hydrogens at δ = 0.07 and 0.43 ppm, respectively. The assignments of all peaks were further supported by additional 2D-NMR experiments (HMQC and COSY). The ^{13}C NMR spectrum of compound **161** showed four high-intensity singlets in the Cp region, two for nitrogen substituted Cp ring at δ = 67.2 and 72.1 ppm, and two for silicon substituted Cp ring at δ = 70.9 and 75.9 ppm. Due to the fact that nitrogen is more electron withdrawing than silicon, the signal for the Me_3SiN-substituted *ipso*-carbon is found at δ = 102.0 ppm, whereas that for Me_2Si-substituted one appears at 70.0 ppm.

Figure 2.4 depicts the molecular structure for compound **161** obtained by a single-crystal X-ray analysis. The crystal and structural refinement data can be found in Table 2.2 of Section 2.3.3. As shown in Figure 2.4, nitrogen is trigonal planar coordinated with a sum of the surrounding angles of 359.76(35)°. The second bridging element, silicon, is in the center of a distorted tetrahedron with tetrahedral angles in a range of 105.73(8)-111.95(10)°. The detail discussion about the measured distortion angles can be found in Section 2.3.3.

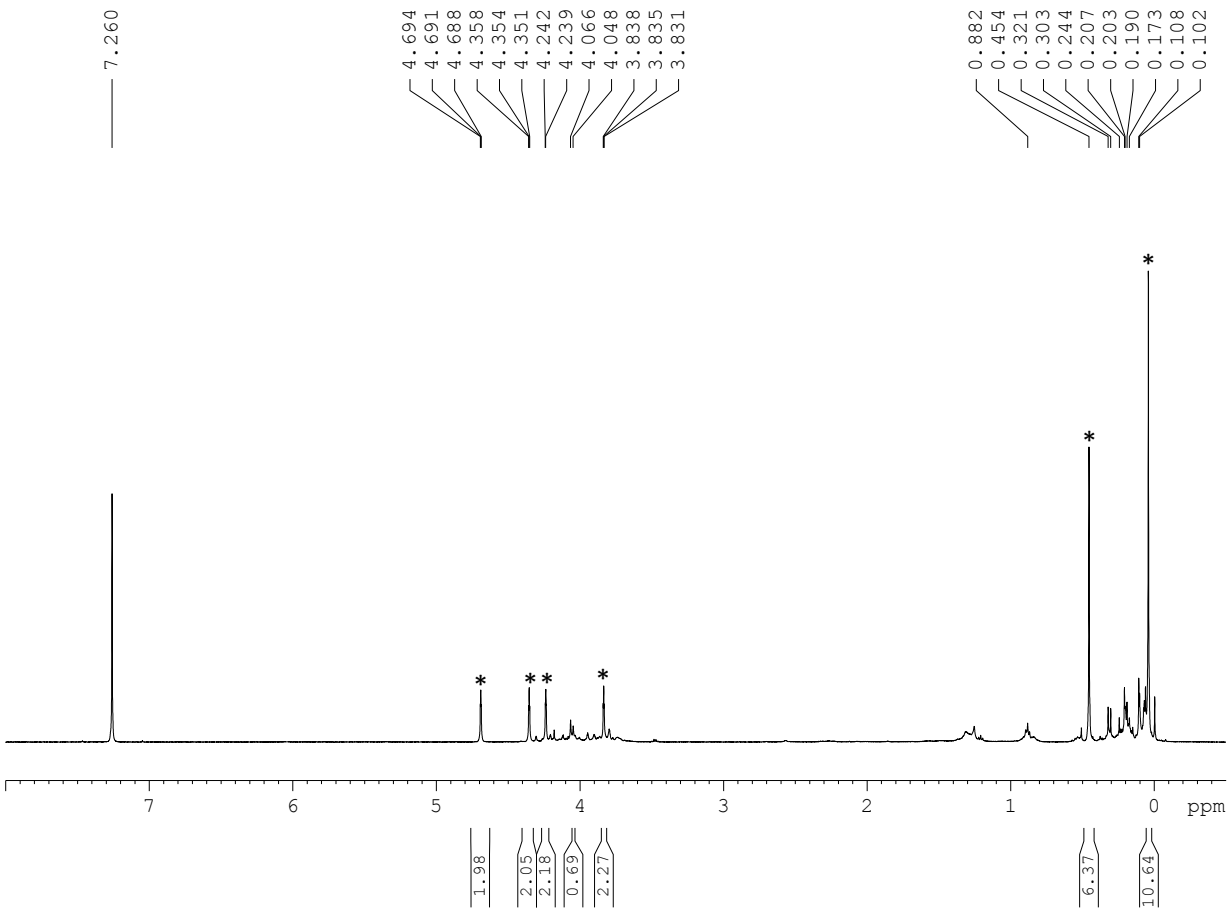

Figure 2.3. ^{1}H NMR spectrum of **161** ($CDCl_3$), taken from an aliquot of the reaction mixture. Peaks marked with * are resulting from compound **161**.

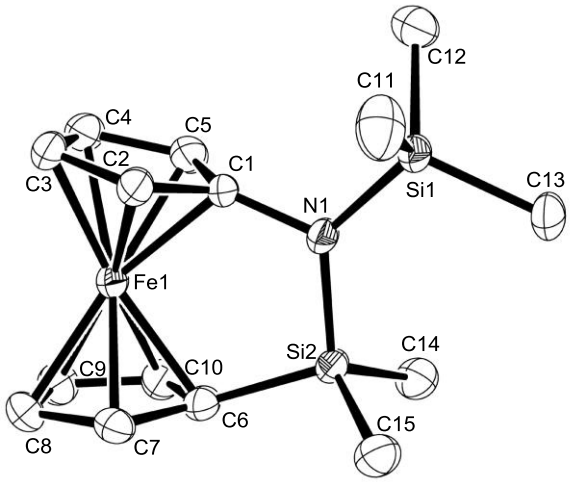

Figure 2.4. Molecular structure of **161** with thermal ellipsoids at the 50% probability level. Hydrogen atoms are omitted for clarity. Selected bond lengths [Å] and bond angles: N1-C1 = 1.442(2); N1-Si1 = 1.7484(17); N1-Si2 = 1.7529(17); Si2-C6 = 1.877(2); Si2-C14 = 1.861(2); Si2-C15 = 1.860(2); Si1-N1-C1 = 115.33(13); Si1-N1-Si2 = 129.86(9); C1-N1-Si2 = 114.57(13); N1-Si2-C6 = 105.73(8); N1-Si2-C14 = 111.35(10); N1-Si2-C15 = 111.95(10); C6-Si2-C14 = 108.91(10); C6-Si2-C15 = 109.44(10); C14-Si2-C15 = 109.35(11); This figure is reprinted with permission from Dey, S; Quail, J. W.; Müller, J. *Organometallics* **2015**, *34*, 3039-3046. Copyright 2015 ACS.

2.3.2. Azastanna[2]ferrocenophane (162)

The syntheses of stanna[1]ferrocenophanes are not as straightforward as their silicon-bridged counterparts.[113] Reaction between tmeda-stabilized dilithioferrocene (**19**, Scheme 1.7) and Me_2SnCl_2 gave oligomers whereas, the similar reaction with tBu$_2$SnCl$_2$ afforded strained [1]FCP.[113] Due to the challenging synthesis of stanna[1]ferrocenophane, we became interested to explore the similar reactions with our system.

Our strategy was to prepare a similar compound as **161** with tin in the bridging position. Following the usual procedure compound **142** was dilithiated and *in situ* reacted with a dilute solution of Me_2SnCl_2. However, the ^{1}H NMR spectrum of the reaction mixture showed broad resonances, which indicated the formation of oligomers **163** as the major product (see Figure 2.5). Our targeted compound **162** was present as a minor product in the reaction mixture. Via vacuum

sublimation from the crude, compound **162** was isolated as a partially pure species in an approximate yield of 14% (Scheme 2.25).

Scheme 2.25. Synthesis of 2,2-Dimethyl-1-trimethylsilyl-1,2-azastanna[2]ferrocenophane (162)

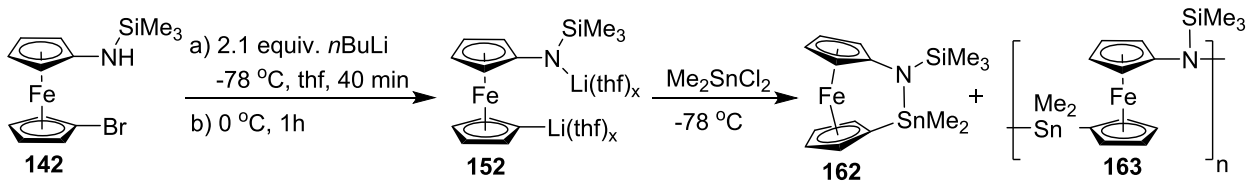

The ^{1}H NMR spectrum of the isolated product shows four equally intense signals in the Cp region, two for nitrogen-substituted Cp ring at δ = 3.78 and 4.23 ppm, and two for tin-substituted Cp ring at δ = 4.45 and 4.69 ppm. The chemical shifts for the Cp signals of compound **162** are very similar to those of **161** and indicate that the molecule is C_s symmetric. The protons of the $NSiMe_3$ and $SnMe_2$ groups are found as two intense singlets for nine and six hydrogens at δ = 0.06 and 0.40 ppm, respectively. The ^{13}C NMR spectrum of compound **162** shows four high-intensity singlets in the Cp region. Among them, peaks at δ = 65.4 and 76.7 ppm are caused by the nitrogen-substituted Cp ring and peaks at δ = 70.6 and 72.9 ppm are caused by the tin-substituted Cp ring. The signals for the *ipso*-carbons, substituted by Me_3NSi and Me_2Sn groups are found as low-intensity singlets at δ = 114.2 and 70.4 ppm, respectively. The similar result is found also for compound **161**, where the nitrogen-substituted ipso carbon shows a chemical shift (δ = 102.0 ppm), significantly higher than the silicon-substituted one (δ = 70.0 ppm; Section 2.3.1).

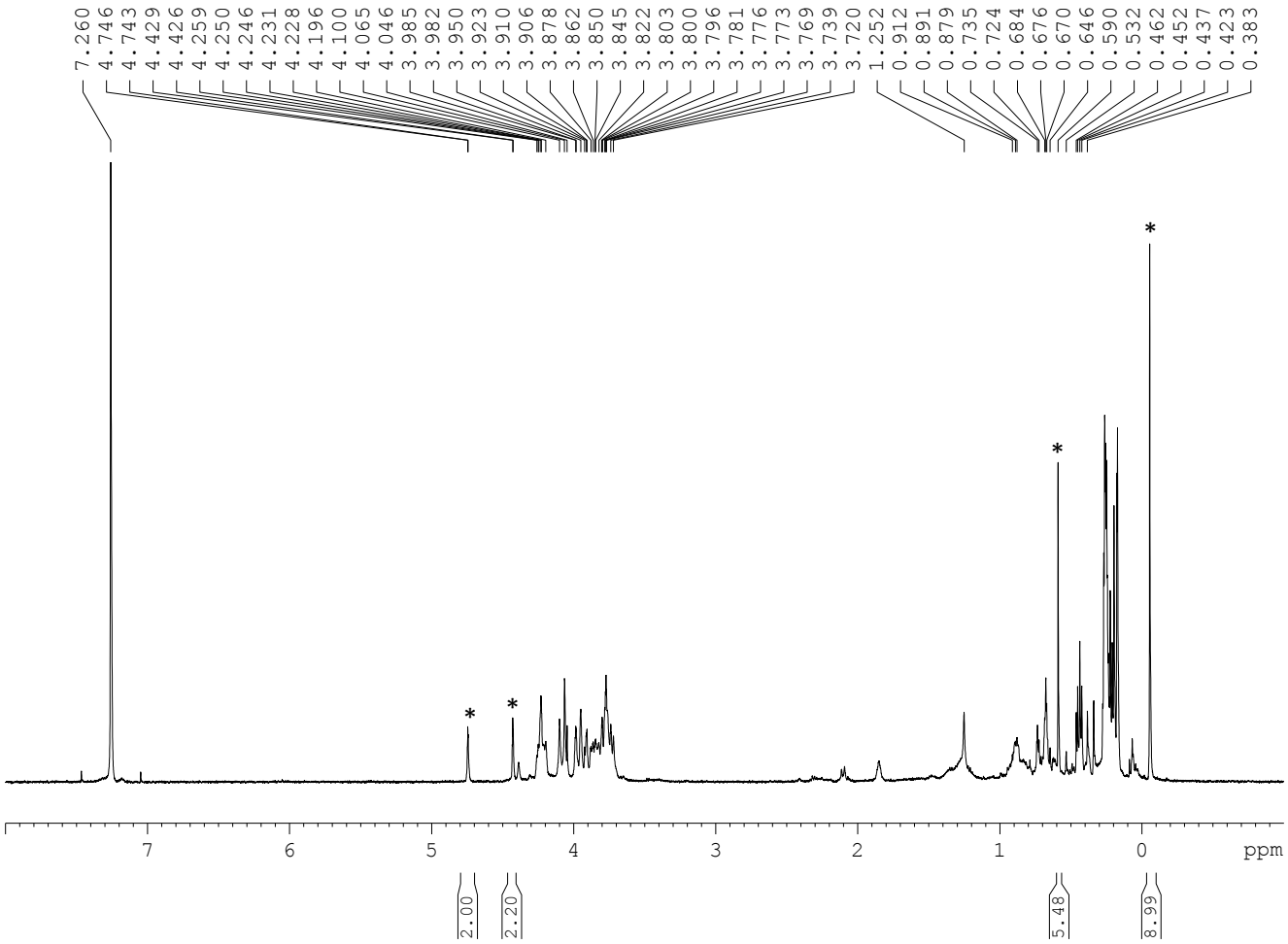

Figure 2.5. ^{1}H NMR spectrum of compound **162** ($CDCl_3$), taken from an aliquot of the reaction mixture. The peaks marked with * are resulting from **162**. The other peaks of **162** presumably overlaps with stronger peaks of **163**.

Suitable crystals for a single-crystal X-ray analysis of **162** could be obtained and the molecular structure could be solved (Figure 2.6). The crystal and structural refinement data can be found in Table 2.2 of Section 2.3.3. Similar to compound **161**, nitrogen is trigonal planar coordinated shown by the sum of the surrounding angles of 359.47(42) and 359.69(42)° for both independent molecules. Tin is present at the center of a distorted tetrahedron, where the tetrahedral angles fall in a range of 98.86(8)-114.79(12)°. The N-Sn bond (2.067(2) / 2.060(2) [Å]) of

compound **162** is significantly longer than the bridging N-Si bond (1.7529(17) [Å]) of compound **161**.

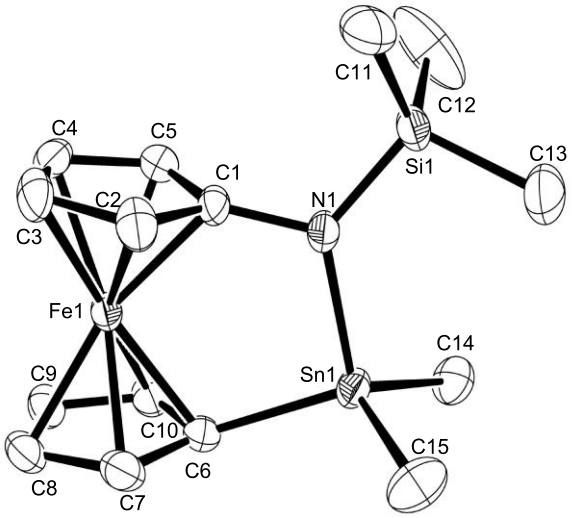

Figure 2.6. Molecular structure of **162** with thermal ellipsoids at the 50% probability level. Hydrogen atoms are omitted for clarity. Selected bond lengths [Å] and bond angles for the two independent molecules: N1-C1 = 1.432(3) / 1.426(3); N1-Si1 = 1.721(2) / 1.723(2); N1-Sn1 = 2.067(2) / 2.060(2); Sn1-C6 = 2.133(2) / 2.129(3); Sn1-C14 = 2.124(3) / 2.122(3); Sn1-C18 = 2.129(3) / 2.130(3); Si1-N1-C1 = 118.72(16) / 117.95(16); Si1-N1-Sn1 = 127.74(11) / 128.29(11); C1-N1-Sn1 = 113.23(15) / 113.23(15); N1-Sn1-C6 = 98.86(8) / 99.14(9); N1-Sn1-C14 = 108.91(10) / 108.62(10); N1-Sn1-C18 = 108.80(10) / 108.78(11); C6-Sn1-C14 = 115.20(11) / 112.92(11); C6-Sn1-C18 = 111.71(12) / 111.34(12); C14-Sn1-C18 = 112.34(11) / 114.79(12). This figure is reprinted with permission from Dey, S; Quail, J. W.; Müller, J. *Organometallics* **2015**, *34*, 3039-3046. Copyright 2015 ACS.

The steric shielding over the elemental dihalides play a significant role in formation of the strained stanna[1]ferrocenophanes.[113] In a previous report by Manners and co-workers, it was observed that the larger groups on the stannyl chloride favor the formation of strained compounds, whereas the smaller groups mostly afford the oligomers.[113] Our system shows reactivity similar to that was found for tmeda-stabilized dilithioferrocene by the Manners *et al.*[113] The low yield of azastanna[2]ferrocenophane **162** can be attributed to the intermolecular condensation reaction which was found as more favorable over intramolecular cyclization. Although we did not do any further investigation to fully understand the reaction mechanism, two possible reaction channels

have been speculated and illustrated in Scheme 2.26. As Cp^- is more reactive than an amide, species **164** can be expected as a viable intermediate in this reaction.

Scheme 2.26. Illustration of the two Parallel Reaction Channels in Salt-metathesis of 152 with Me_2SnCl_2

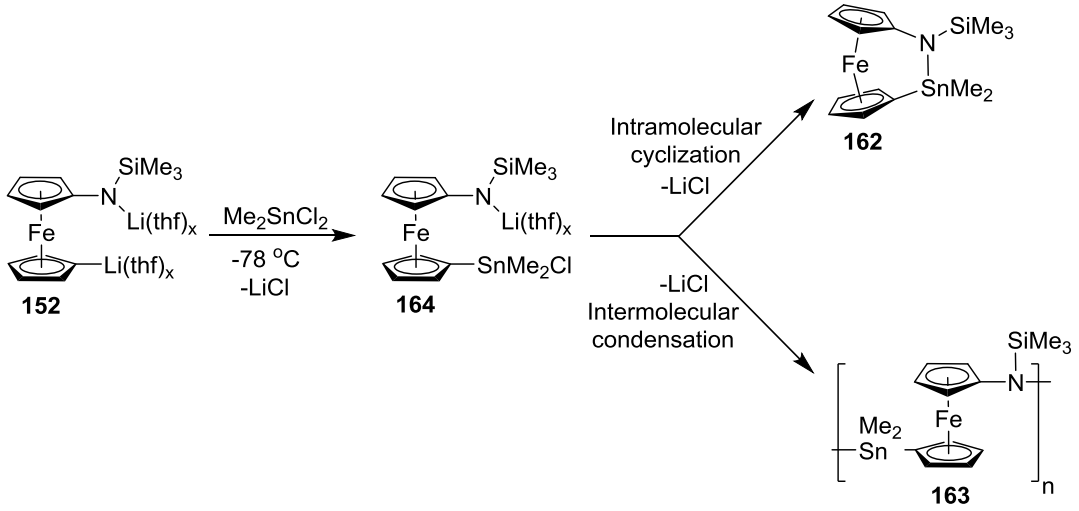

Since the bulkier substituents on tin preferably produced strained compounds,[113] our next plan was to investigate the reaction of dilithio species **152** with a bulky stannyl dichloride such as tBu$_2$SnCl$_2$.

2.3.3. Azastanna[2]ferrocenophane with Increased Bulk on Tin (165)

As shown in Scheme 2.27, the silylated 1-amino-1'-bromoferrocene **142** was first dilithiated and further reacted with a dilute solution of tBu$_2$SnCl$_2$ at -78 °C. The ^{1}H NMR spectrum of the reaction mixture, taken after 1 h of stirring at room temperature, showed a clean conversion of the starting material to the intended product (see Figure 2.7). The crude product was finally purified by vacuum sublimation at 95 °C resulting in compound **165** as red crystals in a yield of 62% (Scheme 2.27).

Scheme 2.27. Synthesis of 2,2-Di-*tert*-butyl-1-trimethylsilyl-1,2-azastanna[2]ferrocenophane (165)

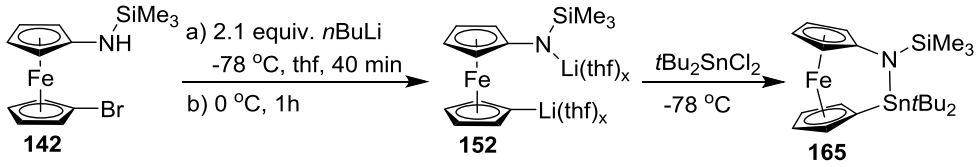

The ^{1}H NMR spectrum of the purified product shows four equally intense signals, two for the nitrogen-substituted Cp ring at δ = 3.80 and 4.26 ppm, and two for tin-substituted Cp ring at δ = 4.36 and 4.69 ppm. This pattern of the NMR signals indicate that the molecule is C_s symmetric. The *tert*-butyl groups appear as an intense singlet at δ = 1.40 ppm, accompanied by two small satellite peaks which were resulting due to the presence of Sn^{117} and Sn^{119} isotopes in the sample. The signals for the $NSiMe_3$ group are found as a high-intensity singlet with relative intensity for nine protons at δ = 0.13 ppm. The ^{13}C NMR spectrum of compound **165** shows four intense singlets in the Cp region, two from the nitrogen-substituted Cp ring at δ = 65.7 and 70.89 ppm, and two from the tin-substituted Cp ring at δ = 70.86 and 77.7 ppm. The signals for the *ipso*-carbons, substituted with $NSiMe_3$ and $SntBu_2$ groups appeared as small singlets at δ = 113.7 and 74.5 ppm, respectively. These values show very close similarities with those for compounds **161** and **162**.

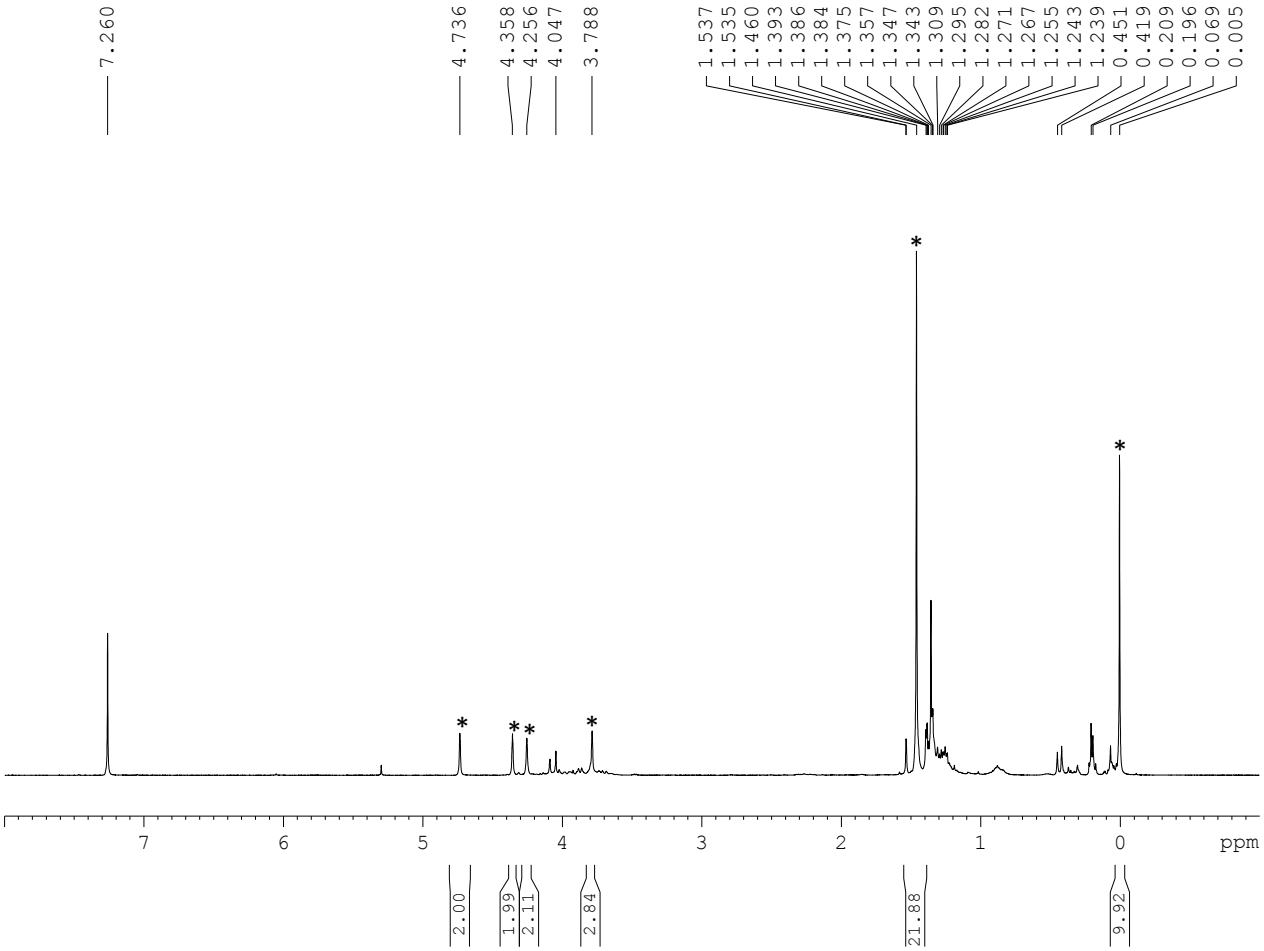

Figure 2.7. ^{1}H NMR spectrum of **165** ($CDCl_3$), taken from an aliquot of the reaction mixture. The peaks marked with * are resulting from compound **165**.

The chemical shifts caused by the Cp protons and carbons of compound **165** are very similar to those of **162**. The similarity is also noticeable in the crystal structures of these two species. Comparison between the bond angles and bond lengths of compounds **162** and **165** reveals that the size of the substituents on tin have little-to-no effect on the overall structure of the strained molecules. As compound **162** could not be isolated in an analytically pure form, species **165** was used for ROP studies. The molecular structure of compound **165**, derived by X-ray diffraction data, is displayed in Figure 2.8.

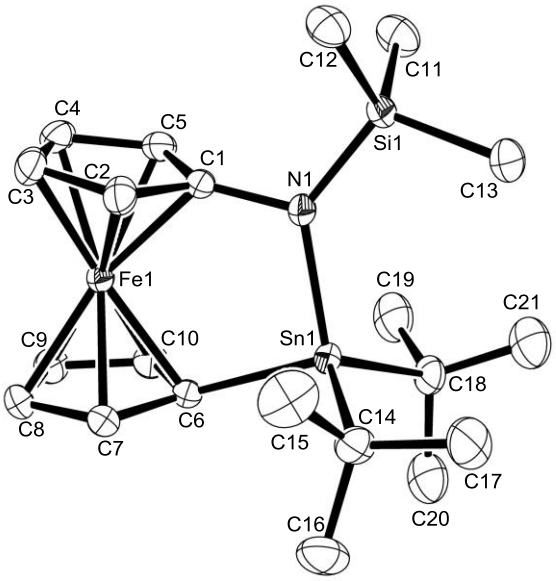

Figure 2.8. Molecular structure of **165** with thermal ellipsoids at the 50% probability level. Hydrogen atoms are omitted for clarity. The *t*Bu group (C18) is disordered; only the main species is shown. Selected bond lengths [Å] and bond angles: N1-C1 = 1.435(2); N1-Si1 = 1.7309(15); N1-Sn1 = 2.0775(14); Sn1-C6 = 2.1526(17); Sn1-C14 = 2.1937(19); Sn1-C18 = 2.1984(18); Si1-N1-C1 = 115.56(11); Si1-N1-Sn1 = 131.94(8); C1-N1-Sn1 = 112.44(10); N1-Sn1-C6 = 98.24(6); N1-Sn1-C14 = 109.92(7); N1-Sn1-C18 = 111.91(7); C6-Sn1-C14 = 108.81(7); C6-Sn1-C18 = 108.58(7); C14-Sn1-C18 = 117.59(8). This figure is reprinted with permission from Dey, S.; Quail, J. W.; Müller, J. *Organometallics* **2015**, *34*, 3039-3046. Copyright 2015 ACS.

Table 2.1. Common Angles [°] to Characterize Compounds 161, 162, and 165

Distortion Angles [e]	**161**	**162** [a]	**165**
α	15.73(13)	9.36(17) {9.45(18)}	10.13(11)
β [b]	6.53(18)	3.4(2) {3.5(2)}	2.31(16)
β' [c]	17.38(15)	19.18(17) {19.12(19)}	18.52(12)
δ	168.62(2)	172.75(2) {172.73(3)}	172.50(2)
τ [d]	3.31(13)	4.2(2) {1.9(2)}	8.08(4)

[a] values for the second independent molecule of the asymmetric unit are shown in braces; [b] β for E = N; [c] β' for E = Si or Sn; [d] τ is defined as the angle between the least squares plane $Cp^{centriod}$-Fe-$Cp^{centroid}$ and the bridging bond vector (N-Sn). [e] The readers are requested to consult Figure 1.2 in introduction.

Table 2.1 shows the common distortion angles for compounds **161**, **162**, and **165**; the crystal and structural refinement data can be found in Table 2.2. The Cp rings of the silicon-bridged species are tilted more strongly (α angle of **161** is ca. 16°) than those of the tin-bridged species (α

angles of **162** and **165** are in a range of ca. 9-10°). Overall, this is a moderate (for **161**) to small (for **162** and **165**) degree of tilting,[104] as a comparison with the known [2]FCPs [α angles for [2]FCPs with the bridging moieties in parentheses: α = 12.82(16)° (Me_2NB-$BNMe_2$),[13] 23.2° (C_2Me_4),[30] 22.6° (CH=CH),[31] 4.19(2)° (Me_2Si-$SiMe_2$),[46] 3.94° (Me_2Ge-$GeMe_2$),[49] 0.7° (Me_2Sn-$SnMe_2$),[50] 13.6° (*t*BuP-P*t*Bu),[55] 18.51(14)° (CH_2S),[66] 18.3(2)° (CH_2PMes),[66] 15.0(4)° and 14.8(3)° (CH_2PPh),[66] 11.8(1)° (CH_2SiMe_2),[66] 11.4(7)° (CH_2PPhMe^+),[66] 10.99(2)° (CH_2GeMe_2),[67] 7.5(1)° (CH_2SnMe_2),[67] -5.5(2) (CH_2ZrCp_2),[68] 23° ($HNSO_2$)[64]]. However, as expected, due to the presence of nitrogen in the bridge, the tilting of our compounds (**161**, **162**, and **165**) were significantly higher than those in related carbasila- and carbastanna[2]ferrocenophane (**66**, **72**, and **74**; see Section 1.2.3), reported by Manners *et al.*[66,67] The two β angles of each of compounds **161**, **162**, and **165** are significantly different, with a small β angle for nitrogen between 2.31(16)° and 6.53(18)°, and larger β angle for silicon or tin between 17.38(15)° and 19.18(17)° (see Table 2.1). These differences can be rationalized from the following simple mechanical model. The lever arm for nitrogen [between 1.426(30) and 1.442(2) Å] is significantly shorter than that for silicon [1.877(2) Å] or for tin [between 2.129(3) and 2.1526(17) Å]. If one assumes that the bridging N-E moiety puts the same force on both the lever arms, the longer lever arm will bend more than the shorter one. The angles between $Cp^{centroid}$-Fe-$Cp^{centroid}$ and bridging bond vector N-E (E = Si, Sn), expressed as τ, are small with values between 1.9(2)° and 8.09(4)° (consult Figure 1.2 in Introduction). This is due to the fact that Me_3Si group on nitrogen tends to have a staggered conformation with the alkyl groups of tin or silicon. Although, we know that the chemical bonds are not hard sticks and the model described here is too simplistic, it is a common way of thinking about the simple force field to rationalize distortions in [2]FCPs.[114]

Table 2.2. The Crystals and Structural Refinement Data of Compounds 161, 162, and 165

Parameters	**161**	**162**	**165**
empirical formula	$C_{15}H_{23}FeNSi_2$	$C_{15}H_{23}FeNSiSn$	$C_{21}H_{35}FeNSiSn$
fw	329.37	420.00	504.16
cryst. size / mm^3	0.070 × 0.070 × 0.150	0.080 × 0.150 × 0.150	0.050 × 0.200 × 0.200
cryst. system, space group	triclinic, $P\bar{1}$	triclinic, $P\bar{1}$	monoclinic, $P2_1/n$
Z	2	4	4
a / Å	6.5140(5)	10.9962(3)	8.6378(2)
b / Å	10.7849(8)	12.7443(4)	15.6700(4)
c / Å	11.7791(9)	13.2851(3)	16.6663(5)
α / °	96.347(2)	80.3890(10)	90
β / °	90.913(2)	80.2710(10)	97.0033(9)
γ / °	98.624(2)	68.5680(10)	90
volume / $Å^3$	812.70(11)	1696.83(8)	2239.03(10)
ρ_{calc} / mg m^{-3}	1.346	1.644	1.496
temperature / K	173(2)	173(2)	173(2)
$\mu_{calc.}$/ mm^{-1}	1.062	2.385	1.821
θ range / °	3.44 to 28.32	2.68 to 27.48	3.46 to 30.54
completeness / %	99.6	99.9	99.8
reflns collected / independent	17418 / 4034	59734 / 7792	51094 / 6851
absorption correction	multiscan	multiscan	multiscan
data $[F_o^2 \geq -3\sigma(F_o^2)]$/ restraints / params	4034 / 0 / 177	7792 / 0 / 353	6851 / 6 / 242
goodness-of-fit	1.025	1.042	1.038
R_1 [I > 2 σ(I)] [a]	0.0346	0.0251	0.0253
wR_2 (all data) [a]	0.0843	0.0569	0.0501
largest diff. peak and hole, $\Delta\rho_{elect}$ / e $Å^{-3}$	0.336 and -0.402	0.457 and -0.451	0.571 and -0.548

[a] $R_1 = [\Sigma||F_o|-|F_c||]/[\Sigma|F_o|]$ for $[F_o^2 > 2\sigma(F_o^2)]$, $wR_2 = \{[\Sigma w(F_o^2-F_c^2)^2]/[\Sigma w(F_o^2)^2]\}^{1/2}$ [all data]

2.3.4. Attempted Ring-opening Polymerization of Compounds 161 and 165

ROPs of compound **161** and **165** were attempted using the common methods of thermal-, transition-metal-catalyzed-, anionic-, and photocontrolled ROPs. In short, no oligomeric or

polymeric material resulted from any of these reactions. Heating of compound **161** at 300 °C in a sealed NMR tube for 21 h gave the unreacted starting material. On the other hand, compound **165** could withstand 200 °C, but further heating to 260 °C gave a waxy solid residue, which was suspended in dry and deoxygenated C_6D_6. After centrifugation an orange supernatant and a black residue were obtained. The ^{1}H NMR spectrum measured from the decanted supernatant solution showed the presence of starting material **165**, (trimethylsilylamino)ferrocene (**140**) and other unidentified product in the reaction mixture (Scheme 2.28). The black residue was identified as metallic tin following the wet tests for metals, described by Vogel *et al.* (Section 4.19).[115]

Scheme 2.28. Investigation of Thermal Ring-opening Polymerization of Compound 165

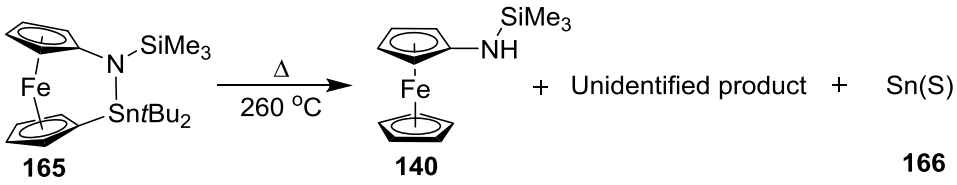

Attempts of photocontrolled ROP with compounds **161** and **165** with 0.10, 0.25 or even 1.0 equivalents of NaCp as initiator were unsuccessful. Similar negative results were obtained when transition-metal-catalyzed ROP was attempted with both monomers. Reactions of compounds **161** and **165** with Karstedt's catalyst in C_6D_6 at 50 °C returned the unreacted starting materials. After unsuccessful attempts via thermal, photocontrolled, and transition-metal-catalyzed polymerization reactions, anionic ROPs were attempted for both the monomers.

In order to evaluate the possibility of anionic ROP, ring-opening reactions were first investigated for compounds **161** and **165**. In a thf solution of the monomer **165**, one equivalent of *n*BuLi was added and the reaction mixture was left at room temperature for 0.5 h. After quenching

the reaction mixture with excess amount of Me_3SiCl, the supernatant was analyzed by ^1H NMR spectroscopy, which showed the quantitative formation of the silylated product **167** (Scheme 2.29).

Scheme 2.29. Anionic Ring-opening Reaction of Compound 165

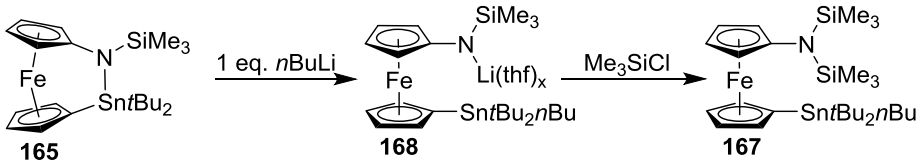

A similar result was obtained when the reaction time was extended from 0.5 h to 6 h, showing that the lithio species **168** is stable in thf. The Cp signals in the ^1H NMR spectrum of species **169** (δ = 3.96, 4.23 ppm in $CDCl_3$)[116] and **170** (δ = 3.66, 3.75, 3.81, 3.83 ppm in CD_2Cl_2)[117] are very similar to the four Cp signals of **167** (δ = 3.71, 3.90, 3.98, 4.27 ppm in $CDCl_3$). Therefore, the peaks of **167** at δ = 3.98 and 4.27 ppm were assigned to the tin-substituted Cp ring, whereas those at δ = 3.71 and 3.90 ppm were assigned to the nitrogen-substituted Cp ring (Figure 2.9).

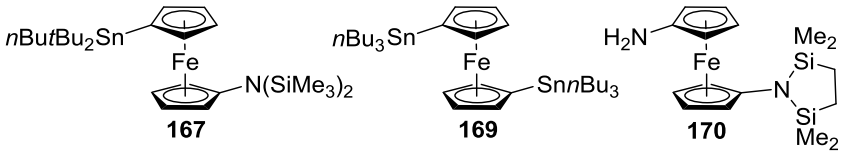

Figure 2.9. Compound **167** and related known species.

A similar ring-opening reaction was also performed with compound **161** when its thf solution was treated with one equivalent of *n*BuLi and after 1 h an excess amount of Me_3SiCl was added. The ^1H NMR spectrum of the reaction mixture indicated the presence of ring-opened product **171** along with the left-over starting material **161** (Scheme 2.30). The Cp signals of compound **171** (δ = 3.71, 3.90, 4.04, and 4.24 ppm) are very similar to those of compound **167**.

Therefore, the peaks at δ = 3.71 and 3.90 ppm could be assigned to the $N(SiMe_3)_2$-substituted Cp ring, whereas the peaks at δ = 4.04 and 4.24 ppm were assigned to silicon-substituted Cp ring.

Scheme 2.30. Anionic Ring-opening Reaction of Compound 161

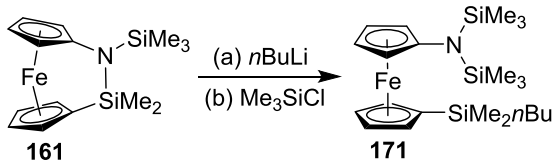

161 **171**

Attempt to polymerize compound **165** by addition of 0.25 equivalents of *n*BuLi in thf solution, followed by quenching with Me_3SiCl resulted in a mixture containing the unreacted starting material, ring-opened compound **167**, and protonated ring-opened compound **172** (Scheme 2.31). On the other hand, a similar reaction with compound **161** resulted only the unreacted starting material and ring-opened product **171** (Scheme 2.31). In order to ensure that the formation of protonated compound **172** was not caused by human error, two simultaneous reactions on compound **165** with 1.0 and 0.25 equivalents of *n*BuLi were performed using the same reagents and solvents. Both the reactions were quenched by Me_3SiCl and reaction mixtures were analyzed by ^1H NMR spectroscopy. Similar to previous attempts, the batch with a full equivalent of *n*BuLi showed only the ring-opened compound **167**, and the reaction with sub-stoichimetric amount of *n*BuLi resulted in a mixture of residual **165**, ring-opened products **167**, and **172** (Scheme 2.31). In addition to ^1H NMR spectroscopy, the mass spectrometric measurements confirmed these results.

Scheme 2.31. Attempted Anionic ROP on Compounds 165 and 161

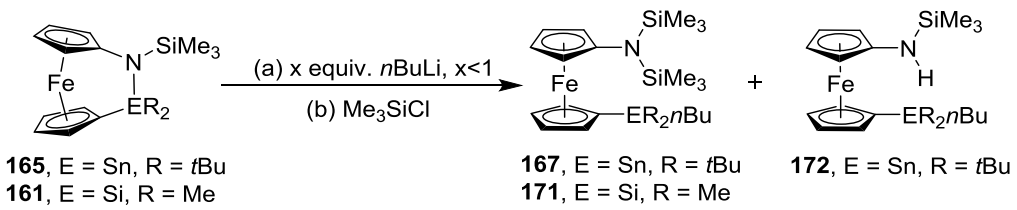

165, E = Sn, R = *t*Bu
161, E = Si, R = Me

167, E = Sn, R = *t*Bu
171, E = Si, R = Me

172, E = Sn, R = *t*Bu

Thus the polymerization attempts using common ring-opening conditions did not result in any polymeric materials. While the silicon-bridged species **161** was thermally robust at 300 °C, the corresponding tin species **165** decomposed at 260 °C. Using a 1:1 ratio of anionic initiator the tin-bridged species **165** cleanly gave the ring-opened product, while the similar condition afforded a sluggish ring-opening reaction for its silicon counterpart **161**. Using sub-stoichiometric amounts of the anionic initiator both of these compounds resulted in a mixture of ring-opened species and unreacted starting materials. These results lead to the following conclusions. First, $n\text{Bu}^-$ reacted with the starting materials (**161** and **165**) and transformed them into anionic species **168** and **173** (Scheme 2.32). These species are equipped with a sterically encumbered $(Me_3Si)N^-$ group, which failed to further react with other monomers. That means that the initiation step for the attempted polymerization worked, but the ring-propagation did not occur.

Scheme 2.32. Anion Initiated Ring-opened Intermediates from Compounds 161 and 165

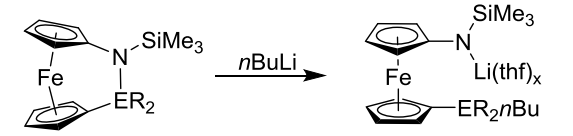

161, E = Si, R = Me
165, E = Sn, R = *t*Bu

173, E = Si, R = Me
168, E = Sn, R = *t*Bu

One possible way to increase the reactivity of [2]FCPs towards anionic ROP was using a less bulky alkyl substituent on nitrogen. To test this hypothesis, an azastanna[2]ferrocenophane

with a neopentyl group on nitrogen was synthesized and its reactivity under anionic conditions was studied.

2.3.5. Azastanna[2]ferrocenophane with Reduced Bulk on Nitrogen (174)

As illustrated in scheme 2.33, 1-bromo-1'-(neopentylamino)ferrocene (**149**) was first dilithiated and reacted with a dilute solution of tBu$_2$SnCl$_2$ at 0 °C. The ^{1}H NMR spectrum of the reaction mixture, taken after 1 h of stirring at ambient temperature, showed a clean conversion of the starting material to the intended product **174**. When the crude product was subjected to crystallization at -78 °C, compound **174** was obtained as red crystals which were contaminated with a small amount of an unknown impurity (Scheme 2.33).

Scheme 2.33. Synthesis of 2,2-Di-*tert*-butyl-1-neopentyl-1,2-azastanna[2]ferrocenophane (174)

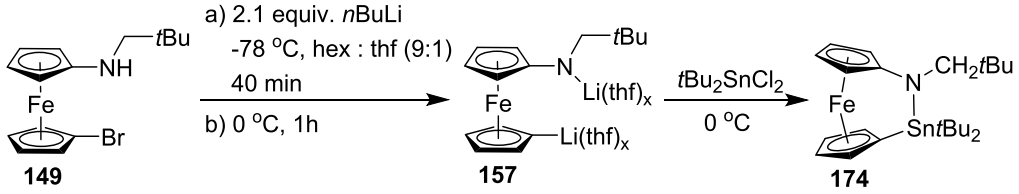

The ^{1}H NMR spectrum of the isolated product shows four equally intense peaks at δ = 3.80, 4.23, 4.57, and 4.72 ppm, which are caused by four pairs of Cp protons. The *tert*-butyl groups on tin appear as a high-intensity singlet at δ = 1.44 ppm, accompanied by two small satellite peaks which are due to Sn^{117} and Sn^{119} isotopes. The neopentyl group on nitrogen shows a singlet for nine hydrogens at δ = 0.89 ppm and another low-intensity singlet for two hydrogens at δ = 3.02 ppm. The ^{13}C NMR spectrum of compound **174** shows four high-intensity singlets in the Cp region at δ = 65.0, 68.7, 70.8, and 77.7 ppm, which indicate that the molecule is C_s symmetric. The *ipso* carbon, substituted with the tBuCH$_2$N group, appears as a small peak at δ = 121.9 ppm. The

isolated product contains a small amount of unknown impurity which shows singlets at δ = 1.46 ppm and 30.7 ppm in ^{1}H and ^{13}C NMR spectra, respectively. As the strained compound **174** could not be isolated in an analytically pure form, this partially purified product was used in subsequent reactions.

2.3.6. Investigation of Anionic Ring-opening Polymerization of Compound 174

In order to evaluate the possibility of anionic ROP, the corresponding ring-opening reaction was first investigated for compound **174**. In a thf solution of this monomer one equivalent of *n*BuLi was added and the reaction mixture was left at room temperature for 4 h. After quenching the reaction mixture with excess amount of Me_3SiCl, the reaction mixture was analyzed by ^{1}H NMR spectroscopy which revealed an incomplete conversion to the ring-opened product **175** (Scheme 2.34). As repeated attempts with 1.0, 1.1, and 1.5 equivalents of *n*BuLi could not significantly improve the quality of the ring-opening reaction, a test anionic ROP was performed with 0.5 equivalent of anionic initiator on **174**. Again, no signs of polymeric material were observed in either the ^{1}H NMR or the mass spectrometric data.

Scheme 2.34. Anionic Ring-opening Reaction and Attempted Polymerization of Compound 174

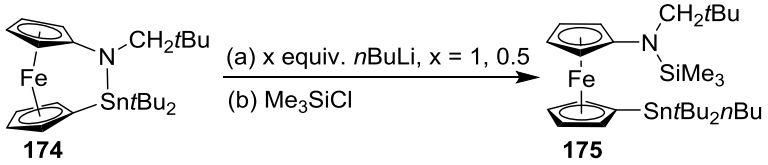

174 **175**

2.4. Aza[2]ferrocenophanes with Phosphorus in the Bridging Position

The measured α angles of the group-14-bridged aza[2]ferrocenophanes were in the range of 10 to 16°, which indicates a presence of low to moderate intrinsic strain. This could be a potential reason behind the unsuccessful ring-opening polymerization of strained compounds **161**, **165**, and **174** (Scheme 2.31 and 2.34). In order to test this speculation, new aza[2]ferrocenophanes with higher molecular strain were required. The easiest way to achieve this goal is to incorporate smaller elements in the bridging position. Due to having a lower covalent radius than silicon, phosphorus [covalent radii: Si 1.11(2) Å; P 1.07(3) Å] was chosen as a candidate.[57] Moreover, the fact that the known phospha[1]ferrocenophanes are capable to ring-open polymerize in a living fashion was another motivation to prepare azaphospha[2]ferrocenophanes.[118]

The majority of the results discussed in Section 2.4, except the synthesis and characterization of compound **179**, can be found in our recent publication.[112]

2.4.1. Azaphospha[2]ferrocenophane (176)

To test if the azaphospha[2]ferrocenophanes are accessible, a trial reaction was performed with starting material **142** (Scheme 2.35). Following some reported synthesis of phospha[1]ferrocenophanes, *t*BuPCl$_2$ was chosen as a reagent for the salt-metathesis reaction.[18,118] As illustrated in Scheme 2.35, compound **142** was first dilithiated and *in situ* reacted with a stoichiometric amount of *t*BuPCl$_2$ at 0 °C. The ^{1}H NMR spectrum of the reaction mixture, taken after 1 h of stirring at ambient temperature, show that the clean conversion of the starting material to the intended product has occurred (see Figure 2.10). After removal all the volatiles, the crude product was further purified by flask-to-flask condensation and compound **176**, contaminated with a small amount of an unknown impurity, was collected as a dark red oil. The ^{1}H NMR spectrum

of the isolated product shows eight equally intense signals at δ = 3.67, 3.73, 3.98, 4.15, 4.88, 4.94, 5.10, and 5.18 ppm in the Cp region, indicating that the molecule has no symmetry. These signals can further be divided into two major groups where each group consists of four peaks. The group with lower chemical shifts (δ = 3.67, 3.73, 3.98, and 4.15 ppm) results from protons of the Me_3SiN-substituted Cp ring, whereas that with higher chemical shifts (δ = 4.88, 4.94, 5.10, and 5.18 ppm) is caused by the P*t*Bu substituted Cp. The aforementioned assignment was done with the help of additional (HMQC and COSY) NMR experiments and increment method to assign ^{1}H NMR peaks for 1,1'-disubstituted ferrocene derivatives.[119] The protons of the *tert*-butyl group are coupled with phosphorus and, therefore, found as a doublet at δ = 1.35 ppm with a coupling constant of J = 12.5 Hz; the Me_3Si group on nitrogen shows a singlet at δ = 0.26 ppm.

Scheme 2.35. Synthesis of 2-*tert*-Butyl-1-trimethylsilyl-1,2-azaphospha[2]ferrocenophane (176)

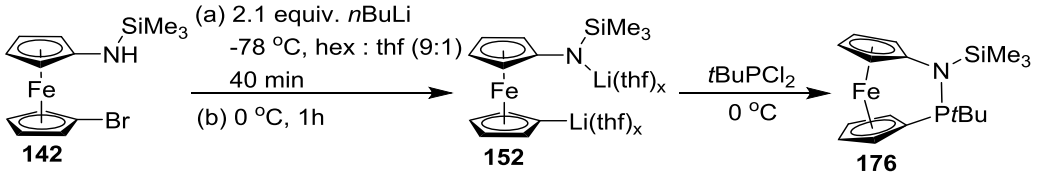

The effect of phosphorus is easily noticeable in ^{13}C NMR spectrum, as many of the P*t*Bu-substituted Cp carbons couple with phosphorus and appeared as doublets with coupling constants in a range of J = 5 to 37 Hz. The primary and tertiary carbons of the *tert*-butyl group also couple with phosphorus and show doublets at δ = 28.7 (J = 18 Hz) and 33.9 (J = 29 Hz) ppm, respectively. The phosphorus of compound **176** appears as a singlet at δ = 147.8 ppm in the ^{31}P{^{1}H} NMR spectrum, which upon coupling with nine methyl protons of *tert*-butyl group converts into a decet (J = 12 Hz) in a proton coupled ^{31}P NMR experiment.

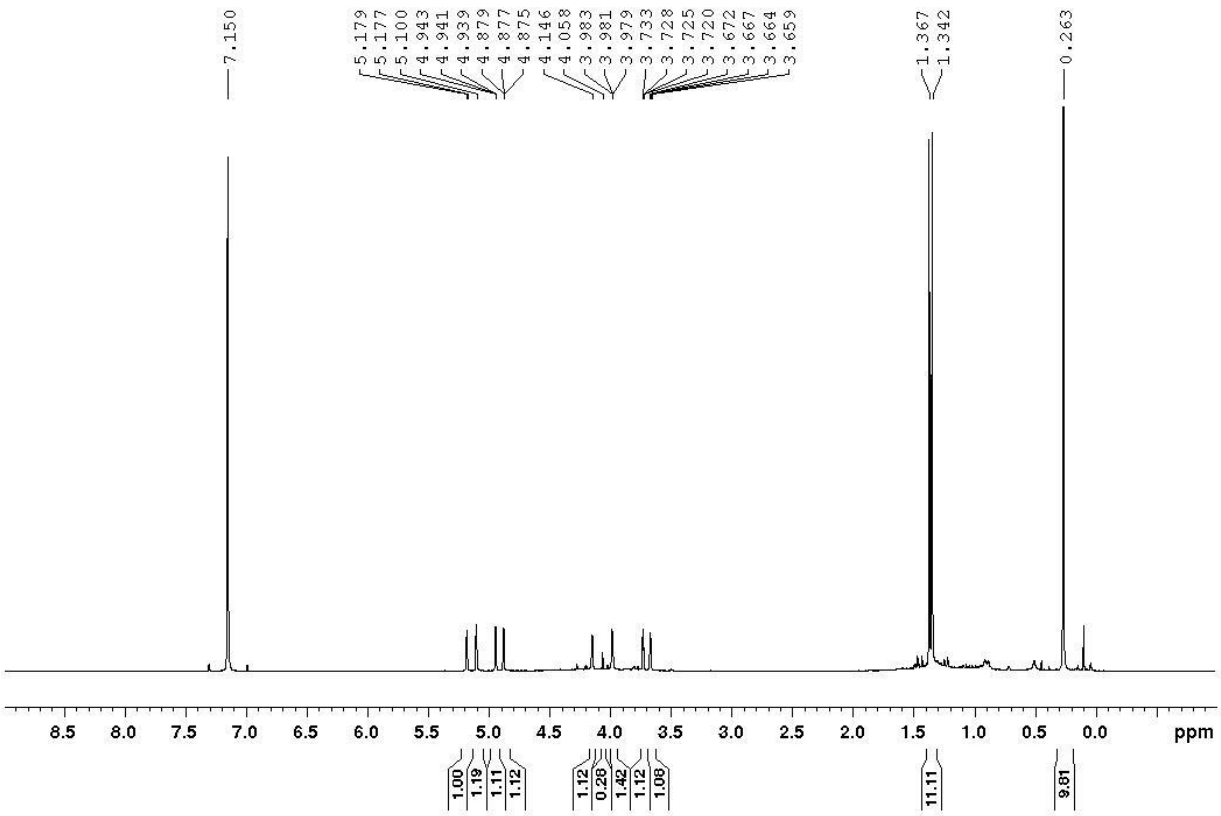

Figure 2.10. ^{1}H NMR spectrum (C_6D_6) of the reaction mixture to synthesize compound **176**. The sample for this spectrum was taken from the clear supernatant of the reaction mixture after 1 h of the addition of *t*BuPCl$_2$. The peak at δ = 4.06 ppm indicates the presence of (trimethylsilylamino)ferrocene (**140**) in the sample.

2.4.2. Sulfurization of Azaphospha[2]ferrocenophane (176)

As species **176** could not be isolated in an analytically pure form, column chromatography was attempted to further purify it. The first trial of purification via column chromatography resulted in decomposition of compound **176** on column material. Therefore, compound **176** was further sulfurized. As illustrated in Scheme 2.36, compound **176** was first dissolved in CH_2Cl_2 and oxidized with an excess amount of elemental sulfur. However, the chromatographic separation on silica gel afforded the targeted compound **177** as minor product and its desilylated counterpart **178**

as major product. Vacuum sublimation of compound **178** led to single crystals which were suitable for X-ray crystallography. In contrast to **178**, species **177** was obtained as a red, waxy solid by vacuum sublimation.

Scheme 2.36. Sulfurization of Compound 176 and Colum Chromatography

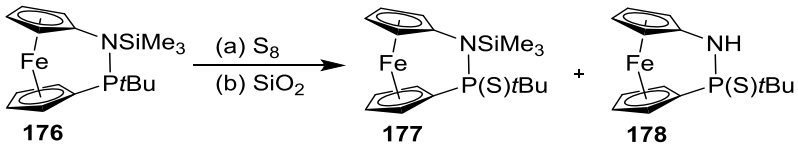

176 **177** **178**

In ^{1}H NMR spectra both compounds **177** and **178** show a similar pattern of the Cp signals as **176**, which supports that these molecules are asymmetric on the NMR timescale (500 MHz) at ambient temperature. The ^{31}P{^{1}H} NMR spectra of compounds **177** and **178** show singlets at δ = 110.4 and 106.1 ppm, respectively. The proton coupled ^{31}P NMR spectrum of compound **177** shows a decet at δ = 110.4 ppm with a coupling constant of J = 18 Hz, which is due to the coupling of phosphorus with the protons of the *tert*-butyl group. On the other hand, in a similar NMR measurement, the phosphorus atom of compound **178** couples with both the *tert*-butyl group and the neighboring amino proton to give an unresolved multiplet at δ = 106.1 ppm.

While Figure 2.11 depicts the molecular structure of compound **178**, the crystal and structural refinement data of the corresponding species can be found in Table 2.3. A comparison of the measured distortion angles of compounds **161**, **165**, and **178** is depicted in Table 2.4. The tilt angle α for this compound was measured as 18.40(11)° which is ca. 3° to 8° larger than those of sila- and tin-bridged aza[2]ferrocenophanes, respectively [**161**, α = 15.73(11)°; **165** , α = 10.13(11)°].[104,112] Like all three previously measured compounds (**161**, **162**, and **165**, Section 2.3), the β angle in species **178** for phosphorus-substituted Cp ring is significantly higher than that of the other Cp ring. This can be explained with a simple mechanical model. One can envision that

the bridging N-E (E = Si, Sn, P) bond puts a certain force toward each Cp ring through lever arms, where the N-Cp bond is the shorter and the N-E bond is the longer lever arm. If one assumes that the bridging N-E moiety puts the same force on both the lever arms, the longer lever arm will bend more than the shorter one. However, the chemical bonds are not hard sticks and one can argue that the analogy of the above described mechanical model is too simple to be realistic.[114]

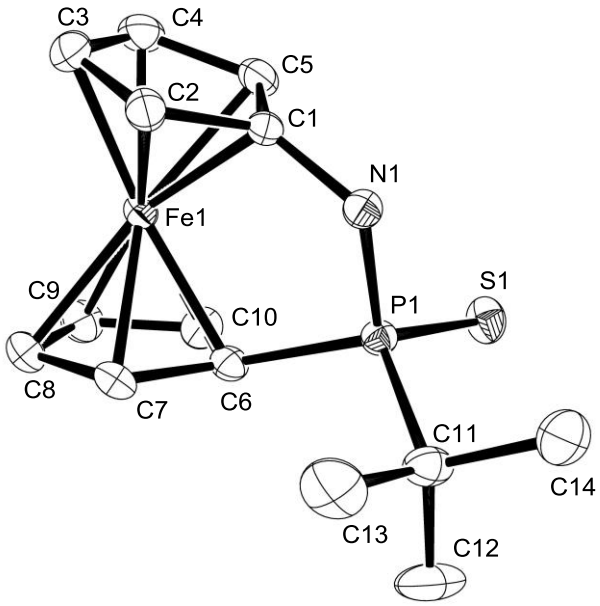

Figure 2.11. Molecular structure of **178** with thermal ellipsoids at 50% probability level. Hydrogen atoms are omitted for clarity. Selected bond lengths [Å] and bond angles: C1-N1 = 1.4425(19); P1-N1 = 1.6835(14); S1-P1 = 1.9678(6); P1-C6 = 1.8094(17); P1-C11 = 1.841(2); C1-N1-P1 = 115.48(11); C6-P1-C11 = 109.75(8); C6-P1-S1 = 110.94(6); C6-P1-N1 = 102.53(7); N1-P1-S1 = 114.96(6); N1-P1-C11 = 106.30(8); C11-P1-S1 = 111.84(7). This figure is reprinted with permission from Dey, S.; Sun, W.; Müller, J. *Inorg. Chem.* **2016**, *55*, 3630-3639. Copyright 2016 ACS.

Table 2.3. Crystal and Structural Refinement Data for Compound 178

Parameters	**178**
empirical formula	$C_{14}H_{18}FeNPS$
fw	319.18
cryst. size / mm^3	0.100 × 0.200 × 0.200
cryst. system, space group	monoclinic, C2/c
Z	8
a / Å	20.4077(4)
b / Å	10.9902(2)
c / Å	15.5010(4)
α / °	90
β / °	124.565(2)
γ / °	90
volume / $Å^3$	2862.95(12)
ρ_{calc} / g cm^{-3}	1.481
temperature / K	173(2)
μ_{calc} / mm^{-1}	1.292
θ range / °	2.21 to 29.01
completeness / %	99.8
reflns collected / independent	26643 / 3791
absorption correction	multi-scan
data [$F_o^2 \geq -3\sigma(F_o^2)$] / restraints / params	3791 / 0 / 166
goodness-of-fit	1.075
R_1 [I > 2 σ(I)] [a]	0.0273
wR_2 (all data) [a]	0.1279
largest diff. peak and hole, $\Delta\rho_{elect}$ / e $Å^{-3}$	0.772 and -1.081

[a] $R_1 = [\Sigma||F_o|-|F_c||]/[\Sigma|F_o|]$ for $[F_o^2 > 2\sigma(F_o^2)]$, $wR_2 = \{[\Sigma w(F_o^2-F_c^2)^2]/[\Sigma w(F_o^2)^2]\}^{1/2}$ [all data]

Table 2.4. Distortion Angles [°] in Aza[2]ferrocenophanes

Numerical acronym	α	β / β' [a]	δ	τ
178	18.40(11)	10.38(15) / 17.10(13)	167.61(2)	20.14(14)
165	10.13(11)	2.31(16) / 18.52(12)	172.50(2)	8.08(4)
161	15.73(13)	6.53(18) / 17.38(15)	168.62(2)	3.31(13)

[a] β for E = N and β' for E = Sn, Si or P (see also Figure 1.2 in the Chapter Introduction).

For a successful ring-propagation, smaller substituents were needed both on bridging nitrogen and phosphorus. Therefore, in order to synthesize polymerizable azaphospha[2]ferrocenophane, an attempt to reduce the steric bulk on phosphorus was done. As phenyl is flat compared to the bulky *tert*-butyl group, $PhPCl_2$ was selected as a reagent for the salt-metathesis reaction. The silylated 1-amino-1'-bromoferrocene **142** as the mostly explored starting material in our chemistry was chosen for this investigation.

2.4.3. An Azaphospha[2]ferrocenophane with Reduced Bulk on Phosphorus (179)

As illustrated in Scheme 2.37, compound **142** was first dilithiated and *in situ* reacted with a dilute solution of $PhPCl_2$ at 0 °C. The ^{1}H NMR spectrum of the reaction mixture, taken after 3 h of stirring at ambient temperature, showed the targeted compound **179** as a major product and oligomeric material **180** as the minor product. Although compound **180** was not isolated and characterized, its presence can clearly be observed from the broader resonances in ^{1}H NMR spectrum of the reaction mixture (see Figure 2.12). The oligomeric species **180** was further evidenced by mass spectrometric measurements of the reaction mixture, which showed peaks for higher molecular weights than that expected for **179**. The formation of compound **180** can be rationalized in a similar way as it was done for compound **163** in Section 2.3.2. Phenyl, being a flat ligand, is unable to provide sufficient steric shielding on phosphorus and, therefore, could not

produce the strained compound (**179**) selectively. Consequently, a part of the dilithiated starting material **152** underwent an intermolecular condensation reaction and gave the oligomers **180**. However, the flask-to-flask condensation from the resulting crude material afforded compound **179** as an analytically pure species in a yield of 64% (Scheme 2.37).

Scheme 2.37. Synthesis of 2-Phenyl-1-trimethylsilyl-1,2-azaphospha[2]ferrocenophane (179)

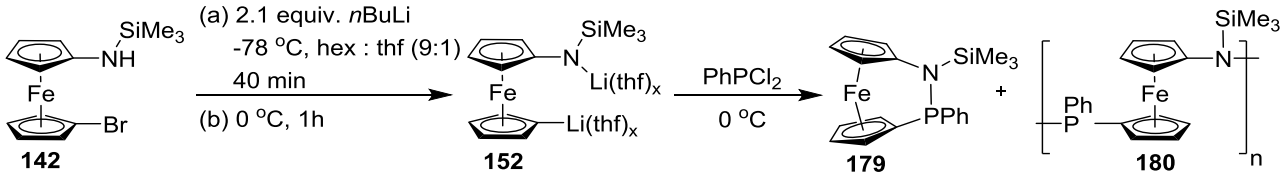

The ^{1}H NMR spectrum of compound **179** shows eight equally intense signals (δ = 3.60, 3.61, 3.78, 4.20, 4.59, 4.91, 5.07, and 5.26 ppm) in the Cp region, which indicate that the molecule is asymmetric. In the proton-coupled ^{31}P NMR spectrum of **179** the phosphorus appeared as a singlet at δ = 120.9 ppm, indicating no coupling with any of the neighboring phenyl protons.

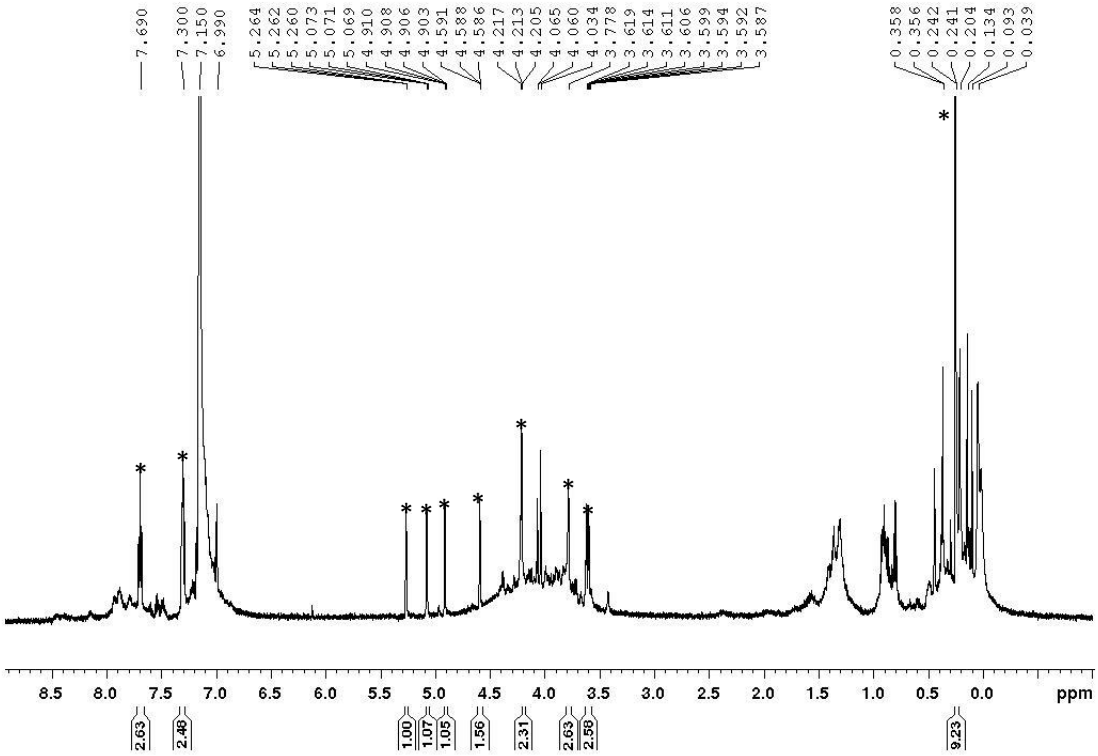

Figure 2.12. ^{1}H NMR spectrum (C_6D_6) of the reaction mixture to synthesize compound **179**. The peaks marked by * are resulting from compound **179**. The sample for this spectrum was taken from the clear supernatant of the reaction mixture after 3 h of the addition of $PhPCl_2$.

As our previous investigation suggested that Me_3Si group reduces the propensity of polymerization (see Section 2.3.4), attempts to use smaller alkyl substituents on nitrogen were undertaken. Accordingly, the two alkyl-substituted aminobromoferrocenes **147** and **149** were employed as starting compounds to synthesize new azaphospha[2]ferrocenophanes. However, in this investigation we stumbled across surprising results and it turned out that the preparation of these species was not as straightforward as anticipated.

2.4.4. Attempts to Synthesize Azaphospha[2]ferrocenophanes with Reduced Bulk on Nitrogen (181 and 186)

As shown in Scheme 2.38, the *in situ* prepared dilithio derivative of compound **147** was reacted with stoichiometric amount of *t*BuPCl$_2$ and the reaction mixture was analyzed by ^{1}H and ^{31}P NMR spectroscopy. Careful inspection of the proton and phosphorus signals showed that a mixture of the three constitutional isomers **181**, **182**, and **183** was present. However, the target compound **181** was present in a very small amount and could not be isolated from the reaction mixture. The 1,1'-disubstituted ferrocene derivative **182** was resulted as a major product in this reaction. Along with these two compounds a [3]FCP **183** was also present in the reaction mixture. However, when the crude material was dissolved in Et$_2$O and the solution was left at room temperature, species **182** slowly transformed into the [3]FCP **183**, while the target compound **181** remained unchanged. This transformation was evident from ^{1}H and ^{31}P NMR spectra measured from aliquots of the reaction mixture after certain time intervals.[112] Detailed characterization and assignments of the relative configuration of compound **183** can be found in Section 2.4.5.

Scheme 2.38. Attempted Synthesis of 1-Benzyl-2-*tert*-butyl-1,2-azaphospha[2]ferrocenophane (181)

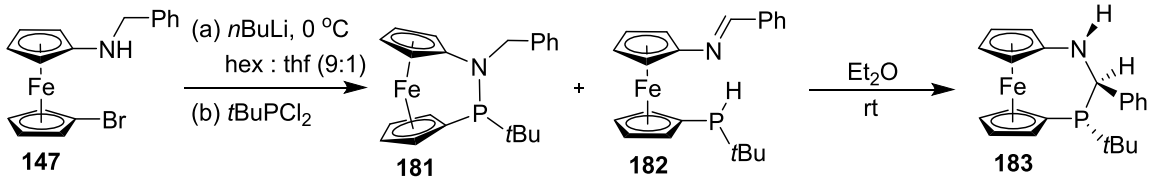

A comparative study, using proton-coupled ^{31}P NMR spectra measured from the reaction mixture after 1.5 and 4.5 h of addition of *t*BuPCl$_2$, clearly revealed that the transformation from **182** to **183** occurred (Figure 2.13).

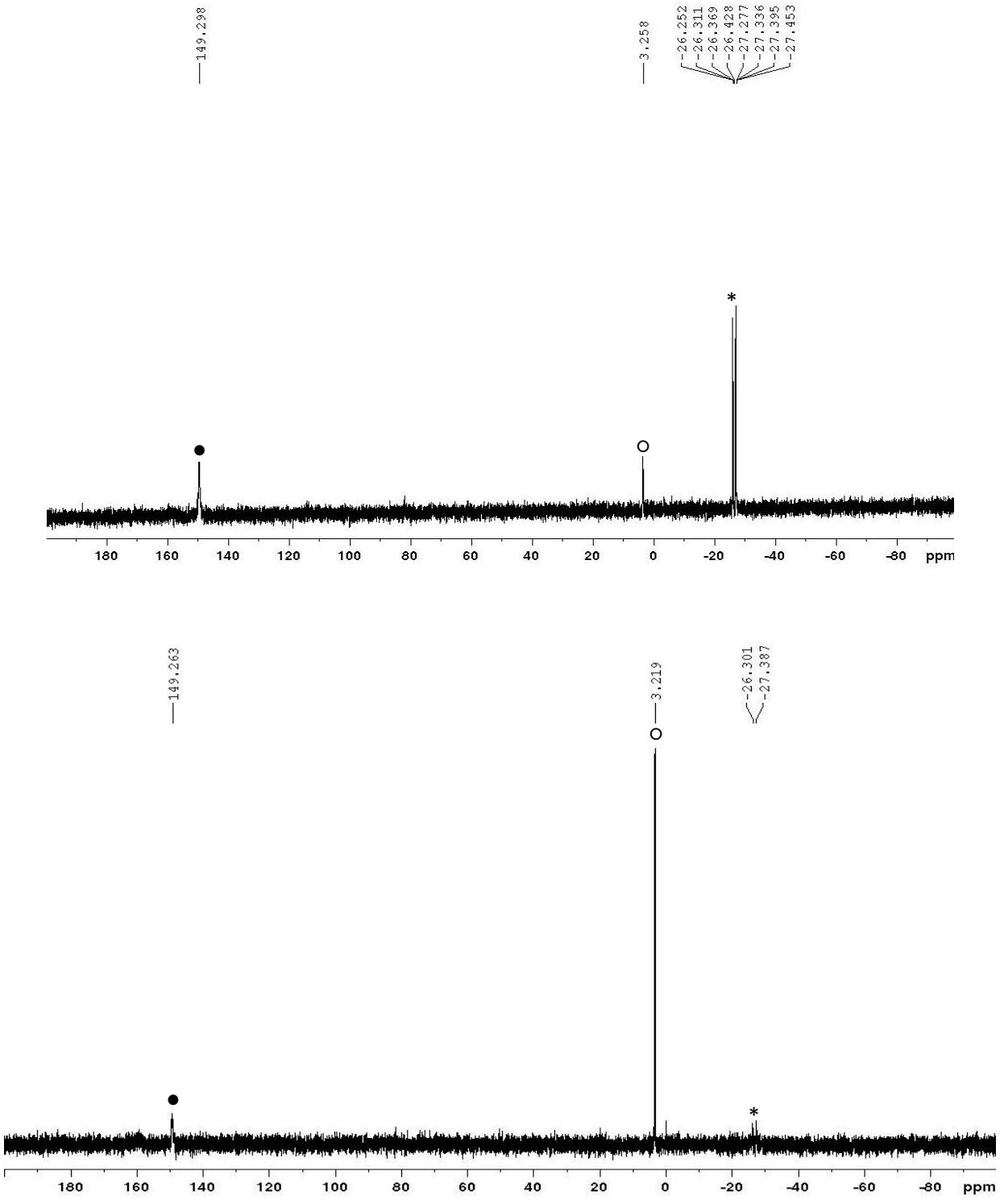

Figure 2.13. Proton coupled ^{31}P NMR spectrum of the isolated crude reaction mixture after 1.5 h (top) and 4.5 h (bottom) of addition of *t*BuPCl$_2$. Peaks for compounds **181**, **182**, and **183** are marked with ●, *, and ○, respectively.

The ^{1}H NMR spectroscopic data revealed that [2]FCP **181** did not isomerize into **182**, while **182** isomerized into **183**. Therefore, it can be concluded that the salt-metathesis reaction proceeded in two parallel and independent reaction channels: one resulted in the targeted compound **181** and the other gave the 1,1'-disubstituted ferrocene derivative **182**. Although we do not have enough experimental evidence to fully understand the reason of formation of **182**, a tentative reaction sequence can be proposed (Scheme 2.39).

Scheme 2.39. Illustration of Two Parallel Reaction Channels of the Salt-metathesis Reaction

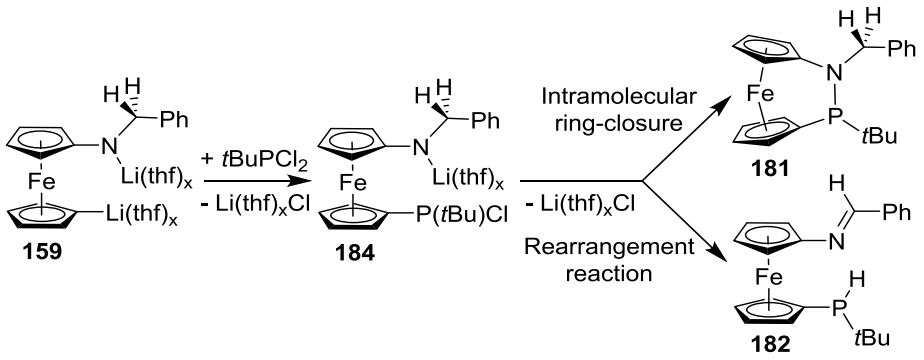

Among the two lithiated sites of species **159**, the carbanion $C_5H_5^-$ is far more nucleophilic than the amide. Therefore, after the first reaction with one equivalent of *t*BuPCl$_2$, species **159** gives a monolithiated intermediate **184** which can either yield the targeted species **181** through a ring-closure reaction, or can produce **182** by following an unknown rearrangement reaction. However, in this case, the experimental evidence showed that the molecular rearrangement prevailed over the ring-closure reaction and, therefore, **182** was formed as the major product (Scheme 2.39). To our best knowledge, no example of similar rearrangement reaction has been reported in the literature.

Even though compounds **181** and **182** could not be isolated as analytically pure species, their formation was unequivocally identified by different NMR experiments. The proton-coupled ^{31}P NMR spectrum of the reaction mixture taken after 1.5 h of addition of *t*BuPCl$_2$ shows three major peaks: one intense doublet of decets at δ = -26.9 ppm and two small multiplets at δ = 3.2 and 149.3 ppm (see Figure 2.13). A comparison of the NMR values suggested that the peak at δ = 149.3 ppm, which is closely related to our previously synthesized [2]FCP **176** (δ = 147.8 ppm), is resulting from compound **181**. As a result of coupling with P*H* proton and the protons of *tert*-butyl group, the phosphorus in compound **182** appears as a doublet of decets at δ = -26.9 ppm (J = 208 and 12 Hz). The unexpected product **182** could also be identified by ^{1}H NMR spectroscopy. While the pattern of the Cp signals indicates that this compound is C_1 symmetric, a singlet at δ = 8.54 ppm shows close similarity with N*H*Ph peak of species **143** (Scheme 2.17) and, therefore, implies the presence of imine proton (N*H*Ph). The signal at δ = 3.65 ppm with an apparent relative intensity of half a hydrogen atom can be interpreted as being part of the doublet resulting from a P*H*tBu proton. The second peak of this doublet was more difficult to find as it overlaps with one Cp signal at δ = 4.06 ppm. Due to the coupling with the phosphorus atom the distance between the two peaks of this doublet is 0.95 ppm equivalent to a coupling constant of 206.0 Hz.[120]

The unexpected formation of 1,1'-disubstituted ferrocene **182** surprised us. It is possible that the presence of six π electrons of the phenyl group of **147** has an unknown electronic effect on the reaction. To explore this possibility, a test reaction was performed using the neopentyl substituted starting material **149**. As illustrated in Scheme 2.40, the *in situ* prepared dilithio salt of compound **149** was reacted with stoichiometric amounts of *t*BuPCl$_2$. However, in this case the 1,1'-disubstituted ferrocene derivative **185** was formed exclusively (see Figure 2.14). No evidence of the targeted [2]FCP **186** was found in ^{1}H and ^{31}P spectra of the crude reaction mixture. Species

185 did not further transform into the [3]FCP **187** on prolonged standing at room temperature or heating at 80 °C in toluene solution. Due to the low reactivity of the 1,1'-disubstituted ferrocene derivative **185**, this compound could be isolated in analytical pure form and, therefore, characterized by standard techniques.

Scheme 2.40. Attempted Synthesis of 1-Neopentyl-2-*tert*-butyl-1,2-azaphospha[2]ferrocenophane (186)

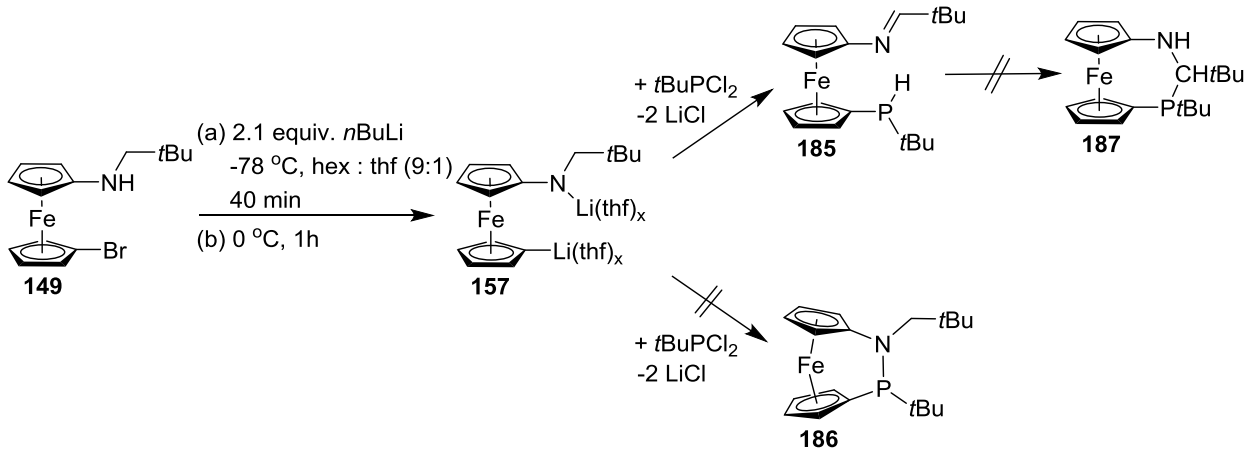

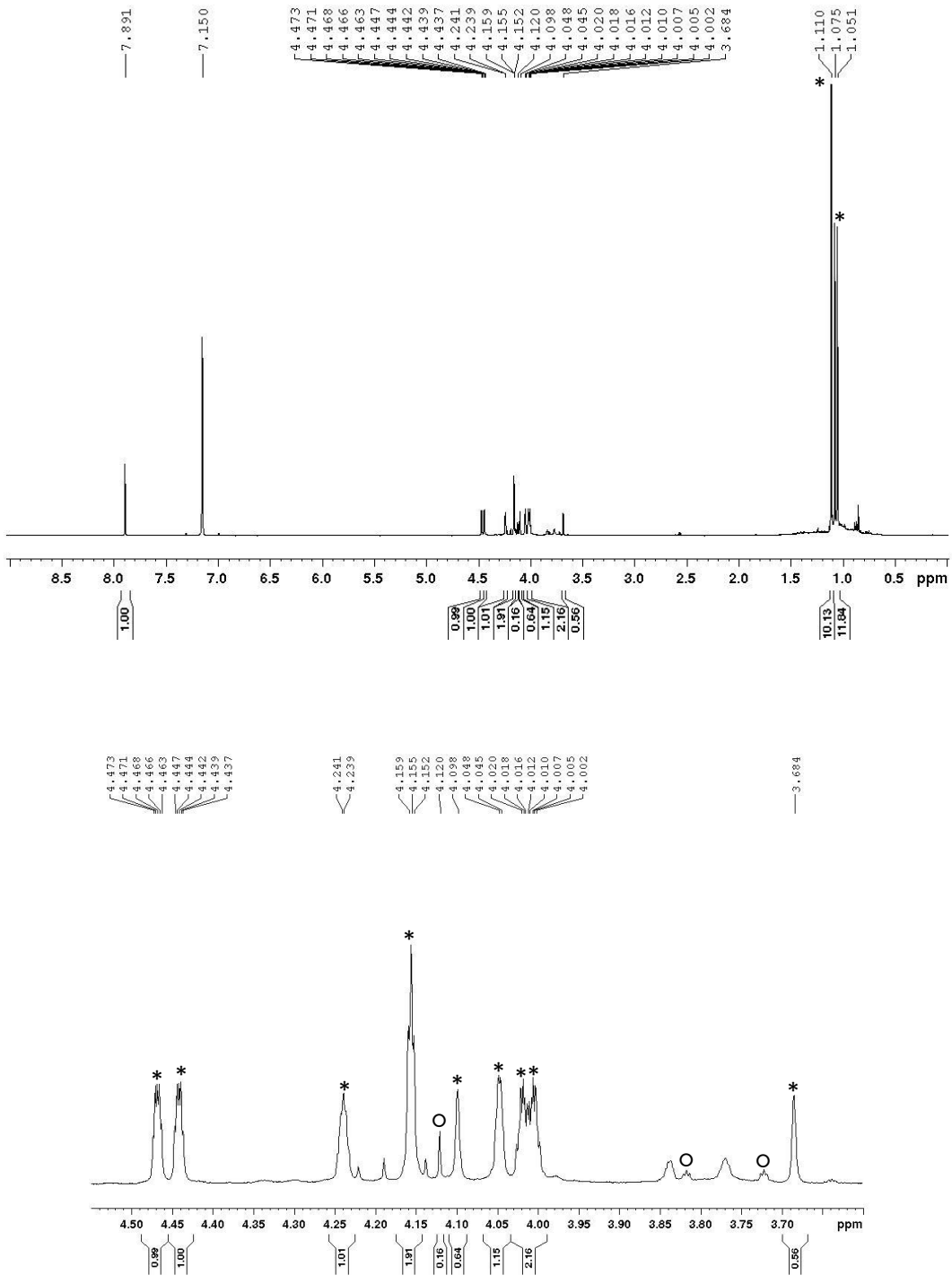

Figure 2.14. Full (top) and extended (bottom) view of ^{1}H NMR spectrum (C_6D_6) of the reaction mixture of the attempted preparation of **186** that resulted in species **185**. Peaks marked by * indicate the signals of compound **185**, whereas those marked by ○ indicate the signals of (neopentylamino)ferrocene.

The ^{1}H NMR spectrum of compound **185** shows six equally intense Cp signals (δ = 4.01, 4.02, 4.05, 4.24, 4.44, 4.47 ppm), each having relative intensity for one proton and a broad singlet (δ = 4.16 ppm) having the relative intensity for two Cp protons. This pattern indicates that no symmetry element is present in the molecule and, therefore, the molecule is C_1 symmetric. The widely spaced doublet at δ = 3.89 ppm (J = 207.0 Hz) and a singlet at δ = 7.89 ppm reveals that compound **185** has PH*t*Bu and NCH*t*Bu moieties. The presence of the PH*t*Bu group is further supported by a proton coupled ^{31}P NMR spectrum, which shows a doublet of decets at δ = -26.7 ppm with coupling constants of J = 208 and 12 Hz. The observed correlations in NOE measurements between NC*Ht*Bu and α-H protons of Cp^{NCHtBu} reveal that the *trans* isomer of compound **185** was formed in this reaction (Figure 2.15).

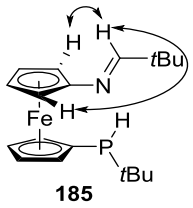

185

Figure 2.15. Selected observed NOE correlations of compound **185** are shown by ↔. Correlations between the Cp protons have been omitted for clarity.

2.4.5. Characterization and Relative Configuration of Azacarbaphospha[3]ferrocenophane (183)

As mentioned above, species **182** was not stable and quantitatively transformed into compound **183** by a non-catalyzed intramolecular hydrophosphination over the course of three hours at room temperature. A comparable intermolecular hydrophosphination has been reported as an equilibrium reaction.[121] A minimum-to-no control over the diastereomeric ratios has been reported for non-catalyzed intermolecular hydrophosphination reactions.[122] There is a current interest of transition-metal-catalyzed hydrophosphination and related bond-forming reactions to

synthesize new phosphorus containing species.[123] A comprehensive review of this field is beyond the scope of this thesis and the readers are being referred to a recent review article.[124]

The newly formed compound could be identified as the [3]FCP **183** by the following tests. First, a mass spectrometric measurement of the reaction mixture containing compound **183** showed the molecular ion peak at 377 amu which would have also been expected for strained species **181** and 1,1'-disubstituted ferrocene **182**. This result indicated that compounds **181**, **182**, and **183** are constitutional isomers. The proton-coupled ^{31}P NMR spectrum, measured from the reaction mixture after 4.5 h of addition of *t*BuPCl$_2$, shows an intense multiplet at δ = 3.2 ppm and a small doublet of decets at δ = -26.9 ppm (see Figure 2.13). This indicates that the PH*t*Bu group, which was causing an intense doublet of decet at δ = -26.9 ppm, has lost the PH proton in the transformation. Moreover, a doublet at δ = 2.23 ppm (J = 12.5 Hz) and a doublet of doublets at δ = 4.20 ppm (J = 12.5 and 5.5 Hz) in the ^{1}H NMR spectrum strongly suggests that a NH-CH(Ph)-P moiety is present in the molecule. The observed coupling constants indicate that the proton on the bridging carbon couples with both amino proton and neighboring phosphorus. Collecting all these evidences, it can be concluded that the newly formed species was the azacarbaphospha[3]ferrocenophane (**183**). Column chromatography and recrystallization of the resulting crude mixture gave compound **183** as a partially pure species. As no suitable single-crystals could be grown for X-ray crystallography, the relative configuration of this compound was determined by ^{1}H-^{1}H COSY and a series of selective gradient NOE measurements (Figure 2.16).

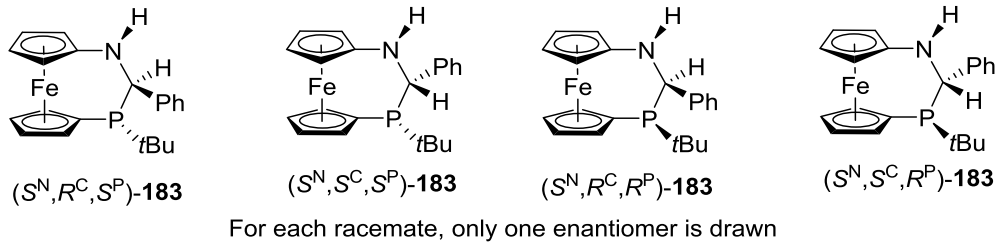

Figure 2.16. Possible diastereomers of compound **183**. This figure is reprinted with permission from Dey, S.; Sun, W.; Müller, J. *Inorg. Chem.* **2016**, *55*, 3630-3639. Copyright 2016 ACS.

Eight stereoisomers could be possible for compound **183**. Among the four racemates only the set with *S* configuration on nitrogen are shown in Figure 2.16. The other racemates which are not shown in Figure 2.16 are (R^N, S^C, R^P)-**183**, (R^N, R^C, R^P)-**183**, (R^N, S^C, S^P)-**183**, and (R^N, R^C, S^P)-**183**. A series of measurements of NOE correlations suggest that compound **183** was a mixture of enantiomers (S^N, R^C, S^P)-**183** and (R^N, S^C, R^P)-**183**. As NOE correlation could not be observed between N*H* proton and the proton on the bridging carbon, it can be concluded that they are in *trans* position (Figure 2.17). A NOE correlation was detected between the bridging CH moiety and *tert*-butyl group on phosphorus, which led to the conclusion that they are *cis* to each other (Figure 2.17). Of course, one would expect that the stereochemical configuration of nitrogen was unstable and prone to rapid inversion at ambient temperature. This point will further be clarified in Section 2.4.6.

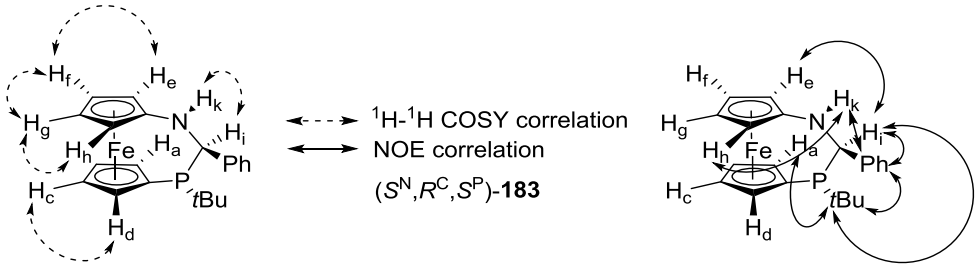

Figure 2.17. Results obtained from ^{1}H-^{1}H COSY experiment and selective gradient NOE experiments with compound (S^N,R^C,S^P)-**183**. Proton H_b of the Cp^{PtBu} was omitted for clarity. Observed ^{1}H-^{1}H COSY correlations of compound **183**: $H_i \leftrightarrow H_k$, $H_e \leftrightarrow H_f$, $H_f \leftrightarrow H_g$, $H_g \leftrightarrow H_h$, $H_c \leftrightarrow H_d$. The chemical shifts for H_a, H_b, and H_c are so close to each other that $H_b \leftrightarrow H_c$, $H_b \leftrightarrow H_a$ COSY correlations are overlapped with the symmetric diagonal base line. Observed NOE correlations of compound **183**: *t*Bu ↔ H of *o*-Ph, *t*Bu ↔ H_i, *t*Bu ↔ H_a, H_i ↔ *ortho*-H of Ph, H_i ↔ H_e, H_k ↔ *ortho*-H of Ph, $H_k \leftrightarrow H_h$. This figure is reprinted with permission from Dey, S; Sun, W.; Müller, J. *Inorg. Chem.* **2016**, *55*, 3630-3639. Copyright 2016 ACS.

The other three racemates were eliminated by comparing expected NOE correlations with observed ones. As no NOE correlation between NH and CH protons could be found, the presence of enantiomers (S^N, S^C, S^P)-**183** and (R^N, R^C, R^P)-**183** could be excluded. Similarly, the observed NOE correlation between the CH proton and the *tert*-butyl group led us to exclude species (S^N, R^C, R^P)-**183** and (R^N, S^C, S^P)-**183**. Finally, due to the lack of observed NOE correlations among NH, CH, and *tert*-butyl groups the racemate (S^N, S^C, R^P)-**183** and (R^N, R^C, S^P)-**183** was ruled out (see Figure 2.18). All these experimental findings were further complemented by DFT calculations.

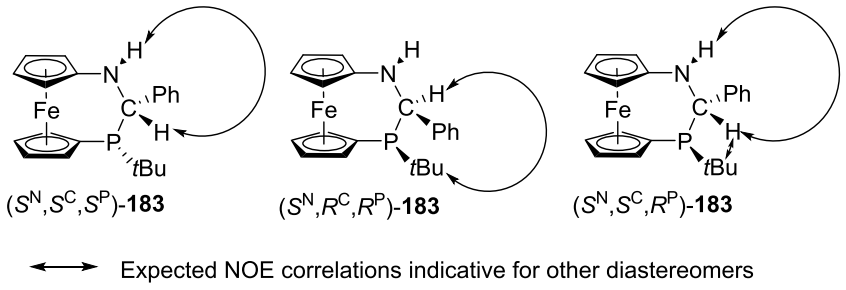

Figure 2.18. Indicative NOE correlations that are expected for the diastereomers (S^N,S^C,S^P)-**183**, (S^N,R^C,R^P)-**183**, and (S^N,S^C,R^P)-**183**, but were not found experimentally. This figure is reprinted with permission from Dey, S. Sun, W.; Müller, J. *Inorg. Chem.* **2016**, *55*, 3630-3639. Copyright 2016 ACS.

2.4.6. DFT Calculations for [2]FCPs (178, 181, 186), 1,1'-Disubstituted Ferrocenes (182, 185), and [3]FCP (183, 187)

In order to better understand the results, DFT calculation was performed. Geometries of compounds **178**, **181-183**, and **185-187** were optimized at the M06/6-311+G(d,p) level of theory.[125] Close similarities between the calculated and measured distortion angles of compound **178** (Table 2.4 and 2.5) indicated that the above mentioned level of theory was suitable to predict realistic molecular structures. The DFT calculations on all these compounds were done by Dr. Jens Müller.

Table 2.5. Calculated Common Angles [°] in [2]FCPs (178, 181, 186) and Different Diastereomers of [3]FCP (183)

Compounds	α	β [a]	β' [a]	δ	τ [b]
178[c]	18.01	10.30	17.02	168.17	21.48
181	17.93	8.56	13.86	167.96	3.07
186	18.15	8.72	13.23	167.92	2.40
(S^N,R^C,S^P)-**183**	7.14	1.19	8.17	174.55	-
(S^N,S^C,S^P)-**183**	5.81	1.12	13.36	175.55	-
(S^N,R^C,R^P)-**183**	7.30	0.83	7.21	174.02	-
(S^N,S^C,R^P)-**183**	7.75	3.40	6.52	173.85	-
(S^N,R^C,S^P)-**183**	9.49	2.96	5.52	172.87	-
(S^N,S^C,S^P)-**183**	7.68	3.18	11.88	174.56	-
(S^N,R^C,R^P)-**183**	7.63	3.26	6.88	173.72	-
(S^N,S^C,R^P)-**183**	7.96	3.51	5.98	173.98	-

[a] β for E = N and β' for E = P, [b] τ is not applicable for [3]FCPs, [c] Measured values for **178** are shown in Table 2.4. This table is reprinted with permission from Dey, S.; Sun. W; Müller, J. *Inorg. Chem.* **2016**, *55*, 3630-3639.

Figure 2.19 compares calculated $\Delta G°$ values for species **181-183** and **185-187**. Calculations for [2]- and [3]FCPs (**181**, **183**, **186**, and **187**) were straightforward, as the relative orientation of the two Cp rings were restricted by the *ansa* bridge; only one optimized geometry was obtained for each of these species. In contrast, the rotational freedom in species **182** and **185**, in particular with respect to the Cp rings, resulted in many optimized geometries of similar

energies. Furthermore, the imine group gave rise to *cis* and *trans* isomers, with the *trans* isomers being around 6 kcal mol^{-1} ($\Delta G°$) preferred over respective *cis* isomers. The fact that the *trans* isomers are significantly more stable was further supported by the experimental finding that showed species **185** and the imines **143** and **145** were obtained exclusively in their *trans* form (Figure 2.1 and 2.15). Moreover, the number of different molecular geometries for the 1,1'-disubstituted ferrocenes (**182** and **185**) was doubled as minima were found for two different positions of the imine group -N=CHR relative to the Cp ring. In Figure 2.19, only the most stable isomer for each species, **182** and **185**, is considered.

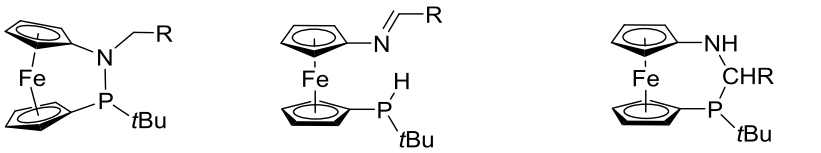

R = Ph (**181**)	*t*Bu (**186**)
0.00	0.00

R = Ph (**182**)	*t*Bu (**185**)
-6.62	-6.83

R = Ph (**183**)	*t*Bu (**187**)
(S^N,R^C,S^P): -7.64	-2.30
(S^N,R^C,R^P): -4.70	-1.58
(S^N,S^C,R^P): -2.00	0.35
(S^N,S^C,S^P): 1.69	7.84

For **182** and **185**, only the most stable isomer was considered

Figure 2.19. Differences in free energies ($\Delta G°$ in kcal mol^{-1}) for isomers **181-183** and **185-187**. This figure is reprinted with permission from Dey, S.; Sun, W.; Müller, J. *Inorg. Chem.* **2016**, *55*, 3630-3639.

For each of the four feasible racemates of the [3]FCPs **183** and **187**, only one enantiomer has been optimized (Figure 2.19). Within each series of the [3]FCPs, **183** (R = Ph) and **187** (R = *t*Bu), the order of thermodynamic stability is the same: the most stable isomer is the (S^N,R^C,S^P)- and the least stable isomer is the (S^N,S^C,S^P) species (Figure 2.19). The difference in free energies between the most and least stable isomer in both series is very similar with 9.33 (**183**) and 10.14 kcal mol^{-1} (**187**) (Figure 2.19). If one considers only the thermodynamically preferred isomer of the [3]FCPs, the [2]FCPs (**181** and **186**) are in both the cases the least stable compounds (Figure

2.19). The relative stabilities of **182** and **185** are with -6.62 and -6.83 kcal mol^{-1}, respectively, nearly identical (Figure 2.19). Whereas species (S^N,R^C,S^P)-**183** is slightly more stable than its precursor **182** ($\Delta G°$ = 1.02 kcal mol^{-1}), for the other case, the relative energies are drastically different and (S^N,R^C,S^P)-**187** is 4.53 kcal mol^{-1} less stable than **185** (Figure 2.19). These facts are in agreement with the experimental findings, as species **182** converts to (S^N,R^C,S^P)-**183**, but species **185** does not give the corresponding [3]FCP **187**, even at higher temperature (Scheme 2.40). The obvious reasons for this different behavior are steric effects. For the [3]FCP **187** two *tert*-butyl groups are forced to be in neighboring positions on the *ansa* bridge, which leads to steric congestion and, therefore, destabilization. This steric effect is illustrated in Figure 2.20, where bond angles around the bridging P- and C-atoms are shown for (S^N,R^C,S^P)-**183** and (S^N,R^C,S^P)-**187**.

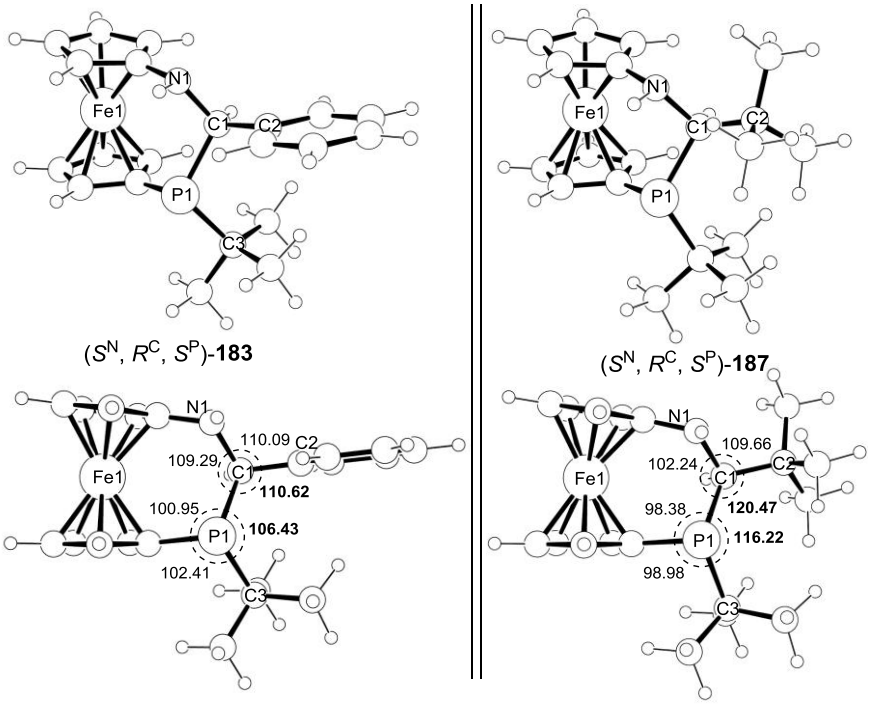

Figure 2.20. Optimized geometries of (S^N,R^C,S^P)-**183** and (S^N,R^C,S^P)-**187**. Bond angles are expressed in °; the tetrahedral angles around C1 involving H atom is not shown. This figure is reprinted with permission from Dey, S.; Sun, W.; Müller, J. *Inorg. Chem.* **2016**, *55*, 3630-3639. Copyright 2016 ACS.

For (S^N,R^C,S^P)-**183**, the bond angles around phosphorus and carbon, respectively, cover narrow ranges (P1: 100.95–106.43°; C1: 107.74–110.62°) whereas, those in (S^N,R^C,S^P)-**187** are significantly wider (P1: 98.38–116.22°; C1: 107.29–120.47°) (Figure 2.20). In particular, the two bond angles C1–P1–C3 and P1–C1–C2, respectively, are with 116.22 and 120.47° in (S^N,R^C,S^P)-**187** significantly larger compared to 106.43 and 110.62° found in (S^N,R^C,S^P)-**183** (Figure 2.20). The widening of these bond angles is a consequence of the steric repulsion between the two adjacent *tert*-butyl groups in (S^N,R^C,S^P)-**187**. One can assume that this steric repulsion energetically disfavors the formation of the [3]FCP (S^N,R^C,S^P)-**187** from the 1,1'-disubstituted ferrocene **185**.

As shown in Figure 2.17, the isolated, racemic [3]FCP **183** did not show NOE correlations between the amino proton and its neighboring CH proton, even though one would expect that a configuration at nitrogen should be instable through a fast inversion of nitrogen. However, an inversion at nitrogen would result in a racemate of **183** that is 5.64 kcal mol^{-1} less stable (Figure 2.19). That means that (S^N,R^C,S^P)-**183** and (R^N,S^C,R^P)-**183** would give (R^N,R^C,S^P)-**183** and (S^N,S^C,R^P)-**183**, respectively, after inversion at nitrogen. Such a large difference in free energy would mean that through inversion at nitrogen, only negligible amounts of the disfavored isomers will be present in equilibrium with the energetically favored isomer.

2.5. Aza[2]ferrocenophanes with Group 13 Elements in the Bridging Position

The surprising results in phosphorus chemistry showed the difficulties in synthesizing strained ferrocenophanes using alkyl- and aryl-substituted starting materials. In order to increase the propensity towards ROP it was intended to synthesize new strained species with group 13 elements in the bridging position. As bora[1]ferrocenophanes have the highest tilt angle of known FCPs,[10,126,127] we became interested in introducing boron in the bridge. Following the results published by previous researchers, $(i\text{Pr})_2\text{NBCl}_2$ was chosen as a reagent for this investigation.[12,111,126,127]

In 2010, Müller and co-workers introduced the first polymerizable galla[1]ferrocenophane, synthesized from a reaction of tmeda-stabilized dilithioferrocene and $(\text{Mamx})\text{GaCl}_2$ (Mamx = 2,4-di-*tert*-butyl-6-[(dimethylamino)methyl]phenyl).[128] Attempts to isolate the sandwich compound resulted poly(ferrocenylgallane) which was characterized with observable tacticity.[128] All previously known gallium-bridged metallocyclophanes were equipped with the bulky and intramolecularly coordinating *trisyl*-based ligands.[128] ROP attempts with all these previously reported [1]FCPs either failed or resulted in extremely sluggish polymerization.[128] Consequently, from the aspect of ROPs the new (Mamx)gallium-bridged [1]FCP was of immense importance.[128] The aforementioned result made us interested to explore gallium-bridged aza[2]ferrocenophanes. As (Mamx) ligand led to the successful reactions in the past, $(\text{Mamx})\text{GaCl}_2$ was chosen as a reagent for this investigation. Again, compound **142** was used as the starting point to prepare [2]FCPs via salt-metathesis reactions. As the reaction presented in Section 2.5.2 was performed during the early stage of my PhD, an un-optimized lithiation procedure was used. As a result, the isolated yield of compound **188** is comparatively lower than other strained species discussed in this thesis.

2.5.1. Contribution from Collaborators

Being the lead researcher of this project, I developed the optimized conditions of the salt-metathesis reaction and prepared the strained compounds **188** and **189**. The other collaborators of this project are Dr. Bidraha Bagh, who synthesized (Mamx)$GaCl_2$ and Hridaynath Bhattacharjee, who prepared the strained compound **190** and starting material (*i*Pr)$_2NBCl_2$.[128,129] The geometry optimization of compound **188** was done by Dr. Jens Müller. Hridaynath Bhattacharjee will be continuing this project as part of his exploration of boron-bridged FCPs.

2.5.2. Azagalla[2]ferrocenophane (188)

As illustrated in Scheme 2.41, the *in situ* prepared dilitho derivative of compound **142** was reacted with a dilute solution of (Mamx)$GaCl_2$ at 0 °C. Careful assignment of peaks in the ^1H NMR spectrum of the reaction mixture, taken after 4 h of stirring at ambient temperature, showed that conversion of the starting material to the intended product happened (see Figure 2.21). When the crude product was further purified by crystallization at -78 °C, analytically pure species **188** was obtained as an amorphous yellow solid in a yield of 43%.

Scheme 2.41. Synthesis of 2-Mamx-1-trimethylsilyl-1,2-azagalla[2]ferrocenophane (188)

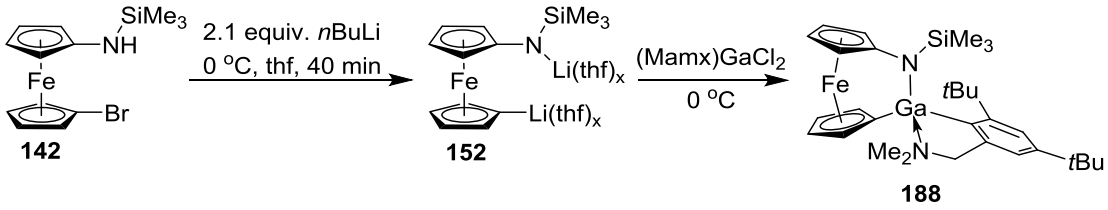

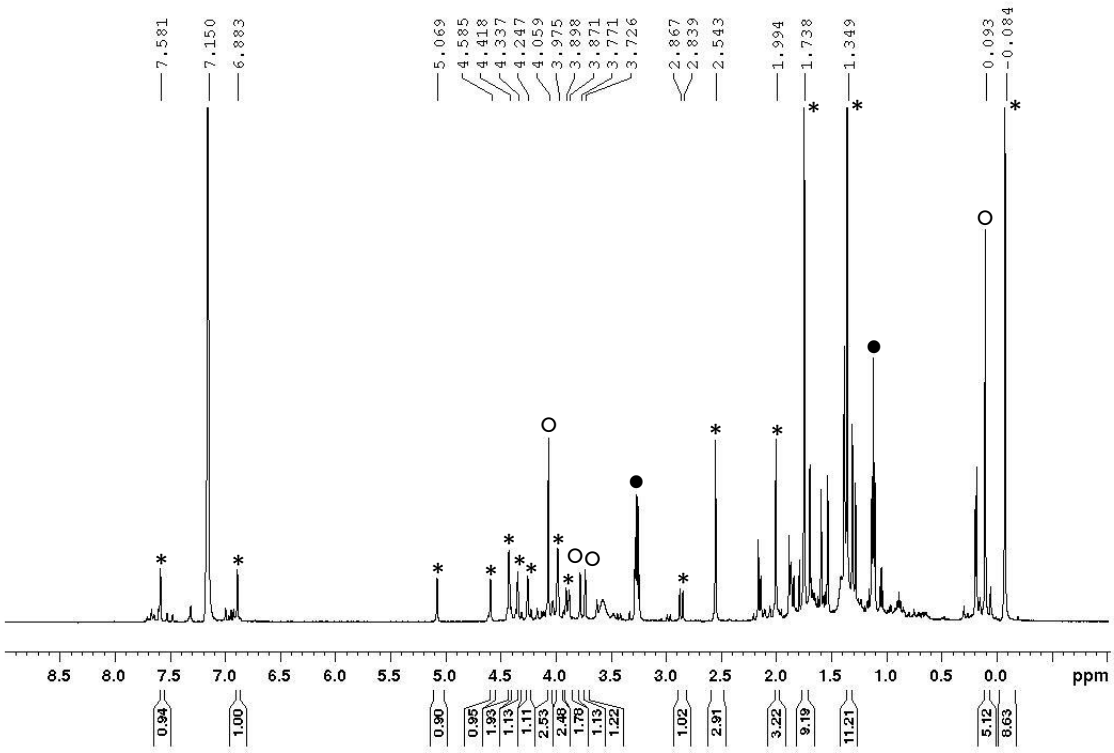

Figure 2.21. ^{1}H NMR spectrum ($CDCl_3$) of the reaction mixture to synthesize **188**. Peaks marked by * indicate the signals of compound **188**, whereas those marked by ○ and ● indicate the signals of (trimethylsilyl)aminoferrocene (**140**) and thf, respectively.

The Cp region of the ^{1}H NMR spectrum of compound **188** shows four signals at δ = 4.25, 4.33, 4.58, and 5.07 ppm, each with a relative intensity for one proton, and two signals at δ = 3.97 and 4.42 ppm, each with a relative intensity for two protons. As expected, the molecule has no symmetry as indicated by this signal pattern. For example, the two methylene protons appear as two doublets at δ = 2.86 and 3.89 ppm with a germinal coupling constant of 14.0 Hz. The ^{13}C NMR spectrum shows eight equally intense signals for proton substituted Cp carbons, which also supports the presence of C_1 symmetry in the molecule. Because of the quadrupolar relaxation of ^{69}Ga and ^{71}Ga nuclei, the signals for *ipso*-carbons, connected to gallium atom, was not detected in

^{13}C NMR spectrum. As no suitable single-crystal for X-ray diffraction could be grown from compound **188**, the molecular structure was optimized at the M06/6-311+G(d,p) level of theory (Figure 2.22).[125] As expected from the values of covalent radii [Si, 1.11(2) Å; Sn, 1.39(4) Å and Ga, 1.22(3) Å][57], the calculated tilt angle for compound **188** (α = 11.11°) is in between those for silicon- and tin-bridged species [**161**, α = 15.73(13)° and **165**, α = 10.13(11)°]. Similar to all four aza[2]ferrocenophanes discussed so far, the calculated β angle on gallium (β' = 21.37°) is higher than that on nitrogen (β = 4.91°). The angle between the least square plane of $Cp^{centroid}$-Fe-$Cp^{centroid}$ and bridging bond vector N-Ga (τ) was calculated as 13.60°, which was higher than the silicon- and tin-bridged species [**161**, τ = 3.31(13)° and **165**, τ = 8.08(4)°], but lower than the phosphorus analog [**178**, τ = 20.14(14)°] (consult Figure 1.2).

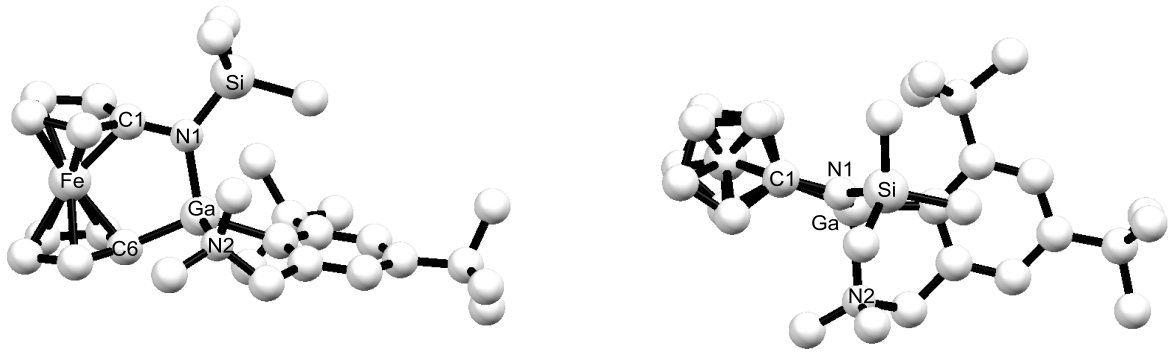

Figure 2.22. Optimized molecular structure of azagalla[2]ferrocenophane **188** by M06/6-311+G(d,p) level of theory. Molecule is shown with views tangent to the plane C1-Fe-C6 and perpendicular to the straight line C1-C2, respectively.

2.5.3. Azabora[2]ferrocenophane (189)

After successful synthesis of gallium-bridged [2]FCP, our next target was incorporating boron in the bridge. As illustrated in Scheme 2.42, starting material **142** was first dilithiated and *in situ* reacted with stoichiometric amount of $(i\text{Pr})_2NBCl_2$ at 0 °C (see Figure 2.23). The

analytically pure compound **189** was obtained by vacuum sublimation of the crude product as a red crystalline solid (Scheme 2.42).

Scheme 2.42. Synthesis of 2-Di(isopropyl)amino-1-trimethylsilyl-1,2-azabora[2]ferrocenophane (189)

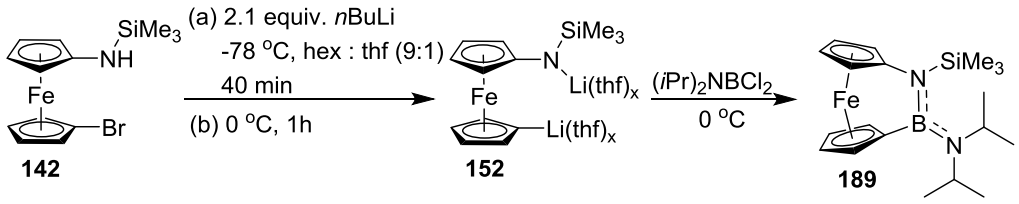

The ^{1}H NMR spectrum of the isolated product shows four equally intense signals in the Cp region at δ = 3.91, 4.21, 4.27, and 4.53 ppm, which indicate that the molecule is C_s symmetric in NMR timescale (500 MHz). Due to a fast rotation around boron and N(*i*Pr)$_2$ bond (B-N bond) two *i*Pr groups appear as a high-intensity doublet at δ = 1.21 ppm with coupling constant of 7 Hz. The C*H*(*i*Pr)$_2$ proton shows a low-intensity septet at δ = 3.72 ppm (J = 7 Hz). The presence of the plane of symmetry is further supported by ^{13}C NMR spectrum of **189**, which shows four equally intense signals at δ = 67.6, 70.6, 72.8, and 76.3 ppm for proton-substituted Cp carbons. Because of the quadrupolar relaxation of ^{11}B nucleus, the signal for boron substituted *ipso* carbon of **189** could not be found in ^{13}C NMR spectrum.

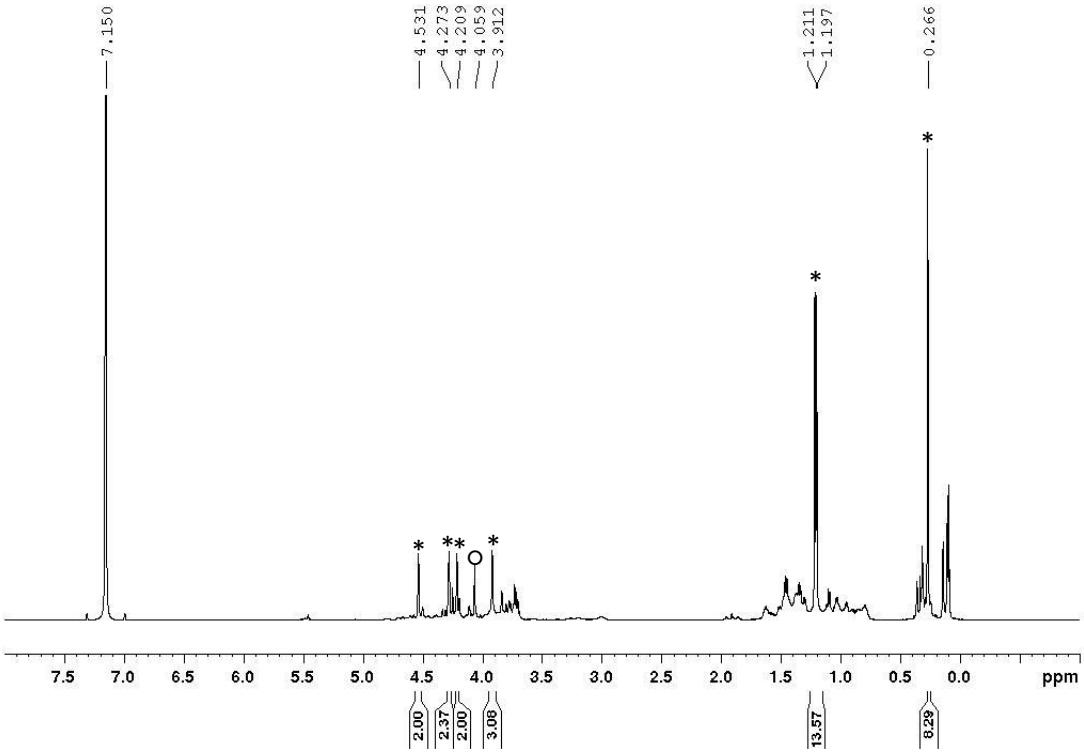

Figure 2.23. ^{1}H NMR spectrum (C_6D_6) of the reaction mixture to synthesize compound **189**. Peaks marked by * indicate the signals of compound **189**, whereas that marked by ○ indicate the signal of an unknown impurity.

Figure 2.24 depicts the molecular structure of compound **189**, determined by X-ray crystallography. Both nitrogen and boron show trigonal planar geometries with the sum of surrounding angles of ca. 360°. Both the B-N bonds show bond lengths [1.472(2) and 1.421(2) Å] close to that in borazine (1.44 Å), which indicate a π electronic conjugation between N1, B1, and N2. The external B1-N2 bond is 0.05 Å shorter than the internal B1-N1 bond, indicating that the extent of π donation towards boron is higher from N2 than N1. The Me_3Si group attracts the π electron cloud from N1. Therefore, the amount of π donation from N1 to B1 is reduced and, as a result, the N1-B1 bond becomes longer, and the tilt angle in **189** decreases. From the aforementioned argument, one can speculate that by replacing Me_3Si with an alkyl group it is possible to increase the tilt-angle of azabora[2]ferrocenophane. To examine this possibility we

then planned to synthesize a new azabora[2]ferrocenophane with an alkyl substituent on bridging nitrogen. Our neopentyl substituted starting material, **149** was used in this investigation.

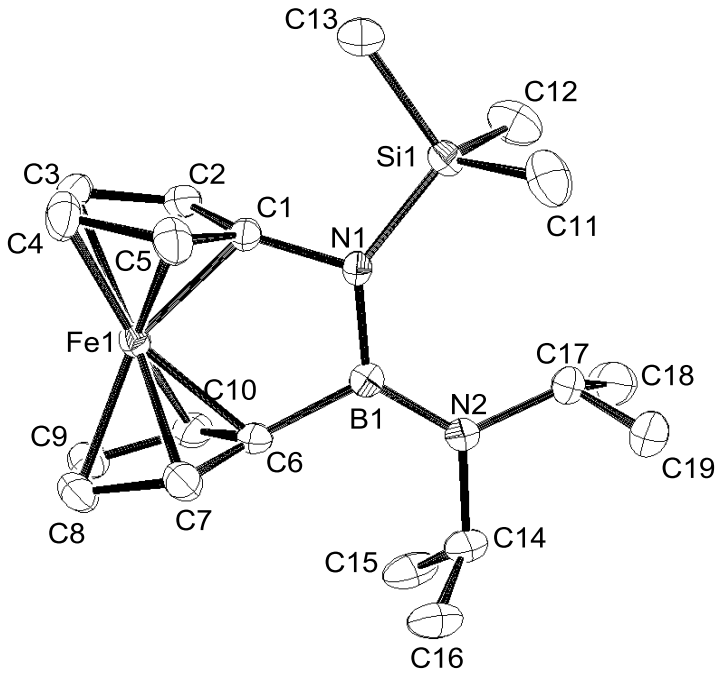

Figure 2.24. Molecular structure of **189** with thermal ellipsoids at 50% probability level. Hydrogen atoms are omitted for clarity. Selected bond lengths [Å] and bond angles: C1-N1 = 1.454(2); B1-N1 = 1.472(2); B1-N2 = 1.421(2); B1-C6 = 1.612(3); N1-Si1 = 1.7823(15); N2-C17 = 1.477(2); C1-N1-B1 = 112.53(14); C6-B1-N1 = 113.81(15); C6-B1-N2 = 119.97(16); N1-B1-N2 = 126.22(16); B1-N1-Si1 = 137.87(12); C1-N1-Si1 = 109.60(11).

2.5.4. Azabora[2]ferrocenophane with Reduced Bulk on Nitrogen (190)

As this part was solely done by Hridaynath Bhattacharjee, I will use only some preliminary result of compound **190** (Table 2.6). The detail of synthesis, characterization, crystal structure, and refinement data of **190** will be depicted in Hridaynath's thesis. As illustrated in Scheme 2.43, a stoichiometric amount of $(i\text{Pr})_2\text{NBCl}_2$ was reacted with an *in situ* prepared dilithio derivative **157**. When the crude product was purified by crystallization, analytically pure species **190** was obtained (Scheme 2.43). Suitable single crystal was collected and measured with X-ray crystallography. To

draw a comparison between the intrinsic strains in compounds **189** and **190**, I will use the tilt angle α (with no estimated standard deviation) of **190** (Table 2.6).

Scheme 2.43. Synthesis of 2-Di(isopropyl)amino-1-neopentyl-1,2-azabora[2]ferrocenophane (190)

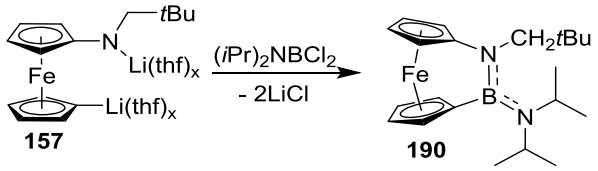

The crystal and structural refinement data for compounds **189** are listed in Table 2.7. Surprisingly, the tilt angle of compound **190** [α = 22.9°] is identical to that of **189** [α = 22.9(1)°]. This fact invalidates our speculation (described in Section 2.5.3). As boron has a lower covalent radii than phosphorus [B, 0.84(3) Å; P, 1.07(3) Å][57], the α angles for azabora[2]ferrocenophanes are significantly higher than its phosphorus analog [**178**, α = 18.40(11)°]. This represents a major increase of intrinsic strain in the aza[2]ferrocenophane molecules, which can play a significant role in ring-opening polymerizations. However, no investigation of ROPs was performed for azabora[2]ferrocenophanes, so far. This field will remain in focus within the Müller group.

Table 2.6. Distortion Angles [°] in Aza[2]ferrocenophanes

Numerical acronym	α	β / β' [a]	δ	τ
178	18.40(11)	10.38(15) / 17.10(13)	167.61(2)	20.14(14)
189	22.9(1)	11.56(17) / 15.01(16)	159.58(2)	2.08(10)
190 [b]	22.9	-	-	-

[a] β for E = N and β' for E = P or B. The readers are requested to consult Figure 1.2 in introduction. [b] Further detail of the distortion angles of **190** will be shown in Hridaynath's thesis.

Table 2.7. Crystal and Structural Refinement Data for Compound 189

Parameters	**189**
empirical formula	$C_{19}H_{31}BFeN_2Si$
fw	382.21
cryst. size / mm^3	0.150 × 0.300 × 0.450
cryst. system, space group	monoclinic, P 1 21/n 1
Z	4
a / Å	6.3615(4)
b / Å	19.7152(13)
c / Å	15.9518(11)
α / °	90
β / °	94.707(2)
γ / °	90
volume / $Å^3$	1993.9(2)
ρ_{calc} / g cm^{-3}	1.273
temperature / K	173(2)
μ_{calc} / mm^{-1}	0.819
θ range / °	3.29 to 28.90
completeness / %	98.7
reflns collected / independent	27865 / 5187
absorption correction	multi-scan
data [$F_o^2 \geq -3\sigma(F_o^2)$] / restraints / params	5187 / 0 / 224
goodness-of-fit	1.071
R_1 [I > 2 σ(I)] [a]	0.0373
wR_2 (all data) [a]	0.1040
largest diff. peak and hole, $\Delta\rho_{elect}$ / e $Å^{-3}$	0.961 and -0.320

[a] $R_1 = [\Sigma||F_o|-|F_c||]/[\Sigma|F_o|]$ for $[F_o^2 > 2\sigma(F_o^2)]$, $wR_2 = \{[\Sigma w(F_o^2-F_c^2)^2]/[\Sigma w(F_o^2)^2]\}^{1/2}$ [all data]

CHAPTER 3

SUMMARY AND CONCLUSION

By adapting a well-known chemical methodology, a new and reliable synthesis of 1-amino-1'-bromoferrocene (**114**) was developed. In order to selectively dilithiate compound **114**, it was further modified into *N*-substituted species **142**, **147**, and **149** by employing known procedures of silylation and reductive amination (Figure 3.1). Thereafter, a stepwise dilithiation technique was optimized for species **142** and **149** employing quenching reactions of lithium species by D_2O to measure success. As the stepwise reaction did not work for **147**, a direct dilithiation procedure was optimized for this compound.

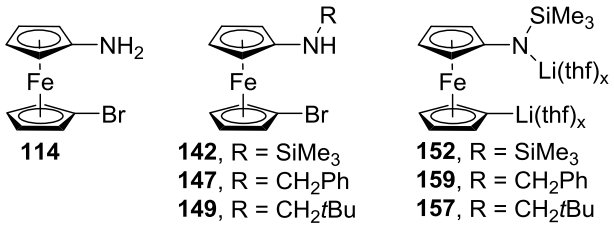

Figure 3.1. Key compound (**114**), starting materials (**142**, **147**, and **149**) and their dilithiated salts (**152**, **159**, and **157**).

The *in situ* prepared dilithio derivative **152** was first used to prepare the three unsymmetrically bridged [2]FCPs **161**, **162**, and **165** (Figure 3.2). As indicated by the measured tilt angles α (α for **161** is approx. 16° whereas, those in **162** and **165** are approx. 10°), the intrinsic strain in these species is expected to be moderate to low. Among the three [2]FCPs, **162** and **165** could be isolated in analytically pure form and, therefore, used in investigations of ROP.

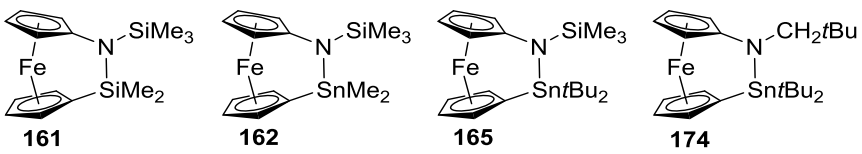

Figure 3.2. Silicon- and tin-bridged aza[2]ferrocenophanes.

Unfortunately, all attempts to polymerize species **161** and **165**, applying common ROP techniques, yielded no polymeric material. Silicon-bridged species **161** turned out as a thermally robust material and did not ring-open even at 300 °C. On the other hand, the tin-bridged species **165** could withstand 200 °C but decomposed at 260 °C. More negative results were obtained when species **161** and **165** were attempted to ring-open polymerize in catalytic and photocontrolled conditions for ROP. None of these species afforded any polymeric material with the reactions of substoichiometric amounts of *n*BuLi. This is not very surprising, as the *n*Bu$^-$ group was transformed by the initiation to a sterically encumbered Cp(Me$_3$Si)N$^-$ group (see Scheme 2.32). Consequently the Me$_3$Si group on nitrogen was replaced with neopentyl group and the new azastanna[2]ferrocenophane **174** was synthesized. However, repeated attempts of anionic ROP with **174** did not produce any polymeric material. Therefore, in order to increase the α angles in aza[2]ferrocenophanes, phosphorus was incorporated as a bridging atom.

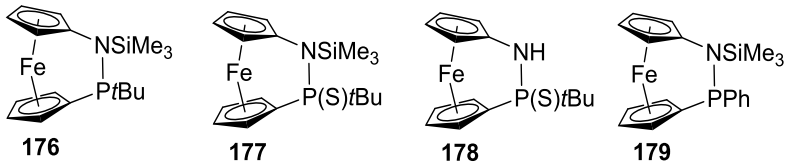

Figure 3.3. Azaphospha[2]ferrocenophanes.

The first examples of azaphospha[2]ferrocenophanes (**176**-**179**) were synthesized and are described in this thesis (Figure 3.3). Comparison of the molecular structure of **178** with silicon- and tin-bridged aza[2]ferrocenophanes (Figure 3.2) revealed an expected distortion in this molecule [**178**, α = 18.40(11)°]. Although, phosphorus-bridged aza[2]ferrocenophane with a bulky group on nitrogen could successfully be synthesized, unexpected results were obtained when the synthesis of similar compounds with reduced bulk on nitrogen was attempted. Even though compounds **147** and **149** could readily be dilithiated, neither dilithio species **159** nor **157** could be

used as a suitable precursor as intended. In salt-metathesis reactions with *t*BuPCl$_2$ both species resulted in 1,1'-disubstituted ferrocene derivatives (**182** and **185**) as major products (Figure 3.4). While compound **185** was produced almost exclusively, compound **182** was obtained as a major component in a mixture of the three constitutional isomers **181**-**183** (Figure 3.4). ^{1}H and ^{31}P NMR spectroscopy revealed that species **182** isomerized to the [3]FCP **183**, whereas **181** remained in unaltered amounts. Contrary to this result, the 1,1'-disubstituted ferrocene **185** did not give the corresponding [3]FCP **187**, neither on long standing at ambient temperature nor on heating a toluene solution to 80 °C.

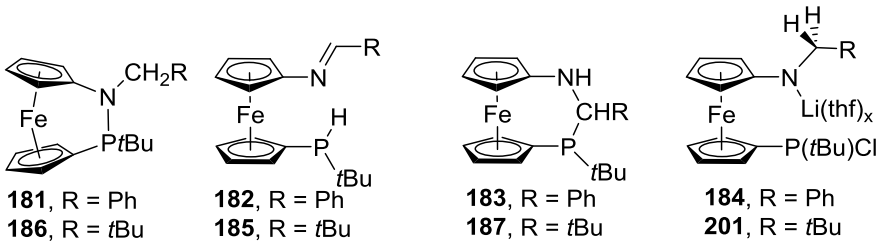

181, R = Ph
186, R = *t*Bu

182, R = Ph
185, R = *t*Bu

183, R = Ph
187, R = *t*Bu

184, R = Ph
201, R = *t*Bu

Figure 3.4. Expected and unexpected products (**181**-**183** and **185**-**187**), and possible intermediates (**184** and **201**) of salt metatheses.

Differences between standard free energies ($\Delta G°$), obtained from optimized geometries at the M06/6-311+G(d,p) level of theory of species **181**-**183** and **185**-**187**, were used to better rationalize the following experimental findings. First, the isolated racemic mixture of **183** [i.e., (S^N,R^C,S^P)-**183** and (R^N,S^C,R^P)-**183**] is the thermodynamically preferred racemate among the four possible mixtures (see Figure 2.16 – 2.19 and Table 2.5). Second, matching with the experimental observations, the isomerization of **182** to **183** is exoergic ($\Delta G°$ = -1.02 kcal mol^{-1}), while that of **185** to **187** is thermodynamically impossible ($\Delta G°$ = 4.53 kcal mol^{-1}; see Figure 2.19). The latter result is a consequence of steric interactions of two adjacent *t*Bu groups on the bridging moiety of the [3]FCP **187** (see Figure 2.20). The most unexpected result in this investigation was the formation of 1,1'-disubstituted ferrocene species **182** and **185**. Although there is not enough

experimental evidence to fully understand the formation of these species, a speculated reaction sequence was discussed (see Scheme 2.39).

A discrepancy was noticed when a small amount of the [2]FCP **181** was formed in the salt-metathesis reaction with compound **147**, whereas no trace of [2]FCP **186** was observed in the reaction mixture starting from compound **149** (consult Figure 3.1 and 3.4). This difference in reactivity can be rationalized in the following way. For ring-closure reaction, the nitrogen-bonded CH_2R (R = Ph and *t*Bu) group must come in the close proximity to the P(*t*Bu)Cl group. Therefore, it can be expected that the increased bulkiness from Ph to *t*Bu on nitrogen will reduce the conversion of intermediate **201** to [2]FCP **186** (consult Figure 3.4). On the other hand, the unexpected products **182** and **185** are flexible over the rotation of the Cp rings and, therefore, NCHR and PH*t*Bu can avoid steric interactions (consult Figure 3.4). As a result, the conversion of intermediates (**184** and **201**) to 1,1'-disubstituted ferrocenes (**182** and **185**) does not significantly change by a switch from R = Ph to *t*Bu.

High intrinsic strain in bora[1]ferrocenophanes[10,126,127] and polymerizable galla[1]ferrocenophane[128] led us interested in synthesizing strained compounds with boron and gallium in the bridge. The optimized geometry of the gallium-bridged compound **188** shows an α angle of 11.11° (Figure 3.5). Following this initial exploration, two azabora[2]ferrocenophanes were prepared, one with a Me_3Si (**189**) and one with a *t*BuCH_2 group (**190**) on the bridging nitrogen atom (Figure 3.5). It was expected that, due to the presence of electron-withdrawing Me_3Si group, the π electron transfer from the bridging nitrogen to boron is lower for **189**, which should result in a smaller α angle. However, the molecular structures obtained by single-crystal X-ray crystallography showed with approx. 22.9° (see Table 2.6) nearly identical tilt angles for both species.

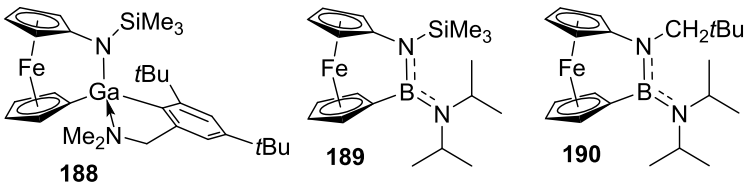

Figure 3.5. Gallium- and boron-bridged aza[2]ferrocenophanes.

The azabora[2]ferrocenophanes **189** and **190** contain boron atoms, which are electronically stabilized by a $(i\text{Pr})_2\text{N}$ group. The π donation from the $(i\text{Pr})_2\text{N}$ moiety significantly reduces the electrophilicity of the bridging boron, which might prevent the ROP of these species with ionic initiators. In order to be prepared for this potential problem, current efforts in the Müller group are concentrated on the preparation of FCPs where boron is not electronically stabilized by an external ligand.

One important aspect of this chemistry is that tmeda ($Me_2NCH_2CH_2NMe_2$) is not needed as a reagent for dilithiation reactions. This is important to note because dilithioferrocene·tmeda is insoluble in most of the common organic solvents and this hinders a perfect control over its concentration in the reaction mixture in respective salt-metathesis reactions. The preparation of the dilithio species **152**, **157**, and **159** result in homogeneous solutions that allow controlling the concentration and stoichiometry of the reactants (Figure 3.1). Moreover, as the clean dilithiation of starting materials can be performed in a solvent mixture of hexanes and thf (hexanes : thf, 9:1), the byproduct LiCl can easily be precipitated, which presumably facilitates the formation of [2]FCPs.

The long term goal of research in the area of strained sandwich compounds is getting access to new metal-containing polymers and derived materials. The first steps toward this goal is the synthesis of suitable monomers. With the thesis on hand, the development of a new family of

[2]FCPs has been described. Initial investigations to use the silicon- and tin-bridged [2]FCPs for the preparation of polymers were conducted. However, these species did not ring-open to give the anticipated metallopolymers. Current efforts in the Müller group are under way to take advantage of the severely tilted boron-bridged aza[2]ferrocenophanes for ROP. The future will reveal if these explorations will bear fruits.

CHAPTER 4

EXPERIMENTAL SECTION

I was the main researcher in this project. All the compounds, except **190**, were synthesized and characterized by me. Compound **190** was synthesized and characterized by Hridaynath Bhattacharjee. All DFT calculations were done by Prof. Dr. Jens Müller. The crystallographic measurements for strained compounds were done by the following SSSC personnel: Dr. Wilson Quail measured compounds **161**, **162**, and **165**; Dr. Wei Sun measured compound **178**; and Dr. Jianfeng Zhu measured compounds **189** and **190**.

4.1. General Synthetic and Characterization Methods

All air-sensitive manipulations were carried out using standard Schlenk and glovebox techniques. Solvents were dried using an MBraun Solvent Purification System and stored under nitrogen over 3 Å molecular sieves. All solvents for NMR spectroscopy were prepared by freeze-pump-thaw cycles and stored under nitrogen over 3 Å molecular sieves. ^{1}H, ^{13}C, ^{11}B, ^{31}P, and ^{119}Sn NMR spectra were recorded on 500 MHz Bruker Avance and 500 MHz Bruker Avance III HD NMR spectrometers at 25 ºC in $CDCl_3$ and C_6D_6. ^{1}H chemical shifts were referenced to the residual protons of the deuterated solvents (δ 7.15 ppm for C_6D_6 and 7.26 ppm for $CDCl_3$); ^{13}C chemical shifts were referenced to the C_6D_6 signal at δ 128.00 ppm and $CDCl_3$ signal at δ 77.00 ppm. ^{1}H NMR assignments for all compounds were supported by additional 2D-NMR experiments (HMQC, COSY) or by applying the published increment method.[119] For compounds **129**, **128**, **132, 139**, **114**, **142**, **161**, **162**, and **165** the mass spectra were measured on a VG 70SE instrument and reported in the form of *m*/*z* (relative intensities) where '*m*/*z*' is the observed mass. For all other compounds the mass data were obtained with a JEOL AccuTOF GCv 4G using field desorption (FD) as the ionization method and reported in the form of $[M^+]$ where $[M^+]$ is the molecular ion

peak. For all analytically pure, solid compounds elemental analyses were performed on a Perkin Elmer 2400 CHN Elemental Analyzer. Due to technical difficulties in analyzing liquids, the elemental analyses could not be performed for liquid and sticky compounds. As the NMR spectra could not be given in this thesis, readers are being referred to our new publications.

Compounds **129**, **128**, **132**, **139**, **114**, **142**, **143**, **145**, **147**, and **149** could not be isolated as analytically pure species. The only impurity was present in each isolated product was the corresponding non-brominated species (**131**, **124**, **126**, **127**, **120**, **140**, **144**, **146**, **148**, and **150**), which could not be removed by standard purification techniques (column chromatography, crystallization and precipitation). As a result, these compounds were used in the next chemical syntheses without further purification. The percentage amounts of the intended products and corresponding non-brominated impurities were determined by the integral values of the signals in the ^{1}H NMR spectrum. The formula weight for each impure compound was calculated on the basis of the amount of non-brominated impurity present in the isolated sample. For an example, let us suppose that we have an isolated product mixture containing a% of compound **A** and b% of compound **B**, where compound **A** (molar mass M_A) is the major product and compound **B** (molar mass M_B) is the minor impurity. For this product mixture, the formula weight of compound **A** (F_A) was calculated as $F_a = [(M_A \times a\%) + (M_B \times b\%)]$. The desired values for elemental analyses were also calculated by a similar procedure. For the aforementioned example, if the desired CHN values for compound **A** are C_a, H_a, and N_a, and those for impurity **B** are C_b, H_b, and N_b, the calculated elemental analyses value for the isolated mixture will be $[(C_a \times a\%) + (C_b \times b\%)]$, $[(H_a \times a\%) + (H_b \times b\%)]$, and $[(N_a \times a\%) + (N_b \times b\%)]$. However, this procedure can only be meaningfully applied, if the compound **B** is present in a small amount. As in our cases the amounts of the non-brominated impurities varied in a range of 2.5% to 7%, we successfully applied this simple

arithmetic procedure to calculate the formula weights, percentage yields and expected elemental analyses values for compounds **129** (with 4% of **131**), **128** (with 4% of **124**), **132** (with 4% of **126**), **139** (with 4% of **127**), **114** (with 6% of **120**), **142** (with 6% of **140**), **143** (with 7% of **144**), **145** (with 2.5% of **146**), **147** (with 2.5% of **148**), and **149** (with 3.5% of **150**). [104,112] The calculated formula weights (g/mole), followed by the numerical acronyms in parentheses: 333.84 (**129**), 305.48 (**128**), 330.80 (**132**), 410.92 (**139**), 275.21 (**114**), 347.39 (**142**), 362.53 (**143**), 346.09 (**145**), 368.10 (**147**), and 347.32 (**149**).[104,112]

4.2. Reagents

*n*BuLi (2.5 M in hexanes), $C_2Br_4H_2$ (98%), ferrocene (98%), Me_2SiCl_2 (≥99.5%), Karstedt's catalyst (2% Pt, in xylene) trimethylacetaldehyde (96%), *tert*-butyldichlorophosphine (1.0 M in Et_2O), $Na[BH_3CN]$ (reagent grade, 95%), and molecular sieves (3 Å pore size) were purchased from Sigma-Aldrich; benzaldehyde (99+%), ClCOOEt (97%), $(COCl)_2$ (98%), $PhCH_2OH$ (99%), Me_3SiCl (≥98%), tBu_2SnCl_2 (98%), and Me_2SCl_2 (99%) were purchased from Alfa Aesar; NEt_3 (reagent grade, 99%), N,N,N',N'-tetramethylethylenediamine (tmeda; 99%, Acros Organics), KOH (pallets), and NaN_3 (reagent grade) were purchased from Fisher Chemicals; Pd-C (10% on activated carbon, reduced) was purchased from Strem Chemicals; elemental sulfur (99%) was purchased from EMD and D_2O (D, 99.9%) was purchased from Cambridge Isotope Laboratories. Silica gel 60 (EMD, Geduran, particle size 0.040–0.063 mm) and alumina (Sigma-Aldrich, activated, neutral, 58 Å pore size) were used for column chromatography. (Mamx)$GaCl_2$,[128] *i*Pr_2NBCl_2,[129] $(LiC_5H_4)_2Fe{\cdot}2/3$tmeda[77], and $(BrC_5H_4)_2Fe$[130] were synthesized according to the literature procedures.

4.3. DFT Calculations

Geometries of species **178**, **181-183**, **185-187**, and **188** were optimized on the M06/6-311+G(d,p) level of theory using GAUSSIAN 09.[125] An ultrafine grid (int = ultrafine) and tight requirements for geometry optimizations (opt = tight) were used for all calculations. Frequency calculations were used to confirm minima and provide thermodynamic information. The notation used for free energies, ΔG°, indicate standard conditions (p = 1 atm; T = 298.15 K). Graphical illustrations of calculated results were done with the help of ORTEP-3 for Windows (version 2.02), extraction of structural parameters from the calculated coordinates of [2]FCP and [3]FCPs were done with the help of Mercury (version 3.6) and CYLview (version 1b).[131,132,133]

4.4. Crystal Structure Determinations

A single crystal was coated with Paratone-N oil, mounted using a Micromount™ (*MiTeGen* - Microtechnologies for Structural Genomics), and frozen in the cold stream of the Oxford Cryojet attached to the diffractometer. Crystal data were collected on a Bruker APEX II diffractometer at -100 °C, using monochromated Mo Kα radiation (λ = 0.71073 Å). An initial orientation matrix and cell was determined by ω scans, and the X-ray data were measured using ϕ and ω scans.[134] The frames were integrated with the Bruker SAINT software package.[135] Data reduction was performed with the APEX2 software package.[134] A multiscan absorption correction (SADABS) was applied.[135] The structure was solved by direct methods and refined using the Bruker SHELXL-2014 software package.[136,137] Non-hydrogen atoms were refined anisotropically; hydrogen atoms were included at geometrically idealized positions but not refined. The isotropic thermal parameters of the hydrogen atoms were fixed at 1.5 or 1.2 times that of the preceding carbon atom. Ellipsoid plots were prepared using ORTEP-3 for Windows.[131] Distortion angles for the [2]FCPs, shown in Tables 2.1, 2.4 and 2.6, were calculated using the programs PLATON.[138] The lists of

bond angles and bond lengths of compounds **161**, **162**, **165**, **178**, and **189** can be found in the Appendix.

4.5. Synthesis of 1-Bromo-1'-(ethoxycarbonyl)ferrocene (129)

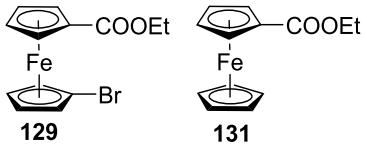

129 **131**

*n*BuLi (2.5 M in hexane, 14.6 mL, 36.5 mmol) was added dropwise to a cold (-78 ºC) solution of 1,1'-dibromoferrocene (**115**) (12.28 g, 35.72 mmol) in thf (100 mL) followed by stirring for 25 min at this temperature. The cold reaction mixture (-78 ºC) containing a red precipitate was added dropwise by a cannula to a stirred solution (cooled at -78 ºC) of ethylchloroformate (68.0 mL, 711 mmol) in thf (100 mL). The reaction mixture was warmed up to r.t. and stirred for 20 h, followed by the addition of deionized water (100 mL) and Et_2O (100 mL). Using a separatory funnel, the aqueous phase was removed and the organic phase was washed with brine (4 × 200 mL) and dried over anhydrous Na_2SO_4. All the volatiles were removed by a rotary evaporator resulting in a red oil (11.96 g). The red oil was subjected to column chromatography on silica gel using a mixture of hexanes and CH_2Cl_2 (1 : 1 by volume) as eluent. The second red band was collected and all the volatiles were removed by high vacuum, resulting in compound **129** as a red oil (8.56 g, 72%), which contained ca. 4% of (ethylcarboxy)ferrocene (**131**) as impurity. ^{1}H NMR ($CDCl_3$): δ 1.35 (t, 3H, $COOCH_2CH_3$), 4.12 (s, 2H, CH-β of Cp^{Br}), 4.29 (q, 2H, $COOCH_2CH_3$), 4.41 (s, 4H, CH-α of Cp^{Br}, CH-β of Cp^{COOEt}), 4.82 (s, 2H, CH-α of Cp^{COOEt}). $^{13}C\{^1H\}$ NMR ($CDCl_3$): δ 14.5 ($COOCH_2CH_3$), 60.3 ($COOCH_2CH_3$), 68.8 (C-β of Cp^{Br}), 69.6 (*ipso*-C-COOEt), 71.6 (C-α of Cp^{Br}), 72.2 (C-α of Cp^{COOEt}), 73.6 (CH-β of Cp^{COOEt}), 78.1 (*ipso*-C-Br), 170.3 (-*C*OO-). MS (70 eV): *m/z* (%) 336 (100) [M^+], 308 (38) [$M^+ - 2CH_2$]. HRMS (70 eV): calcd for $C_{13}H_{13}BrFeO_2$, 335.9448; found, 335.9449. Anal. Calcd for a mixture of $C_{13}H_{13}BrFeO_2$ (336.99;

96%) and $C_{13}H_{14}FeO_2$ (258.10; 4%): C, 46.90; H, 3.95. Found: C, 46.59; H, 3.87. Note: The ^{1}H NMR (in $CDCl_3$) of the isolated product shows small peaks at δ 4.18 (s, 5H, Cp), 4.20 (q, 2H, COOC*H*$_2$CH$_3$), 4.37 (s, 2H, Cp^{COOEt}), and 4.79 (s, 2H, Cp^{COOEt}) ppm which are resulting from the non-bromo impurity **131**. The missing peak (for COOCH$_2$C*H*$_3$) of the byproduct **131** presumably overlaps with the stronger signals resulting from the major product **129**.

4.6. Synthesis of 1-Bromo-1'-carboxyferrocene (128)

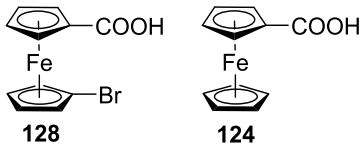

128 **124**

Compound **129** (8.56 g, 25.6 mmol) and KOH (55.42 g, 987.8 mmol) were dissolved in a mixture of EtOH (780 mL) and deionized water (80 mL). After the solution was heated under reflux for 40 h, deionized water (100 mL) was added to the reaction mixture at r.t. The aqueous phase was washed with CH_2Cl_2 (4 × 200 mL; discarded) and acidified by conc. HCl(aq) (60 mL) to give a yellow precipitate, which was extracted by CH_2Cl_2 (3 × 100 mL). After the CH_2Cl_2 phase was dried over anhydrous Na_2SO_4, all volatiles were removed in a rotary evaporator, resulting in product **128** as an orange powder (6.05 g, 77%) which contained ca. 4% of carboxyferrocene (**124**) as an impurity. ^{1}H NMR ($CDCl_3$): δ 4.20 (pst, 2H, CH-β of Cp^{Br}), 4.49 (pst, 2H, CH-α of Cp^{Br}), 4.51 (pst, 2H, CH-β of Cp^{COOH}), 4.91 (pst, 2H, CH-α of Cp^{COOH}), 11.95 (bs, 1H, COO*H*). ^{13}C{^{1}H} NMR ($CDCl_3$): δ 69.3 (C-β of Cp^{Br}), 70.1 (*ipso*-C-COOH), 71.9 (C-α of Cp^{Br}), 72.7 (C-α of Cp^{COOH}), 74.6 (CH-β of Cp^{COOH}), 78.1 (*ipso*-C-Br), 176.1 (*C*OOH). MS (70 eV): *m/z* (%) 308 (100) [M$^+$], 165 (57) [M$^+$ - CpBr]. HRMS (70 eV): calcd for $C_{11}H_9BrFeO_2$, 307.9135; found, 307.9127. Anal. Calcd for a mixture of $C_{11}H_9BrFeO_2$ (308.94; 96%) and $C_{11}H_{10}FeO_2$ (230.04; 4%): C, 43.36; H, 3.00. Found: C, 43.50; H, 2.89. Note: The ^{1}H NMR of the isolated product (in $CDCl_3$) shows small peaks at δ 4.26 (s, 5H, Cp) and 4.85 (s, 2H, Cp^{COOH}) ppm which are resulting from

the non-bromo impurity **124**. The other peaks (for Cp^{COOH} and COO*H*) of the byproduct **124** presumably overlap with stronger signals of the major product **128**.

4.7. Synthesis of 1-Azidocarbonyl-1'-bromoferrocene (132)

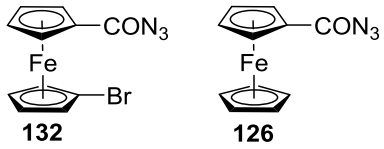

132 **126**

$(COCl)_2$ (1.6 mL, 19 mmol) was added dropwise to a solution of compound **128** (1.82 g, 5.95 mmol) in CH_2Cl_2 (35 mL), followed by the addition of DMF (four drops). After stirring the solution for 3 h, all the volatiles were removed under high vacuum. To a solution of the so-obtained red solid in CH_2Cl_2 (35 mL), nBu$_4$NBr (0.015 g, 0.046 mmol) and an aqueous solution of NaN_3 (0.575 g, 8.84 mmol in 7.0 mL of deionized water) were added. The biphasic solution was stirred for 16 h at r.t., followed by the addition of deionized water (100 mL). The aqueous phase was removed by a separatory funnel, and the organic phase was washed with deionized water (4 x 200 mL) and dried over anhydrous Na_2SO_4. All volatiles were removed by a rotary evaporator resulting in compound **132** as a brown powder (1.83 g, 93%) which contained ca. 4% of (azidocarbonyl)ferrocene (**126**) as an impurity. ^{1}H NMR ($CDCl_3$): 4.19 (pst, 2H, CH-β of Cp^{Br}), 4.49 (pst, 2H, CH-α of Cp^{Br}), 4.54 (pst, 2H, CH-β of Cp^{CON3}), 4.87 (pst, 2H, CH-α of Cp^{CON3}). ^{13}C{^{1}H} NMR ($CDCl_3$): δ 69.3 (C-β of Cp^{Br}), 70.3 (*ipso*-C-$COON_3$), 72.0 (C-α of Cp^{Br}), 72.3 (C-α of Cp^{CON3}), 75.1 (CH-β of Cp^{CON3}), 78.4 (*ipso*-C-Br), 175.9 (*C*OON_3). MS (70 eV): *m/z* (%) 333 (13) [M^+], 305 (29) [M^+ - N_2]. HRMS (70 eV): calcd for $C_{11}H_8BrFeN_3O$, 332.9200; found, 332.9198. Anal. Calcd for a mixture of $C_{11}H_8BrFeN_3O$ (333.95; 96%) and $C_{11}H_9FeN_3O$ (255.06; 4%): C, 40.05; H, 2.46; N, 12.74. Found: C, 39.94; H, 2.20; N, 12.64. Note: The ^{1}H NMR (in $CDCl_3$) of the isolated product shows small peaks at δ 4.26 (s, 5H, Cp) and 4.83 (s, 2H, Cp^{CON3})

ppm which are resulting from the non-bromo impurity **126**. The missing peak (for Cp^{CON3}) of the byproduct **126** presumably overlaps with other stronger signals of the major product **132**.

4.8. Synthesis of Benzyl N-(1'-bromoferrocen-1-yl)carbamate (139)

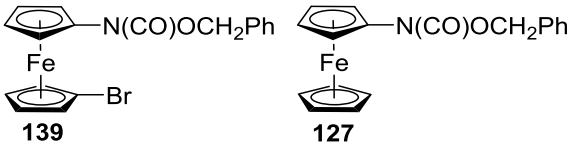

139 **127**

A solution of compound **132** (3.05 g, 9.22 mmol) in $PhCH_2OH$ (15.0 mL) was heated at 90 ºC for 2 h resulting in a color change from burgundy red to yellow. The yellow solution was cooled to r.t. and all volatiles were removed under high vacuum. The mixture was further purified by column chromatography on silica gel (hexanes : CH_2Cl_2 : NEt_3; 15 : 83 : 2 by volume). The product **139** was obtained as a golden yellow crystalline solid (3.35 g, 88%) which contained ca. 4% of benzyl N-ferrocenyl-carbamate (**127**) as an impurity. ^{1}H NMR ($CDCl_3$): δ 4.04 (s, 2H, CH-β of $Cp^{NHCOOBz}$), 4.09 (s, 2H, CH-β of Cp^{Br}), 4.38 (s, 2H, CH-α of Cp^{Br}), 4.52 (s, 2H, CH-α of $Cp^{NHCOOBz}$), 5.18 (s, 2H, C*H*$_2$Ph), 6.00 (bs, 1H, N*H*), 7.25 – 7.42 (m, 5H, *Ph*). ^{13}C{^{1}H} NMR ($CDCl_3$): δ 62.8 (*C*H_2Ph), 66.7 (C-β of $Cp^{NHCOOBz}$), 67.0 (*ipso*-C-NH), 67.9 (C-β of C^{Br}), 69.1 (C-α of $Cp^{NHCOOBz}$), 71.1 (C-α of Cp^{Br}), 78.9 (*ipso*-C-Br), 128.2 (C of Ph), 128.3 (*ipso*-C of Ph), 128.6 (C of Ph), 136.2 (C=O). MS (70 eV): *m/z* (%) 413 (37) [M^+], 335 (2) [M^+ - HPh], 278 (26) [M^+ - $NHCOOCH_2Ph$]. HRMS (70 eV): calcd for $C_{18}H_{16}BrFeNO_2$, 412.9714; found, 412.9700. Anal. Calcd for a mixture of $C_{18}H_{16}BrFeNO_2$ (414.08; 96%) and $C_{18}H_{17}FeNO_2$ (335.18; 4%): C, 52.70; H, 3.94; N, 3.41. Found: C, 52.87; H, 3.61; N, 3.38. Note: The ^{1}H NMR (in $CDCl_3$) of the isolated product shows no peak of the non-bromo impurity **127**. One can assume that the peaks resulting from byproduct **127** overlap with the stronger signals of the major product **139**.

4.9. Synthesis of 1-Amino-1'-bromoferrocene (114)

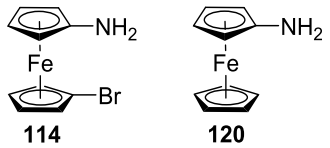

114 **120**

Pd-C (0.99 g) was added to a solution of compound **139** (4.32 g, 10.5 mmol) in dry and deoxygenated *i*PrOH (160 mL) taken in a Schlenk flask. After the reaction flask was purged with hydrogen by six consecutive cycles of evacuation and refilling, and a balloon, filled with hydrogen gas, was placed on the well stirred reaction mixture for 2.5 h. All the volatiles were removed under high vacuum and the resulting black solid was suspended in dry Et_2O (100 mL). All insoluble materials were filtered off by Schlenk filtration, resulting in a bright yellow solution which, after removal of all the volatiles, resulted in a yellow crystalline solid. This yellow solid was dissolved in CH_2Cl_2 (75 mL) and the organic phase was washed by an aqueous NaOH solution (6 M, 5 × 20 mL) and deionized water (20 mL). After drying the organic phase over anhydrous Na_2SO_4, all volatiles were removed under high vacuum to give a yellow solid, which according to ^{1}H NMR spectroscopy was composed of 1-amino-1'-bromoferrocene (**114**, 85%) and aminoferrocene (**120**, 15%). Some of the aminoferrocene (**120**) was removed by sublimation (96 h; 38 °C oil bath temperature; p ~ 10^{-2} mbar). Further sublimation (24 h; 60 °C oil bath temperature; p ~ 10^{-2} mbar) gave product **114** as a yellow amorphous solid contaminated with ca. 6% of compound **120** (2.03 g, 70%). ^{1}H NMR (C_6D_6): δ 2.08 (bs, 2H, N*H*$_2$), 3.57 (pst, 2H, Cp^{Br}), 3.68 (pst, 2H, Cp^{NH2}), 3.71 (pst, 2H, Cp^{NH2}), 4.12 (pst, 2H, Cp^{Br}). $^{13}C\{^1H\}$ NMR (C_6D_6): δ 60.0 (C of Cp^{NH2}), 65.7 (C of Cp^{NH2}), 67.5 (C of Cp^{Br}), 71.1 (C of Cp^{Br}), 79.9 (*ipso*-C-Br), 107.9 (*ipso*-C-NH_2). MS (70 eV): *m/z* (%) 279 (100) [M^+], 199 (10) [M^+ - HBr]. HRMS (70 eV): calcd for $C_{10}H_{10}BrFeN$, 278.9346; found, 278.9357. Anal. Calcd for a mixture of $C_{10}H_{10}BrFeN$ (279.94; 94%) and $C_{10}H_{11}FeN$ (201.05; 6%): C, 43.91; H, 3.72; N, 5.12. Found: C, 43.86; H, 3.29; N, 4.90. Note: The ^{1}H NMR

(in C_6D_6) of the isolated product shows small peaks at δ 1.85 (s, 2H, NH_2) and 3.97 (s, 5H, Cp) ppm which are resulting from the non-bromo impurity **120**. The other peaks (for Cp^{NH2}) of the byproduct **120** presumably overlap with the stronger signals of the major product **114**.

4.10. Synthesis of 1-Bromo-1'-(trimethylsilylamino)ferrocene (142)

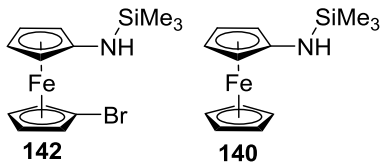

Compound **114** (0.28 g, 1.0 mmol) was suspended in hexanes (20.0 mL), NEt_3 (1.2 mL, 8.6 mmol) was added, followed by addition of a solution of chlorotrimethylsilane (0.20 mL, 1.6 mmol) in hexanes (4.0 mL). After stirring the solution for 20 h at r.t, all the insoluble materials were removed by a Schlenk filtration resulting in a red solution. After removal of all the volatiles under high vacuum, compound **142** was left behind as a red oil (0.32 g, 92%) which contained ca. 6% of (trimethylsilylamino)ferrocene (**140**) as an impurity. ^{1}H NMR ($CDCl_3$): δ 0.23 (s, 9H, Si(CH_3)$_3$), 2.42 (bs, 1H, NH), 3.85 (pst, 2H, CH of $Cp^{NHSiMe3}$), 3.88 (pst, 2H, CH of $Cp^{NHSiMe3}$), 3.99 (pst, 2H, CH of Cp^{Br}), 4.25 (pst, 2H, CH of Cp^{Br}). ^{13}C{^{1}H} NMR ($CDCl_3$): δ 0.18 (Si(*C*H$_3$)$_3$), 59.64 (C of $Cp^{NHSiMe3}$), 65.24 (C of $Cp^{NHSiMe3}$), 67.62(C-β of Cp^{Br}), 70.87(C-α of Cp^{Br}), 79.07 (*ipso*-C-Br), 109.34 (*ipso*-C-NHSiMe$_3$). MS (70 eV): *m/z* (%) 353 (76) [M^+], 273 (16) [M^+ - Br]. HRMS (70 eV): calcd for $C_{13}H_{18}BrFeNSi$, 350.9741; found, 350.9745. Note: Due to technical difficulties in analyzing liquids, an elemental analysis could not be performed for this compound. The ^{1}H NMR (in $CDCl_3$) of the isolated product shows a small peak at δ 4.06 (s, 5H, Cp) which is resulting from the non-bromo impurity **140**. Other peaks (for $Cp^{NHSiMe3}$, NH, and Si*Me*$_3$) of the byproduct **140** presumably overlap with the stronger signals of the major product **142**.

4.11. Synthesis of 1-Benzylidenimino-1'-bromoferrocene (143)

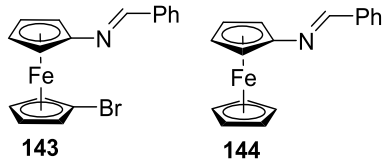

Compound **114** (0.250 g, 0.908 mmol) was dissolved in toluene (40 mL) and benzaldehyde (3.80 mL, 37.6 mmol) was added. After stirring the reaction mixture for 3 h at ambient temperature, all volatiles were removed under high vacuum, resulting in compound **143** as a dark red, sticky solid (0.325 g, 99%) which contained ca. 7% of benzylidenimino-ferrocene (**144**) as an impurity. NOE measurements revealed this imine to be the *trans* isomer. ^{1}H NMR (C_6D_6): δ 3.76 (pst, 2H, Cp^{Br}), 4.02 (pst, 2H, Cp^{NCHPh}), 4.24 (pst, 2H, Cp^{Br}), 4.50 (pst, 2H, Cp^{NCHPh}), 7.10-7.14 (m, 3H, *m*-H, *p*-H of Ph), 7.87 (m, 2H, *o*-H of Ph), 8.48 (s, 1H, NC*H*Ph). ^{13}C{^{1}H} NMR (C_6D_6): δ 65.6 (s, Cp^{NCHPh}), 68.8 (s, Cp^{Br}), 69.9 (s, Cp^{NCHPh}), 71.9 (s, Cp^{Br}), 79.5 (s, *ipso*-C-Br), 106.8 (s, *ipso*-C-N), 128.5 (s, C of Ph), 128.9 (s, C of Ph), 130.7 (s, C of Ph), 137.4 (s, *ipso*-C of Ph), 158.5 (s, N*C*HPh). MS (FDI): m/z (%) 367 (100) [M^+]. HRMS (FDI; m/z): $[M]^+$ calc for $C_{17}H_{14}BrFeN$, 366.9659; found 366.9671. Anal. Calcd for a mixture of $C_{17}H_{14}BrFeN$ (368.06, 93%) and $C_{17}H_{15}FeN$ (289.16, 7%): C, 56.54; H, 3.93; N, 3.88. Found: C, 56.32; H, 3.64; N, 3.72. Note: The ^{1}H NMR (in C_6D_6) of the isolated product shows a small peak at δ 4.05 (s, 5H, Cp) which is resulting from the non-bromo impurity **144**. The other peaks (for Cp^{NCHPh} and NC*HPh*) of the byproduct **144** presumably overlap with the stronger signals of the major product **143**.

4.12. Synthesis of 1-Bromo-1'-[(2,2-dimethylpropyliden)imino]ferrocene (145)

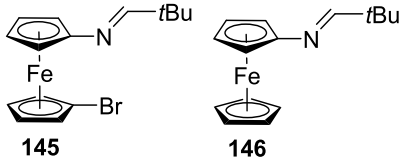

Compound **114** (0.373 g, 1.36 mmol) was dissolved in toluene (60 mL), pivalaldehyde (0.50 mL, 4.6 mmol) was added, followed by the addition of 3Å mole sieves (ca. 4 g). After stirring the reaction mixture for 4 h at ambient temperature, all insoluble materials were filtered off and volatiles were removed under high vacuum resulting in compound **145** as a dark red, sticky solid (0.450 g, 96%) which contained ca. 2–3 % of [(2,2-dimethylpropyliden)imino]ferrocene (**146**) as an impurity. NOE measurements revealed this imine to be the *trans* isomer. ^{1}H NMR (C_6D_6): δ 1.08 (s, 9H, *t*Bu), 3.77 (pst, 2H, Cp^{Br}), 3.93 (pst, 2H, Cp^{NCHtBu}), 4.22 (pst, 2H, Cp^{Br}), 4.35 (pst, 2H, Cp^{NCHtBu}), 7.86 (s, 1H, NC*H*t*Bu). ^{13}C{^{1}H} NMR (C_6D_6): δ 27.0 (s, NCHC(CH_3)$_3$), 36.9 (s, NCH*C*Me$_3$), 65.5 (s, Cp^{NCHtBu}), 68.6 (s, Cp^{Br}), 69.1 (s, Cp^{NCHtBu}), 71.8 (s, Cp^{Br}), 78.9 (s, *ipso*-C-Br), 107.5 (s, *ipso*-C-N), 170.6 (s, N*C*H*t*Bu). MS (FDI): m/z (%) 347 (100) [M^+]. HRMS (FDI; m/z): $[M]^+$ calc for $C_{15}H_{18}BrFeN$, 346.9972; found 346.9961. Anal. Calcd for a mixture of $C_{15}H_{18}BrFeN$ (348.07, 97.5%) and $C_{15}H_{19}FeN$ (269.17, 2.5%): C, 52.14; H, 5.26; N, 4.05. Found: C, 52.30; H, 5.03; N, 3.95. Note: The ^{1}H NMR (in C_6D_6) of the isolated product shows a small peak at δ 4.06 (s, 5H, Cp) which is resulting from the non-bromo impurity **146**. Other peaks (for Cp^{NCHtBu}, NC*H*t*Bu, and NC*HCMe*$_3$) of the byproduct **146** presumably overlap with the stronger signals of the major product **145**.

4.13. Synthesis of 1-Benzylamino-1'-bromoferrocene (147)

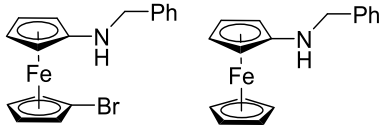

147 **148**

$NaBH_3CN$ (0.307 g, 4.89 mmol) was added to a glacial acetic acid solution (8 mL) of compound **143** (0.336 g, 0.927 mmol). After 18 h of stirring at ambient temperature, an aqueous solution of NaOH (10 mL; 6 M) was added to the yellow reaction mixture followed by addition of

CH_2Cl_2 (20 mL). From this point on the manipulation was done under air. The organic phase was separated, washed with water (2 × 20 mL), and dried over anhydrous Na_2SO_4. The partially purified compound was obtained as yellow solid by column chromatography on silica gel (hexanes : NEt_3, 9 : 1). Crystallization from a 1 : 1 mixture of hexanes and CH_2Cl_2 at -23 °C gave yellow crystals of compound **147** (0.156 g, 46%) which contained ca. 2–3% of (benzylamino)ferrocene (**148**) as an impurity. ^{1}H NMR (C_6D_6): δ 2.42 (s, 1H, NH), 3.60 (s, 2H, Cp^{NH}), 3.74 (s, 2H, Cp^{Br}), 3.77 (s, 2H, Cp^{NH}), 3.89 (s, 2H, NC*H*$_2$Ph), 4.25 (s, 2H, Cp^{Br}), 7.11 (t, 1H, *p*-H of Ph), 7.18 (q, 2H, *m*-H of Ph), 7.30 (d, 2H, *o*-H of Ph). ^{13}C{^{1}H} NMR (C_6D_6): δ 51.5 (s, N*C*H$_2$Ph), 58.0 (s, Cp^{NH}), 65.6 (s, Cp^{NH}), 67.1 (s, Cp^{Br}), 70.5 (s, Cp^{Br}), 79.3 (s, *ipso*-C-Br), 112.8 (s, *ipso*-C-N), 127.4 (s, Ph), 128.1 (s, Ph), 128.71 (s, Ph), 140.1 (s, *ipso*-C of Ph). MS (FDI): m/z (%) 369 (100) [M^+]. HRMS (FDI; m/z): $[M]^+$ calc for $C_{17}H_{16}BrFeN$, 368.9816; found 368.9819. Anal. Calcd for a mixture of $C_{17}H_{16}BrFeN$ (370.07, 97.5%) and $C_{17}H_{17}FeN$ (291.18, 2.5%): C, 55.55; H, 4.40; N, 3.81. Found: C, 55.19; H, 4.28; N, 3.63. Note: The ^{1}H NMR (in C_6D_6) of the isolated product mixture shows a small peak at δ 4.08 (s, 5H, Cp) which is resulting from the non-bromo impurity **148**. Other peaks (for Cp^{NH}, N*H*, and NC*H*$_2$*Ph*) of the byproduct **148** presumably overlap with the stronger signals of the major product **147**.

4.14. Synthesis of 1-Bromo-1'-(neopentylamino)ferrocene (149)

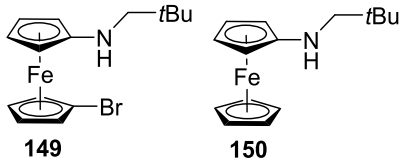

149 **150**

$NaBH_3CN$ (0.283 g, 4.50 mmol) was added to a glacial acetic acid solution (6 mL) of compound **145** (0.280 g, 0.809 mmol). After 18 h of stirring at ambient temperature, an aqueous solution of NaOH (10 mL; 6 M) was added to the yellow reaction mixture, followed by addition

of CH_2Cl_2 (20 mL). From this point on the manipulation was done under air. The organic phase was separated, washed with water (2 × 20 mL), and dried over anhydrous Na_2SO_4. The partially purified compound was obtained as yellow solid by column chromatography on silica gel (hexanes : NEt_3; 9 : 1) as eluent. Crystallization from a 1 : 1 mixture of hexanes and CH_2Cl_2 at -23 °C gave compound **149** as a yellow, waxy solid (0.156 g, 56%) which contained ca. 3-4% of (neopentylamino)ferrocene (**150**) as an impurity. ^{1}H NMR (C_6D_6): δ 0.86 (s, 9H, *t*Bu), 2.29 (br. s, 1H, N*H*), 2.60 (br. d, J = 3 Hz, 2H, NHC$\underline{H_2}$*t*Bu), 3.65 (pst, 2H, Cp^{NH}), 3.80 (pst, 2H, Cp^{Br}), 3.82 (pst, 2H, Cp^{NH}), 4.30 (pst, 2H, Cp^{Br}). ^{13}C{^{1}H} NMR (C_6D_6): δ 27.6 (s, C(*C*H$_3$)$_3$), 31.5 (s, *C*Me$_3$), 57.8 (s, Cp^{NH}), 58.8 (s, N*C*H$_2$*t*Bu), 65.5 (s, Cp^{NH}), 67.0 (s, Cp^{Br}), 70.4 (s, Cp^{Br}), 79.4 (s, *ipso*-C-Br), 113.7 (s, *ipso*-C-N). MS (FDI): m/z (%) 349 (100) [M^+]. HRMS (FDI; m/z): $[M]^+$ calc for $C_{15}H_{20}BrFeN$, 349.0129; found 349.0129. Anal. Calcd for a mixture of $C_{15}H_{20}BrFeN$ (350.08, 96.5%) and $C_{15}H_{21}FeN$ (271.19, 3.5%): C, 51.98; H, 5.83; N, 4.04. Found: C, 52.35; H, 5.48; N, 3.93. $\underline{\text{Note:}}$ The ^{1}H NMR (in C_6D_6) of the isolated product shows a small peak at δ 4.12 (s, 5H, Cp) which is resulting from the non-bromo impurity **150**. Other peaks (for Cp^{NH}, N*H*, and NC*H$_2$tBu*) of the byproduct **150** presumably overlapped with the stronger signals of the major product **149**.

4.15. Test Lithiation and Deuteration of Compounds 147 and 149, and Formation of 160 and 158

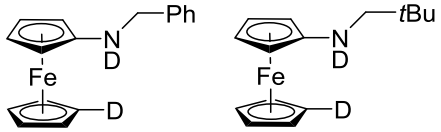

160 **158**

*n*BuLi (0.09 mL, 0.2 mmol) was added dropwise to a 0 ºC cooled solution of compound **147** (0.042 g, 0.11 mmol) in a mixture of hexanes and thf (5.0 mL; hexanes : thf; 9:1), resulting in a color change from pale yellow to bright orange. After the reaction mixture was stirred for 40 min

at 0 ºC, D_2O (0.05 mL, 3 mmol) was added dropwise over 1 min, followed by removal of the cold bath. After 15 min stirring at ambient temperature, a ^1H NMR spectrum (C_6D_6) was measured from a sample of the supernatant clear solution. ^1H NMR of **160** (C_6D_6): δ 3.67 (m, 2H, CH_2), 3.76 (pst, 2H, Cp^D), 3.85 (pst, 2H, Cp^D), 4.07 (s, 4H, $Cp^{NDCH2Ph}$).

A similar experiment was performed with compound **149**, when *n*BuLi (0.12 mL, 0.30 mmol) was added dropwise to a -78 ºC cooled solution of **149** (0.050 g, 0.14 mmol) in a mixture of hexanes and thf (5 mL; hexanes : thf; 9:1), resulting in a color change from pale yellow to bright orange. After the reaction mixture was stirred for 40 min at -78 ºC, the cold bath was replaced by an ice bath, followed by stirring of the reaction mixture at 0 °C for 1 h. D_2O (0.10 mL, 5.5 mmol) was added dropwise over 2 min. The reaction mixture was warmed to ambient temperature and, after stirring for 15 min, a ^1H NMR spectrum was measured from a sample of the supernatant clear solution. ^1H NMR of **158** (C_6D_6): δ 0.85 (s, 9H, CMe_3) 2.56 (m, 2H, CH_2), 3.72 (pst, 2H, Cp^D), 3.82 (pst, 2H, Cp^D), 4.12 (s, 4H, $Cp^{NDCH2tBu}$).

4.16. Synthesis of 2,2-Dimethyl-1-trimethylsilyl-1,2-azasila[2]ferrocenophane (161)

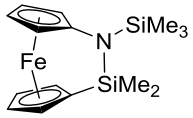

161

*n*BuLi (0.40 mL, 1.0 mmol) was added dropwise to a -78 ºC cooled solution of compound **142** (0.17 g, 0.49 mmol) in thf (24.0 mL), resulting in a color change from pale yellow to bright orange. After the reaction mixture was stirred for 40 min at -78 ºC, the cold bath was replaced by an ice bath, followed by stirring of the reaction mixture at 0 °C for 1 h. The resulting deep red solution was cooled to -78 ºC and a solution of Me_2SiCl_2 (0.064 g, 0.50 mmol) in thf (5.0 mL) was added dropwise over 5 min. The reaction mixture was warmed up to ambient temperature and

stirred for 4 h. After all volatiles were removed under high vacuum, the product was dissolved in hexanes (15.0 mL) and LiCl was removed by a Schlenk filtration. From this red solution, solvents were removed under high vacuum, resulting in a red, sticky solid. Product **161** was obtained by vacuum sublimation (45 °C oil bath temperature; p ~ 10^{-2} mbar) in form of red crystals (0.085 g, 53%). ^{1}H NMR (C_6D_6): δ 0.07 (s, 9H, Si(CH_3)$_3$), 0.43 (s, 6H, (CH_3)$_2$Si), 3.80 (pst, 2H, CH of Cp^{NSiMe3}), 4.23 (pst, 2H, CH of Cp^{NSiMe3}), 4.27 (pst, 2H, CH of Cp^{SiMe2}), 4.63 (pst, 2H, CH of Cp^{SiMe2}). ^{13}C{^{1}H} NMR (C_6D_6): δ 0.7 (Si(*C*H$_3$)$_3$), 3.0 (Si(*C*H$_3$)$_2$), 67.2 (C of Cp^{NSiMe3}), 70.0 (*ipso*-C-SiMe$_2$), 70.9 (C of Cp^{SiMe2}), 72.1 (C of Cp^{NSiMe3}), 75.9 (C of Cp^{SiMe2}), 102.0 (*ipso*-C-NSiMe$_3$). MS (70 eV): *m/z* (%) 329 (100) [M^+], 314 (16) [M^+ - Me]. HRMS (70 eV; m/z): calcd for $C_{15}H_{23}FeNSi_2$, 329.0718; found, 329.0724. Anal. Calcd for $C_{15}H_{23}FeNSi_2$: C, 54.70; H, 7.04; N, 4.25. Found: C, 55.01; H, 6.73; N, 4.29.

4.17. Synthesis of 2,2-Dimethyl-1-trimethylsilyl-1,2-azastanna[2]ferrocenophane (162)

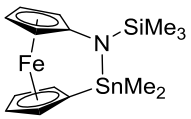

162

*n*BuLi (0.57 mL, 1.4 mmol) was added dropwise to a -78 ºC cooled solution of compound **142** (0.25 g, 0.72 mmol) in thf (36.0 mL), resulting in a color change from pale yellow to bright orange. After the reaction mixture was stirred for 40 min at -78 ºC, the cold bath was replaced by an ice bath, followed by stirring of the reaction mixture at 0 °C for 1 h. The resulting deep red solution was cooled to -78 ºC and a solution of Me_2SnCl_2 (0.15 g, 0.68 mmol) in thf (5.0 mL) was added dropwise over 5 min. The reaction mixture was warmed up to ambient temperature and stirred for 4 h. After all volatiles were removed under high vacuum, the product was dissolved in hexanes (15.0 mL) and LiCl was removed by a Schlenk filtration. From this red solution, solvents

were removed under high vacuum, resulting in a red, sticky solid. Product **162** was obtained by vacuum sublimation (120 °C oil bath temperature; p ~ 10^{-2} mbar) in form of red crystals which sublimed together with a red, sticky oil (0.043 g, approx. 14%). According to ^{1}H NMR data, the isolate mixture was composed out of compound **162** (ca. 90%) and 1-trimethylsilylamino-1'-(chlorodimethylstannyl)ferrocene (ca. 10%). ^{1}H NMR (C_6D_6): δ 0.06 (s, 9H, Si(CH_3)$_3$), 0.40 (s, 6H, (CH_3)$_2$Sn), 3.78 (pst, 2H, CH of Cp^{NSiMe3}), 4.23 (pst, 2H, CH of Cp^{NSiMe3}), 4.45 (pst, 2H, CH of Cp^{SnMe2}), 4.69 (pst, 2H, CH of Cp^{SnMe2}). ^{13}C{^{1}H} NMR (C_6D_6): δ -2.04 (Si(CH_3)$_3$), 1.3 (Sn(CH_3)$_2$), 65.4 (C of Cp^{NSiMe3}), 70.4 (*ipso*-C-SnMe$_2$), 70.6 (C of Cp^{SnMe2}), 72.9 (C of Cp^{SnMe2}), 76.7 (C of Cp^{NSiMe3}), 114.2 (*ipso*-C-NSiMe$_3$). ^{119}Sn NMR (C_6D_6): δ 83.2. MS (70 eV): *m/z* (%) 421 (100) [M^+], 391 (17) [M^+ - 2Me]. HRMS (70 eV; *m/z*): calcd for $C_{15}H_{23}FeNSi_2$, 420.9971; found, 420.9973. Note: As compound **162** could not be isolated as analytically pure species no elemental analysis was done for this compound.

4.18. Synthesis of 2,2-Di-*tert*-butyl-1-trimethylsilyl-1,2-azastanna[2]ferrocenophane (165)

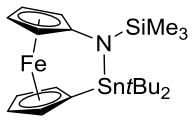

165

*n*BuLi (0.48 mL, 1.2 mmol) was added dropwise to a -78 ºC cooled solution of compound **142** (0.20 g, 0.57 mmol) in thf (29.0 mL), resulting in a color change from pale yellow to bright orange. After the reaction mixture was stirred for 40 min at -78 ºC, the cold bath was replaced by an ice bath, followed by stirring of the reaction mixture at 0 °C for 1 h. The resulting deep red solution was cooled to -78 ºC and a solution of *t*Bu$_2$SnCl$_2$ (0.17 g, 0.56 mmol) in thf (6.0 mL) was added dropwise over 5 min. The reaction mixture was warmed up to ambient temperature and stirred for 4 h. After all volatiles were removed under high vacuum, the product was dissolved in

hexanes (20.0 mL) and LiCl was removed by a Schlenk filtration. From this red solution, solvents were removed under high vacuum, resulting in a red, sticky solid. Product **165** was obtained by vacuum sublimation (95 °C oil bath temperature; p ~ 10^{-2} mbar) in form of red crystals (0.18 g, 62%). ^{1}H NMR (C_6D_6): δ 0.13 (s, 9H, Si(CH_3)$_3$), 1.40 (s, 18H, Sn[C(CH_3)$_3$]$_2$), 3.80 (pst, 2H, CH of $Cp^{NHSiMe3}$), 4.26 (pst, 2H, CH of $Cp^{NHSiMe3}$), 4.36 (pst, 2H, CH of Cp^{SntBu2}), 4.69 (pst, 2H, CH of Cp^{SntBu2}). ^{13}C{^{1}H} NMR (C_6D_6): δ 1.8 (Si(CH_3)$_3$), 31.3 (Sn[C(CH_3)$_3$]$_2$), 34.2 (Sn[C(CH$_3$)$_3$]$_2$), 65.7 (C of Cp^{NSiMe3}), 70.9 (C of Cp^{SntBu2}), 70.9 (C of Cp^{NSiMe3}), 74.5 (*ipso*-C-Sn*t*Bu$_2$), 77.7 (C of Cp^{SntBu2}), 113.7 (*ipso*-C-NSiMe$_3$). ^{119}Sn NMR: δ 44.1 (C_6D_6); 44.8 ($CDCl_3$). MS (70 eV): *m/z* (%) 505 (22) [M^+], 391 (100) [M^+ - 2*t*Bu]. HRMS (70 eV; m/z): calcd for $C_{21}H_{35}FeNSiSn$, 505.0910; found, 505.0907. Anal. Calcd for $C_{21}H_{35}FeNSiSn$: C, 50.03; H, 7.00; N, 2.78. Found: C, 49.97; H, 7.22; N, 2.81.

4.19. Attempted Thermal ROP of Compounds 165 and 161

In an evacuated and sealed NMR tube compound **165** (0.020 g, 0.040 mmol) was heated at temperatures of 200 ºC (for 40 min). During the heating no significant change of viscosity was observed. When the sample was further heated at 260 ºC for another 40 min a black solid with a red waxy mass was resulted. The sealed tube was removed from the oven and cooled to ambient temperature. Inside a glovebox the sealed tube was opened and C_6D_6 (0.5 mL) was added. An orange solution with a solid black residue was resulted. The orange supernant was then decanted from a solid black residue. The ^{1}H NMR spectrum of the supernant showed signals of the starting material, of (trimethylsilylamino)ferrocene (**140**), and of unidentified species. Mass spectrometry confirmed the presence of starting material and (trimethylsilylamino)ferrocene. The black residue was then dissolved in conc. HCl, which resulted in evolution of gas. Neutralization by 6 M NaOH (aq.) gave a white precipitate, which disolved in excess amount of NaOH (aq.). The precipitate did

not change its color after long exposure to air showing that the black residue did not contain any iron. This confirmatory wet test identifies the black residue as metallic tin.

Compound **161** (0.020 g, 0.061 mmol) was taken in an evacuated and sealed NMR tube and heated at 200 ºC for 40 min while the compound melted and the vapor started to condense on the inner wall of the NMR tube. No significant change of viscosity was observed even when the compound was further heated at 260 ºC (40 min) and 300 ºC (21 h). The sealed tube was then cooled to ambient temperature and opened inside a glovebox. The sample completely dissolved in C_6D_6 (0.5 mL). The NMR spectrum of the resulting solution indicated only the presence of starting material.

4.20. Attempted Catalytic ROP of Compounds 165 and 161

Karstedt's catalyst (7.0 μL, 0.016 mmol) was added to a solution of compound **165** (0.015 g, 0.030 mmol) in C_6D_6 (0.5 mL). After 24 h of storing at room temperature, ^{1}H NMR spectroscopy revealed the presence of only starting reagents. After 65 h at 50 ºC, again, only starting materials were detected by ^{1}H NMR spectroscopy.

A similar experiment was performed with compound **161**. Karstedt's catalyst (8.0 μL, 0.018 mmol) was added to a solution of compound **161** (0.012 g, 0.036 mmol) in C_6D_6 (0.5 mL) and the solution was heated to 50 ºC for 65 h. The ^{1}H NMR spectrum of the resulting reaction mixture showed only the peaks of starting material and Karstedt's catalyst.

4.21. Anionic Ring-opening Reactions of Compounds 165 and 161, and Formation of 167 and 171

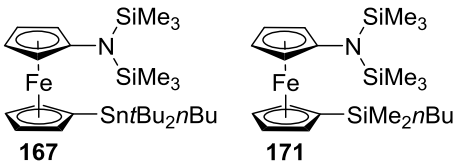

167 **171**

1.6 M *n*BuLi (19 μL, 0.030 mmol) was added to a solution of compound **165** (0.014 g, 0.028 mmol) in thf (0.5 mL). After 0.5 h at r.t., with shaking of the NMR sample occasionally once in every 5 to 10 min, Me_3SiCl (30 μL, 0.24 mmol) was added to the reaction mixture. All volatiles were removed and the resulting red sticky oil was dissolved in $CDCl_3$ (0.5 mL). The ^1H NMR spectrum of the resulting solution showed [{$(Me_3Si)_2N$}H_4C_5][(*n*Bu*t*Bu_2Sn)H_4C_5]Fe (**167**) as the main product.

Characterization of [{$(Me_3Si)_2N$}H_4C_5][(*n*Bu*t*Bu_2Sn)H_4C_5]Fe (167). ^1H NMR ($CDCl_3$): δ0.22 (s, 18H, [Si(CH_3)$_3$]$_2$), 0.96 (t, 3H, CH_3), 1.06 (m, 2H, CH_2-Sn), 1.23 (s, 18H, Sn[C(CH_3)$_3$]$_2$), 1.44 (m, 2H, CH_2), 1.70 (m, 2H, CH_2), 3.71 (pst, 2H, CH of $Cp^{NHSiMe3}$), 3.89 (pst, 2H, CH of $Cp^{NHSiMe3}$), 3.98 (pst, 2H, CH of Cp^{SntBu2}), 4.27 (pst, 2H, CH of Cp^{SntBu2}). $^{13}C\{^1H\}$ NMR ($CDCl_3$): δ 3.5 (Si(*C*H$_3$)$_3$), 9.6 (*C*H$_3$), 13.7 (*C*H$_2$), 27.6 (*C*H$_2$), 28.2 (*C*H$_2$), 29.7 (Sn[*C*(CH$_3$)$_3$]$_2$), 31.5 (Sn[C(*C*H$_3$)$_3$]$_2$), 63.7 (C of Cp), 65.3 (C of Cp), 68.8 (*ipso*-C-Sn*t*Bu$_2$) 73.2 (C of Cp), 74.8 (C of Cp), 107.9 (*ipso*-C-N[SiMe$_3$]$_2$). ^{119}Sn NMR ($CDCl_3$): δ -32.2. HRMS (FD): calcd for $C_{28}H_{53}FeNSi_2Sn$, 635.2088; found, 635.2079.

A similar experiment was performed with compound **161**. *n*BuLi (1.6 M, 19 μL, 0.030 mmol) was added to a solution of compound **161** (0.010 g, 0.030 mmol) in thf (0.5 mL). After the solution was left at r.t. for 1 h, Me_3SiCl (30 μL, 0.24 mmol) was added. All the volatiles were removed and the resulting sticky red oil was dissolved in $CDCl_3$ (0.5 mL). The ^1H NMR and ^{13}C NMR spectra revealed the presence of starting material (**161**) along with [{$(Me_3Si)_2N$}H_4C_5][(*n*$BuMe_2Si$)H_4C_5]Fe (**171**). A similar reaction mixture was left for 6 h as reaction time and subsequently quenched with excess amount of Me_3SiCl. After removing all the volatiles, 0.5 mL of $CDCl_3$ was added. The ^1H NMR and ^{13}C NMR spectra indicated a similar

reaction mixture as that found after 1 h. The presence of ring-opened compound was also confirmed by observed [M^+] measured in ACCU-TOF mass spectrometer.

Characterization of [{(Me$_3$Si)$_2$N}H$_4$C$_5$][(*n*BuMe$_2$Si)H$_4$C$_5$]Fe (171). ^{1}H NMR ($CDCl_3$): δ0.21 (s, 24H, Si(CH_3)$_2$, Si(CH_3)$_3$), 0.65 (m, 2H, CH_2), 0.88 (m, 2H, CH_2), 1.32 (t, 2H, CH_3), 3.72 (pst, 2H, CH of Cp^{NHSiMe3}), 3.90 (pst, 2H, CH of Cp^{NHSiMe3}), 4.04 (pst, 2H, CH of Cp$^{Sn\mathit{t}Bu2}$), 4.24 (pst, 2H, CH of Cp$^{Sn\mathit{t}Bu2}$). ^{13}C{^{1}H} NMR ($CDCl_3$): δ -2.1 (Si(*C*H$_3$)$_2$), 3.5 (Si(*C*H$_3$)$_3$), 13.8 (*C*H$_3$), 16.7 (*C*H$_2$), 26.3 (*C*H$_2$), 26.6 (*C*H$_2$), 63.5 (C of Cp), 65.3 (C of Cp), 70.5 (*ipso*-C-Sn*t*Bu$_2$) 73.3 (C of Cp), 73.5 (C of Cp), 108.1 (*ipso*-C-N[SiMe$_3$]$_2$). HRMS (FD): calcd for $C_{22}H_{41}FeNSi_3$, 459.1896; found, 459.1884.

4.22. Attempted Anionic ROP of Compounds 165 and 161, and Formation of 167, 172, and 171

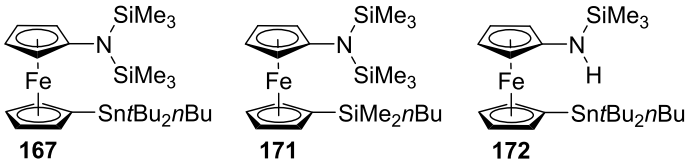

1.6 M *n*BuLi (7 μL, 0.011 mmol) was added to a solution of compound **165** (0.024 g, 0.048 mmol) in thf (0.85 mL). After 6 h at r.t., with occasionally shaking of the NMR sample, Me$_3$SiCl (30 μL, 0.24 mmol) was added to the reaction mixture. All volatiles were removed and the resulting red sticky oil was dissolved in $CDCl_3$ (0.5 mL). The ^{1}H NMR spectrum of the resulting solution showed the peaks of starting material (**165**), [{(Me$_3$Si)$_2$N}H$_4$C$_5$][(*n*Bu*t*Bu$_2$Sn)H$_4$C$_5$]Fe (**167**), and [{(Me$_3$Si)HN}H$_4$C$_5$][(*n*Bu*t*Bu$_2$Sn)H$_4$C$_5$]Fe (**172**). The presence of ring-opened compounds was further confirmed by mass spectrometry (MS (FD): *m/z* 563 (**172**) and 635 (**167**) [M^+]).

A similar experiment was performed with compound **161**, when *n*BuLi (1.6 M, 9 μL, 0.014 mmol) was added to a solution of **161** (0.020 g, 0.061 mmol) in thf (1.00 mL). After the solution

was stored at r.t. for 6 h, Me_3SiCl (30 μL, 0.24 mmol) was added. All the volatiles were removed and the resulting red sticky oil was dissolved in $CDCl_3$ (0.5 mL). The ^1H NMR spectrum revealed the presence of starting material (**161**) along with [{$(Me_3Si)_2N$}H_4C_5][(nBuMe$_2$Si)H_4C_5]Fe (**171**).

4.23. Attempted Photo-controlled ROP of Compounds 165 and 161

A solution of compound **165** (0.025 g, 0.076 mmol) in thf in an NMR tube was treated with (i) 0.10 equivalents, (ii) 0.25 equivalents, and (iii) 1.0 equivalents of Na(C_5H_5). The three solutions were placed in a 5 ºC bath and irradiated for 5 h. All volatiles were removed and the resulting red sticky solid was dissolved in C_6D_6 (0.5 mL). In each case, the ^1H NMR spectrum of the resulting solution showed only the peaks of starting reagents. The similar experiments were performed with compound **161** which also resulted only in unreacted starting reagents (^1H NMR spectroscopy).

4.24. Synthesis of 2,2-Di-*tert*-butyl-1-neopentyl-1,2-azastanna[2]ferrocenophane (174)

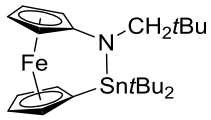

174

nBuLi (0.35 mL, 0.88 mmol) was added dropwise to a -78 ºC cooled solution of compound **149** (0.146 g, 0.420 mmol) in a solvent mixture of hexanes and thf (10 mL; hexanes : thf, 9 : 1), resulting in a color change from pale yellow to bright orange. After the reaction mixture was stirred for 40 min at -78 ºC, the dry ice bath was replaced by an ice bath, followed by stirring of the reaction mixture at 0 °C for 1 h. A solution of tBu$_2$SnCl$_2$ (0.128 g, 0.421 mmol) in hexanes (5 mL) was added dropwise over 2 min. The reaction mixture was warmed to ambient temperature and stirred for 1 h. After all volatiles were removed under high vacuum, the product was dissolved in hexanes (15.0 mL) and LiCl was removed by a Schlenk filtration. From this red solution, solvents were removed under high vacuum, resulting in a red, sticky liquid. Product **174** was obtained by

crystallization in Et_2O at -80 °C in form of red crystals (0.150 g, 71%). ^1H NMR (C_6D_6): δ 0.89 (s, 9H, $NCH_2C(CH_3)_3$), 1.44 (s, 18H, $Sn[C(CH_3)_3]_2$), 3.02 (s, 2H, NCH_2tBu), 3.80 (pst, 2H, CH of $Cp^{NHCH2tBu}$), 4.23 (pst, 2H, CH of $Cp^{NHCH2tBu}$), 4.57 (pst, 2H, CH of Cp^{SntBu2}), 4.72 (pst, 2H, CH of Cp^{SntBu2}). $^{13}C\{^1H\}$ NMR (C_6D_6): δ 28.7 ($NCH_2C(CH_3)_3$), 31.2 ($Sn[C(CH_3)_3]_2$), 34.7 ($Sn[C(CH_3)]_2$), 35.3 (NCH_2CMe_3), 65.0 (C of $Cp^{NCH2tBu}$), 68.7 (C of Cp^{SntBu2}), 69.4 (NCH_2tBu), 70.8 (C of Cp^{NSiMe3}), 77.7 (C of Cp^{SntBu2}), 121.9 (*ipso*-C-NCH_2tBu). MS (FD): *m/z* 503 [M^+]. HRMS (FD): calcd for $C_{23}H_{37}FeNSn$, 503.1297; found, 503.1314. Note: This compound contains a small amount of unknown impurity which shows a small peak at 1.46 ppm in ^1H NMR and another small peak at 30.7 ppm in ^{13}C NMR. As no isolation procedure could be successful to isolate the strained compound in an analytically pure form, this isolated product mixture was used in further chemical transformation without purification. Anal. Calcd for $C_{23}H_{37}FeNSn$: C, 55.02; H, 7.43; N, 2.79. Found: C, 52.25; H, 7.27; N, 2.34. The significant difference between calculated and found values is due to the presence of impurity in the sample.

4.25. Anionic Ring-opening Reaction of Compound 174 and Formation of 175

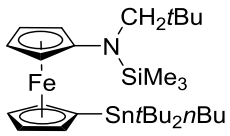

175

1.6 M *n*BuLi (9.0 μL, 0.014 mmol) was added to a solution of compound **174** (0.007 g, 0.01 mmol) in thf (0.5 mL). After 4 h at r.t., with shaking of the NMR sample occasionally once in every 5 to 10 min, Me_3SiCl (30 μL, 0.24 mmol) was added to the reaction mixture. All volatiles were removed and the resulting red sticky oil was dissolved in $CDCl_3$ (0.5 mL). The ^1H NMR spectrum of the resulting solution showed starting material (**174**) along with [{$(Me_3Si)(CH_2tBu)$}NH_4C_5][($nButBu_2Sn$)H_4C_5]Fe (**175**) as ring-opened compound.

Characterization of [{(Me$_3$Si)(CH$_2$*t*Bu)}NH$_4$C$_5$][(*n*Bu*t*Bu$_2$Sn)H$_4$C$_5$]Fe (175). ^{1}H NMR (C_6D_6): δ 0.33 (s, 9H, Si(C*H*$_3$)$_3$), 0.91 (s, 9H, NCH$_2$C(C*H*$_3$)$_3$), 1.33 (s, 18H, Sn[C(C*H*$_3$)$_3$]$_2$), 2.97 (s, 2H, NC*H*$_2$*t*Bu), 3.95 (s, 2H, CH of Cp^{NHCH2tBu}), 3.98 (s, 2H, CH of Cp^{NHCH2tBu}), 4.11 (pst, 2H, CH of Cp^{SntBu2}), 4.34 (pst, 2H, CH of Cp^{SntBu2}). Signals for *n*Bu group appear as small peaks in the region of δ = 0.60 – 2.00 ppm. MS (FD): *m/z* 633 [M$^+$].

4.26. Attempted Anionic ROP of Compound 174

1.6 M *n*BuLi (19 μL, 0.030 mmol) was added to a solution of compound **174** (0.014 g, 0.028 mmol) in thf (0.5 mL). After 0.5 h at r.t., with shaking of the NMR sample occasionally once in every 5 to 10 min, Me$_3$SiCl (30 μL, 0.24 mmol) was added to the reaction mixture. All volatiles were removed and the resulting red sticky oil was dissolved in $CDCl_3$ (0.5 mL). The ^{1}H NMR spectrum of the resulting solution showed [{(Me$_3$Si)(CH$_2$*t*Bu)}NH$_4$C$_5$][(*n*Bu*t*Bu$_2$Sn)H$_4$C$_5$]Fe (**175**) along with the starting material **174**.

4.27. Synthesis of 2-*Tert*-butyl-1-trimethylsilyl-1,2-azaphospha[2]ferrocenophane (176)

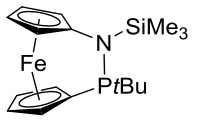

176

*n*BuLi (0.40 mL, 1.0 mmol) was added dropwise to a -78 ºC cooled solution of compound **142** (0.164 g, 0.472 mmol) in a solvent mixture of hexanes and thf (10 mL; hexanes : thf, 9 : 1), resulting in a color change from pale yellow to bright orange. After the reaction mixture was stirred for 40 min at -78 ºC, the dry ice bath was replaced by an ice bath, followed by stirring of the reaction mixture at 0 °C for 1 h. A solution of *t*BuPCl$_2$ (0.45 mL, 1.0 M in Et$_2$O) was added dropwise over 2 min. The reaction mixture was warmed to ambient temperature and stirred for 3 h. After all volatiles were removed under high vacuum, the product was dissolved in hexanes (15.0

mL) and LiCl was removed by a Schlenk filtration. From this red solution, solvents were removed under high vacuum, resulting in a red, sticky liquid. Product **176** was obtained by flask-to-flask condensation (60 °C; p ~ 10^{-2} mbar) in form of a red sticky oil (0.110 g, 65%). ^{1}H NMR (C_6D_6): δ 0.26 (s, 9H, Si(CH_3)$_3$), 1.35 (d, J = 12.5 Hz, 9H, PC(CH_3)$_3$), 3.67 (m, 1H, H of Cp^{NSiMe3}), 3.73 (m, 1H, H of Cp^{NSiMe3}), 3.98 (m, 1H, H of Cp^{NSiMe3}), 4.15 (m, 1H, H of Cp^{NSiMe3}), 4.88 (m, 1H, H of Cp^{PtBu}), 4.94 (m, 1H, H of Cp^{PtBu}), 5.10 (m, 1H, H of Cp^{PtBu}), 5.18 (m, 1H, H of Cp^{PtBu}). ^{13}C{^{1}H} NMR (C_6D_6): δ 2.1 (d, J = 6 Hz, Si(CH_3)$_3$), 28.7 (d, J = 18 Hz, PC(CH_3)$_3$), 33.9 (d, J = 29 Hz, PCMe$_3$), 66.3 (s, Cp^{NSiMe3}), 66.6 (s, Cp^{NSiMe3}), 69.4 (s, Cp^{NSiMe3}), 70.97 (s, Cp^{NSiMe3}), 70.99 (d, J = 9 Hz, Cp^{PtBu}), 74.1 (s, Cp^{PtBu}), 76.6 (d, J = 5 Hz, Cp^{PtBu}), 77.4 (d, J = 37 Hz, Cp^{PtBu}), 80.4 (d, J = 37 Hz, *ipso*-C-P), 117.7 (d, J = 7 Hz, *ipso*-C-N). ^{31}P NMR (C_6D_6): δ 147.8 (decet, J = 12 Hz). MS (FDI): m/z (%) 359 (100) [M^+]. HRMS (FDI; m/z): [M]$^+$ calc for $C_{17}H_{26}FeNPSi$, 359.0922; found 359.0937. Note: Due to the technical difficulty in analyzing sticky liquids, an elemental analysis could not be performed for this compound.

4.28. Sulfurization of Compound 176, and Formation of 177 and 178

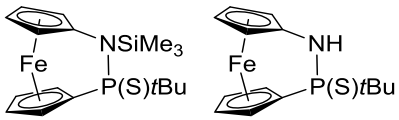

177 **178**

Under an atmosphere of air, elemental sulfur (0.406 g, 12.7 mmol) was added to a solution of compound **176** (0.094 g, 0.26 mmol) in CH_2Cl_2 (10 mL) and this reaction mixture was stirred for 3 h at ambient temperature. After removal of all volatiles under high vacuum, the solid yellow mass was used for column chromatography on silica gel (hexanes : Et_3N, 20 : 1). Two fractions were obtained from red bands and, after removing all volatiles under high vacuum, each compound was purified by vacuum sublimation (100 °C; p ~ 10^{-2} mbar). While from the first band compound

177 was obtained as a red, waxy solid (0.022 g, 22%), the second band gave compound **178** as a red, crystalline solid (0.034 g, 41%). The obtained crystals were used for single crystal X-ray analysis.

Characterization of 177. ^{1}H NMR (C_6D_6): δ 0.32 (s, 9H, Si(CH_3)$_3$), 1.41 (d, J = 17.5 Hz, 9H, C(CH_3)$_3$), 3.72 (m, 2H, Cp^{NSiMe3}), 3.97 (m, 1H, Cp^{NSiMe3}), 4.06 (m, 1H, Cp^{NSiMe3}), 4.18 (m, 1H, Cp$^{PS\textit{t}Bu}$), 4.69 (m, 1H, Cp$^{PS\textit{t}Bu}$), 4.77 (m, 1H, Cp$^{PS\textit{t}Bu}$), 5.71 (m, 1H, Cp$^{PS\textit{t}Bu}$). ^{13}C{^{1}H} NMR (C_6D_6): δ 2.2 (s, Si(CH$_3$)$_3$), 27.4 (d, J = 3 Hz, PC(CH$_3$)$_3$), 39.2 (d, J = 63 Hz, PCMe$_3$), 69.4 (s, Cp^{NSiMe3}), 69.5 (s, Cp^{NSiMe3}), 70.3 (s, Cp^{NSiMe3}), 72.0 (d, J = 11 Hz, Cp$^{P\textit{t}Bu}$), 72.6 (d, J = 9 Hz, Cp$^{P\textit{t}Bu}$), 73.1 (s, Cp^{NSiMe3}), 74.1 (d, J = 10 Hz, Cp$^{P\textit{t}Bu}$), 78.3 (d, J = 13 Hz, Cp$^{P\textit{t}Bu}$), 80.3 (d, J = 90 Hz, *ipso*-C-P), 96.2 (d, J = 8 Hz, *ipso*-C-N). ^{31}P NMR (C_6D_6): δ 110.4 (decet, J = 18 Hz). MS (70 eV): m/z (%) 391 (100) [M$^+$], 334 (85) [M$^+$ - *t*Bu], 73 (26) [SiMe$_3^+$]. HRMS (70 eV; m/z): [M]$^+$ calc for $C_{17}H_{26}FeNPSSi$, 391.0642; found 391.0636. Anal. Calcd for $C_{17}H_{26}FeNPSSi$ (391.37): C, 52.17; H, 6.70, N, 3.58. Found: C, 52.75; H, 6.42; N; 3.41.

Characterization of 178. ^{1}H NMR (C_6D_6): δ 1.24 (d, J = 17.5 Hz, 9H, PC(CH_3)$_3$), 2.53 (br. d, J = 8.5 Hz, 1H, NH), 3.61 (m, 1H, Cp^{NH}), 3.84 (m, 1H, Cp^{NH}), 3.97 (m, 1H, Cp^{NH}), 4.09 (m, 1H, Cp^{NH}), 4.28 (m, 1H, Cp$^{PS\textit{t}Bu}$), 4.74 (m, 1H, Cp$^{PS\textit{t}Bu}$), 5.41 (m, 1H, Cp$^{PS\textit{t}Bu}$), 5.87 (m, 1H, Cp$^{PS\textit{t}Bu}$). ^{13}C{^{1}H} NMR (C_6D_6): δ 25.5 (d, J = 2 Hz, PC(CH$_3$)$_3$), 38.5 (d, J = 67 Hz, PCMe$_3$), 67.9 (s, Cp^{NH}), 70.4 (s, Cp^{NH}), 71.7 (d, J = 12 Hz, Cp^{NH}), 73.0 (d, J = 9 Hz, Cp$^{P\textit{t}Bu}$), 73.3 (d, J = 4 Hz, Cp$^{P\textit{t}Bu}$), 73.91 (s, Cp^{NH}), 73.95 (d, J = 9 Hz, Cp$^{P\textit{t}Bu}$), 73.90 (d, J = 90 Hz, *ipso*-C-P), 82.7 (d, J = 15 Hz, Cp$^{P\textit{t}Bu}$), 94.1 (d, J = 9 Hz, *ipso*-C-P). ^{31}P NMR (C_6D_6): δ 106.1 (m). MS (70 eV): m/z (%) 319 (100) [M$^+$], 263 (77) [M$^+$ - *t*Bu]. HRMS (70 eV; m/z): [M]$^+$ calc for $C_{14}H_{18}FeNPS$, 319.0247; found 319.0257. Anal. Calcd for $C_{14}H_{18}FeNPS$ (319.18): C, 52.68; H, 5.68, N, 4.39. Found: C, 53.09, H, 5.08, N, 4.31.

4.29. Synthesis of 2-Phenyl-1-trimethylsilyl-1.2-azaphospha[2]ferrocenophane (179)

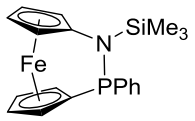

179

*n*BuLi (0.45 mL, 1.1 mmol) was added dropwise to a -78 ºC cooled solution of compound **142** (0.185 g, 0.533 mmol) in a solvent mixture of hexanes and thf (10 mL; hexanes : thf, 9 : 1), resulting in a color change from pale yellow to bright orange. After the reaction mixture was stirred for 40 min at -78 ºC, the dry ice bath was replaced by an ice bath, followed by stirring of the reaction mixture at 0 °C for 1 h. A solution of $PhPCl_2$ (0.093 g, 0.52 mmol) in hexanes (5 mL) was added dropwise over 2 min. The reaction mixture was warmed to ambient temperature and stirred for 3 h. After all volatiles were removed under high vacuum, the product was dissolved in hexanes (15.0 mL) and LiCl was removed by a Schlenk filtration. From this red solution, solvents were removed under high vacuum, resulting in a red, sticky liquid. Product **179** was obtained by flask-to-flask condensation (60 °C; p ~ 10^{-2} mbar) in form of a red sticky oil (0.130 g, 64%). ^{1}H NMR (C_6D_6, 500 MHz): 0.24 (9H, Si(CH_3)$_3$), 3.60 (s, 1H, H of Cp^{NSiMe3}), 3.61 (s, 1H, H of Cp^{NSiMe3}), 3.78 (s, 1H, H of Cp^{NSiMe3}), 4.20 (s, 1H, H of Cp^{NSiMe3}), 4.59 (s, 1H, H of Cp^{PPh}), 4.91 (s, 1H, H of Cp^{PPh}), 5.07 (s, 1H, H of Cp^{PPh}), 5.26 (s, 1H, H of Cp^{PPh}), 7.16 (t, 1H, *p*-H of Ph), 7.30 (t, 2H, *m*-H of Ph), 7.69 (t, 2H, *o*-H of Ph). ^{13}C{^{1}H} NMR (C_6D_6, 126 MHz): 0.9 (d, J = 7 Hz, Si(*C*H_3)$_3$), 65.8 (s, C of Cp^{NSiMe3}), 66.1 (s, C of Cp^{NSiMe3}), 67.6 (s, C of Cp^{NSiMe3}), 69.9 (s, C of Cp^{NSiMe3}), 72.9 (d, J = 8.0 Hz, C of Cp^{PPh}), 73.6 (s, C of Cp^{PPh}), 74.5 (d, J = 32 Hz, C of Cp^{PPh}), 78.9 (s, C of Cp^{PPh}), 84.6 (d, J = 30 Hz, *ipso*-C-P of Cp^{PPh}), 119.5 (d, J = 6 Hz, *ipso*-C-N of Cp^{NSiMe3}), 128.5 (d, J = 4 Hz, C of Ph), 128.8 (s, C of Ph), 129.0 (s, C of Ph), 143.9 (d, J = 26 Hz, *ipso*-C-P of Ph). ^{31}P NMR (C_6D_6, 203 MHz): 120.9. MS(FDI): m/z (%) 379 (100). HRMS (FDI; m/z): $[M]^+$ calcd for

$C_{19}H_{22}FeNPSi$, 379.0609; found 379.0609. Note: Due to the technical difficulty in analyzing liquid an elemental analysis could not be performed for this compound.

4.30. Attempt to Synthesize 1-Benzyl-2-*tert*-butyl-1,2-azaphospha[2]ferrocenophane (181)

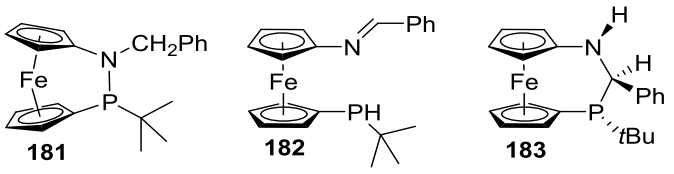

*n*BuLi (0.21 mL, 0.53 mmol) was added dropwise to a 0 ºC cooled solution of compound **147** (0.091 g, 0.25 mmol) in a mixture of hexanes and thf (5.0 mL; hexanes : thf; 9:1), resulting in a color change from pale yellow to bright orange. After the reaction mixture was stirred for 40 min at 0 ºC, a solution of *t*BuPCl$_2$ (0.25 mL, 1.0 M in Et_2O) was added dropwise over 2 min, followed by removal of the cold bath. After 1 h of stirring at ambient temperature, all the volatiles were removed under high vacuum and the resulting sticky solid was dissolved in Et_2O (12 mL). After removing all LiCl by Schlenk filtration, the red solution was kept at ambient temperature and NMR spectra were measured at t = 1.5 h, 2.5 h, and 4.5 h from aliquots of the Et_2O solution (t = 0 refers to the moment of addition of *t*BuPCl$_2$). After 48 h at ambient temperature, all volatiles were removed under high vacuum. An attempt to isolate **183** by column chromatography on alumina (hexanes : NEt_3; 92 : 8) resulted in compound **183** contaminated with targeted [2]FCP (**181**). Crystallization from a hexanes solution under air, letting the solvent slowly evaporate at ambient temperature, resulted in compound **183**, (0.023 g, 24%) that contained small amounts of impurities. Suitable single crystal for structural determination were not obtained for compound **183**.

Characterization of Compound 183. ^{1}H NMR (C_6D_6): δ 0.92 (d, J = 11.0 Hz, 9H, PC(CH_3)$_3$), 2.23 (d, J = 12.5 Hz, 1H, NH), 3.64 (m, 1H, Cp^{NH}), 3.76 (m, 1H, Cp^{NH}), 3.90 (m, 1H, Cp^{NH}), 3.96 (m, 1H, Cp^{NH}), 4.20 (dd, J = 12.5 and 5.5 Hz, 1H, C*H*Ph), 4.22 (m, 1H, Cp^{PtBu}), 4.26

(m, 2H, Cp^{PtBu}), 4.36 (m, 1H, Cp^{PtBu}), 7.10 (t, 1H, *p*-H of Ph), 7.17 (q, 2H, *m*-H of Ph), 7.37 (d, 2H, *o*-H of Ph). $^{13}C\{^1H\}$ NMR (C_6D_6): δ 28.2 (d, J = 16 Hz, P*C*Me$_3$), 29.9 (d, J = 12 Hz, PC(*C*H$_3$)$_3$), 56.5 (s, N*C*HPh), 64.7 (s, Cp^{NH}), 66.1 (s, Cp^{NH}), 67.1 (s, Cp^{NH}), 69.4 (d, J = 28 Hz, Cp^{PtBu}), 69.8 (d, J = 27 Hz, *ipso*-C-P), 71.5 (s, Cp^{NH}), 71.8 (d, J = 7 Hz, Cp^{PtBu}), 72.2 (d, J =10 Hz, Cp^{PtBu}), 80.6 (d, J = 44 Hz, Cp^{PtBu}), 106.0 (s, *ipso*-C-N), 128.8 (d, J = 8 Hz, Ph), 128.9 (s, Ph), 142.2 (d, J = 16 Hz, *ipso*-C of Ph). ^{31}P NMR (C_6D_6): δ 3.2 (m). MS (FDI): m/z (%) 377 (100) [M^+]. HRMS (FDI; m/z): $[M]^+$ calc for $C_{21}H_{24}FeNP$, 377.0996; found 377.0990.

Tentative Characterization of Compound 181. ^1H NMR (C_6D_6): δ 1.00 (d, J = 15.0 Hz, 9H, PC(C*H*$_3$)$_3$), 3.77 (m, 1H, Cp), 4.39 (m, 1H, Cp), 4.43 (m, 1H, Cp), 4.52 (s, 1H, Cp), 4.83 (m, 1H, Cp), 4.86 (m, 1H, Cp). ^{31}P NMR (C_6D_6): δ 149.3. Note: Missing signals of other Cp protons presumably overlap with stronger signals of compounds **182** and **183**.

Characterization of Compound 182. ^1H NMR (C_6D_6): δ 1.01 (d, J = 12.0 Hz, 9H, PC(C*H*$_3$)$_3$), 3.86 (d, J = 206.0 Hz, 1H, P*H*tBu) 4.06 (m, 1H, Cp), 4.13 (m, 2H, Cp), 4.16 (m, 2H, Cp), 4.26 (m, 1H, Cp), 4.59 (m, 1H, Cp), 4.61 (m, 1H, Cp), 7.07-7.15 (m, 3H, *m*-H, *p*-H of Ph), 7.88 (m, 2H, *o*-H of Ph), 8.54 (s, 1H, NC*H*Ph). ^{31}P NMR (C_6D_6): δ -26.9 (doublet of decets, J = 208 and 12 Hz). MS (FDI): m/z (%) 377 (100) [M^+]. HRMS (FDI; m/z): $[M]^+$ calc for $C_{21}H_{24}FeNP$, 377.0996; found 377.1001. Note: The signal for P*H*tBu shows a doublet with J = 206 Hz with one signal at δ = 3.65 ppm and the second signal at δ = 4.06 ppm overlapped with one signal of a Cp proton. The MS data were taken from the isolated crude that contained compound **182** as the major compound.

4.31. Attempted synthesis of 1-Neopentyl-2-*tert*-butyl-1,2-azaphospha[2]ferrocenophane (186) and Formation of 1-(*Tert*-butylphosphanyl)-1'-[(2,2-dimethylpropyliden)imino]ferrocene (185)

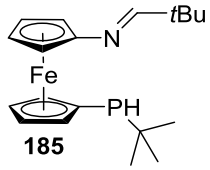

185

*n*BuLi (0.32 mL, 0.80 mmol) was added dropwise to a -78 ºC cooled solution of compound **149** (0.130 g, 0.374 mmol) in a mixture of hexanes and thf (10 mL; hexanes : thf; 9 : 1), resulting in a color change from pale yellow to bright orange. After the reaction mixture was stirred for 40 min at -78 ºC, the cold bath was replaced by an ice bath, followed by stirring of the reaction mixture at 0 °C for 1 h. A solution of *t*BuPCl$_2$ (0.37 mL, 1.0 M in Et$_2$O) was added dropwise over 2 min. The reaction mixture was warmed up to ambient temperature and stirred for 3 h. After all volatiles were removed under high vacuum, the product was dissolved in hexanes (15.0 mL) and LiCl was removed by a Schlenk filtration. From this orange solution, solvents were removed under high vacuum, resulting in a yellow, sticky solid, which was further purified by crystallization in hexanes at -78 ºC. Isolation of these low melting crystals resulted in product as a red oil at ambient temperature (0.070 g, 52%). ^{1}H NMR (C_6D_6): δ 1.06 (d, J = 12.0 Hz, 9H, PC(C*H*$_3$)$_3$), 1.11 (s, 9H, NCHC(C*H*$_3$)$_3$), 3.89 (d, J = 207.0 Hz, 1H, P*H*t*Bu*), 4.01 (m, 1H, CH-β of Cp^{NCHtBu}), 4.02 (m, 1H, CH-β of Cp^{NCHtBu}), 4.05 (m, 1H, CH-α of Cp^{PHtBu}), 4.16 (m, 2H, CH-β of Cp^{PHtBu}), 4.24 (m, 1H, CH-α of Cp^{PHtBu}), 4.44 (m, 1H, CH-α of Cp^{NCHtBu}), 4.47 (m, 1H, CH-α of Cp^{NCHtBu}), 7.89 (s, 1H, NC*H*t*Bu*). ^{13}C{^{1}H} NMR (C_6D_6): 27.1 (s, NCHC(*C*H$_3$)$_3$), 27.7 (d, J = 3 Hz, P*C*Me$_3$), 29.8 (d, J = 13 Hz, PC(*C*H$_3$)$_3$), 37.0 (s, NCH*C*Me$_3$), 63.9 (s, C-α of Cp^{NCHtBu}), 64.1 (s, C-α of Cp^{NCHtBu}), 67.76 (s, C-β of Cp^{NCHtBu}), 67.79 (s, C-β of Cp^{NCHtBu}), 72.3 (s, 2C-β of Cp^{PHtBu}), 72.7 (d, J = 7 Hz, C-α of Cp^{PHtBu}), 76.7 (d, J = 9 Hz, *ipso*-C-P), 77.9 (d, J = 34 Hz, C-α of Cp^{PHtBu}), 106.6 (s, *ipso*-C-N),

170.0 (s, N*C*H*t*Bu). ^{31}P NMR (C_6D_6): δ -26.7 (doublet of decets, J = 208 and 12 Hz). MS (FDI): m/z (%) 357 (100) [M^+]. HRMS (FDI; m/z): $[M]^+$ calc. for $C_{19}H_{28}FeNP$, 357.1309; found 357.1319. Note: Due to technical difficulty in analyzing liquids, an elemental analysis could not be performed for this compound.

4.32. Synthesis of 2-Mamx-1-trimethylsilyl-1,2-azagalla[2]ferrocenophane (188)

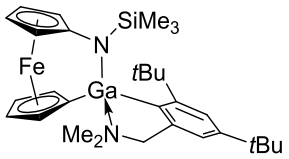

188

*n*BuLi (0.9 mL, 2.25 mmol) was added dropwise to a 0 ºC cooled solution of compound **142** (0.374 g, 1.08 mmol) in thf (12 mL), resulting in a color change from pale yellow to bright orange. The reaction was stirred at this temperature for an additional 40 min. A solution of (Mamx)$GaCl_2$ (0.382 g, 0.987 mmol) in thf (6.0 mL) was added dropwise to it over 5 min. The reaction mixture was warmed up to ambient temperature and stirred for 4 h. After all volatiles were removed under high vacuum, the product was dissolved in hexanes (20.0 mL) and LiCl was removed by a Schlenk filtration. From this red solution, solvents were removed under high vacuum, resulting in a red, sticky solid. Product **188** was obtained by crystallization in Et_2O at -23 °C in form of red crystals (0.272 g, 43%). ^{1}H NMR (C_6D_6, 500 MHz): δ -0.09 (s, 9H, Si(C*H*$_3$)$_3$), 1.35 (s, 9H, C(C*H*$_3$)$_3$), 1.74 (s, 9H, C(C*H*$_3$)$_3$), 2.00 (s, 3H, NC*H*$_3$), 2.55 (s, 3H, NC*H*$_3$), 2.86 (d, J = 14 Hz, 1H, C*H*$_2$NMe$_2$), 3.89 (d, J = 14 Hz, 1H, C*H*$_2$NMe$_2$), 3.97 (s, 2H, H of Cp^{NSiMe3}), 4.25 (s, 2H, H of Cp^{GaMamx}), 4.33 (s, H, 1H of Cp^{GaMamx}), 4.42 (s, 2H, 1H of Cp^{NSiMe3}), 4.58 (s, 1H, H of Cp^{GaMamx}), 5.07 (s, 1H, H of Cp^{GaMamx}), 6.88 (s, 1H, H of Ph), 7.58 (s, 1H, H of Ph). ^{13}C{^{1}H} NMR (C_6D_6, 126 MHz): δ 1.4 (s, Si(*C*H$_3$)$_3$), 31.6 (s, C(*C*H$_3$)$_3$), 33.2 (s, C(*C*H$_3$)$_3$), 34.8 (s, *C*(CH$_3$)$_3$), 37.3 (s, *C*(CH$_3$)$_3$), 44.8 (s, N*C*H$_3$), 46.7 (s, N*C*H$_3$), 65.2 (s, C of Cp^{NSiMe3}), 65.5 (s, C of Cp^{NSiMe3}), 67.9

(s, *C*H_2NMe_2), 69.1 (s, C of Cp^{GaMamx}), 69.7 (s, C of Cp^{NSiMe3}), 70.1 (s, C of Cp^{GaMamx}), 71.9 (s, C of Cp^{GaMamx}), 76.4 (s, C of Cp^{NSiMe3}), 78.2 (s, C of Cp^{GaMamx}), 112.0 (*ipso*-C-N of Cp^{NSiMe3}), 119.3 (C of Ph), 121.5 (C of Ph), 142.1 (*ipso*-C-*t*Bu of Ph), 151.0 (*ipso*-C-*t*Bu of Ph), 157.8 (*ipso*-C-CH_2NMe_2 of Ph). MS(70 eV): m/z (%) 586 (100). HRMS (70 eV; m/z): $[M]^+$ calcd for $C_{30}H_{45}FeGaN_2Si$, 586.1957; found 586.1942. Anal. Calcd for $C_{30}H_{45}FeGaN_2Si$ (587.3570): C, 61.35; H, 7.72; N, 4.77. Found: C, 61.07; H, 7.90; N; 4.56.

4.33. Synthesis of 2-Di(isopropyl)amino-1-trimethylsilyl-1,2-azabora[2]ferrocenophane (189)

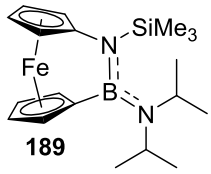

189

*n*BuLi (0.41 mL, 1.03 mmol) was added dropwise to a -78 ºC cooled solution of compound **142** (0.171 g, 0.492 mmol) in a solvent mixture of hexanes and thf (10 mL; hexanes : thf, 9 : 1), resulting in a color change from pale yellow to bright orange. After the reaction mixture was stirred for 40 min at -78 ºC, the dry ice bath was replaced by an ice bath, followed by stirring of the reaction mixture at 0 °C for 1 h. A solution of *i*Pr_2NBCl_2 (0.090 g, 0.494 mmol) in hexanes (6 mL) was added dropwise over 2 min. The reaction mixture was warmed to ambient temperature and stirred for 2 h. After all volatiles were removed under high vacuum, the product was dissolved in hexanes (15.0 mL) and LiCl was removed by a Schlenk filtration. From this red solution, solvents were removed under high vacuum, resulting in a red, sticky liquid. Product **189** was obtained by vacuum sublimation (60 °C; p ~ 10^{-2} mbar) in form of red crystals (0.103 g, 55%). ^{1}H NMR (C_6D_6, 500 MHz): δ 0.26 (s, 9H, Si(CH_3)$_3$), 1.20 (d, J = 7 Hz, 12H, N[CH(CH_3)$_2$]$_2$), 3.72 (septet, J = 7 Hz, 2H, N[CH(CH$_3$)$_2$]$_2$), 3.91 (pst, 2H, α-H of Cp^{NSiMe3}), 4.21 (pst, 2H, β-H of Cp^{NSiMe3}), 4.27 (pst,

2H, β-H of Cp^{BNiPr2}), 4.53 (pst, 2H, α-H of Cp^{BNiPr2}). $^{13}C\{^{1}H\}$ NMR (C_6D_6, 126 MHz): δ 2.4 ($Si(CH_3)_3$), 25.0 ($N[CH(CH_3)_2]_2$), 47.8 ($N[CHMe_2]_2$), 67.6 (s, α-C of Cp^{NSiMe3}), 70.6 (s, β-C of Cp^{NSiMe3}), 72.8 (s, β-C of Cp^{BNiPr2}), 76.3 (s, α-C of Cp^{BNiPr2}), 98.4 (s, *ipso*-C-N of Cp^{NSiMe3}). ^{11}B NMR (C_6D_6, 160 MHz): δ 34.4. MS(FDI): m/z (%) 382 (100). HRMS (70 eV; m/z): $[M]^+$ calcd for $C_{19}H_{31}BFeN_2Si$, 382.1699; found 382.1707. Anal. Calcd for $C_{19}H_{31}BFeN_2Si$ (382.2110): C, 59.71; H, 8.18; N, 7.33. Found: C, 59.61; H, 8.33; N; 7.23.

REFERENCES

(1) Koch, R.; Weidenbruch, M. *Angew. Chem. Int. Ed.* **2002**, *41*, 1861–1863.

(2) Mathey, F. *Chem. Rev.* **1990**, *90*, 997–1025.

(3) Vanderark, L. A; Clark, T. J.; Rivard, E.; Manners, I.; Slootweg, J. C.; Lammertsma, K. *Chem. Commun.* **2006**, 3332–3333.

(4) Liebman, J. F.; Greenberg, A. *Chem. Rev.* **1976**, 311–365.

(5) Foucher, D. A.; Tang, B.-Z.; Manners, I. *J. Am. Chem. Soc.* **1992**, *114*, 6246–6248.

(6) Rinehart, K. L.; Curby, R. J. *J. Am. Chem. Soc.* **1957**, *79*, 3290–3291.

(7) Rinehart, K. L.; Frerichs, A. K.; Kittle, P. A.; Westman, L. F.; Gustafson, D. H.; Pruett, R. L.; McMahon, J. E. *J. Am. Chem. Soc.* **1960**, *82*, 4111–4112.

(8) Neuse, E.; Rosenberg, H. *Polym. Rev.* **1970**, *4*, 1–145.

(9) Osborne, A. G., Whiteley, R. H. *J. Organomet. Chem.* **1975**, 101, 27–28.

(10) Herbert, D. E.; Mayer, U. F. J.; Manners, I. *Angew. Chem. Int. Ed.* **2007**, *46*, 5060–5081.

(11) Musgrave, R. A.; Russell, A. D.; Manners, I. *Organometallics* **2013**, *32*, 5654–5667.

(12) Berenbaum, A.; Braunschweig, H.; Dirk, R.; Englert, U.; Green, J. C.; Jäkle, F.; Lough, A. J.; Manners, I. *J. Am. Chem. Soc.* **2000**, *122*, 5765–5774.

(13) Braunschweig, H.; Seeler, F.; Sigritz, R. *J. Organomet. Chem.* **2007**, *692*, 2354–2356.

(14) Finckh, W.; Tang, B. Z.; Foucher, D. A.; Zamble, D. B.; Ziembinski, R.; Lough, A.; Manners, I. *Organometallics* **1993**, *12*, 823–829.

(15) Foucher, D. A.; Edwards, M.; Burrow, R. A.; Lough, A. J.; Manners, I. *Organometallics* **1994**, *13*, 4959–4966.

(16) Jäkle, F.; Rulkens, R.; Zech, G.; Foucher, D. A.; Lough, A. J.; Manners, I. *Chem.—Eur. J.* **1998**, *4*, 2117–2128.

(17) Schachner, J. A.; Lund, C. L.; Quail, J. W.; Müller, J. *Organometallics* **2005**, *24*, 785–787.

(18) Butler, I. R.; Cullen, W. R.; Einstein, F. W. B.; Rettig, S. J.; Willis, A. J. *Organometallics* **1983**, *2*, 128–135.

(19) Evans, C. E. B.; Lough, A. J.; Grondey, H.; Manners, I. *New J. Chem.* **2000**, *24*, 447–453.

(20) C. Green, J. *Chem. Soc. Rev.* **1998**, *27*, 263–271.

(21) MacLachlan, M. J.; Ginzburg, M.; Coombs, N.; Coyle, T. W.; Raju, N. P.; Greedan, J. E.; Ozin, G. A.; Manners, I. *Science* **2000**, *287*, 1460–1463.

(22) Arsenault, A. C.; Puzzo, D. P.; Manners, I.; Ozin, G. A. *Nat. Photonics* **2007**, *1*, 468–472.

(23) Ma, Y.; Dong, W.-F.; Hempenius, M. A.; Möhwald, H.; Vancso, G. J. *Nat. Mater.* **2006**, *5*,

724–729.

(24) Gädt, T.; Ieong, N. S.; Cambridge, G.; Winnik, M. A.; Manners, I. *Nat. Mater.* **2009**, *8*, 144–150.

(25) Guérin, G.; Raez, J.; Wang, X. S.; Manners, I.; Winnik, M. A. *Prog. Colloid Polym. Sci.* **2006**, *132*, 152–160.

(26) Rider, D. A.; Manners, I. *Polym. Rev.* **2007**, *47*, 165–195.

(27) Heo, R. W.; Lee, T. R. *J. Organomet. Chem.* **1999**, *578*, 31–42.

(28) Bellas, V.; Rehahn, M. *Angew. Chem. Int. Ed.* **2007**, *46*, 5082–5104.

(29) Tan, T.-S.; Fletcher, J. L.; McGlinchey, M. J. *J. Chem. Soc., Chem. Commun.* **1975**, 771–772.

(30) Laing, M. B.; Trueblood, K. N. *Acta Crystallogr.* **1965**, *19*, 373–381.

(31) Buretea, M. A.; Tilley, T. D. *Organometallics* **1997**, *16*, 1507–1510.

(32) Yasufuku, K.; Aoki, K.; Yamazaki, H. *Inorg. Chem.* **1977**, *16*, 624–628.

(33) Hafner, K.; Mink, C.; Lindner, H. J. *Angew. Chem. Int. Ed.* **1994**, *33*, 1479–1480.

(34) Brandt, P. F.; Compton, D. L.; Rauchfuss, T. B. *Organometallics* **1998**, *17*, 2702–2706.

(35) Herberhold, M.; Dörfler, U.; Wrackmeyer, B. *J. Organomet. Chem.* **1997**, *530*, 117–120.

(36) Braunschweig, H.; Kupfer, T. *J. Am. Chem. Soc.* **2008**, *130*, 4242–4243.

(37) Braunschweig, H.; Grünewald, B.; Schwab, K.; Sigritz, R. *Eur. J. Inorg. Chem.* **2009**, 4860–4863.

(38) Bauer, F.; Braunschweig, H.; Schwab, K. *Organometallics* **2010**, *29*, 934–938.

(39) Bhattacharjee, H.; Müller, J. *Coord. Chem. Rev.* **2016**, *314*, 114–133.

(40) Braunschweig, H.; Kupfer, T. *Eur. J. Inorg. Chem.* **2012**, 1319–1332.

(41) Bauer, F.; Braunschweig, H.; Gruß, K.; Kupfer, T. *Organometallics* **2011**, *30*, 2869–2884.

(42) Bauer, F.; Braunschweig, H.; Gruß, K.; Lambert, C.; Pandey, K. K.; Radacki, K.; Reitzenstein, D. *Chem.—Eur. J.* **2011**, *17*, 5230–5233.

(43) Kondo, T.; Yamamoto, K.; Kumada, M. *J. Organomet. Chem.* **1972**, *43*, 315–321.

(44) Kumada, M.; Kondo, T.; Mimura, K.; Yamamoto, K.; Ishikawa, M. *J. Organomet. Chem.* **1972**, *43*, 307–314.

(45) Kumada, M.; Kondo, T.; Mimura, K.; Ishikawa, M.; Yamamoto, K.; Ikeda, S.; Kondo, M. *J. Organomet. Chem.* **1972**, *43*, 293–305.

(46) Dement, V. V; Cervantes-lee, F.; Parkanyi, L.; Sharma, H.; Pannell, K. H. *Organometallics* **1993**, *12*, 1983–1987.

(47) Wagner, H.; Baumgartner, J.; Marschner, C. *Organometallics* **2007**, *26*, 1762–1770.

(48) Finckh, W.; Tang, B. Z.; Lough, A.; Manners, I. *Organometallics* **1992**, *11*, 2904–2911.

(49) Mochida, K.; Shibayama, N.; Goto, M. *Chem. Lett.* **1998**, 339–340.

(50) Herberhold, M.; Steffl, U.; Milius, W.; Wrackmeyer, B. *Angew. Chem. Int. Ed.* **1996**, *35*, 1803–1804.

(51) Herberhold, M.; Steffl, U.; Milius, W.; Wrackmeyer, B. *Angew. Chem. Int. Ed.* **1997**, *36*, 1508–1510.

(52) Herberhold, M.; Steffl, U.; Milius, W.; Wrackmeyer, B. *Chem.—Eur. J.* **1998**, *4*, 1027–1032.

(53) Herberhold, M.; Steffl, U.; Wrackmeyer, B. *J. Organomet. Chem.* **1999**, *577*, 76–81.

(54) Allcock, H. R.; Lavin, K. D.; Riding, G. H.; Suszko, P. R.; Whittle, R. R. *J. Am. Chem. Soc.* **1984**, *106*, 2337–2347.

(55) Tanimoto, Y.; Ishizu, Y.; Kubo, K.; Miyoshi, K.; Mizuta, T. *J. Organomet. Chem.* **2012**, *713*, 80–88.

(56) Moser, C.; Belaj, F.; Pietschnig, R. *Chem.—Eur. J.* **2009**, *15*, 12589–12591.

(57) Cordero, B.; Gómez, V.; Platero-Prats, A. E.; Revés, M.; Echeverría, J.; Cremades, E.; Barragán, F.; Alvarez, S. *Dalt. Trans.* **2008**, 2832–2838.

(58) Nelson, J. M.; Lough, A. J.; Manners, I. *Angew. Chem. Int. Ed.* **1994**, *33*, 989–991.

(59) Nelson, J. M.; Lough, A. J.; Manners, I. *Organometallics* **1994**, *13*, 3703–3710.

(60) Russell, A. D.; Gilroy, J. B.; Lam, K.; Haddow, M. F.; Harvey, J. N.; Geiger, W. E.; Manners, I. *Chem.—Eur. J.* **2012**, *18*, 8000–8003.

(61) Russell, A. D.; Gilroy, J. B.; Lam, K.; Haddow, M. F.; Harvey, J. N.; Geiger, W. E.; Manners, I. *Chem.—Eur. J.* **2014**, *20*, 16216–16227.

(62) Braunschweig, H.; Hupp, F.; Kramer, T.; Mager, J. *Inorg. Chem.* **2013**, *52*, 9060–9065.

(63) Abramovitch, R. A.; Azogu, C. I.; Sutherland, R. G. *J. Chem. Soc. Chem. Commun.* **1969**, *291*, 1439–1440.

(64) Abramovitch, R. A.; Atwood, J. L.; Good, M. L.; Lampert, B. A. *Inorg. Chem.* **1975**, *14*, 3085–3089.

(65) Chao, S.; Robbins, J. L.; Wrighton, M. S. *J. Am. Chem. Soc.* **1983**, *105*, 181–188.

(66) Resendes, R.; Nelson, J. M.; Fischer, A.; Jäkle, F.; Bartole, A.; Lough, A. J.; Manners, I. *J. Am. Chem. Soc.* **2001**, *123*, 2116–2126.

(67) Bartole-scott, A.; Resendes, R.; Ja, F.; Lough, A. J.; Manners, I. *Organometallics* **2004**, *23*, 6116–6126.

(68) Bartole-Scott, A.; Lough, A. J.; Manners, I. *Polyhedron* **2006**, *25*, 429–436.

(69) Hardy, C. G.; Zhang, J.; Yan, Y.; Ren, L.; Tang, C. *Prog. Polym. Sci.* **2014**, *39*, 1742–1796.

(70) Arimoto, F. S.; Haven, A. C. *J. Am. Chem. Soc.* **1955**, *77*, 6295–6297.

(71) Pietschnig, R. *Chem. Soc. Rev.* **2016**, DOI: 10.1039/C6CS00196C.

(72) Dragutan, I.; Dragutan, V.; Fischer, H. *J. Inorg. Organomet. Polym. Mater.* **2008**, *18*, 311–324.

(73) Seyferth, D.; Withers, H. P.; Fellmann, J. D.; Garrou, P. E.; Martin, S. *Organometallics* **1982**, *1*, 1283–1288.

(74) Brandt, P. F.; Rauchfuss, T. B. *J. Am. Chem. Soc.* **1992**, *114*, 1926–1927.

(75) Rosenberg, H.; Rausch. M. D *US Pat.* 3060215, **1962**.

(76) Rosenberg, H. *US Pat.* 3426053, **1969**.

(77) Butler, I. R.; Cullen, W. R.; Ni, J.; Rettig, S. J. *Organometallics* **1985**, *4*, 2196–2201.

(78) Masson, G.; Beyer, P.; Cyr, P. W.; Lough, A. J.; Manners, I. *Macromolecules* **2006**, *39*, 3720–3730.

(79) Pudelski, J. K.; Manners, I. *J. Am. Chem. Soc.* **1995**, *117*, 7265–7266.

(80) Rulkens, R.; Lough, A. J.; Manners, I. *J. Am. Chem. Soc.* **1994**, *116*, 797–798.

(81) Ni, Y.; Rulkens, R.; Manners, I. *J. Am. Chem. Soc.* **1996**, *118*, 4102–4114.

(82) Mizuta, T.; Onishi, M.; Miyoshi, K. *Organometallics* **2000**, *19*, 5005–5009.

(83) Mizuta, T.; Imamura, Y.; Miyoshi, K. *J. Am. Chem. Soc.* **2003**, *125*, 2068–2069.

(84) Tanabe, M.; Manners, I. *J. Am. Chem. Soc.* **2004**, *126*, 11434–11435.

(85) Reddy, N. P.; Yamashita, H.; Tanaka, M. *J. Chem. Soc. Chem. Commun.* **1995**, *2*, 2263–2264.

(86) Ni, Y.; Rulkens, R.; Pudelski, J. K.; Manners, I. *Macromol. Rapid Commun.* **1995**, *16*, 637–641.

(87) Sheridan, J. B.; Temple, K.; Lough, J.; Manners, I. *J. Chem. Soc. Dalt. Trans.* **1997**, 711–713.

(88) Temple, K.; Jäkle, F.; Sheridan, J. B.; Manners, I. *J. Am. Chem. Soc.* **2001**, *123*, 1355–1364.

(89) Hussein, M. A.; Asiri, A. M. *Des. Monomers Polym.* **2012**, *15*, 207–251.

(90) Nguyen, P.; Gómez-Elipe, P.; Manners, I. *Chem. Rev.* **1999**, *99*, 1515–1548.

(91) Nelson, J. M.; Rengel, H.; Manners, I. *J. Am. Chem. Soc.* **1993**, *115*, 7035–7036.

(92) Nelson, J. M.; Nguyen, P.; Petersen, R.; Rengel, H.; Macdonald, P. M.; Lough, A. J.; Manners, I.; Raju, N. P.; Greedan, J. E.; Barlow, S.; O'Hare, D. *Chem.—Eur. J.* **1997**, *3*, 573–584.

(93) Herbert, D. E.; Gilroy, J. B.; Staubitz, A.; Haddow, M. F.; Harvey, J. N.; Manners, I. *J. Am. Chem. Soc.* **2010**, *132*, 1988–1998.

(94) Gilroy, J. B.; Russell, A. D.; Stonor, A. J.; Chabanne, L.; Baljak, S.; Haddow, M. F.; Manners, I. *Chem. Sci.* **2012**, *3*, 830–841.

(95) Masson, G.; Lough, A. J.; Manners, I. *Macromolecules* **2008**, *41*, 539–547.

(96) Herbert, D. E.; Mayer, U. F. J.; Gilroy, J. B.; López-Gómez, M. J.; Lough, A. J.; Charmant, J. P. H.; Manners, I. *Chem.—Eur. J.* **2009**, *15*, 12234–12246.

(97) Butler, I. R.; Quayle, S. C. *J. Organomet. Chem.* **1998**, *552*, 63–68.

(98) Bildstein, B.; Malaun, M.; Kopacka, H.; Wurst, K.; Mitterböck, M.; Ongania, K.; Opromolla, G.; Zanello, P. *Organometallics* **1999**, *18*, 4325–4336.

(99) Bertogg, A.; Camponovo, F.; Togni, A. *Eur. J. Inorg. Chem.* **2005**, 347–356.

(100) Lai, L.-L.; Dong, T.-Y. *J. Chem. Soc. Chem. Commun.* **1994**, 2347–2348.

(101) Jana, R.; Kumar, M. S.; Singh, N.; Elias, A. J. *J. Organomet. Chem.* **2008**, *693*, 3780–3786.

(102) Butler, D. C. D.; Richards, C. J. *Organometallics* **2002**, *21*, 5433–5436.

(103) Scriven, E. F. V; Turnbull, K. *Chem. Rev.* **1988**, *88*, 297–368.

(104) Dey, S.; Quail, J. W.; Müller, J. *Organometallics* **2015**, *34*, 3039–3046.

(105) Wrackmeyer, B.; Maisel, H. E.; Herberhold, M. *J. Organomet. Chem.* **2001**, *639*, 727–732.

(106) Shafir, A.; Fiedler, D.; Arnold, J. *Chem. Commun.* **2003**, 2598–2599.

(107) Rittinghaus, S.; Färber, C.; Bruhn, C.; Siemeling, U. *Dalt. Trans.* **2014**, *43*, 3508–3520.

(108) Dangerfield, E. M.; Plunkett, C. H.; Win-Mason, A. L.; Stocker, B. L.; Timmer, M. S. M. *J. Org. Chem.* **2010**, *75*, 5470–5477.

(109) Metallinos, C.; Zaifman, J.; Dodge, L. *Org. Lett.* **2008**, *10*, 3527–3530.

(110) Bailey, W. F.; Luderer, M. R.; Jordan, K. P. *J. Org. Chem.* **2006**, *71*, 2825–2828.

(111) Sadeh, S.; Schatte, G.; Müller, J. *Chem.—Eur. J.* **2013**, *19*, 13408–13417.

(112) Dey, S.; Sun, W.; Müller, J. *Inorg. Chem.* **2016**, *55*, 3630–3639.

(113) Rulkens, R.; Lough, A. J.; Manners, I. *Angew. Chem. Int. Ed.* **1996**, *35*, 1805–1807.

(114) Comba, P.; Hambley, T. W.; Martin, B. *Molecular Modeling of Inorganic Compounds*; 3rd ed.; Wiley-VCH: Weinheim, Germany, 2009.

(115) Svehla, G. *Vogel's Qualitative Inorganic Analysis*, 5th ed.; Longman: New York, **1979**; pp 237–241.

(116) Guillaneux, D.; Kagan, H. B. *J. Org. Chem.* **1995**, *60*, 2502–2505.

(117) Wrackmeyer, B.; Klimkina, E. V.; Milius, W. *Inorg. Chem. Commun.* **2004**, *7*, 412–416.

(118) Patra, S. K.; Whittell, G. R.; Nagiah, S.; Ho, C. L.; Wong, W. Y.; Manners, I. *Chem.—Eur. J.* **2010**, *16*, 3240–3250.

(119) Pickett, T. E.; Richards, C. J. *Tetrahedron Lett.* **1999**, *40*, 5251–5254.

(120) Gorenstein, D. G. In *Phosphorus-31 NMR*; Academic Press, New York, 1984; pp 551–552.

(121) Andrieu, J.; Camus, J.-M.; Poli, R.; Richard, P. *New J. Chem.* **2001**, *25*, 1015–1023.

(122) Szabó, A.; Petneházy, I.; Jászay, Z. M. *Heteroat. Chem.* **2003**, *14*, 235–240.

(123) Rosenberg, L. *ACS Catal.* **2013**, *3*, 2845–2855.

(124) Koshti, V.; Gaikwad, S.; Chikkali, S. H. *Coord. Chem. Rev.* **2014**, *265*, 52–73.

(125) Zhao, Y.; Truhlar, D. G. *Theor. Chem. Acc.* **2008**, *120*, 215–241.

(126) Sadeh, S.; Bhattacharjee, H.; Khozeimeh Sarbisheh, E.; Quail, J. W.; Müller, J. *Chem.—Eur. J.* **2014**, *20*, 16320–16330.

(127) Bhattacharjee, H.; Martell, J. D.; Khozeimeh Sarbisheh, E.; Sadeh, S.; Quail, J. W.; Müller, J. *Organometallics* **2016**, *35*, 2156–2164.

(128) Bagh, B.; Gilroy, J. B.; Staubitz, A.; Müller, J. *J. Am. Chem. Soc.* **2010**, *132*, 1794–1795.

(129) Gerrard, W.; Hudson, H. R.; Mooney, E. F. *J. Chem. Soc.* **1960**, *11*, 5168–5172.

(130) Shafir, A.; Power, M. P.; Whitener, G. D.; Arnold, J. *Organometallics* **2000**, *19*, 3978–3982.

(131) Farrugia, L. J. *J. Appl. Crystallogr.* **1997**, *30*, 565.

(132) Mercury; http://www.ccdc.cam.ac.uk/mercury.

(133) Legault, C. CYLview (http://www.cylview.org), 2009.

(134) *Bruker APEX2, 2014.3-0 ed.*; Bruker AXS Inc., Madison, WI, USA, 2014.

(135) *Bruker SAINT and SADABS v834a ed.*;Bruker AXS Inc., Madison, WI, USA, 2013.

(136) G. M. Sheldrick, SHELXL , Program for the Solution of Crystal Structures ; University of Göttingen, Göttingen, Germany.

(137) Sheldrick, G. M. *Acta Crystallogr. Sect. A Found. Crystallogr.* **2007**, *64*, 112–122.

(138) Spek, A. L. *PLATON, A Multipurpose Crystallographic Tool*; University of Utrecht, Utrecht, The Netherlands, 2011.

APPENDIX

Bond lengths and angles of compound **161** are depicted in Tables A1 and A2, respectively. Data of two independent molecules of compound **162** are shown in Tables A3 and A4, where the first molecule is marked as A and the second one is marked as B. As the *tert*-butyl group of compound **165** is disordered around C18, the major species is marked as C19A, C20A, and C21A; and the minor species is marked as C19B, C20B, and C21B (Tables A5 and A6). Bond lengths and angles of compound **178** and **189** can be found in Tables A7 and A8; and A9 and A10, respectively. Syntheses and characterizations of strained compounds **174**, **179**, **188**, and **189** have not been published. Readers can get an idea about the purity of the isolated products from their ^{1}H NMR spectra, which are shown in Figures A1 to A4.

Table A1. Bond Lengths [Å] of Compound 161

Fe1-C1	2.0019(19)	Fe1-C6	2.004(2)
Fe1-C10	2.025(2)	Fe1-C7	2.027(2)
Fe1-C2	2.033(2)	Fe1-C5	2.036(2)
Fe1-C4	2.059(2)	Fe1-C3	2.061(2)
Fe1-C9	2.071(2)	Fe1-C8	2.073(2)
Si2-N1	1.7529(17)	Si2-C15	1.860(2)
Si2-C14	1.861(2)	Si2-C6	1.877(2)
Si1-N1	1.7484(17)	Si1-C12	1.854(2)
Si1-C11	1.861(3)	Si1-C13	1.864(2)
N1-C1	1.442(2)	C1-C5	1.431(3)
C1-C2	1.432(3)	C2-C3	1.425(3)
C6-C10	1.439(3)	C3-C4	1.414(4)
C7-C8	1.427(3)	C4-C5	1.432(3)
C8-C9	1.415(3)	C6-C7	1.439(3)
C9-C10	1.421(3)		

Table A2. Bond Angles [°] of Compound 161

C1-Fe1-C6	93.01(8)	C1-Fe1-C10	113.98(9)
C6-Fe1-C10	41.84(9)	C1-Fe1-C7	112.20(8)

C6-Fe1-C7	41.83(9)	C10-Fe1-C7	68.88(9)
C1-Fe1-C2	41.55(8)	C6-Fe1-C2	113.49(8)
C10-Fe1-C2	151.04(9)	C7-Fe1-C2	102.96(9)
C1-Fe1-C5	41.49(8)	C6-Fe1-C5	111.45(9)
C10-Fe1-C5	102.74(10)	C7-Fe1-C5	148.35(9)
C2-Fe1-C5	69.08(9)	C1-Fe1-C4	69.44(8)
C6-Fe1-C4	151.54(10)	C10-Fe1-C4	124.31(10)
C7-Fe1-C4	165.63(10)	C2-Fe1-C4	68.34(10)
C5-Fe1-C4	40.93(9)	C1-Fe1-C3	69.45(8)
C6-Fe1-C3	153.78(9)	C10-Fe1-C3	163.44(10)
C7-Fe1-C3	126.00(10)	C2-Fe1-C3	40.73(8)
C5-Fe1-C3	68.54(10)	C4-Fe1-C3	40.14(10)
C1-Fe1-C9	154.09(9)	C6-Fe1-C9	69.80(9)
C10-Fe1-C9	40.58(9)	C7-Fe1-C9	68.07(9)
C2-Fe1-C9	163.41(10)	C5-Fe1-C9	125.97(10)
C4-Fe1-C9	117.16(10)	C3-Fe1-C9	132.89(9)
C1-Fe1-C8	152.01(9)	C6-Fe1-C8	69.95(9)
C10-Fe1-C8	68.19(9)	C7-Fe1-C8	40.71(8)
C2-Fe1-C8	124.41(10)	C5-Fe1-C8	165.46(10)
C4-Fe1-C8	134.34(9)	C3-Fe1-C8	117.04(9)
C9-Fe1-C8	39.93(9)	N1-Si2-C15	111.95(10)
N1-Si2-C14	111.35(10)	C15-Si2-C14	109.35(11)
N1-Si2-C6	105.73(8)	C15-Si2-C6	109.44(10)
C14-Si2-C6	108.91(10)	N1-Si1-C12	109.19(10)
N1-Si1-C11	110.57(11)	C12-Si1-C11	108.85(13)
N1-Si1-C13	109.21(9)	C12-Si1-C13	109.84(11)
C11-Si1-C13	109.17(12)	C1-N1-Si1	115.33(13)
C1-N1-Si2	114.57(13)	Si1-N1-Si2	129.86(9)
C5-C1-C2	107.44(18)	C5-C1-N1	126.34(19)
C2-C1-N1	125.80(19)	C5-C1-Fe1	70.55(12)
C2-C1-Fe1	70.41(11)	N1-C1-Fe1	118.66(14)
C3-C2-C1	108.3(2)	C3-C2-Fe1	70.68(13)
C1-C2-Fe1	68.05(12)	C4-C3-Fe1	69.84(13)
C4-C3-C2	108.1(2)	C3-C4-Fe1	70.02(13)
C2-C3-Fe1	68.59(12)	C1-C5-Fe1	67.96(12)
C3-C4-C5	108.34(19)	C10-C6-Si2	125.86(16)
C5-C4-Fe1	68.70(12)	C10-C6-Fe1	69.84(12)
C1-C5-C4	107.8(2)	Si2-C6-Fe1	107.84(10)

C4-C5-Fe1	70.37(13)	C8-C7-Fe1	71.38(13)
C10-C6-C7	105.54(18)	C9-C8-Fe1	69.94(13)
C7-C6-Si2	124.93(16)	C8-C9-Fe1	70.13(12)
C7-C6-Fe1	69.93(12)	C9-C10-Fe1	71.43(13)
C8-C7-C6	109.3(2)	C8-C9-C10	108.2(2)
C6-C7-Fe1	68.24(12)	C10-C9-Fe1	67.98(12)
C9-C8-C7	107.6(2)	C9-C10-C6	109.3(2)
C7-C8-Fe1	67.91(12)	C6-C10-Fe1	68.32(12)

Table A3. Bond Lengths [Å] of Two Independent Molecules of Compound 162

Fe1A-C1A	2.024(2)	Fe1A-C10A	2.026(2)
Fe1A-C6A	2.027(2)	Fe1A-C7A	2.030(3)
Fe1A-C5A	2.035(3)	Fe1A-C2A	2.040(3)
Fe1A-C4A	2.045(3)	Fe1A-C3A	2.049(3)
Fe1A-C8A	2.055(3)	Fe1A-C9A	2.056(3)
Sn1A-N1A	2.067(2)	Sn1A-C14A	2.124(3)
Sn1A-C15A	2.129(3)	Sn1A-C6A	2.133(2)
Si1A-N1A	1.721(2)	Si1A-C11A	1.851(3)
Si1A-C12A	1.852(4)	Si1A-C13A	1.870(3)
N1A-C1A	1.432(3)	C1A-C2A	1.423(4)
C1A-C5A	1.423(4)	C2A-C3A	1.422(4)
C6A-C10A	1.431(4)	C3A-C4A	1.405(4)
C7A-C8A	1.422(4)	C4A-C5A	1.418(4)
C8A-C9A	1.408(4)	C6A-C7A	1.433(4)
C9A-C10A	1.425(3)	Fe1B-C10B	2.023(3)
Fe1B-C6B	2.022(2)	Fe1B-C7B	2.029(3)
Fe1B-C2B	2.026(3)	Fe1B-C5B	2.038(3)
Fe1B-C1B	2.030(2)	Fe1B-C4B	2.044(3)
Fe1B-C3B	2.039(3)	Fe1B-C8B	2.056(3)
Fe1B-C9B	2.052(3)	Sn1B-C14B	2.122(3)
Sn1B-N1B	2.060(2)	Sn1B-C15B	2.130(3)
Sn1B-C6B	2.129(3)	Si1B-C12B	1.847(3)
Si1B-N1B	1.723(2)	Si1B-C11B	1.861(3)
Si1B-C13B	1.861(3)	C1B-C5B	1.422(4)
N1B-C1B	1.426(3)	C2B-C3B	1.414(4)
C1B-C2B	1.424(3)	C3B-C4B	1.388(5)
C6B-C10B	1.432(4)	C4B-C5B	1.412(4)

C7B-C8B	1.414(4)	C6B-C7B	1.435(4)
C8B-C9B	1.399(5)	C9B-C10B	1.428(4)

Table A4. Bond Angles [°] of Two Independent Molecules of Compound 162

C1A-Fe1A-C10A	115.80(10)	C1A-Fe1A-C6A	98.38(10)
C10A-Fe1A-C6A	41.37(10)	C1A-Fe1A-C7A	117.76(11)
C10A-Fe1A-C7A	68.65(11)	C6A-Fe1A-C7A	41.39(10)
C1A-Fe1A-C5A	41.04(10)	C10A-Fe1A-C5A	104.54(11)
C6A-Fe1A-C5A	117.03(10)	C7A-Fe1A-C5A	154.17(10)
C1A-Fe1A-C2A	40.98(10)	C10A-Fe1A-C2A	152.07(10)
C6A-Fe1A-C2A	116.07(11)	C7A-Fe1A-C2A	105.56(12)
C5A-Fe1A-C2A	68.23(11)	C1A-Fe1A-C4A	69.05(10)
C10A-Fe1A-C4A	124.86(12)	C6A-Fe1A-C4A	156.30(12)
C7A-Fe1A-C4A	162.31(12)	C5A-Fe1A-C4A	40.67(10)
C2A-Fe1A-C4A	68.09(12)	C1A-Fe1A-C3A	69.02(10)
C10A-Fe1A-C3A	163.49(12)	C6A-Fe1A-C3A	155.07(12)
C7A-Fe1A-C3A	124.48(12)	C5A-Fe1A-C3A	68.07(12)
C2A-Fe1A-C3A	40.70(11)	C4A-Fe1A-C3A	40.15(12)
C1A-Fe1A-C8A	157.22(11)	C10A-Fe1A-C8A	68.22(11)
C6A-Fe1A-C8A	69.41(10)	C7A-Fe1A-C8A	40.74(11)
C5A-Fe1A-C8A	161.69(11)	C2A-Fe1A-C8A	126.10(12)
C4A-Fe1A-C8A	128.85(11)	C3A-Fe1A-C8A	114.00(11)
C1A-Fe1A-C9A	154.71(11)	C10A-Fe1A-C9A	40.86(10)
C6A-Fe1A-C9A	69.52(10)	C7A-Fe1A-C9A	68.26(11)
C5A-Fe1A-C9A	123.71(11)	C2A-Fe1A-C9A	164.31(11)
C4A-Fe1A-C9A	113.22(11)	C3A-Fe1A-C9A	130.08(10)
C8A-Fe1A-C9A	40.06(11)	N1A-Sn1A-C14A	108.91(10)
N1A-Sn1A-C15A	108.80(10)	C14A-Sn1A-C15A	112.34(11)
N1A-Sn1A-C6A	98.86(8)	C14A-Sn1A-C6A	115.20(11)
C15A-Sn1A-C6A	111.71(12)	N1A-Si1A-C11A	110.01(12)
N1A-Si1A-C12A	111.80(15)	C11A-Si1A-C12A	107.94(19)
N1A-Si1A-C13A	107.18(14)	C11A-Si1A-C13A	109.50(17)
C12A-Si1A-C13A	110.4(2)	C1A-N1A-Si1A	118.72(16)
C1A-N1A-Sn1A	113.23(15)	Si1A-N1A-Sn1A	127.74(11)
C2A-C1A-C5A	106.9(2)	C2A-C1A-N1A	125.7(2)
C5A-C1A-N1A	127.4(2)	C2A-C1A-Fe1A	70.12(14)
C5A-C1A-Fe1A	69.88(14)	N1A-C1A-Fe1A	122.49(16)

C3A-C2A-C1A	108.4(3)	C3A-C2A-Fe1A	69.97(15)
C1A-C2A-Fe1A	68.90(14)	C4A-C3A-Fe1A	69.79(15)
C4A-C3A-C2A	108.0(2)	C3A-C4A-Fe1A	70.06(15)
C2A-C3A-Fe1A	69.33(14)	C4A-C5A-Fe1A	70.06(15)
C3A-C4A-C5A	108.1(2)	C10A-C6A-Fe1A	69.28(14)
C5A-C4A-Fe1A	69.27(14)	C10A-C6A-Sn1A	125.79(19)
C4A-C5A-C1A	108.6(2)	Fe1A-C6A-Sn1A	106.87(11)
C1A-C5A-Fe1A	69.08(14)	C8A-C7A-Fe1A	70.59(15)
C10A-C6A-C7A	105.9(2)	C9A-C8A-Fe1A	70.00(15)
C7A-C6A-Fe1A	69.43(14)	C8A-C9A-Fe1A	69.95(15)
C7A-C6A-Sn1A	123.66(19)	C9A-C10A-Fe1A	70.70(14)
C8A-C7A-C6A	109.0(2)	C6B-Fe1B-C2B	116.53(12)
C6A-C7A-Fe1A	69.19(14)	C6B-Fe1B-C7B	41.49(11)
C9A-C8A-C7A	108.2(2)	C2B-Fe1B-C7B	105.23(12)
C7A-C8A-Fe1A	68.67(15)	C10B-Fe1B-C1B	116.40(11)
C8A-C9A-C10A	107.8(2)	C7B-Fe1B-C1B	117.03(11)
C10A-C9A-Fe1A	68.43(14)	C10B-Fe1B-C5B	104.99(13)
C9A-C10A-C6A	109.2(2)	C7B-Fe1B-C5B	153.47(11)
C6A-C10A-Fe1A	69.35(14)	C6B-Fe1B-C3B	155.73(14)
C6B-Fe1B-C10B	41.46(11)	C2B-Fe1B-C3B	40.70(12)
C10B-Fe1B-C2B	152.96(11)	C1B-Fe1B-C3B	69.07(10)
C10B-Fe1B-C7B	68.82(12)	C6B-Fe1B-C4B	155.78(13)
C6B-Fe1B-C1B	98.28(10)	C2B-Fe1B-C4B	67.73(13)
C2B-Fe1B-C1B	41.10(10)	C1B-Fe1B-C4B	68.83(11)
C6B-Fe1B-C5B	116.74(11)	C3B-Fe1B-C4B	39.76(14)
C2B-Fe1B-C5B	68.00(12)	C10B-Fe1B-C9B	41.01(11)
C1B-Fe1B-C5B	40.90(11)	C7B-Fe1B-C9B	67.99(13)
C10B-Fe1B-C3B	162.75(14)	C5B-Fe1B-C9B	125.09(13)
C7B-Fe1B-C3B	124.80(14)	C4B-Fe1B-C9B	113.96(14)
C5B-Fe1B-C3B	67.71(13)	C10B-Fe1B-C8B	68.26(12)
C10B-Fe1B-C4B	124.78(15)	C7B-Fe1B-C8B	40.51(12)
C7B-Fe1B-C4B	162.68(14)	C5B-Fe1B-C8B	162.98(13)
C5B-Fe1B-C4B	40.47(12)	C4B-Fe1B-C8B	129.74(12)
C6B-Fe1B-C9B	69.45(11)	N1B-Sn1B-C14B	108.62(10)
C2B-Fe1B-C9B	163.02(12)	C14B-Sn1B-C6B	112.92(11)
C1B-Fe1B-C9B	155.86(12)	C14B-Sn1B-C15B	114.79(12)
C3B-Fe1B-C9B	129.52(12)	N1B-Si1B-C12B	110.50(14)
C6B-Fe1B-C8B	69.28(11)	C12B-Si1B-C13B	109.75(18)

C2B-Fe1B-C8B	125.18(13)	C12B-Si1B-C11B	108.45(16)
C1B-Fe1B-C8B	156.09(13)	C1B-N1B-Si1B	117.95(16)
C3B-Fe1B-C8B	113.98(12)	Si1B-N1B-Sn1B	128.29(11)
C9B-Fe1B-C8B	39.81(13)	C5B-C1B-N1B	126.5(2)
N1B-Sn1B-C6B	99.14(9)	C5B-C1B-Fe1B	69.85(15)
N1B-Sn1B-C15B	108.78(11)	N1B-C1B-Fe1B	122.46(16)
C6B-Sn1B-C15B	111.34(12)	C3B-C2B-Fe1B	70.13(17)
N1B-Si1B-C13B	107.32(12)	C4B-C3B-Fe1B	70.30(18)
N1B-Si1B-C11B	111.91(14)	C3B-C4B-Fe1B	69.94(18)
C13B-Si1B-C11B	108.88(17)	C4B-C5B-Fe1B	69.97(18)
C1B-N1B-Sn1B	113.23(15)	C10B-C6B-Fe1B	69.31(15)
C5B-C1B-C2B	106.0(2)	C10B-C6B-Sn1B	125.4(2)
C2B-C1B-N1B	127.4(2)	Fe1B-C6B-Sn1B	106.81(11)
C2B-C1B-Fe1B	69.30(14)	C8B-C7B-Fe1B	70.75(17)
C3B-C2B-C1B	108.8(3)	C9B-C8B-Fe1B	69.94(17)
C1B-C2B-Fe1B	69.60(14)	C8B-C9B-Fe1B	70.24(17)
C4B-C3B-C2B	108.1(3)	C9B-C10B-Fe1B	70.57(16)
C2B-C3B-Fe1B	69.17(15)	C9B-C10B-H10B	125.7
C3B-C4B-C5B	108.4(3)	C6B-C7B-Fe1B	69.00(15)
C5B-C4B-Fe1B	69.56(16)	C9B-C8B-C7B	108.4(3)
C4B-C5B-C1B	108.7(3)	C7B-C8B-Fe1B	68.74(15)
C1B-C5B-Fe1B	69.24(15)	C8B-C9B-C10B	108.1(3)
C10B-C6B-C7B	106.0(2)	C10B-C9B-Fe1B	68.41(16)
C7B-C6B-Fe1B	69.52(15)	C9B-C10B-C6B	108.5(3)
C7B-C6B-Sn1B	123.9(2)	C6B-C10B-Fe1B	69.24(14)
C8B-C7B-C6B	108.9(3)		

Table A5. Bond Lengths [Å] of Compound 165

Fe1-C6	2.0236(17)	Fe1-C1	2.0252(17)
Fe1-C10	2.0293(18)	Fe1-C7	2.0355(18)
Fe1-C5	2.0385(18)	Fe1-C2	2.0428(18)
Fe1-C4	2.0524(19)	Fe1-C3	2.0539(19)
Fe1-C9	2.0618(18)	Fe1-C8	2.0674(18)
Sn1-N1	2.0775(14)	Sn1-C6	2.1526(17)
Sn1-C14	2.1937(19)	Sn1-C18	2.1984(18)
Si1-N1	1.7309(15)	Si1-C13	1.865(2)
Si1-C12	1.8663(19)	Si1-C11	1.871(2)

N1-C1	1.435(2)	C1-C5	1.430(3)
C1-C2	1.436(3)	C2-C3	1.427(3)
C6-C7	1.437(2)	C3-C4	1.414(3)
C7-C8	1.424(3)	C4-C5	1.431(3)
C8-C9	1.414(3)	C6-C10	1.437(2)
C9-C10	1.427(3)	C14-C17	1.526(3)
C14-C16	1.525(3)	C18-C21A	1.509(5)
C14-C15	1.535(3)	C18-C20A	1.523(5)
C18-C19B	1.496(8)	C18-C21B	1.578(8)
C18-C20B	1.512(8)	C18-C19A	1.553(5)

Table A6. Bond Angles [°] of compound 165

C6-Fe1-C1	97.78(7)	C6-Fe1-C10	41.53(7)
C1-Fe1-C10	114.91(7)	C6-Fe1-C7	41.46(7)
C1-Fe1-C7	118.11(7)	C10-Fe1-C7	68.62(7)
C6-Fe1-C5	117.13(7)	C1-Fe1-C5	41.22(7)
C10-Fe1-C5	104.21(8)	C7-Fe1-C5	154.76(7)
C6-Fe1-C2	114.90(7)	C1-Fe1-C2	41.33(7)
C10-Fe1-C2	151.05(7)	C7-Fe1-C2	105.17(8)
C5-Fe1-C2	68.84(8)	C6-Fe1-C4	157.01(8)
C1-Fe1-C4	69.24(7)	C10-Fe1-C4	125.58(8)
C7-Fe1-C4	161.50(8)	C5-Fe1-C4	40.95(8)
C2-Fe1-C4	68.36(8)	C6-Fe1-C3	153.82(8)
C1-Fe1-C3	69.29(7)	C10-Fe1-C3	164.56(8)
C7-Fe1-C3	123.74(8)	C5-Fe1-C3	68.56(8)
C2-Fe1-C3	40.76(8)	C4-Fe1-C3	40.28(9)
C6-Fe1-C9	69.60(7)	C1-Fe1-C9	153.77(8)
C10-Fe1-C9	40.83(7)	C7-Fe1-C9	68.00(8)
C5-Fe1-C9	123.20(8)	C2-Fe1-C9	164.86(8)
C4-Fe1-C9	113.64(8)	C3-Fe1-C9	130.92(8)
C6-Fe1-C8	69.61(7)	C1-Fe1-C8	157.65(8)
C10-Fe1-C8	68.33(8)	C7-Fe1-C8	40.61(7)
C5-Fe1-C8	161.05(8)	C2-Fe1-C8	126.21(8)
C4-Fe1-C8	128.49(8)	C3-Fe1-C8	113.94(8)
C9-Fe1-C8	40.04(8)	N1-Sn1-C6	98.24(6)
N1-Sn1-C14	109.92(7)	C6-Sn1-C14	108.81(7)

N1-Sn1-C18	111.91(7)	C6-Sn1-C18	108.58(7)
C14-Sn1-C18	117.59(8)	N1-Si1-C13	109.85(9)
N1-Si1-C12	109.85(8)	C13-Si1-C12	108.11(10)
N1-Si1-C11	111.05(9)	C13-Si1-C11	109.44(11)
C12-Si1-C11	108.49(10)	C1-N1-Si1	115.56(11)
C1-N1-Sn1	112.44(10)	Si1-N1-Sn1	131.94(8)
C5-C1-N1	127.05(17)	C5-C1-C2	107.20(16)
N1-C1-C2	125.71(16)	C5-C1-Fe1	69.89(10)
N1-C1-Fe1	123.63(12)	C2-C1-Fe1	69.99(10)
C3-C2-C1	108.23(18)	C3-C2-Fe1	70.04(11)
C1-C2-Fe1	68.68(10)	C4-C3-Fe1	69.81(11)
C4-C3-C2	108.17(17)	C3-C4-Fe1	69.92(11)
C2-C3-Fe1	69.20(10)	C1-C5-Fe1	68.89(10)
C3-C4-C5	108.25(17)	C7-C6-Fe1	69.71(10)
C5-C4-Fe1	69.00(10)	C7-C6-Sn1	123.38(13)
C1-C5-C4	108.13(17)	Fe1-C6-Sn1	107.27(7)
C4-C5-Fe1	70.05(11)	C8-C7-Fe1	70.90(11)
C7-C6-C10	105.73(15)	C9-C8-Fe1	69.77(11)
C10-C6-Fe1	69.44(10)	C8-C9-Fe1	70.19(11)
C10-C6-Sn1	126.67(13)	C9-C10-Fe1	70.81(11)
C8-C7-C6	109.43(16)	C16-C14-C15	110.00(19)
C6-C7-Fe1	68.83(10)	C16-C14-Sn1	108.07(13)
C9-C8-C7	107.70(16)	C15-C14-Sn1	108.59(13)
C7-C8-Fe1	68.49(10)	C21A-C18-C20A	110.9(3)
C8-C9-C10	108.15(16)	C20A-C18-C19A	108.5(3)
C10-C9-Fe1	68.36(10)	C20B-C18-C21B	108.4(4)
C9-C10-C6	108.98(16)	C21A-C18-Sn1	115.08(19)
C6-C10-Fe1	69.02(10)	C20A-C18-Sn1	106.8(2)
C16-C14-C17	109.38(18)	C21B-C18-Sn1	111.3(3)
C17-C14-C15	108.38(19)	C19B-C18-C21B	109.5(4)
C17-C14-Sn1	112.41(15)	C19B-C18-Sn1	107.9(3)
C19B-C18-C20B	113.0(4)	C20B-C18-Sn1	106.8(3)
C21A-C18-C19A	107.2(3)	C19A-C18-Sn1	108.23(18)

Table A7. Bond Lengths [Å] of Compound 178

Fe1-C1	1.9773(16)	Fe1-C6	1.9803(16)
Fe1-C7	2.0162(17)	Fe1-C5	2.0256(18)
Fe1-C10	2.0283(17)	Fe1-C2	2.0327(18)
Fe1-C4	2.0614(19)	Fe1-C3	2.0644(17)
Fe1-C8	2.0707(18)	Fe1-C9	2.0815(19)
S1-P1	1.9678(6)	P1-N1	1.6835(14)
P1-C6	1.8094(17)	P1-C11	1.841(2)
C1-C5	1.432(2)	C1-C2	1.435(2)
C1-N1	1.4425(19)	C5-C4	1.432(2)
C6-C10	1.445(2)	C4-C3	1.421(3)
C7-C8	1.421(2)	C3-C2	1.417(3)
C8-C9	1.418(3)	C6-C7	1.446(2)
C9-C10	1.421(2)	C11-C14	1.523(3)
C11-C13	1.530(3)	C11-C12	1.530(3)

Table A8. Bond Angles [°] of Compound 178

C1-Fe1-C6	91.93(6)	C1-Fe1-C7	108.00(7)
C6-Fe1-C7	42.40(6)	C1-Fe1-C5	41.90(7)
C6-Fe1-C5	108.68(7)	C7-Fe1-C5	144.23(7)
C1-Fe1-C10	115.96(7)	C6-Fe1-C10	42.24(7)
C7-Fe1-C10	70.13(7)	C5-Fe1-C10	102.86(8)
C1-Fe1-C2	41.90(6)	C6-Fe1-C2	114.57(7)
C7-Fe1-C2	100.59(8)	C5-Fe1-C2	69.81(7)
C10-Fe1-C2	153.74(7)	C1-Fe1-C4	69.64(7)
C6-Fe1-C4	148.59(7)	C7-Fe1-C4	166.62(8)
C5-Fe1-C4	41.02(7)	C10-Fe1-C4	123.05(8)
C2-Fe1-C4	68.58(8)	C1-Fe1-C3	69.37(7)
C6-Fe1-C3	154.95(8)	C7-Fe1-C3	126.33(7)
C5-Fe1-C3	68.79(7)	C10-Fe1-C3	161.72(8)
C2-Fe1-C3	40.46(7)	C4-Fe1-C3	40.29(8)
C1-Fe1-C8	147.35(7)	C6-Fe1-C8	69.72(7)
C7-Fe1-C8	40.67(7)	C5-Fe1-C8	169.00(8)
C10-Fe1-C8	68.36(7)	C2-Fe1-C8	121.02(7)
C4-Fe1-C8	137.78(7)	C3-Fe1-C8	117.50(7)
C1-Fe1-C9	156.38(7)	C6-Fe1-C9	69.58(7)

C7-Fe1-C9	68.53(8)	C5-Fe1-C9	129.06(8)
C10-Fe1-C9	40.42(7)	C2-Fe1-C9	159.75(7)
C4-Fe1-C9	119.11(8)	C3-Fe1-C9	132.41(8)
C8-Fe1-C9	39.95(8)	N1-P1-C6	102.53(7)
N1-P1-C11	106.30(8)	C6-P1-C11	109.75(8)
N1-P1-S1	114.96(6)	C6-P1-S1	110.94(6)
C11-P1-S1	111.84(7)	C5-C1-C2	108.20(14)
C5-C1-N1	126.62(14)	C2-C1-N1	124.06(15)
C5-C1-Fe1	70.86(10)	C2-C1-Fe1	71.12(10)
N1-C1-Fe1	114.31(11)	C1-C5-C4	107.30(16)
C1-C5-Fe1	67.24(10)	C4-C5-Fe1	70.83(11)
C3-C4-Fe1	69.97(10)	C3-C4-C5	108.15(16)
C2-C3-Fe1	68.56(9)	C5-C4-Fe1	68.15(10)
C3-C2-Fe1	70.97(11)	C2-C3-C4	108.73(15)
C10-C6-P1	120.45(13)	C4-C3-Fe1	69.74(10)
C10-C6-Fe1	70.66(9)	C3-C2-C1	107.59(16)
P1-C6-Fe1	108.12(8)	C1-C2-Fe1	66.98(9)
C8-C7-Fe1	71.72(10)	C10-C6-C7	107.00(14)
C9-C8-Fe1	70.44(10)	C7-C6-P1	129.21(13)
C8-C9-Fe1	69.62(10)	C7-C6-Fe1	70.12(9)
C9-C10-Fe1	71.80(10)	C8-C7-C6	107.81(15)
C14-C11-C12	110.38(18)	C6-C7-Fe1	67.48(9)
C14-C11-P1	108.13(14)	C9-C8-C7	108.72(15)
C12-C11-P1	107.84(15)	C7-C8-Fe1	67.60(10)
C14-C11-C13	109.71(18)	C8-C9-C10	108.42(16)
C13-C11-C12	109.13(18)	C10-C9-Fe1	67.77(10)
C13-C11-P1	111.63(15)	C9-C10-C6	108.04(16)
C1-N1-P1	115.48(11)	C6-C10-Fe1	67.11(9)

Table A9. Bond Lengths [Å] of Compound 189

Fe1-C1	1.9618(17)	Fe1-C6	1.9776(18)
Fe1-C10	2.0147(19)	Fe1-C7	2.0151(18)
Fe1-C2	2.0194(18)	Fe1-C5	2.0222(18)
Fe1-C3	2.060(2)	Fe1-C9	2.0631(19)
Fe1-C8	2.0672(19)	Fe1-C4	2.0683(19)
Si1-N1	1.7823(15)	Si1-C13	1.862(2)

Si1-C11	1.865(2)	Si1-C12	1.865(2)
N1-C1	1.454(2)	N1-B1	1.472(2)
N2-B1	1.421(2)	N2-C17	1.477(2)
N2-C14	1.482(2)	C1-C5	1.431(3)
C1-C2	1.433(3)	C2-C3	1.435(3)
C6-C7	1.446(2)	C3-C4	1.418(3)
C6-B1	1.612(3)	C4-C5	1.429(3)
C14-C16	1.525(3)	C6-C10	1.445(3)
C17-C19	1.531(3)	C7-C8	1.430(3)
C14-C15	1.522(3)	C8-C9	1.423(3)
C17-C18	1.533(3)	C9-C10	1.428(3)

Table A10. Bond Angles [°] of Compound 189

C1-Fe1-C6	85.87(7)	C1-Fe1-C10	107.47(7)
C6-Fe1-C10	42.44(8)	C1-Fe1-C7	108.22(8)
C6-Fe1-C7	42.44(7)	C10-Fe1-C7	69.56(8)
C1-Fe1-C2	42.15(7)	C6-Fe1-C2	106.72(8)
C10-Fe1-C2	98.71(9)	C7-Fe1-C2	145.05(8)
C1-Fe1-C5	42.08(7)	C6-Fe1-C5	107.93(8)
C10-Fe1-C5	145.34(8)	C7-Fe1-C5	100.89(8)
C2-Fe1-C5	69.60(8)	C1-Fe1-C3	70.40(7)
C6-Fe1-C3	147.75(8)	C10-Fe1-C3	124.08(9)
C7-Fe1-C3	166.31(9)	C2-Fe1-C3	41.18(8)
C5-Fe1-C3	68.64(9)	C1-Fe1-C9	148.26(8)
C6-Fe1-C9	70.96(8)	C10-Fe1-C9	40.99(8)
C7-Fe1-C9	68.83(9)	C2-Fe1-C9	123.96(9)
C5-Fe1-C9	166.40(8)	C3-Fe1-C9	119.85(9)
C1-Fe1-C8	149.11(8)	C6-Fe1-C8	70.91(7)
C10-Fe1-C8	68.75(8)	C7-Fe1-C8	41.00(8)
C2-Fe1-C8	164.25(9)	C5-Fe1-C8	126.14(8)
C3-Fe1-C8	138.32(8)	C9-Fe1-C8	40.30(9)
C1-Fe1-C4	70.30(7)	C6-Fe1-C4	148.75(8)
C10-Fe1-C4	164.25(9)	C7-Fe1-C4	126.17(9)
C2-Fe1-C4	68.87(9)	C5-Fe1-C4	40.89(8)
C3-Fe1-C4	40.18(9)	C9-Fe1-C4	138.28(8)
C8-Fe1-C4	121.49(8)	N1-Si1-C13	108.50(9)
N1-Si1-C11	112.23(9)	C13-Si1-C11	105.94(13)

N1-Si1-C12	112.90(9)	C13-Si1-C12	106.00(13)
C11-Si1-C12	110.82(11)	C1-N1-B1	112.53(14)
C1-N1-Si1	109.60(11)	B1-N1-Si1	137.87(12)
B1-N2-C17	123.30(15)	B1-N2-C14	123.56(16)
C17-N2-C14	113.12(15)	C5-C1-C2	107.28(16)
C5-C1-N1	126.33(16)	C2-C1-N1	126.00(16)
C5-C1-Fe1	71.22(10)	C2-C1-Fe1	71.07(10)
N1-C1-Fe1	117.58(11)	C1-C2-C3	107.96(17)
C1-C2-Fe1	66.78(10)	C3-C2-Fe1	70.92(11)
C4-C3-Fe1	70.24(11)	C4-C3-C2	108.27(17)
C3-C4-Fe1	69.59(12)	C2-C3-Fe1	67.90(11)
C4-C5-Fe1	71.28(11)	C3-C4-C5	107.88(17)
C7-C6-B1	125.61(16)	C5-C4-Fe1	67.83(10)
C7-C6-Fe1	70.17(10)	C4-C5-C1	108.51(17)
B1-C6-Fe1	110.19(11)	C1-C5-Fe1	66.70(10)
C8-C7-Fe1	71.45(11)	C7-C6-C10	105.34(16)
C9-C8-Fe1	69.70(11)	C10-C6-B1	126.53(16)
C8-C9-Fe1	70.01(11)	C10-C6-Fe1	70.15(10)
C9-C10-Fe1	71.32(11)	C8-C7-C6	109.42(17)
N2-C14-C16	114.87(16)	C6-C7-Fe1	67.39(10)
N2-C17-C18	112.89(17)	C9-C8-C7	107.80(17)
N2-B1-C6	119.97(16)	C7-C8-Fe1	67.55(10)
C15-C14-C16	112.01(18)	C8-C9-C10	107.89(18)
N2-C17-C19	111.99(18)	C10-C9-Fe1	67.69(11)
C19-C17-C18	112.15(18)	C9-C10-C6	109.46(17)
N2-B1-N1	126.22(16)	C6-C10-Fe1	67.41(10)
N1-B1-C6	113.81(15)	N2-C14-C15	112.87(16)

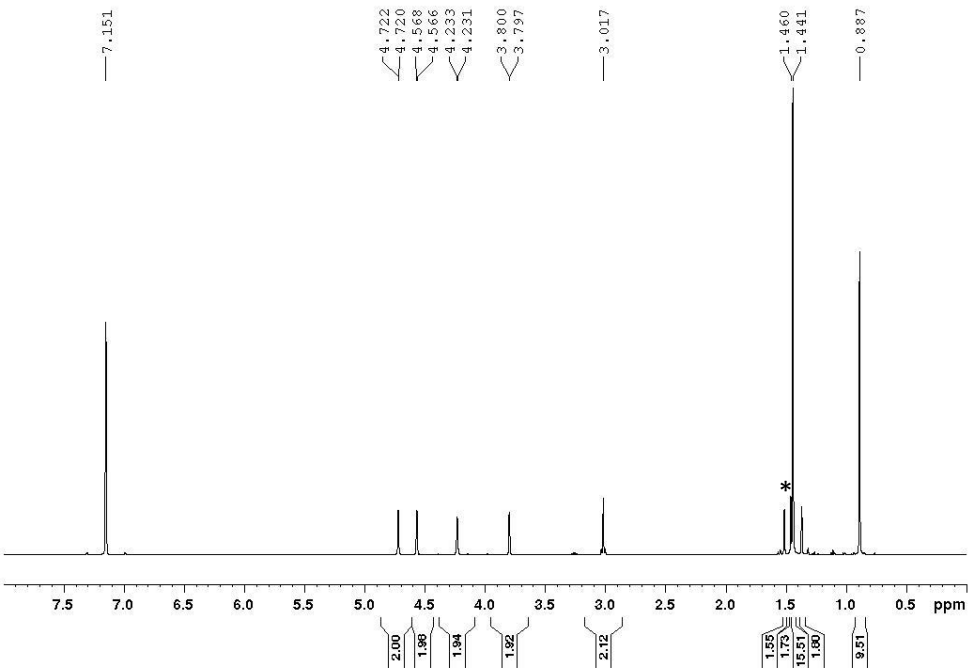

Figure A1. [1]H NMR spectrum of the isolated compound **174**. The peak marked with * is resulting from an unknown impurity.

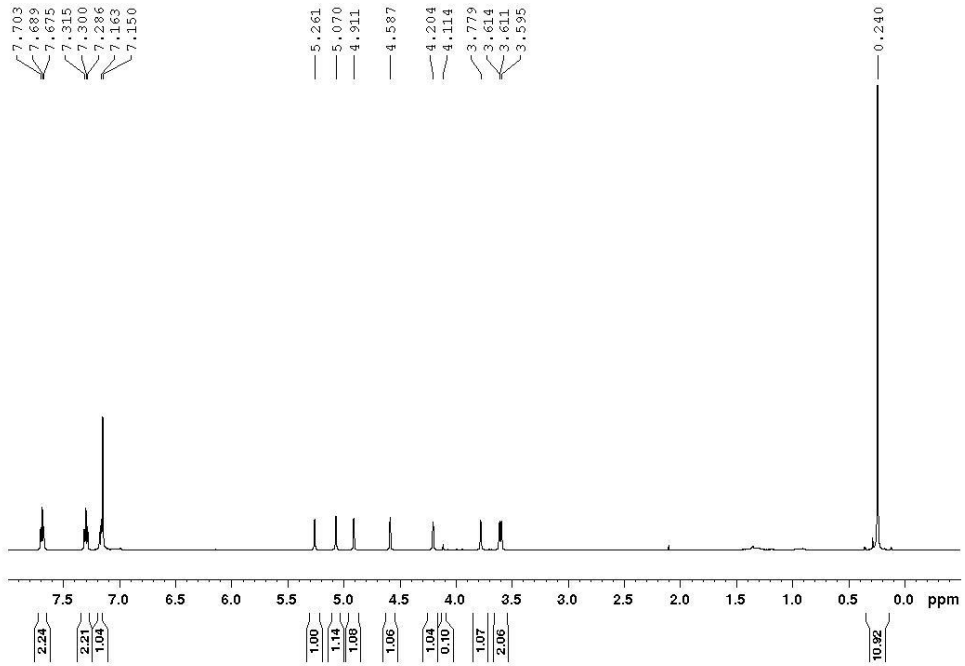

Figure A2. [1]H NMR spectrum of the isolated compound **179**.

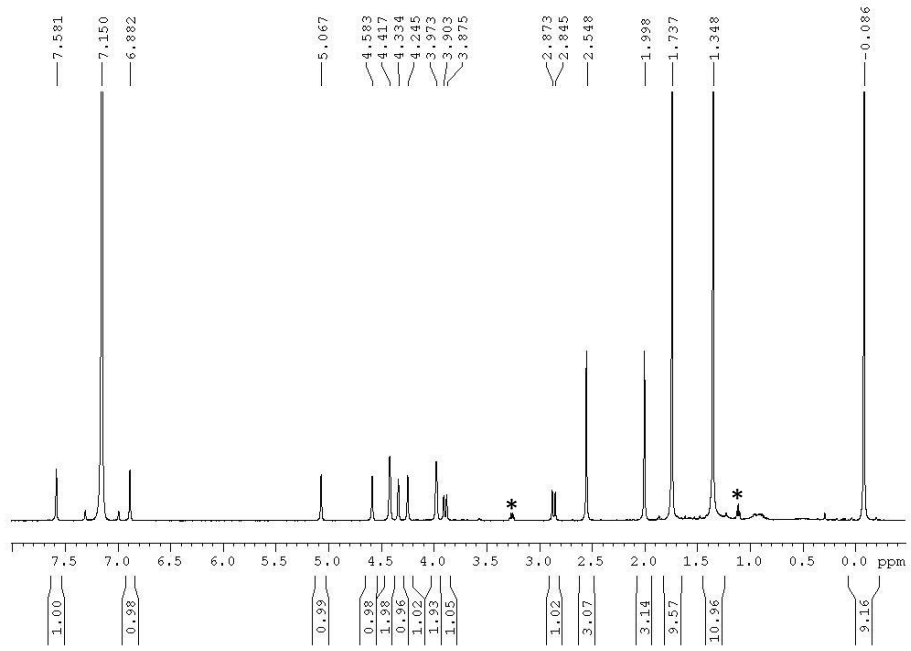

Figure A3. ^{1}H NMR spectrum of the isolated compound **188**. The peaks marked with * are resulting from Et_2O, which was used to crystallize compound **188**.

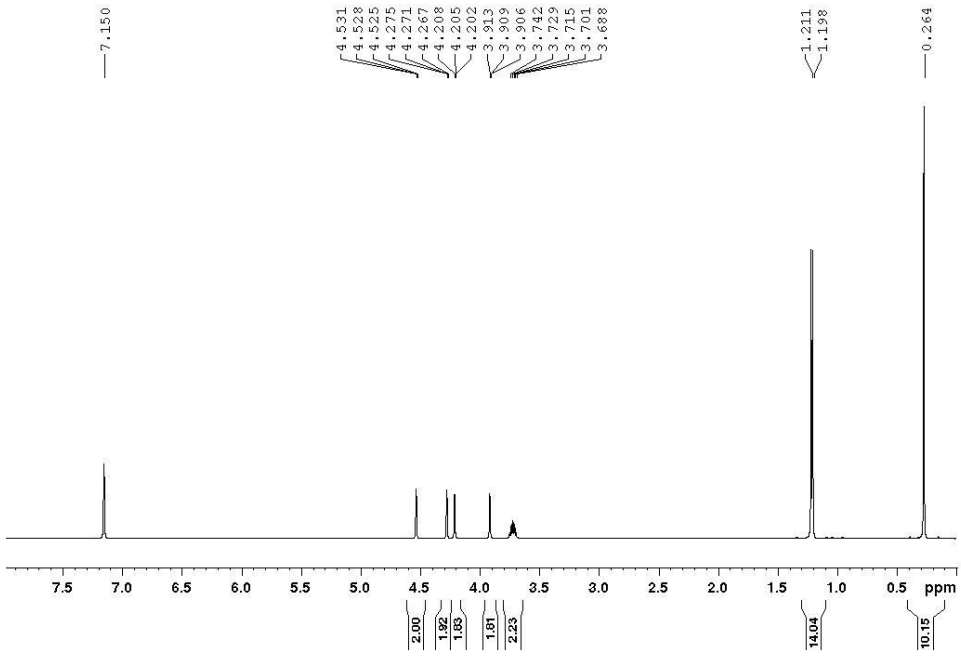

Figure A4. ^{1}H NMR spectrum of the isolated compound **189**.